Terms and Conditions of Use of Digitised Theses from Trinity College Library Dublin

Copyright statement

All material supplied by Trinity College Library is protected by copyright (under the Copyright and Related Rights Act, 2000 as amended) and other relevant Intellectual Property Rights. By accessing and using a Digitised Thesis from Trinity College Library you acknowledge that all Intellectual Property Rights in any Works supplied are the sole and exclusive property of the copyright and/or other IPR holder. Specific copyright holders may not be explicitly identified. Use of materials from other sources within a thesis should not be construed as a claim over them.

A non-exclusive, non-transferable licence is hereby granted to those using or reproducing, in whole or in part, the material for valid purposes, providing the copyright owners are acknowledged using the normal conventions. Where specific permission to use material is required, this is identified and such permission must be sought from the copyright holder or agency cited.

Liability statement

By using a Digitised Thesis, I accept that Trinity College Dublin bears no legal responsibility for the accuracy, legality or comprehensiveness of materials contained within the thesis, and that Trinity College Dublin accepts no liability for indirect, consequential, or incidental, damages or losses arising from use of the thesis for whatever reason. Information located in a thesis may be subject to specific use constraints, details of which may not be explicitly described. It is the responsibility of potential and actual users to be aware of such constraints and to abide by them. By making use of material from a digitised thesis, you accept these copyright and disclaimer provisions. Where it is brought to the attention of Trinity College Library that there may be a breach of copyright or other restraint, it is the policy to withdraw or take down access to a thesis while the issue is being resolved.

Access Agreement

By using a Digitised Thesis from Trinity College Library you are bound by the following Terms & Conditions. Please read them carefully.

I have read and I understand the following statement: All material supplied via a Digitised Thesis from Trinity College Library is protected by copyright and other intellectual property rights, and duplication or sale of all or part of any of a thesis is not permitted, except that material may be duplicated by you for your research use or for educational purposes in electronic or print form providing the copyright owners are acknowledged using the normal conventions. You must obtain permission for any other use. Electronic or print copies may not be offered, whether for sale or otherwise to anyone. This copy has been supplied on the understanding that it is copyright material and that no quotation from the thesis may be published without proper acknowledgement.

DEVELOPMENT OF SALMON CALCITONIN (sCT) NANOPOROUS/NANOPARTICULATE MICROPARTICLES FOR PULMONARY DELIVERY

Presented by:

Maria Inês Amaro, M.Pharm., M.P.S.I.

being a thesis for the degree of Doctor in Philosophy in Pharmaceutics

at the

University of Dublin, Trinity College

Under the direction and supervision of

Professor Anne Marie Healy B.Sc. (Pharm.), Ph.D., F.T.C.D., M.P.S.I.

Associate Professor Lidia Tajber, B.Sc. (Pharm.), Ph.D.

and

Professor Owen I. Corrigan

B.Sc. (Pharm.) (N.U.I.), M.A., Ph.D. (N.U.I.), F.T.C.D., F.P.S.I.

2013

DECLARATION

This thesis is submitted by the undersigned to the University of Dublin, Trinity College, for the examination for the degree of Doctor of Philosophy. This thesis is my own work and effort and it has not been submitted as an exercise for a degree at this or any other University. Where other sources of information have been used, they have been acknowledged. I agree that the Library may lend or copy the thesis upon request.

X

Maria Inês Amaro

SUMMARY

The studies in this thesis focus on the development and production by spray drying of porous microparticulate systems designed for the pulmonary delivery of a therapeutic peptide – salmon calcitonin. The nanoporous/nanoparticulate microparticles (NPMPs) developed are composite systems comprising stabilising excipient, trehalose and raffinose with bioactive. In all cases the physicochemical characteristics were studied by differential scanning calorimetry (DSC), thermogravimetric analysis (TGA), gas chromatography with flame ionisation detector (GC-FID), infrared spectroscopy (IR), X-ray powder diffraction (XRPD) and dynamic vapour sorption (DVS). Particle morphology was visualised by scanning electron microscopy (SEM). Other micromeritic characteristics of NPMPs, i.e., specific surface area, particle size, bulk and tap densities were also assessed. *In-vitro* deposition of powders was evaluated using a Next Generation Impactor (NGI). Studies directed at elucidating the pharmacokinetics of salmon calcitonin from particles administered by powder insufflation in rats were also performed.

One-factor-at-a-time (OFAT) optimisation studies on the spray drying process of raffinose and trehalose were initially performed. The effects of altering inlet temperature, feed flow rate and feed concentration on powder physicochemical properties were investigated. Powders were amorphous in nature. Microparticles were spherical and porous with a median particle size ≤ 3μm. Bulk and tap densities were low, ~0.11 and ~0.18 g/cm^3, respectively. Residual solvent content in both powder types was ~3-4% for the majority of samples. By choosing appropriate spray drying conditions, stickiness of sugar NPMPs could be decreased and the yield increased.

The OFAT did not fully cover the different parameters of the spray drying process, therefore, the effect of four parameters (air inlet temperature, gas flow, feed rate and feed concentration) on the production and characteristics of sugar NPMPs were evaluated by a 2^4 factorial experimental design. Five responses were studied: yield, geometric median particle size (d_{50}), residual solvent content (RSC), specific surface area (SSA) and outlet temperature (T_{outlet}). The design of experiment (DOE) conducted revealed that the most significant factors affecting raffinose and trehalose powders were as follows: yield - gas flow and pump setting; particle size and specific surface area – gas flow rate; residual solvent and outlet temperature – inlet temperature. It was found that particles of the same size with increasing surface area will present higher powder deposition in stages with a cut-off point less than 5 μm. A linear relationship was found to exist between SSA and the *in-vitro* deposition of the sugar NPMPs.

The NPMPs were then prepared by co-spray drying trehalose with raffinose or with hydroxypropyl-β-cyclodextrin (HPβCD) and, raffinose with HPβCD at different ratios. The

inclusion of raffinose or HPβCD in trehalose and raffinose NPMPs resulted in powders with improved physicochemical characteristics, physical stability and aerodynamic behaviour, compared to spray dried raffinose and trehalose particles. As for raffinose and trehalose NPMPs, these composite particles were regarded as suitable for pulmonary delivery.

Sugar-based nanoporous/nanoparticulate microparticles loaded with salmon calcitonin (sCT) could be produced using the same process conditions as for raffinose, trehalose and sugar composite NPMPs. The addition of peptide to the systems did not affect powder aerosol deposition, with a fine particle fraction (FPF) less than 5 μm of more than 80%. Peptide processing stability was found to be better for raffinose and raffinose:cyclodextrin systems than for systems containing trehalose as the stabilising agent. Preliminary pharmacokinetic studies indicated that sCT dry powder formulations had a similar pharmacokinetic profile as sCT solution.

Raffinose and raffinose:HPβCD NPMPs could be produced by spray drying in larger dimension spray dryers such as the Niro Mobile Minor and Niro SDMicro. Powders presented, in general, higher geometric median particle size and residual solvent content and smaller SSA than those produced using the Büchi Mini spray dryer B-290. However, the *in-vitro* deposition studies showed NPMP powders produced in the Niro Mobile Minor presented similar deposition profiles and deposition parameters to those spray dried with the Büchi Mini Spray Dryer, while powders prepared on the Niro SDMicro powders had higher fine particle fractions than those prepared with the Büchi instrument.

ACKNOWLEDGMENTS

Desejo agradecer em especial a minha orientadora Doutora Anne Marie Healy, pela oportunidade, orientação, disponibilidade, atenção dispensada e pequenas conversas sobre a vida! À Doutora Lidia Tajber e Professor Corrigan pela orientação e atenção dispensada. Ao Doutor Carsten Ehrhardt por toda a orientação e disponibilidade em todas as conferencias nas quais participamos.

Ao Luís Pedro pelo apoio, incentivo, compreensão e encorajamento, durante todo este período. Obrigada, pela paciência, por todos os almoços cozinhados, filmes, musicas, jogos e mimo!

À minha família, em particular, aos meus pais e irmãos sempre presentes e curiosos sobre o meu trabalho. Mãe obrigada por tudo ao longo destes curtos 29 anos! Pai sem os seus docinhos nunca la teria chegado!

Aos pais, irmão e avós do Luís, obrigada pelos biscoitos da Belmira, vinho e pão alentejano, bolo podre e ginginha!

Aos meus amigos, Inêsinha, Gui, Teresa, Ruca, Bruno e Andrea obrigada pela conversa, cafés, almoços e jantares.

To Anita, Christine, Evelyn, Fred, Joanne, Johanna, Krzysziof, Marisia, Stefano, Stephany and Vicent Caron, for the moments shared in the fantastic, amazing, awsome Trinity labs. Joanne and Christine, thank you for all the long conversations and for putting up with my warm-blooded temper!

A todo o pessoal técnico do Trinity.

Aos meus amigos e parceiros de escalada, Jenny, Niamh, Peter K. and Peter W.

Por fim, obrigada a cidade de Dublin, à Guinness e ao Jameson por todos os momentos proporcionados.

Thank you everyone!

PRESENTATIONS ASSOCIATED WITH THIS THESIS

POSTER PRESENTATIONS

- "Characterisation of sugar nanoporous/nanoparticulate microparticles (NPMPs) and optimisation of the spray drying process for their production" 23rd AAPS Annual Meeting and Exposition, Los Angeles, November 2009 [M.I. Amaro, L. Tajber, O.I. Corrigan, A.M. Healy]
- "Optimisation of the spray drying process for the production of sugar nanoporous/nanoparticulate microparticles - carriers of peptides and proteins for pulmonary delivery" All-Ireland Pharmacy Schools Conference, Belfast, March 2010 [M.I. Amaro, L. Tajber, O.I. Corrigan, A.M. Healy]
- "Design of experiment to study the effect of spray dryer operating variables on sugar powders intended for inhalation" UK-PharmSci 2010 – The Science of Medicines, Nottingham, September 2010 [M.I. Amaro, L. Tajber, O.I. Corrigan, A.M. Healy]
- "Characterisation, aerodynamic behaviour and bioactivity of salmon calcitonin-loaded nanoporous/nanoparticulate microparticles (NPMPs)" 24th AAPS Annual Meeting and Exposition, New Orleans, November 2010 [M.I. Amaro, F. Tewes, L. Tajber, O.I. Corrigan, A.M. Healy]
- "Salmon calcitonin loaded raffinose microparticles for pulmonary delivery" All-Ireland Pharmacy Schools Conference, Dublin, April 2011 [M.I. Amaro, L. Tajber, O.I. Corrigan, A.M. Healy]
- "Formulation and stability of sugar-based salmon calcitonin-loaded nanoporous/nanoparticulate microparticles (NPMPs) for inhalation" ISAM 2011 Congress, Rotterdam 2011 M.I. Amaro, F. Tewes, L. Tajber, O.I. Corrigan, A.M. Healy]
- "Physicochemical, physical stability and aerosolisation properties of trehalose/cyclodextrin microparticles" 25th AAPS Annual Meeting and Exposition, Washington DC, October 2011 [M.I. Amaro, L. Tajber, O.I. Corrigan, A.M. Healy]
- "Characterisation and pharmacokinetic studies of salmon calcitonin:sugar nanoporous/nanoparticulate microparticles (NPMPs) for pulmonary delivery" 8th World Meeting on Pharmaceutics, Biopharmaceutics and Pharmaceutical Technology, Istanbul, March 2012 [M. I. Amaro, O. Gobbo, F. Tewes, L. Tajber, O.I. Corrigan, C. Ehrhardt, A.M. Healy]

JOURNAL ARTICLES

- Amaro M.I., Tajber L., Corrigan O.I., Healy A.M., 2010. Design of experiment to study the effect of spray dryer operating variables on sugar powders intended for inhalation. *Journal of Pharmacy and Pharmacology*, 62 (10), pp 1413-1414
- Amaro M.I., Tajber L., Corrigan O.I., Healy A.M., 2011. Optimisation of spray drying process conditions for sugar nanoporous microparticles (NPMPs) intended for inhalation. *International Journal of Pharmaceutics*, 421(1), pp 99-109.

TABLE OF CONTENTS

ABBREVIATIONS

BA – butyl acetate

bp – bulk density

cAMP - cyclic adenosine monophosphate

CD – circular dicroyism

d_{aer} –aerodynamic diameter

d_{50} - geometric median particle size

DOE - design of experiment

DPIs - dry powder inhalers

DSC - differential scanning calorimetry

DVS - dynamic vapour sorption

EA – ethyl acetate

EIA - enzyme immuno-assay

EtOH - ethanol

FPF - fine particle fraction

GC-FID - gas chromatography with flame ionisation detector

GSD- geometric standart deviation

hCT – human calcitonin

HPLC – high performance liquid chromatography

HPβCD - hydroxypropyl-β-cyclodextrin

IP – induction port

IR - infrared spectroscopy

m_0 - dry sample mass

MA – mouth adaptor

MeOH – metanol

MM- Niro Mobile Minor

MMAD-mass median aerodynamic diameter

NPMPs - nanoporous/nanoparticulate microparticles

OFAT - One-factor-at-a-time

PA –propyl acetate

PLGA - poly(lactic-co-glycolic acid)

RH – relative humidity

R5W -raffinose pentahydrate

RSC - residual solvent content

sCT – salmon calcitonin

SEM - scanning electron microscopy

SDM – Niro SDMicro

SSA - specific surface area

T_c - recrystallisation temperature

T2W - trehalose dehydrate

T_g – glass transition

TGA - thermogravimetric analysis

T_{inlet} - inlet temperature

T_m - melting temperature

T_{outlet} - outlet temperature

tp – tap density

t.s.c. – total solid concentration

XRPD - X-ray powder diffraction

ΔH_c - recrystallisation enthalpy

ΔH_m - melting enthalpy

ORIGIN AND SCOPE

Pulmonary drug delivery using dry powder inhalers (DPIs) is an important research area, impacting on the treatment of respiratory diseases such as asthma and chronic obstructive pulmonary disease. Inhalation allows non-invasive drug targeting. In recent years, it has become an alternative for systemic delivery of peptides and proteins, improving their bioavailability and effectiveness (Patton, 1996; Patton et al., 2004; Daniher et al., 2008). Over the past 40 years, DPIs have been marketed with various devices and formulations, the Exubera™ product by Nektar/Pfizer being the most recent example of marketed pulmonary delivery of a protein (Hickey, 2005; Chan, 2006). Currently many investigations are being pursued by the pharmaceutical industry such as the AIR system (Alkermes/Eli Lilly), the Technosphere system (Mannkind) and Kos inhaled insulin (Kos Pharm/Abbott) for Type I/II diabetes, and Granulocyte-colony-stimulating factor (G-CSF) for Neutropenia (Amgen)(Kunda, N.K. et al., 2012). The inhalers employ the patient's inspiratory flow as the means of dispersion and entrainment of the aerosol into the lungs (Hickey, 2005; Campen and Venthoye, 2007; Daniher and Zhu, 2008; Pilcer and Amighi, 2010). The lung is an attractive option for peptide and protein delivery due to the large and highly vascularised absorptive surface area of the alveolar region (~100 m^2), thin non-ciliated epithelial barrier (0.1-0.2 μm), relatively low enzymatic activity, and most importantly, the avoidance of hepatic first pass metabolism (Patton, 1996).

The DPI aerosol cloud should be constituted by particles with aerodynamic diameters between 1 and 3 μm with good dispersibility (good flow) to efficiently deliver the drug into the lower regions, i.e., alveolar, of the lungs (Johnson, 1997; Koushik and Kompella, 2004; Chow et al., 2007).

Spray drying is a commonly used technique which may be employed to produce powders of fine particle size (Masters, 1991). The process consists of the atomisation of a feed solution into droplets that dry rapidly because of their high surface area and intimate contact with the drying gas. Dried powder is protected from overheating by rapid removal from the drying zone. The final product can be removed from the air stream by cyclones and/or filters (Masters, 1991).

Where the protein/peptide to be used for pulmonary delivery is of low dose and high potency, it may be desirable to formulate it with a carrier material (inert excipient) to increase the volume of powder loaded and delivered from the DPI device. Protection of protein structure is critical in both processing and storage of the final formulation (Ní Ógáin et al., 2011).

Non-reducing sugars, such as raffinose and trehalose, possess properties which make them promising excipients for protection of biomolecules. They appear to be effective stabilisers of proteins in the amorphous state (Colaco et al., 1992; Johnson, 1997; Maury et al., 2005). Studies

by Lopéz-Diéz et al. (2004), Maury et al. (2005), Yoshii et al. (2008) and Ní Ógáin et al. (2011) have established the protective action of trehalose and raffinose on protein integrity, reducing loss of bioactivity. Carpenter and Crowe (1988, 1989) suggested the water replacement theory to explain the protective action of the sugar compounds, where the formation of H-bonding between the excipient and the biomolecule occurs when water is removed, maintaining the structural integrity of the peptide/protein. A second theory of protein protection through the use of such sugars was proposed by Franks et al. (1991) based on the formation of an amorphous glass during drying, which provides a rigid matrix around the protein molecules to restrict and stabilise their motion.

Ní Ógáin et al. (2011) studied the production of raffinose and trehalose nanoporous microparticles (NPMPs) for inhalation, evaluating different ratios of methanol:n-butyl acetate (MeOH:BA) solvent system for the solution to be spray dried, and concluded that NPMPs spray dried from 80:20 (v/v) MeOH:BA displayed favourable micromeritic characteristics, suggesting potential suitability for pulmonary delivery. The porous morphology of the particles was found to improve the aerosolisation properties compared to equivalent non-porous spray dried particles. Ní Ógáin et al. (2011) also demonstrated that a model protein, lysozyme, could be incorporated into the carrier particles at a ratio of 1:4 (w/w) protein:carrier, while still retaining the characteristic porous morphology. The same author presented a short study on the spray drying of salmon calcitonin:trehalose composite system, with retention of peptide bioactivity and conformation (Ní Ógáin, 2008). However, the spray drying process developed to produce NPMPs of the two sugars was not optimised in terms of product characteristics or yield. Following on from the work of Ní Ógáin et al. (2011) the initial studies in this thesis investigate the effect of operating parameters of a Büchi B-290 laboratory spray dryer and feed solution concentration, in order to optimise the production of raffinose and trehalose NPMP powders, intended to be used as carriers of biomolecules for inhalation.

The amorphous nature of the sugar NPMPs raised an issue of stability, since amorphous solids are known to be less stable physically and chemically than the corresponding crystals (Yu, 2001, Newman et al., 2012), and will spontaneously sorb (adsorb or absorb) a significant amount of water vapour from their surroundings unless stored under completely dry conditions. This sorbed water vapour can markedly change the physical and chemical properties of the sugars, accelerate hydrolytic degradation, isomerisation, and/or crystallisation processes and, thus can have a significant impact upon their use and function in pharmaceutical dosage forms (Hancock and Shamblin, 1998). Different studies have observed a rapid water absorption and recrystallisation of amorphous raffinose and trehalose powders when exposed to ~75% relative

humidity (RH) for 24 hours (Hogan and Buckton, 2001; Charmathy et al., 2010; Shebor et al., 2010). Ní Ógáin et al. (2010) reported that the exposure to 60% RH for 24 h of trehalose:lysozyme or raffinose:lysozyme NPMPs composites resulted in particle morphology change and amorphous state collapse into crystalline state. This author (Ní Ógáin, 2008) also reported the enhancement of trehalose stability, when co-spray drying with hydropropyl-β-cyclodextrin. Hence, this excipient was included in the studies presented in this thesis.

The need to enhance the stability and prevent recrystallisation of the non-reducing sugars NPMPs was therefore pivotal in the studies presented in this thesis, before testing the NPMPs feasibility to be used as carriers of a peptide, salmon calcitonin, for systemic delivery via the lungs.

The scope of this thesis was:

- To spray dry sugar nanoporous/nanoparticulate microparticles (NPMPs) assessing the effect of operating parameters of a Büchi B-290 laboratory spray dryer and feed solution concentration, in order to optimise the production of NPMPs. To research the physicochemical properties of the prepared powders to ensure their suitability for later incorporation of peptides and proteins, as a system designed for pulmonary delivery.
- To access the production of NPMPs using a different co-solvent system by replacement of butyl acetate with propyl acetate, a solvent of the same chemical family but presenting a lower boiling point.
- To spray dry composite systems comprising of a mixture of excipients and/or excipient: peptide at different mass ratios, using optimised spray drying conditions. To investigate the production process, particle characteristics, *in vitro* and *in vivo* activity and storage stability of peptide-containing NPMPs.
- To assess the feasibility of transferring the spray drying process of NPMPs to a larger dimensions laboratory spray dryer, Niro SDMicro, and to assess the scale up of processing using the Niro Mobile Minor, a pilot scale spray dryer. To investigate the powders physicochemical properties of the particles produced to determine if they are comparable to those produced in the laboratory scale using a Büchi B-290 Mini Spray dryer.

CHAPTER 1

INTRODUCTION

1. INTRODUCTION

1.1 PULMONARY DRUG DELIVERY

Pulmonary drug delivery is routinely used in the treatment of respiratory diseases such as asthma, cystic fibrosis, chronic obstructive pulmonary disease and emphysema. Over the past two decades inhalation therapy has become an attractive option for systemic drug delivery expanding the potential applications of this field. In fact, the lungs are an efficient port of entry for drugs into the bloodstream due to the large and highly vascularised surface area (80-100 m^2/adult and 5 L blood/min respectively), in addition to its thin and highly absorptive membrane (0.1-0.2 μm), for the absorption of drugs (Newhouse, 2007; Daniher and Zhu, 2008; Pilcer and Amighi, 2010).

Nowadays, some of the most promising therapeutic agents are peptides and proteins, such as insulin, interferon β and α_1 proteinase inhibitor, which could be inhaled instead of injected. In contrast to oral delivery, where a drug can be heavily metabolised and altered by the enzymes of the gut and liver (first pass metabolism), the lungs have only a small fraction of the drug-metabolising enzymes and efflux transporter activity of the gut and liver (Patton, 1996; Patton et al., 2004). Thus, small molecules can be delivered in their true form and efficiently into the body through the lungs, without the production of a complex array of metabolites and, large molecules such as peptides and proteins avoid digestion and degradation before reaching the blood stream (Patton, 1996; Patton et al., 2004; Newhouse, 2007; Daniher and Zhu, 2008). Another advantage of the pulmonary route is the fact that it is a non-invasive delivery route.

The devices that are employed to deliver drugs to the lungs may be divided into three categories: propellant-driven metered dose inhaler (pMDI), dry powder inhalers (DPIs), and nebulisers. Each of these systems delivers aerosols by a different principle, and the chemistry associated with the product varies significantly among them (Hickey, 2005; Campen, 2007). A good delivery device has to generate an aerosol of suitable size and provide reproducible drug dosing; it should protect the physical and chemical stability of the drug formulation. The ideal inhalation system must be a simple, convenient, inexpensive and portable device (Pilcer and Amighi, 2010).

The metered dose inhaler is one of the most widely used methods of aerosol drug delivery because of its reliability and low cost. However, its use is limited by the need for the patient to coordinate MDI actuation with breath inhalation and from the deposition of a sometimes

significant amount of drug, driven by the propellant blast, to the back of the throat instead of the lung (Campen, 2007; Pilcer and Amighi, 2010).

The nebuliser platform atomises an aqueous based drug solution or suspension by air jet or ultrasonic mechanisms. It is typically used for delivering doses over multiple breaths, and to infants, elderly and critically ill patients. Advances in nebuliser technology, including more compact ultrasonic mechanisms, have overcome some traditional limitations of the bulky, complicated and expensive units. Nebulisers remain appealing due to the independence of aerosol generation from inhalation manoeuvre, and relatively easy formulation handling (Campen, 2007; Pilcer and Amighi, 2010).

The dry powder platform presents medication to the patient as a dry powder. The device combines powder technology with device design to disperse dry particles as an aerosol in a patient's inspiratory airflow. It is "breath-actuated" in contrast to nebulisers and most MDIs, requiring little or no coordination of actuation and inhalation, which results in more efficient lung delivery (Campen, 2007; Islam and Galdki, 2008; Pilcer and Amighi, 2010).

Pharmaceutical aerosols are inhaled through the mouth and into the respiratory tract for local or systemic delivery. In sequential order the route consists of the oropharynx, larynx, trachea, bronchi, bronchioles and alveoli. The larger bronchioles and the upper respiratory tract have ciliated epithelia, forming the mucociliary escalator. Gas exchange occurs in the distal bronchioles and alveoli, which are extremely thin and are bordered by a profuse network of capillaries (Kwok and Chan, 2006). The alveolar epithelium is composed of a thin, non-ciliated, non-mucus-covered cell layer consisting of type I and type II alveolar epithelial cells. A thin epithelial lining fluid, mainly composed of surfactant, covers the type I and II alveolar epithelial cells (Newhouse, 2007). Aerosol deposition is dependent on three mechanisms: inertial impaction, sedimentation, and diffusion. Inertial impaction is the principal mechanism of deposition of large particles; the inertia of a particle will tend to cause it to move in its initial path when the supporting airstream is suddenly deflected by branching of airways. It is directly dependent on particle terminal settling velocity, airstream velocity and inversely dependent on airway radius. Thus, the larger the particles, the faster it is, the greater the air velocity and the smaller the airway, the greater will be the probability of deposition by inertial impaction (Stuart, 1976; Scheuch et al., 2006). Sedimentation or settling under the force of gravity is dependent on particle density and size. Every particle that is allowed to fall in air will accelerate to a terminal settling velocity at which the force of gravity is balanced by the resistance of air through which the particle is falling; it is the main mechanism of deposition of particles having diameters of 0.1

μm to more than 50 μm (Stuart, 1976; Scheuch et al., 2006). Diffusion or Brownian motion involves particles of very small diameter, 0.2 – 0.5 μm; particles are displaced by bombardment due to random motion of gas molecules in the air, leading to an irregular and unoriented movement of particles, which can cause contact with an airway wall (Stuart, 1976; Scheuch et al., 2006).

For any mechanism of deposition the particle size and density are very important in defining where particle deposition occurs. Deposition in the central and distal lung regions is achieved when particles present an aerodynamic diameter between 1 and 3 μm (Hickey, 1996). Particles of > 5 μm diameter are deposited mainly in the oropharynx by inertial impaction and are then swallowed into the gastro-intestinal tract (Chow et al., 2007).

Particles that deposit along the airways need to overcome the absorption barriers such as mucus layer and alveolar lining fluid layer, to be absorbed (in case of drugs) as well as, the alveolar epithelium and basement membrane, which act to varying extents by inhibiting drug permeation into the circulation, the competing cellular uptake pathways - particle phagocytosis by macrophages, and proteolytic degradation that can limit the amount of intact drug available for absorption.

In the design of formulations for pulmonary delivery focus should be on particle engineering issues that are of vital importance to achieve correct lung deposition and to overcome pulmonary barriers, without disregarding the drug stability and safety.

1.1.1 Dry powder inhalers

Over the past 40 years, dry powder inhalers (DPIs) have been marketed with various devices and formulations (Figure 1.1) (Hickey, 2005; Kwok and Chan, 2006). The inhalers employ the patient's inspiratory flow as the means of dispersion and entrainment of the aerosol into the lungs (Hickey, 2005; Campen and Venthoye, 2007; Daniher and Zhu, 2008; Pilcer and Amighi, 2010). Hence, no propellants are required. The DPI device should assist in the generation of very fine particulates of medication in a way that enables them to avoid the impaction barriers that normally operate in the lung to prevent the ingress of potentially harmful particles. These barriers include the oropharynx and, for deep lung delivery, the air-conducting bronchi and bronchioles (Campen and Venthoye, 2007). Studies have demonstrated that aerosol particles must present a specific aerodynamic diameter: < 5 μm, to clear the oropharyngeal impaction barrier; < 3 μm, to reach the terminal bronchi and the alveoli (Figure 1.2) (Johnson, 1997; Hickey, 2005; Campen and Venthoye, 2007; Chow et al, 2007; Daniher and Zhu, 2008; Pilcer and Amighi,

2010). However, the respiratory pattern of patients during aerosol intake may influence the deposition of inhaled particles, because mean flow rates of particles in each region of the airways is governed by the breathing volume and frequency of breathing (Campen and Venthoye, 2007; Islam and Gladki, 2008). DPIs can provide single- or multi-doses via oral inhalation, depending on the design of the powder reservoir and metering components (Islam and Gladki, 2008).

Characteristics of the ideal DPI system will include most or all of the following attributes (Campen and Venthoye, 2007): simple and comfortable to use; compact and economical to produce; highly reproducible fine-particle dosing; a reproducible emitted dose; physically and chemically stable powder; minimal extrapulmonary loss of drug (low oropharyngeal deposition, low device retention, and low exhaled loss); multidose system; powder protected from external environment and can be used in all climates and protected from moist exhaled air; overdose protection and indicate number of doses delivered and/or remaining.

Figure 1.1 Photographs of some currently available DPI devices: (A) Aerolizer™, (B) Easyhaler™, (C) Turbohaler™, (D) Diskhaler™, (E) Novolizer™, (F) NEXT™, (G) Clickhaler™, (H) MAGhaler™, (I) Spinhaler™, (J) Handihaler™ (Islam and Gladki, 2008)

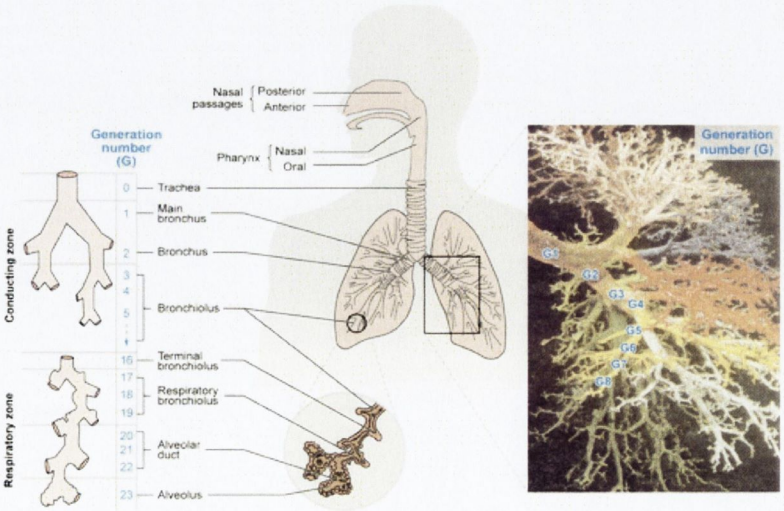

Kleinstreuer C, et al. 2008.
Annu. Rev. Biomed. Eng. 10:195–220.

Figure 1.2 Respiratory tract.

1.1.1.1 Bulk powder properties

The respirable powders (powders capable of penetrating and depositing within the lungs) of a DPI cannot be characterised by single particle studies; bulk properties must also be assessed for ease of manufacture and for thorough knowledge of system performance. Primary bulk properties include particle size and its distribution, bulk density, and surface area; which along with particle electrostatics, shape, surface morphology, hygroscopicity, affect secondary bulk powder characteristics such as powder flow, handling, consolidation, and dispersability (Campen and Venthoye, 2007; Chow et al., 2007; Pilcer and Amighi, 2010). Table 1.1 presents the powder properties that affect the aerosol delivery, as reported by Chow et al. (2007).

Table 1.1 Particle/powder properties that affect the aerosol delivery (Chow et al., 2007).

Particle characteristics	Effects on formulation
Process parameters: temperature, pressure, solvents, pH, additives, yield, recovery, manufacturing complexity	Process economics, development risks and costs
Solid state: crystalinity, polymorphism, hygroscopicity, impurities, solubility, dissolution rate	Physical and chemical stability, bioavailability, toxicity
Particle size distribution, shape, porosity/density	Aerosolisation behavior, in vitro and in vivo deposition profiles, bioavailability
Surface morphology, energetics and electrostatics	Powder handling, inhaler filling, dose metering,
Powder bulk density, agglomeration, cohesiveness, flow properties	storage stability, shelf.life, dose uniformity and consistency
Co-formulation/blending; composition/coating	Dose uniformity Modified and extended release, toxicity
Formulation, dispersion media	Type of inhaler Mode of administration

The particle aerodynamic diameter (d_{aer}) is the most appropriate particle-size expression in inhalation. As discussed above, this particle characteristic will affect the mechanism of its deposition in the lungs. It is defined as the diameter of a sphere of unit density, which reaches the same velocity in the air stream as a non-spherical particle of arbitrary density (Johnson, 1997; Bosquilon et al., 2001; Chow et al, 2007; Pilcer and Amighi; 2010).The aerodynamic diameter can be defined by equation 1:

$$d_{aer} = d\sqrt{\left(\frac{\rho}{\rho_1 \chi}\right)} \qquad \text{(Eq. 1)}$$

Where d is the geometric mean diameter, ρ is the particle density and ρ_1 is the reference density of a sphere, with ρ_1= 1 g/cm^3 and χ is the dynamic shape factor (equal to one for a sphere) (Johnson, 1997; Bosquilon et al., 2001; Chow et al., 2007; Pilcer and Amighi; 2010). The shape factor is a dimensionless measure of the deviation from sphericity; is the ratio of the actual

resistance force experienced by a non-spherical falling particle to the resistance force experienced by a sphere having the same volume. Thus d_{aer} can be reduced by: decreasing the particle density, decreasing the geometric mean diameter and increasing the dynamic shape factor (Pilcer and Amighi; 2010).

In addition to the aerodynamic diameter of primary particles, the dispersibility of the particles has to be taken into consideration as it will define particle deposition. Powder dispersion is strongly related to interparticulate interactions including: Van der Waals forces; electrostatics forces; capillary forces; and mechanical interlocking. Van der Waals forces become noticeable when the particles are sufficiently close (0.2–1.0 nm) to one another and when the particles are small (<20 μm). Surface roughness, geometrical structure and deformation of individual particles can significantly change the van der Waals forces; when these forces increase the particles become highly cohesive (Zeng et al., 2001; Daniher and Zhu, 2008). Electrostatic forces can occur by tribo-electric charging or by the potential difference when particles of different work functions are brought into contact; the resulting Coulomb attraction makes the powder adhesive (Daniher and Zhu, 2008). Capillary forces arise from the dynamic condensation of water molecules onto particle surfaces; a water meniscus is formed between contact points of adjacent surfaces as liquid is drawn by capillary action, inducing an attractive force. Controlling moisture content aids in reducing capillary forces, but care must be taken to avoid increasing the surface charge of the particles (Pilcer and Amighi; 2010). Mechanical interlocking due to surface features or roughness is a prominent mechanism that prevents particle dispersion; these forces are related to the diameter of the pores between particles and interfacial tension due to hydrogen bonding of water (Telko and Hickey, 2005; Pilcer and Amighi; 2010). Particle aggregates and agglomerates are the main outcome of the action of these forces. The strength of these and the impact of aerodynamic forces generated upon inhalation are critical to powder dispersion.

Particle shape may affect the flow properties of a powder by changing interparticulate and/or frictional forces between the particles. In general, if the particle shape can reduce both interparticulate and frictional forces, then it is said to be favourable for good powder flow. The majority of pharmaceutical powders consist of spherical particles since this shape is believed to produce the least interparticulate friction and, hence, the best flow properties under normal conditions. Another aspect of particle morphology that is known to affect powder flow is the surface roughness and presence of porosity. Studies by Tabor (1977) demonstrated that surface roughness can greatly reduce the adhesion between solids, due to the high surface asperities,

which can prise the surfaces apart and break the adhesions occurring at the lower asperities. The cohesion between non-porous particles by contact surfaces is proportional to the specific surface area (Chew et al., 2000). Porous microparticles have potential advantages over non-porous materials as they have reduced interparticulate attractive forces and improved flow characteristics, low bulk densities and exhibit smaller aerodynamic diameters than their geometric diameters, facilitating greater deposition in the lower pulmonary region, with potential for improved efficiency of administration to the lungs in the dry form (Healy et al., 2008). The presence of porosity is reflected in a high specific surface area (SSA) value (Papelis et al., 2003; Healy et al., 2008).

Porous microparticles in the form of Pulmospheres™ have been produced by spray drying an emulsion formulation consisting of a bioactive agent, surfactant, and a blowing agent, such as fluoroalkane. It was postulated that the blowing agent is vaporised and forced through the thin surface wall to form pores in the particles, with the stabilising surfactant remaining in the spray dried product (Chow et al., 2007; Healy et al. 2008). Healy et al. (2008), Nolan et al. (2009, 2010) and Ní Ógaín et al. (2010) reported the production of nanoporous microparticles (NPMPs) of different materials such as bendroflumethiazide, budesonide, sodium cromoglicate, trehalose by spray drying a co-solvent system in which the solute is more soluble in one solvent than another. Ammonium carbonate was added to the bendroflumethiazide solution as a formulation enhancer, acting as a pore forming agent (Healy et al. 2008).

As mentioned above, powders consisting of porous particles present lower bulk density than non-porous powders. The bulk density of a powder is the ratio of the mass of an untapped powder sample to its volume, including the contribution of the interparticulate and intraparticulate void volume. Hence, the bulk density depends on both the density of powder particles and the spatial arrangement of particles in the powder bed (Ph. Eur., 2012). The average number of contact points between particles increases as bulk density increases, and the interparticulate forces at these contact points must be overcome to produce a dispersed aerosol cloud. Therefore, a powder of low bulk density may be more easily dispersed as an aerosol than an equivalent powder with high bulk density (Campen and Venthoye, 2007).

1.1.1.2 Assessment of aerosol deposition

The overall efficiency of any inhalation system is given mathematically by the product of the fraction of emitted dose (ED), dose delivered to the lung (i.e., fine particle fraction, FPF) and lung bioavailability. Both ED and FPF are normally determined *in vitro* using a multistage cascade

impactor (MSCI) (e.g., Andersen cascade impactor (ACI) or next generation impactor (NGI)) and predominantly governed by both the particulate properties and inhaler design. FPF is measured as the mass of particles (with reference to the ED) below a certain cut-off diameter, usually < 5 μm or < 3 μm. The desirable product characteristics include high FPF and ED, high dose consistency and uniformity and, ideally, independence of the type of device and inhalation flow rate. Thus, apart from the correct aerodynamic particle size (often expressed as the mass median aerodynamic diameter, MMAD), the particles should have a relatively narrow particle size distribution (PSD) and should be readily aerosolisable at relatively low aerodynamic dispersion forces (Chow et al. 2007). The MMAD takes account of particle aggregates and gives therefore the ultimate aerodynamic behaviour of the aerosol. In addition, comparison of MMAD with d_{aer} provides information on dry powder cohesiveness and aerosolisation properties (Bosquillon et al., 2001). Powders intended for delivery into the deep lung require an MMAD between 1-3 μm; particles with MMAD ≤ 0.5 μm are exhaled (Campen and Ventoyhe, 2007).

1.1.2 Pulmonary delivery of peptides and proteins

Proteins and peptides are polyamino acids, that is, a chain of amino acids covalently linked by peptide bonds (primary structure) and differing in their structure. Peptides are formed by dozens of amino acids (up to 50) organised in a periodic spatial arrangement of the polypeptide chain backbone that can be designated as alpha-helices and beta-sheets. Proteins present a more complex structure: after the polypeptide chain is formed this structure undertakes a 3-dimensional conformation; the arrangement of these subunits relative to each other constitutes the quaternary structure (Kwok and Chan, 2006; Creighton, 2010).

Peptides and proteins are degraded by digestive enzymes and their oral bioavailability, without advanced delivery systems, is generally poor. The most common route of administration for pharmaceutical peptides and proteins is parenteral (invasive), including intravenous, subcutaneous and intramuscular injections. Inhalation delivery is non-invasive and provides a potential route for protein and peptide delivery. Many pharmaceutical peptides and proteins have been investigated for potential delivery as aerosols for local and systemic diseases. Exubera™ was a marketed insulin dry powder inhaler that presented good stability and bioavailability, but was withdrawn due to poor sales (Kwok and Chan, 2006). Insulin was found to have a pulmonary bioavailabily of 8 to 25% (Patton, 1999). Miacalcin™ a nasal formulation of salmon calcitonin, by Sandoz Pharmaceuticals, is commonly used in the treatment of Paget's disease with three daily administrations being as effective as injectable calcitonin (Patton, 2000; Bhandari et al. 2010). Salmon calcitonin has been reported to have a pulmonary bioavailability

between 11 and 18% (Patton, 2000; Clark et al., 2008). These two examples demonstrate the potential use of the airways for delivery of macromolecules.

The great advantage of pulmonary delivery is the large surface area for absorption that the lungs present, as well as the low levels of drug metabolism and enzymatic breakdown here. However, the lungs also have pulmonary clearance and metabolic pathways to guard against foreign macromolecules and to renew the lung epithelial cells. These natural defence mechanisms include catabolic enzymes such as the serine endo-peptidases, trypsin, chymotrypsin, and various elastases that are either membrane-bound or secreted by respiratory macrophages and epithelial cells that can reduce the bioavailability of the peptides and proteins (Patton, 1996; Baginski et al., 2011). Whilst the lungs show higher systemic bioavailabilities for macromolecules than any other non-invasive route of delivery i.e.,oral and nasal, small natural peptides still suffer from high enzymatic degradation, whereas peptide hydrolysis decreases or is even absent with increasing molecular weight (Patton, 1996; Kwok and Chan, 2006).

Peptide and protein therapeutics requires an accurate dose consistency, physico-chemical stability as well as a constant and efficient deposition in the respiratory tract (Irngartinger et al., 2004). The biological activity of peptides and proteins is strongly dependent on their molecular structure. Biochemical or physical alterations in the protein structure may lead to a change or loss of biological activity. Physical degradation refers to changes in the non-covalent interactions within or between peptide/protein molecules. It can occur independently or via biochemical degradation, and results in alterations to the higher order structures (secondary and above). Common types of physical degradation include denaturation, aggregation, precipitation and adsorption (Kwok and Chan, 2006; Creighton, 2010). The risks of biochemical and physical degradation depend on many physicochemical factors, such as temperature, pH, storage humidity, formulation constituents, delivery device and manufacturing process, amongst others. These must be well studied and controlled to maintain the stability and efficacy of protein products (Kwok and Chan, 2006).

Formulation of protein powders for pulmonary delivery is especially challenging as it requires not only that the powders can flow and disperse, but also stability of the proteins. The success of the final product is also dependant on the resistance of peptides and proteins to the manufacturing process.

1.2 SPRAY DRYING

Spray drying is a commonly used technique which may be employed to produce powders of fine particle size for dry powder inhalers (Masters, 2002). Spray drying is utilised extensively in food products, cosmetics, active pharmaceutical ingredient (API) production and pharmaceutical formulations. The process consists of the atomisation of a feed solution into droplets that dry rapidly because of their high surface area and intimate contact with the drying gas. Dried powder is protected from overheating by rapid removal from the drying zone. The final product can be removed from the air stream by cyclones and/or filters (Masters, 2002). Additionally, spray drying has the advantages of: being a continuous process that it is easy to scale up; controlling the physical properties of the resulting product by the manipulation of the process parameters and selection of equipment; quick drying suitable for heat-sensitive products such as peptides, proteins and enzymes; being a cost-effective process, with possibility of full automation (Celik and Wendell, 2010). However, as with any other process, spray drying also presents limitations: has poor thermal efficiency at low inlet temperatures and the exhaust air stream contains heat requiring heat exchange equipment to remove it (Celik and Wendell, 2010).

A spray drying process consists of four steps: (a) atomisation of feed solution into a spray; (b) spray-air contact involving flow and mixing; (c) drying of sprayed droplets at elevated temperatures; and (d) separation of dried product from the air (Chow et al., 2007).

(a) Atomisation

Formation of the atomized spray requires the application of a force. Several types of driving force can be employed: centrifugal, kinetic, pressure and ultrasonic energy, which are selected depending on the required droplet size (Masters, 2002). A bigger emphasis will be given to kinetic nozzles such as the two fluid nozzle.

Centrifugal atomizers utilize either a rotating disk or wheel to disintegrate the liquid stream into droplets (Masters, 1991). These devices form a low-pressure system, and a wide variety of spray characteristics can be obtained for a given product through combinations of feed rate, atomizer speed, and atomizer design. The droplet size distribution is fairly narrow for a given method and process conditions but the mean droplet size can be varied from as small as 15 μm to as large as 250 μm, depending on the amount of energy transmitted to the liquid (Celik and Wendell, 2010).

Kinetic energy nozzles apply kinetic energy in the form of two-fluid or pneumatic atomisation. Atomisation is accomplished by impacting the liquid feed with high-velocity air, which results in

high frictional forces that cause the feed to disintegrate into droplets. To achieve optimal frictional conditions, this high relative velocity between liquid and air can be achieved by either expanding the air to sonic velocities or destabilising the thin liquid film by rotating it within the nozzle prior to spray-air contact. The main advantage of this type of atomisation is that the liquid is relatively low velocity as it exist the nozzle; therefore, the droplets require a shorter flight path for drying (Masters, 2002; Celik and Wendell, 2010).

There are several two-fluid nozzle designs: external mixing nozzle in which the liquid and air come into contact outside the nozzle; internal mixing design with the air and liquid contacting within the nozzle head; a pneumatic cup design, with liquid-air contact occurring at the rim of a rotating nozzle head (Celik and Wendell, 2010).

In general, two-fluid nozzles are capable of producing small droplet sizes over a wide range of feed rates. These droplets are then carried away from the nozzle by momentum of the spray and the expanding atomizing air. The most important variable involved in the control of droplet size is the mass ratio of airflow to feed rate (ALR –air to liquid ratio). An increase in this ratio causes a decrease in droplet size. This ratio generally ranges from 0.1 to 10. At ratios approaching 0.1, atomisation is difficult even for low-viscosity feeds while a ratio of 10 approaches the limit above which atomisation occurs using excess energy without an appreciable decrease in particle size (Masters, 1991).

Sprays formed by two-fluid nozzles are symmetrical with respect to the nozzle axis and have a cone-shaped pattern. In general, an increase in air pressure will increase the spray angle if the feed rate is maintained at a constant level as long as the maximal angle has not been obtained. Spray angle is maintained if an increase in airflow is accompanied by an increase in feed rate resulting in a similar air-to-feed ratio.

Another type of kinetic nozzle is the three-fluid nozzle. The spray characteristics obtained by two- and three-fuid nozzles are similar when atomizing low-viscosity feeds at up to intermediate feed rates. Use of a second air stream with three-fluid nozzles causes a waste of energy, except for high feed rates of low-viscosity feeds (Celik and Wendell, 2010).

Pressure nozzles apply hydraulic pressure. The feed liquid is pressurised by a pump and forced through a nozzle orifice as a high-speed film that readily disintegrates into fine droplets. The feed is made to rotate within the nozzle, resulting in a cone-shaped spray pattern emerging from the nozzle orifice. The differential pressure across the orifice determines the droplet diameter.

Pressure nozzles are generally used to form coarse spray-dried particles (120 to 300 μm) with good flow properties (Celik and Wendell, 2010).

Sonic energy atomizers are not commonly used. As the name indicates, sonic energy and vibrations are used to produce droplets. The advantages of these nozzles resides in the operation at low pressures and having a wide flow channels suggesting their suitability for abrasive and corrosive materials (Masters,1991).

The function of any atomizer is to produce as homogeneous a spray as possible. The nature of the feed (surface tension, viscosity, density, etc), the characteristics of the spray, and the desired properties of the resulting dried product play a very important role in the selection of the atomizer (Celik and Wendell, 2010).

(b) Spray-air contact

Spray-air contact is determined by the position of the atomizer in relation to the air inlet. Inlet air is introduced to the drying chamber via an air disperser and heated to the desired temperature. Spray droplet movement is classified according to the dryer chamber layout and can be designated as cocurrent, countercurrent or mixed flow (Masters, 1991; Chow et al., 2007; Celik and Wendell, 2010).

Cocurrent flow is the configuration in which the spray and drying air pass through the dryer in the same direction. This arrangement is ideal for heat-sensitive products. Spray evaporation is rapid, the drying air cools as droplets are dried, and overall evaporation times are short. The particles are not subject to heat degradation (Büchi, 2009; Masters, 1991; Celik and Wendell, 2010).

Countercurrent flow is the configuration in which the spray and air enter at the opposite ends of the dryer. This arrangement has excellent heat utilisation. It is well suited for non-heat-sensitive materials degradation (Büchi, 2009; Masters, 1991; Celik and Wendell, 2010).

Mixed flow is the configuration in which both co- and countercurrent flows are incorporated. The advantage of this type of arrangement is that coarse free-flowing products can be produced in relatively small drying chambers. In this system particles are subject to higher particle temperature degradation (Büchi, 2009; Masters, 1991; Celik and Wendell, 2010).

(c) Droplet drying

When droplets of the spray come into contact with the drying air, evaporation takes place from the saturated vapour film which is quickly established at the droplet surface. Due to the high specific surface area and the existing temperature and moisture gradients, an intense heat and mass transfer results in efficient drying. The evaporation leads to a cooling of the droplet and thus to a small thermal load. The drying chamber design and air flow rate provide a short droplet residence time (<10 miliseconds) in the chamber, so that the desired droplet moisture removal is completed and product removed from the dryer before product temperatures can rise to the outlet drying air temperature. Hence, there is little likelihood of heat damage to the product (Büchi, 2009; Celik and Wendell, 2010).

Drying of a spray droplet has been divided into two phases. In the first phase (constant rate period), the rate of evaporation is constant and the liquid feed temperature increases rapidly to the wet bulb temperature (T_{wb}) (lowest temperature attained by the surface of the droplets during evaporation and is dependent upon the evaporative cooling effect). As the relative humidity in the inlet air stream is decreased, drying rate increases, evaporative cooling increases and T_{wb} decreases. The temperature of the interior of the droplet is usually 10–15 °C lower than T_{wb}. Dissolved solute is transported via diffusion and convection to the droplet surface. This phase lasts until a solid phase (crust) begins to form at the surface of the droplet. At this point, solute concentration at the surface has reached a critical solute concentration (C_{crit}) that depends on the solubility of the solute at T_{wb} (S_{wb}). At C_{crit}, diffusion of the solvent through this barrier is slower than the heat transfer, and the system enters the second phase of drying. Drying and evaporation rate decline in the second phase (falling rate phase) and particle size does not undergo further reduction. The temperature of the particle will rise until it equals the dry bulb temperature of air (T_{db}), concurrently the temperature of the particle interior will rise to T_{db} (temperature of the surface of the dried particles after evaporation of most of the water, and is usually close to T_{outlet}). The particle remains at the drying-air outlet temperature before collection (Vehring et al., 2007; Abdul-Fattah et al., 2007).

(d) Separation

Powder separation from the drying air follows the drying stage. In principal, two systems are used to separate the product from the drying medium: (1) primary separation of the drying product takes place at the base of the drying chamber; (2) total recovery of the dried product in the separation equipment. The most common separation equipment is the cyclone. Based on

inertial forces, the particles are separated to the cyclone wall as a down-going strain and removed. Other systems are electrostatic precipitators, textile (bag) filters or wet collectors like scrubbers (Büchi, 2009; Masters, 1991; Celik and Wendell, 2010). The system can be further modified for better product recovery and larger production scale, particularly for thermolabile materials such as proteins and peptides. For instance, by replacing the bag-filter unit with a vacuum system, the drying airflow resistance can be reduced, thus allowing the protein product to be dried at a lower inlet air temperature. Design of high-efficiency cyclone separation is also essential for this technology to be economically acceptable on an industrial scale (Chow et al., 2007).

1.2.1 Particle morphology

Previously it was discussed that when the droplet enters in contact with the drying air, solute starts to concentrate at the droplet surface until a crust is formed. The thickness of the crust is dependent on the drying velocity, with high rates resulting in large particles with a thin shell and low density, whereas a low drying velocity produces small particles with a thick shell and high density (Masters, 2002). Depending on the nature of the component, different solidification mechanisms are triggered once the critical solute concentration is reached. The resulting particles can have a range of different morphologies, depending on their size and the properties of their shells in the final stages of the drying process. Solid hollow spheres can be formed, if the shell becomes rigid quickly and does not buckle or fold. Otherwise, dimpled or wrinkled particles are formed (Vehring, 2007). Porous particles can also be formed, examples have already been reported in section 1.1.1.2. Healy et al., 2008, Ní Ógáin et al., 2008 and Paluch et al., 2012 have described the formation of the nanoporous/nanoparticulate microparticles, which are also presented in this thesis. NPMPs formation is postulated as follows: during the atomisation stage of the spray-drying process, droplets are formed containing the solute (excipient or drug or both) in the co-solvent mix; rapid drying of these droplets proceeds on contact with the warm drying gas and the more volatile solvent phase in which the solute is more soluble, evaporates to a greater extent, resulting in the droplet becoming richer in the less volatile solvent component, in which the solute is less soluble. The fall in the solubility of the solute may be dramatic and it may condense out initially as a nanosized liquid phase within the droplet. As drying proceeds and further solvent loss occurs, the solute phase droplets become less fluid and come closer together, and the solute may precipitate out as primary nanoparticles which agglomerate together either at the particle surface (forming an outer shell) or within the particle,leading to

nanoparticulate microparticle formation (Healy et al., 2008; Nolan et al., 2009; Ní Ógáin et al., 2010; Paluch et al., 2012).

Paluch et al. (2012) have recently reported a novel morphology classification system (MCS) using four simple descriptors such as shape, surface properties, visual morphology and interior of the particle. This was used to classify the particles presented in this thesis. The developed MCS system introduced a code for shape description: 1 for predominantly spherical and 2 for irregular/non-spherical. A second symbol indicating the surface description: A for smooth surface particle and B for crumpled particles. A third symbol to describe the class of visual morphology with three different variants: I nonporous, II porous with nano-sized pores, and III conglomerates of nanoparticles. A last symbol described the interior of the particles and it is possible to distinguish: α for solid/continuous, β for hollow, γ for unknown, and δ for hollow with nanoparticulate content (Paluch et al., 2012).

1.2.2 Peptide and protein stabilisation during spray drying

Spray drying can cause physical degradation of peptides and proteins conformational changes, aggregation, denaturation and adsorption to surfaces (Lai and Topp, 1999). Dry powders resulting from processing are usually sensitive to moisture, the main cause of chemical instability of peptides and proteins in the solid state (Maa et al., 1998; Lai and Topp, 1999). Hence, it is necessary to process these macromolecules with care to maintain their physical stability as well as provide protection from moisture. To satisfy these requirements, peptides and proteins are usually formulated as amorphous glasses.

The glassy preparation derives its stabilising properties from its high viscosity. The principle is to add a glass-forming excipient typically a carbohydrate, polymer or organic salts among others, to a solution of the pharmaceutically active material and to dry this solution under conditions that result in the formation of an amorphous glassy matrix in which the pharmaceutically active material is protected from degradation (Hatley and Blair, 1999; Telko and Hickey, 2005). Franks et al. (1991) described a possible mechanism of glassy immobilisation for protection of proteins: the formation of an amorphous glass during drying, provides a rigid matrix around the protein molecules to restrict and stabilise their motion. Carpenter and Crowe (1988, 1989) suggested the water replacement theory to explain the protective action of the sugar compounds, where the formation of H-bonding between the excipient and the biomolecule occurs when water is removed, maintaining the structural integrity of the peptide/protein. The mobility restriction and H-bonding provided by the glass forming excipient is thought to reduce the peptide and protein reactivity. However the amorphous state is sensitive to temperature and moisture. A

raise in temperature and in moisture will provide the molecular mobility for molecules to revert back to the crystalline state and protection of protein is lost (Lai and Topp, 1999; Hatley and Blair, 1999). Another concern in terms of use of amorphous powders for pulmonary delivery is their high surface area due to the reduced particle size, resulting in rapid moisture uptake. Water acts as a plasticiser to lower the glass transition temperature (T_g) (temperature at which the glassy state transits to rubbery state due to the onset of long range coordinated molecular motion)(approx. 10°C reduction per 1% water in sugar-containing formulations), which will enhance molecular mobility required for nucleation if the T_g approaches the storage temperature. It is thus important to keep the powder dry in order to maintain the high T_g, or to use excipients with a high T_g, or to store the powders at a low temperature (Kwok and Chan, 2006).

Chan et al. (2004) studied the aggregation of salmon calcitonin (sCT) when co-spray dried with mannitol and stored at different relative humidities (RH). sCT was amorphous and resistant to processing; powders were stable when stored at low RH (<30%); aggregation levels were found to be reduced in formulations with 30% mannitol (amorphous) which was opposite to formulations with 70% mannitol (crystalline) that presented high levels of agglomeration. The agglomeration of sCT is known to impair its bioactivity.

Spite of the high energetic level of the amorphous state, the use of glass forming excipients in peptides and protein formulations has been widely used, proving to be the best option.

1.2.3 Spray dryer instruments used in the presented studies

Three different spray dryers were used in the work presented in this thesis. Chapter 7 will focus on a comparison between powders produced using these spray dryers. The scale-up process involves the design of a spray dryer so that it operates at the specified capacity and produces a powder that meets the product specification resulting from earlier process development (Masters, 2002). The major difficulties in scaling-up the spray drying process include the thermal exchange and losses, variable yields and, mostly, differing geometries of atomisers or turbines, drying chambers and cyclones (Raffin et al., 2006). As a result, industrial design is largely based on intuition and practical experience (Zlokarnik 2002). When scaling-up a spray drying process, several areas have to be analysed, as the overall drying process is composed of the following steps: i) atomisation, ii) mixing of droplets and drying gas, iii) drying (drying kinetics and residence time) and iv) separation (Thybo et al., 2008). Scale-up from a pilot to a production scale spray dryer will often require the use of a larger dimensions atomizer, making atomisation a very important step in up-scaling (Thybo et al., 2008).

Raffin et al. (2006) have successfully produced pantoprazole-loaded microparticles by spray drying at the laboratory and pilot scale, using a two-fluid nozzle and co-current flow, with pilot scale resulting in an improvement of powders characteristics such as, morphology and specific surface area.

Thybo et al. (2008) attempted spray drying process scale-up from pilot to production scale using an atomized droplet size criterion. It was reported that the criterion does not account for differences between droplet-drying gas mixing and residence time distribution within between the two spray dryers. Therefore, production scale experiments are required in order to obtain similar product characteristics as in pilot scale.

A study by Büchi (2008) on the scale-up from the Büchi Mini spray dryer B-290 to the Niro mobile Minor, reported extensively on a theoretical approach to predict the process parameters for the larger scale spray dryer. It was defined that the most important process conditions, to be kept constant in order to achieve the same particle size and residual solvent content in the produced powders were the outlet temperature, the droplet size and the outlet vapour concentration, must be kept constant in order to achieve the same particle size and residual solvent content in the produced powders.

Gil et al. (2010) proposed a scale-up method for spray drying processes consisting of two steps – a thermodynamic step and an atomisation and particle formation step. The thermodynamic step was based on maintaining the vapour concentration of the drying gas at a constant level, which was particularly important when producing amorphous materials since the residual solvent level in the solid strongly affects its glass transition temperature. The control of this parameter was based on prior knowledge attained from lab-scale work. Regarding atomisation and particle formation, droplet size and particle size estimation was based on experimental data of particle apparent density, droplet density and droplet average size fitted into a model equation allowing for an estimation of particle size. The approach is simple to use but requires prior knowledge on the product/drying behaviour.

During scale-up there is a great opportunity to improve powder properties, such as, greater ability to produce and dry larger droplets in the larger drying chambers of the commercial units, which is an advantage if the purpose is to obtain large and denser particles for solid oral dosage forms. In the case of particles for inhalation, however, the scale-up challenge is to keep particle properties unchanged. The main characteristics and mode of operation of each spray dryer are hence presented in this section.

(a) **Büchi Mini spray dryer B-290**

A Büchi Mini spray dryer B-290 was used for the majority of studies (chapter 3, 4, 5 and 6); it is a laboratory scale spray dryer with the feasibility of spray drying aqueous and organic solutions with very short set-up times, an effective integrated nozzle cleaning mechanism and a high degree of flexibility due to the availability of different cylinder (drying chamber) geometries designed to cater for different types of solutions to be spray dried (Figure 1.3). The two versions have the intent to optimise the yield depending on the process. For work involving organic solvents a cylinder with vertical outlet geometry is recommended (Figure 1.4) (Büchi, 2009).

The standard method of operation for the Mini Spray Dryer B-290 is in a suction mode with a two-fluid nozzle and with an air and solution set–up in co-current mode. The reduced-pressure environment within the system prevents any possible contamination in the case of leakage. The nozzle may also be thermostatically controlled by use of a cooling system (Büchi, 2009).

Pharmaceutical applications of spray drying the feed solution may be prepared by dissolving or suspending the materials (drug and excipients) in water, organic solvents or combinations of water and organic solvents or organic solvents mixtures. Although evaporating organic solvents by spray drying process is very efficient because of the resulting shorter residence time, when compared with the evaporation of water, the risk of explosion makes the use of air as drying gas very hazardous. Therefore, an inert gas, usually nitrogen, replaces air as the process drying gas. When nitrogen is the drying gas, there is the need to work in a closed-mode, where the gas is recycled (moisture removed) and reused. When using air, the process operates in an open-mode with release of the exhaust to the atmosphere (Celik and Wendell, 2010). The open-mode operates under vacuum (sucking mode) as a standard. However, if the exhaust is aggressive and could lead to a corrosion of the aspirator, the instrument can also be driven without vacuum (blowing mode). The closed cycle is operated in a sucking mode.

The inert loop B-295 (condenser) is required to safely spray dry inflammable solvents; an operating principle uses a combination of the spray dryer B-290 and the inert loop B-295 to provide a closed loop circulation under inert conditions. The absence of oxygen prevents the formation of a ignitable mixture. At the same time, the solvent contained in the gas stream is cooled and consequently condensed. The regenerated flow is then returned again to the spray dryer – operation in closed mode. The dehumidifier B-296 is also used when spray drying in the closed mode to remove water content from the drying gas (Büchi, 2009).

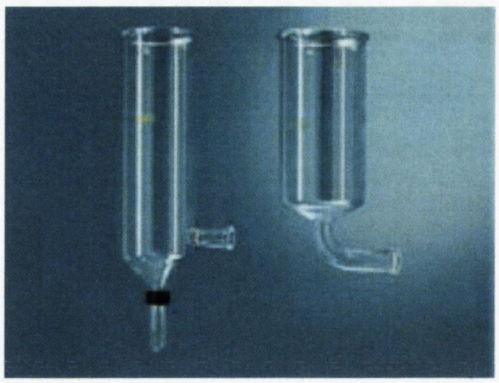

Figure 1.3 Geometries of drying chamber (left) lateral outlet and (right) vertical outlet (Büchi, 2009).

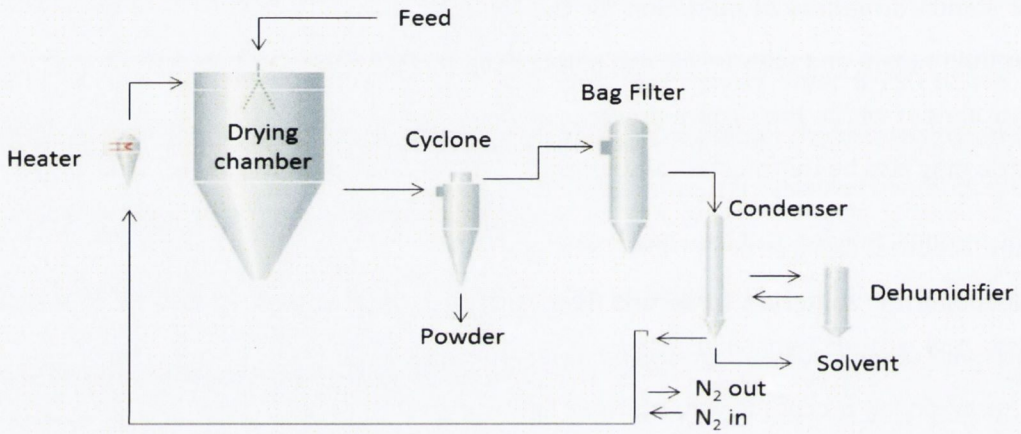

Figure 1.4 Schematic illustration of Büchi Mini spray dryer B-290 set-up.

(b) **GEA Niro S/A SDMicro**

The SDMicro™ is a fully functional spray drying plant at the laboratory scale. This spray dryer was design to retain the same air flow pattern as a full scale production model. It operates in blow mode with a two-fluid nozzle and with an air and solution set–up in co-current mode. The resulting equipment can make test volumes of product at the smallest possible scale (100-200 ml). The intrinsically safe operation makes the SDMicro™ suitable for use with nitrogen for products dissolved in organic solvents, without the requirement of an inert-loop as is the case for the Büchi B-290 Mini spray dryer. Compressed air is used for drying of aqueous fluids. The cyclone is used for the initial powder collection and the bag filter collects fine particles passing through the cyclone. The cyclone may be by-passed completely for collecting very fine powders in the bag filter (GEA Niro, 2012). This instrument operates in a blow mode contrary to the Büchi B-290 Mini spray dryer when using nitrogen as the drying gas.

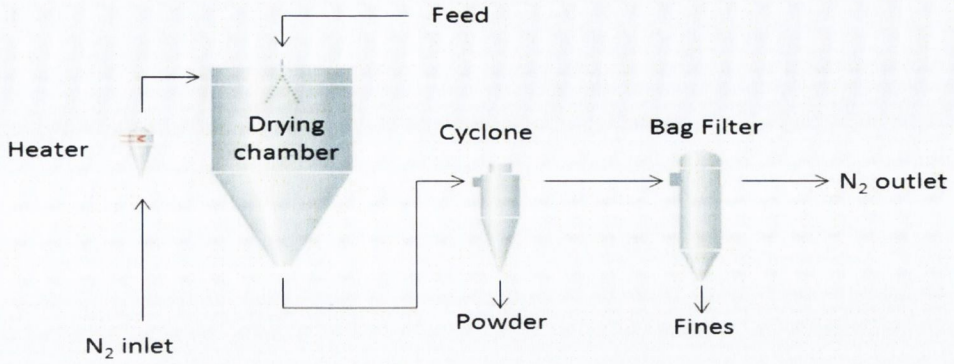

Figure 1.5 Schematic illustration of Niro A/S SDMicro spray dryer set-up.

(c) **GEA Niro Mobile Minor**

The Niro Mobile Minor is a pilot plant spray dryer. Small quantities of solutions, suspensions, and emulsions can be dried into representative powder samples. This spray dryer can be fitted with one of three alternative atomizing systems: rotary atomizer, co-current two-fluid nozzle; fountain two-fluid nozzle. The co-current two fluid nozzle was selected for our experiments; it is located in the centre of the chamber roof. The atomisation is created by compressed air at a pressure of 0.5-2.0 bar. The feed and atomizing gas are passed separately to the nozzle head where the atomisation takes place. The Mobile Minor permits a second point of entry of feed solution in the middle of the drying chamber, as well as the ability to operate in aseptic conditions and in a closed mode, when organic solvents are spray dried and nitrogen gas is used as the drying gas (GEA Niro, 2012).

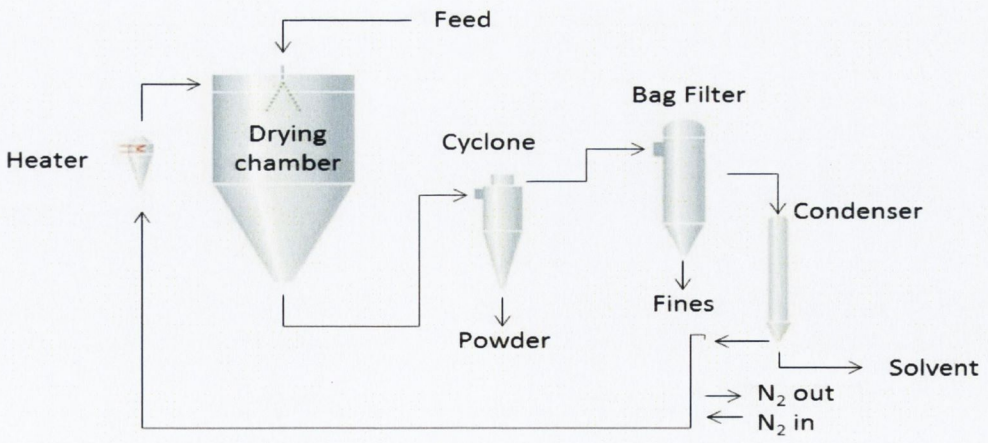

Figure 1.6 Schematic illustration of Niro Mobile Minor spray dryer set-up.

Table 1.2 resumes the technical features of the three spray dryers. All three spray dryers have different geometries and size, resulting in different load capacities (sample volume and drying

air). Operation with a two fluid nozzle and in co-current mode is possible in the three models. The pilot scale spray dryer presents a higher water evaporation capacity as well as the possibility to spray dry at higher temperatures. At the laboratory scale (Büchi Mini Spray dryer and Niro SDMicro) the spray drying is performed indifferent modes: closed versus open and, suction versus blowing. Such difference will impact on particle drying, since in the open mode the drying gas is constantly replaced, as in the closed mode the drying gas is recycled with removal of solvent and moisture content being dependent of auxiliary equipment as condensers and dehumidifiers.

Table 1.2 Technical features of the three spray drying instruments used in the presented studies. N/P – not published

Technical features	Mini Spray Dryer B-290	Niro SD Micro	Niro Mobile Minor
Water evaporation capacity	1.0 kg/h, higher for organic solvents	1.0 kg/h, higher for organic solvents	0.5-6.0 kg/h, higher for organic solvents
Sample volume	30 ml – 1 l	min 100 - 200 ml	100 ml – 10 l
Drying air flow rate	Up to 40 kg/h	Up to 30 kg/h	.80 kg/l at 200 °C
Atomisation flow rate for two-fluid nozzle	0.1 – 1.0 kg/h at 5-8 bar	6 kg/h at 0.5 bar	4 – 25 kg/h at 0.5 – 6.0 bar
Maximum inlet temperature	220 °C	200 °C	350 °C
Spray chamber size (diameter/cylindrical height)	165 mm/600 mm		800 mm/620 mm
Nozzle types	Two-fluid nozzle	Two –fluid nozzle	Rotary atomiser, two-fluid nozzle in co-current or fountain mode
Operating conditions	Open, optional cycle with inert-loop B-295, sucking mode	Open, blowing mode	Open, optional closed cycle with inert loop
Achieved particle size	2 -25 µm	N/P	2 - 80 µm

1.3. SALMON CALCITONIN

Calcitonin (CT) is a polypeptide hormone composed of 32 amino acids (aa) with an N-terminal disulfide bridge between positions 1 and 7 and a C-terminal proline amide residue (Motta et al., 1998); it is produced by the parafollicular cells of the thyroid gland in mammals and by the ultimobranchial gland of birds and fish. Secreted in response to increased serum calcium levels, it has a regulatory function in calcium-phosphorus metabolism, by moving the calcium from blood to bone, enhancing calcium deposition, inhibiting calcium resorption from bone, and decreasing urinary calcium excretion (Arbine and Drake, 1993; Patton, 2000). Osteoclast-mediated bone resorption is inhibited by CT through the regulation of both the number and activity of osteoclasts. Therefore, CT is a potent drug for various bone metabolism diseases such as Paget's disease, hypercalcemia and osteoporosis (Arbine and Drake, 1993; Patton, 2000). The signal transduction of CT to osteoclast is initiated by its binding to the CT receptor, which belongs to a subfamily of GTP-binding (G)-protein-coupled receptors, followed by activation of G-proteins. Activated G-proteins in turn induce the activation of adenylyl cyclase and phospholipase C to generate the intracellular second messenger molecules, cyclic adenosine 3P,5P-monophosphate (cAMP) and inositol phosphates (IPs) with, cAMP likely to be more important for the action of CT in osteoclasts (Katayama et al., 2001).

Calcitonin from five species – human, salmon, porcine, bovine and ovine – have been identified, and porcine, human and salmon calcitonin have been synthesised (Arbine and Drake, 1993; Patton, 2000). Salmon calcitonin (sCT) has the most similar structure to human calcitonin (hCT). It only differs in 16 aa, has the greatest biological activity, undergoes the least amount of degradation by serum factors, has the longest half-life; and shows the highest affinity for receptors in bones and kidneys (Patton, 2000).

Calcitonin is usually administered intravenously, intraperitoneally or subcutaneously. However a nasal formulation is also available, Miacalcin® (sCT formulation) by Sandoz Pharmaceuticals; it is commonly used in the treatment of Paget's disease with three daily administrations being as effective as injectable calcitonin (Patton, 2000; Bhandari et al. 2010).

Amphiphilic secondary structures have been shown to be important elements in the functional properties of many peptides and segments of larger proteins. Native salmon calcitonin appears to comprise a single α-helix from residue 8 to residue 23 (helix-breaking proline), and a hydrophilic random-coil segment from residue 23 to the carboxyl-terminal proline amide (Moe and Keiser, 1985). Epand and Epand (1986) studied the effect of conformational changes in sCT

native structure reporting that conformation flexibility is key to the peptide bioactivity and modification in the structure might also affect the peptide binding to receptors.

Patton (2000), Chan et al. (2004), Clark et al. (2008), Ní Ógáin (2008) have reported different formulations of sCT for pulmonary delivery, underpinning the need for stabilisation of the peptide in order to take advantage of its biological activity. These studies also showed the potential for systemic delivery of sCT via the lungs.

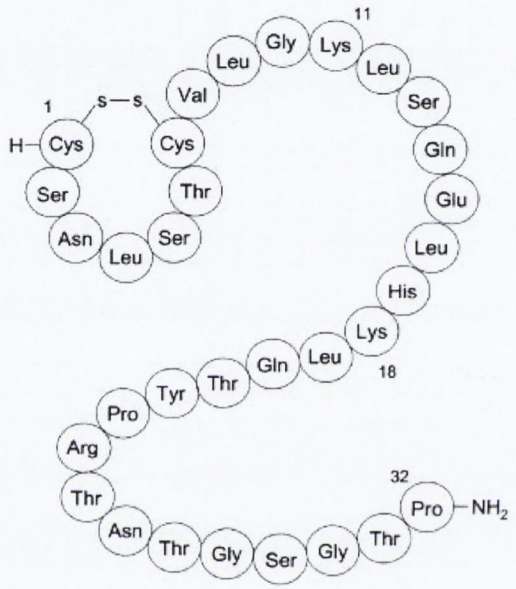

Figure 1.7 Amino acid sequence of salmon calcitonin (sCT). The N-terminus is stabilised by a disulfide bridge between Cys1 and Cys7, the C-terminus is naturally amidated.

1.4 BACKGROUND ON EXCIPIENTS USED

1.4.1 Raffinose (raffinose pentahydrate)

Raffinose is a naturally occurring trisaccharide isolated from a variety of plants including beet sugar molasses, cottonseed meal, and the seeds of various food legumes (Berman, 1970). Its chemical name is α-D-galactopyranosyl-(1→6)-α-D-glucopyranosyl (1→2)-α-D-fructofuranoside and it normally exist as the pentahydrate crystal with no known ability to exist as a stable unsolvated or anhydrous crystal, although it has been shown to form intermediates at lower hydrate level and to become amorphous upon desiccation by spray drying or heating to 80 or 100 °C (Bernan, 1970; Kajiwara et al., 1999; Hogan and Buckton, 2001; Bates et al., 2007; Charmathy et al., 2010). Three water molecules have been reported to locate in a tunnel of the raffinose structure, while two other water molecules are situated outside the tunnel. The hydrogen bonding between water molecules and raffinose in the molecular structure is complex

(Jeffrey and Huang, 1990; Cheng and Lin, 2005). Cheng and Lin (2005) reported thermogram results from DSC indicating that three endothermic peaks at 56, 73 and 85 °C were observed, likely corresponding to the loss of the first, second, and remaining molecules of water, respectively, which corresponded to a total weight loss during TGA analysis of ~ 15%, almost equal to the loss of 5 mol of water from raffinose pentahydrate.

The amorphous form of raffinose (T_g ~116 °C) is of interest because of its ability to protect proteins and related pharmaceutical materials subjected to lyophilisation and spray drying (Kajiwara et al., 1999; Davidson and Sun, 2001; Ní Ógáin, 2008; Charmathy et al., 2010). The ability of raffinose to maintain the integrity of materials during these processes is attributed to its hydrogen bonding properties and its tendency to form a highly viscous glass (Kajiwara et al., 1999; Davidson and Sun, 2001; Charmathy et al., 2010).

Studies by Foster et al. (1996) determined the extent of thermally-induced aggregation in low molecular weight urokinase in the presence of raffinose among other sugars, concluding that sugars were effective, concentration-dependent, inhibitors of aggregation. Fisher et al. (2001) showed raffinose exerted a cytoprotective effect on pulmonary grafts during preservation; Ní Ógaín et al. (2010) have proven the protective action of raffinose on lysozyme in microparticles produced for pulmonary delivery.

Table 1.3 Raffinose pentahydrate molecular structure, formula and weight, and its solubility.

Molecular structure	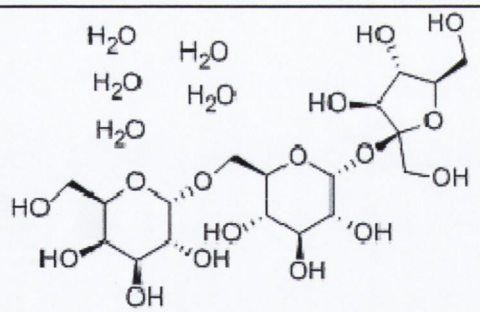
Molecular formula	$C_{12}H_{32}O_{16}.5H_2O$
Molecular weight (g.mol^{-1})	594.51
Solubility	soluble in water (10g/100g H_2O at 20 °C)

1.4.2 Trehalose (trehalose dihydrate)

Trehalose, also known as α-D-glucopyranosyl-(1-1)-α-D-glucopyranoside, is a disaccharide of glucose. Due to the linkage of the two glucopyranose rings occurring at the reducing end of the glycosyl residues (α-carbons), trehalose is a non-reducing sugar and the glycosidic bond is not cleaved by α-glycosidase (Higasiyama, T., 2002; Césaro et al., 2008; Ohtake and Wang, 2011). It is widely distributed in nature (plants, fungi, etc), protecting organisms against various stresses, such as dryness, freezing, and osmopressure (by stabilisation of membranes) (Higasiyama, T., 2002; Ohtake and Wang, 2011).

Trehalose is commonly found in the dihydrate form which is charactersed by its low hygroscopicity, even when exposed to 92% relative humidity (Ohtake and Wang, 2011). The dehydration of the dihydrate crystal occurs at 97 °C and the anhydrous crystal melts at 210 °C (Sussich et al., 1998; Nagase et al., 2002; Sussich and Cesàro, 2008; Ohtake and Wang, 2011). Trehalose can be presented in three isomeric forms: α, α -, α, β- and β, β -trehalose, the only naturally occurring form is the α, α isomer (Césaro et al., 2008). The anhydrous form of trehalose presents three polymorphs: α, γ and β (Sussich et al., 1998; Sussich and Cesàro, 2008; Ohtake and Wang, 2011). The melting points of these forms are, respectively: 126°C, 118-122 °C and 210-215 °C (Césaro et al., 2008). During various desiccation processes, including freeze and spray drying, trehalose readily dries as an amorphous material with a high glass transition temperature (T_g ~120 °C) (Sussich et al., 1998; Nagase et al., 2002; Sussich and Cesàro, 2008; Ohtake and Wang, 2011).

Trehalose has been used to stabilise simple systems, such as lipids and proteins, as well as more complex biologicals, including viruses, bacteria, and tissues. This ability has been attributed to the fact that it can sorb water and crystallise and phase separate from the protein/peptide, thus acting as a desiccant removing large amounts of water that may otherwise result in detrimental crystallisation of the protein/peptide itself (Moran and Buckton, 2007). Studies by Lopéz-Diéz et al. (2004), Maury et al. (2005), Yoshii et al. (2008) and Ní Ógáin et al. (2011) among others have established the protective action of trehalose on protein integrity, avoiding loss of bioactivity.
Trehalose is more commonly used than raffinose. Trehalose production was initially by yeast extraction which presented a high cost. However, Higashiyama (2002) reported a novel process of trehalose production: starch is liquefied by a thermostable α-amylase and is debranched by isoamylase, with the formed amylose being converted into trehalose by the two enzymes, MTSase and MTHase. By this process, the production cost of trehalose was reduced to approximately one hundredth of its initial cost. Raffinose on the other hand, is still directly

extracted from its natural sources (soybeans, beet, sugar molasses, etc), existing in a concentration range between 0.3% and 6% of fresh weight, requiring large quantities (167-334 kg) to produce 1 kg of raffinose, presenting the process high cost (Mussato and Mancilha, 2007).

Table 1.4 Trehalose dihydrate molecular structure, formula and weight, and its solubility.

Molecular structure	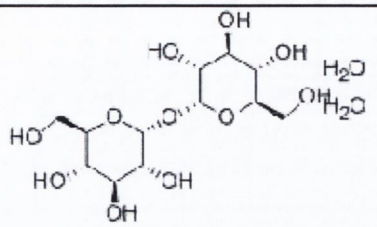
Molecular formula	$C_{12}H_{22}O_{11}.2H_2O$
Molecular weight ($g.mol^{-1}$)	378.33
Solubility	Trehalose is freely soluble in water (40.6-69g/100g H_2O at 20°C), practically insoluble in ethanol and slightly soluble in methanol

1.4.3 Hydroxypropyl-β-cyclodextrin

Cyclodextrins (CD) are cyclic (α-1,4)-linked oligosaccharides of α-D-glucopyranose, obtained by enzymatic degradation of starch, containing a relatively hydrophobic central cavity and hydrophilic outer surface. Owing to back of free rotation about the bonds connecting the glucopyranose units, the cyclodextrins are not perfectly cylindrical molecules but are toroidal or cone shaped. Based on this architecture, the primary hydroxyl groups are located on the narrow side of the torus while the secondary hydroxyl groups are localised on the wider edge (Figure 1.7) (Loftsson and Brewster, 1996). Therefore, CDs have hydrophilic cavity exteriors (hydroxyl groups – polar) and hydrophobic cavity interiors (apolar). The α-cyclodextrin (αCD) comprises six glucopyranose units, the β-cyclodextrin (βCD) seven, and the γ-cyclodextrin (γCD) eight units. For pharmaceutical purposes numerous derivatives have been prepared by etherification or the introduction of other functional groups at the 2-, 3- and 6-hydroxyl groups of the glucose residues. These changes improve solubility and prevent crystallisation giving rise to an amorphous product. One of the most studied derivatives is the hydroxypropyl-β-cyclodextrin (HPβCD) produced by replacement of βCD hydroxyl groups by hydroxypropyl ones, resulting in amorphous form (Loftsson and Brewster, 1996; Muňoz-Ruiz and Paronen, 1997; Davis and Brewsrter, 2004).

One property that characterises cyclodextrines is their ability to form inclusion complexes with hydrophobic molecules. A dynamic equilibrium between free CDs, free drug molecules and their

formed inclusion complexes is established if drug molecules are of sufficient size and have appropriate properties for the formation of inclusion complexes. The formation of inclusion complexes is possible with the entire drug molecule or only a portion of it (Davis and Brewster, 2004). By forming the inclusion complex with the cyclodextrin the drug solubility can be greatly enhanced (e.g., hydrocortisone solubility in water is 33 times greater when complexated with HPβCD), as well as drug stability, with the cyclodextrin acting as a shield against degradation agents shuch as enzymes (Loftsson and Brewster, 1996).

Cyclodextrins can be used to achieve the following: enhance solubility, enhance bioavailability by increasing drug molecules permeability, enhance stability by complex formation or by increasing a system thermal stability (increasing glass transition temperature), convert liquids and oils to free-flowing powders, reduce evaporation and stabilize flavours, reduce odours and tastes, reduce haemolysis, prevent admixture incompatibilities (Shao et al., 1992; Loftsson and Brewster, 1996; Davis and Brewster, 2004).

Muňoz-Ruiz and Paronen (1997) studied the physical characteristics (particle size, morphology, thermal behaviour and water activity) of different cyclodextrins. HPβCD was found to be constituted by spherical particles (by SEM) with an average particle size ~10 μm; powder residual moisture was 4.75% with complete removal when exposed to 160 °C; DSC measurements only showed a broad endotherm between 20 and 130 °C that was attributed to water loss. HPβCD has been reported to have an aqueous solubility of 60% (w/w) (Loftsson and Brewster, 1996; Davis and Brewster, 2004).

Branchu et al. (1999) tested the use of sucrose and HPβCD as stabilising excipients in the spray-drying of a model protein, β-galactosidase. Spray-drying significantly inactivated the enzyme; when spray drying in the presence of sucrose inactivation still occured. However, after spray drying β-galactosidase in the presence of HPβCD, or HPβCD and sucrose, full catalytic activity was exhibited on reconstitution. Furthermore, the reconstituted product was unchanged in terms of molecular weight, charge, and thermal stability.

Sigurjónsdóttir et al. (1999) studied the application of HPβCD as a potential stabiliser of salmon calcitonin (sCT) in aqueous solutions. The cyclodextrin was found to prevent sCT aggregation in solution and 54-75% inhibition of tryptic enzymatic degradation. It should be noted that trypsin is present in the lung lining fluid; these studies suggest a potential use of HPβCD to prevent sCT degradation in the lung fluid.

Ungaro et al. (2006) prepared large porous particles containing cyclodextrin for the sustained release of insulin in the lungs. Large porous particles made of poly(lactic-co-glycolic acid) (PLGA) were produced by the double emulsion-solvent evaporation technique. Hydroxypropyl-β-cyclodextrin was tested as excipient to optimise the aerodynamic behaviour of the microparticles. A controlled release of insulin and HPβCD from the system can be achieved by selecting appropriate ratio of components. HPβCD-containing large porous particles had flow properties and dimensions suitable for aerosolisation and deposition in deep regions of the lung following inhalation, and thus a potential system for protein pulmonary delivery developed.

The aforementioned studies clearly demonstrated that HPβCD can be useful stabilising excipient in the preparation of spray-dried peptide and protein pharmaceuticals.

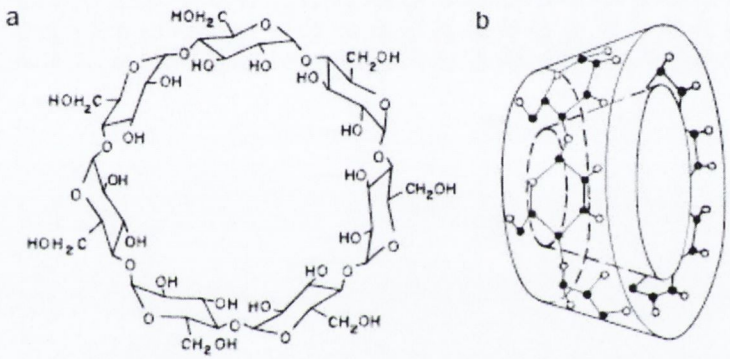

Figure 1.7 a) the chemical structure and (b) the toroidal shape of the *β*-cyclodextrin molecule (Loftsson and Brewster, 1996).

CHAPTER 2

MATERIALS AND METHODS

2.1 MATERIALS

Name	Supplier	Product number	Lot
Acetonitrile > 99.9% HPLC grade	Fisher Scientific, Ireland	A/0626/17	-
Atipamezole hydrochloride solution (Antisedan)	Pfizer, Ireland	-	-
n-Butyl acetate >99%, extra pure	Merck, Germany Sigma-Aldrich	10974 402842	- -
Calcitonin (Salmon) Ph.Eur. (as Calcitonin acetate; 5128, 1 IU/mg)	Polypeptide Laboratories, Sweden	-	108112-01
Compressed air	Jun Air LTD, UK	-	-
Coumarin-6, laser grade	Polysciences, Inc, USA	8037L	543680
Ethanol	Lab Scan Analytical Sciences, Ireland	-	-
Ethyl acetate >99.8%, GC grade	Fluka, Germany	45758	1320047
Foetal bovine serum	Sigma-Aldrich, Ireland	F7524	-
Forskolin	Sigma-Aldrich, Ireland	F6886	109K5057
L-Glutamine solution	Sigma-Aldrich, Ireland	G7513	-
Hydrogen gas	BOC, Ireland	-	-
Helium gas	BOC, Ireland	-	-
Hydroxy-propyl-β-cyclodextrin	Aldrich, Ireland Janssen Biotech N.V., Belgium	33,260-7 30.222.55	S35156-516 07H-221/1
Insulin solution from bovine pancreas	Sigma, Ireland	I0516	118K8401
3-Isobutyl-1-methylxanthine	Sigma-Aldrich, Ireland	I7018	44708221
Ketamine (Vetalar)	Pfizer, Ireland	-	-
Medetomidine hydrochloride (Domitor)	Pfizer, Ireland	-	-
MEM Non-essential amino acid solution	Sigma-Aldrich, Ireland	M7145	RNBB4233
Methanol HPLC grade	Fisher Scientific	M/4056/17I	-
Methanol	Lab Scan Analytical Sciences, Ireland	-	-
Nitrogen gas	BOC, Ireland	-	-
Liquid nitrogen	BOC, Ireland	-	-
Penicillin-streptomycin solution stabilised	Sigma-Aldrich, Ireland	P4333	-
Phenol	Sigma-Aldrich, Ireland	P5566	1423856
Phosphate buffered saline	Sigma-Aldrich, Ireland	D8537	-
1-Propanol	Sigma-Aldrich, Ireland	82090	0001450449
Potassium bromide	Sigma-Aldrich, Ireland	9881	19H0757
Propyl acetate	Aldrich, Ireland	133108	STBB8727V
d-Raffinose pentahydrate	Sigma, Ireland	R0250	077K1842

			039K0016 080M0049V
RPMI-1640 Medium with 25 mM HEPES	Sigma-Aldrich, Ireland	R5886	-
Salmon calcitonin	AmbioPharm, Inc., USA	Api1184	RD010610
Sodium chloride	Merck, Germany	-	K26025300 905
Sulfuric acid 95-97%	Sigma-Aldrich, Ireland	07208	81230
d-(+)-Trehalose dihydrate	Sigma, Ireland	T9531	018K7350 058K7357 020M7023V
Trifluoroacetic acid	Riedel-de Haën, Germany Sigma-Aldrich, Ireland	34957 302031	7317A BCBC7950V
Trypsin-EDTA solution	Sigma-Aldrich, Ireland	T3924	-
Water, deionised	Purite Prestige Analyst HP, Purite Limited, Thames, UK	-	-

2.2 METHODS

2.2.1 Spray drying

Systems were spray dried as solutions using a Büchi Mini spray dryer B-290 operating in the closed mode with a high-performance cyclone and an inert loop B295 accessory (Büchi, Switzerland) or a GEA Niro SDMicro™ spray dryer (GEA Niro, Denmark). In both cases, nitrogen was used as the drying gas in a co-current mode.

Spray drying conditions are described in Appendix I.

The preparation of the systems to be spray dried was based on previous work by Ní Ógáin (2008): excipients and/or peptide, in appropriate concentration, were dissolved in a solvent composition of methanol and butyl acetate or propyl acetate. Solvent mixture ratios are described in Appendix I. Excipients were weighed, methanol was added first for complete dissolution of solute; butyl acetate was added after complete dissolution of the excipients. Peptide addition was prior to spray drying of the solution.

All samples were collected into amber glass jars with screw-top lids, which were then stored in a desiccator at 4°C.

Yields were calculated by dividing the powder quantity collected by the quantity introduced into the feed solution, giving the yield per cent by weight (%).

2.2.2 Scanning electron microscopy (SEM)

Particle morphology was visualised by field emission scanning electron microscopy. SEM micrographs of spray dried materials were made by means of a MiraTescan XMU (Czech Republic) or a Zeiss Ultraplus Thermal Field (Germany) microscope. Samples were fixed on aluminium stubs using double-sided adhesive tape and sputter-coated with gold. Visualisation was performed at 5 kV and photomicrographs were taken at different magnifications in more than one region of the sample.

2.2.3 X-ray powder diffraction (XRPD)

The solid state nature of powders was determined by X-ray powder diffraction measurements using a Rigaku miniFlex II desktop X-ray diffractometer (Japan) with Haskris (USA) WA1 cooling unit. The Rigaku miniFlex II Diffractometer consists of a vertical goniometer with a 1.25° dispersion slit, a 1.25° antiscatter slit and a 0.3 mm receiving slit. The Cu anode X-ray tube was

operated at 30 kV and 15 mA in combination with a Ni filter to give monochromatic Cu Kα X-rays. Measurements were taken from 5° to 40° on the two θ scale at a step size of 0.05°/s. A minimum of two analyses was performed.

2.2.4 Thermal analysis

2.2.4.1 Differential scanning calorimetry (DSC)

DSC scans were taken for all the raw materials and spray dried powders by means of a power compensated Mettler Toledo DSC 821^e (Switzerland) differential scanning calorimeter with a LabPlant RP-100 refrigerated cooling system. Nitrogen was used as the purge gas. Samples were loaded into 40 µL sealed aluminium pans with three vent holes and scanned over a temperature range of 25–200/300°C with a scanning rate of 10°C/min (Ní Ógáin et al., 2011). Weights of ~4 mg were tested. The DSC system was controlled by Mettler Toledo STAR^e software (version 6.10). The glass transition temperature was defined as the midpoint of the transition and the recrystallisation and melting points are reported as the onsets of the exo/endothermic processes. Presented results are the average of triplicate analyses

2.2.4.2 Thermogravimetric analysis (TGA)

Thermogravimetric analysis was used to determine the amount of residual solvent content (RSC) contained in samples after spray drying, as previously described (Ní Ógáin et al., 2011). All measurements were performed with a Mettler TG 50 (Switzerland) module linked to a Mettler MT5 balance. Sample sizes of ~4 mg were used. To avoid interference from moisture in the air, the sample chamber was purged with dry nitrogen at a flow rate of 25 ml/min. A temperature range of 25 – 200/300/350 °C was employed with a heating rate of 10 °C/min. The TGA system was controlled by Mettler Toledo STARe software (version 6.10) and the RSC was defined as the weight loss in TGA between 25 and 130 °C. Presented results are the average of triplicate analyses

2.2.5 Residual solvent content by gas chromatography with flame ionisation detector (GC-FID)

The residual solvent content of methanol and butyl acetate in the spray-dried samples was quantified by gas chromatography with flame ionization detection (GC-FID). A PerkinElmer Clarus® 500 with auto sampler and Supelco SPB-GC column (60 m x 0.25 mm x 0.5 µm, 35% phenyl, 65% dimethyl polysiloxane filling) (European Pharmacopoeia 7th Edition, 2012) was employed. Helium at 8 psi pressure was used as a carrier gas. The oven temperature was 50 °C

and the detector temperature was set to 325 °C. Samples were prepared by dissolving between 100 and 200 mg of the spray dried powder in 1 ml purified water. Both solvents were assayed based on individual calibration curves with internal standards of n-propanol and ethyl acetate respectively. The injection volume was 1.0 µl and the retention times were as follows: methanol: 3 min 57 s, n-propanol: 4 min 34 s, ethyl acetate: 5 min 0 s and butyl acetate: 12 min 50 s of the total 15 min method length. Solubility of butyl acetate and ethyl acetate was reported to be 0.7 g/100 ml and 8.3 g/10 0ml, respectively (Seidell, 2010); all working solutions were bellow these limits. Presented values are the average ± standard deviation of three measurements. This method complements TGA, with discrepancies attributed to moisture absorbed from atmosphere.

2.2.6 Particle size analysis

Particle size distributions of the spray-dried powders were determined using a Mastersizer 2000 laser diffraction instrument (Malvern Instruments, UK) with a dry powder sample dispersion accessory (Scirocco 2000). Pressure was set at 2 bar and a vibration feed rate of 50% was used in order to achieve an obscuration between 0.5 % and 6 %; refractive and absorption indexes were chosen appropriate for the material measured (Ní Ógáin, 2008). Samples were run at least in duplicate. Mastersizer 2000 software was used for data evaluation. The d_{50} reported is the geometric median particle size; the d_{10} and d_{90} are the particle diameters at 10 % and 90 % of the cumulative volume distribution, respectively. The span of the volume distribution, a measure of the width of the distribution relative to the median diameter, was calculated according to the following equation (Maa et al., 1997):

$$span = \frac{d_{90} - d_{10}}{d_{50}}$$

2.2.7 Density measurements

2.2.7.1 Bulk and tap density

Bulk density (bp) was determined by weighing the amount of powder required to occupy a 1 ml volume in a 1 ml graduated glass syringe (Lennox Laboratory supplies, Ireland); tap density (tp) was determined by vertically tapping this sample onto a level bench top surface from a height of 5 cm 100 times and calculating the ratio of the mass to the tapped volume of the sample. Each sample was measured in triplicate and density is expressed as an average ± standard deviation.

2.2.7.2 True density by helium pycnometry

True density was measured using a AccuPyc 1330 Pycnometer Micromeritics™ (USA) using helium (99.995 % purity) to determine the volume of the sample. A 1 cm^3 sample cup was used. The instrument was calibrated before analysis. Samples were dried for at least 12 h prior to analysis using a vacuum oven (Gallencamp, UK) operated at 25 °C and −600 mbar pressure. Each sample was analysed in triplicate; results are expressed as average ± standard deviation.

2.2.8 Specific surface area (SSA) analysis by Brunauer, Emmett, Teller (BET) method and porosity analysis by Barret, Joyner, Heyner (BJH), t-plot and Dubinin-Astakhov method

Specific surface area of spray dried powders was measured by gas adsorption using a Micromeritics Gemini VI surface area and pore size analyzer (Micromeritics, U.K.). Adsorption measurements were performed with nitrogen gas as the analytical (adsorptive) gas and helium as the reference gas for free space (physical volume that the gas occupies in the sample cell) measurements. Prior to analysis the samples were degassed under nitrogen gas, using a Micromeritics SmartPrep degasser for 12-24h at 25 °C to remove residual solvents that may have become physically adsorbed onto the surface (European Pharmacopoeia 7th Edition, 2012; Ní Ógáin et al., 2010). The evacuation conditions used in the analysis were as follows: rate of 500 mmHg/min, time 1 min. Equilibration time for adsorption was 10 seconds. The amounts of nitrogen gas adsorbed at a range of relative pressures (P/P_0): $0.05 < P/P_0 < 1$ were evaluated for micropore volume and area determination using t-plot and Dubinin-Astakhov models (Quantachrome, 2009). Adsorption data for relative pressures $0.05 < P/P_0 < 0.35$ were determined to calculate SSA by the BET equation (Gregg and Sing, 1982); and adsorption data for relative pressures $0.35< P/P_0 <1$ was used to calculate the pore size and pore size distribution using the BJH model (Quantachrome, 2009). Analyses were performed in duplicate for each sample and are expressed as average ± standard deviation.

2.2.9 *In vitro* aerosol deposition studies using the next generation impactor (NGI)

The *in vitro* aerosol deposition of the dry powders was evaluated using apparatus E of the European Pharmacopeia, a Next Generation Impactor (NGI, Copley Scientific Limited, Nottingham, UK) operated under pharmacopoeial conditions. The NGI is a cascade impactor with 7 stages to give five cut-off diameters in the 0.54-6.12 micron range at all flow rates between 30 and 100 l/min, and a micro-orifice collector (MOC) (Copley, 2010; European Pharmacopoeia, 2011). The air flow passes through the impactor in a saw tooth pattern with particle separation and sizing being achieved by successively increasing the velocity of the airstream as it passes

through each stage by forcing it through a series of nozzles containing progressively reducing jet sizes (Copley, 2010).

As previously described by Tewes et al. (2010), the flow rate was adjusted to achieve a pressure drop of 4 kPa in the powder inhaler (Handihaler®, Boehringher Ingelheim, Ingelheim, Germany) and the time of aspiration was adjusted to obtain a flow of 4 L. The dry powder inhaler was loaded with a no. 3 hard gelatin capsule loaded with 20 ± 2 mg of powder for each test. After dissolution in an appropriate volume of solvent, particle deposition in the device, the throat and the stages and the filter was determined by a suitable method (Table 2.1). Each test was repeated three times. The total amount of particles with aerodynamic diameters smaller than 5.0 µm was calculated by interpolation from the inverse of the standard normal cumulative mass distribution less than stated size cut-off against the natural logarithm of the cut-off diameter of the respective stages. This amount was considered as the fine particle fraction (FPF) (or respirable fraction) and expressed as a percentage of the emitted recovered dose (ED). The mass median aerodynamic diameter (MMAD) of the particles was determined from the same plot as the particle size corresponding to the 50 % point of the cumulative distribution, and the geometric standard deviation (GSD) as = $\sqrt{\frac{size\ X}{size\ Y}}$, where *X* is the particle size corresponding to the 84% point and size Y is the particle size corresponding 16 % point of the cumulative distribution (Bosquillon et al., 2001; European Pharmacopoeia 7th Edition, 2012). Presented values are expressed as average ± standard deviation.

Table 2.1 Methods of determination of deposited powder

Material	Collecting Solvent	Method of analysis
Trehalose **Raffinose** **T or R:sCT** **T:R:sCT**	H_2O	phenol-sulfuric acid colorimetric detection
HP-β-CD + coumarin-6 **R: HP-β-CD + coumarin-6** **T: HP-β-CD + coumarin-6**	80 % EtOH	Fluorescence detection: λ_{ex} = 485 nm λ_{em} = 520 nm

2.2.9.1 Phenol-sulfuric acid colorimetric detection

NGI deposition of all sugar powders with no inclusion of cyclodextrin were determined by the phenol-sulfuric acid colorimetric method in microplate format as previously described by Masuko et al. (2005). The sulfuric acid promotes the conversion of all non-reducing sugars to

reducing sugars; these form a complex with the phenol turning the solution into a yellow-orange solution the absorbance of which is measured by UV spectroscopy at 490 nm (Fournier, 2001). Absorbance measurements were carried out using a Fluostar optima microplate reader (BMG Labtech, Germany) using clear 96 well flat bottomed plates (Sarstedt, Inc., Germany). In each well was added 50 µl sample, 30 µl phenol 5% and 150 µl sulfuric acid 95-97%, followed by incubation for 5 min at 90 °C in a static water bath; the plate was subsequently cooled in a room temperature water bath before absorbance measurements were made (Masuko, 2005). All sample and standard measurements were carried out in duplicate/triplicate. Calibration curves were prepared in triplicate.

2.2.9.2 Fluorescence detection

For NGI analyses of cyclodextrin powders, a fluorescent dye coumarin-6 was incorporated at a low load (0.2 % by weight of excipient or excipient:API content) during spray-drying, to enable subsequent quantitation of powder as previously described by Ní Ógáin et al. (2011). Fluorescence measurements were carried out using a Fluostar optima microplate reader (BMG Labtech, Germany) using black 96 well flatbottomed plates (Sarstedt, Inc., Germany) and a 200 µl sample volume, with excitation and emission wavelengths as in Table 2.1. All sample and standard measurements were carried out in duplicate/triplicate. Calibration curves were prepared in triplicate, with the same spray-dried batch of powder and collecting solvent as used in the NGI analysis, and was either freshly prepared or checked simultaneously with each analysis.

2.2.10 Dynamic vapour sorption (DVS)

Vapour sorption by spray dried powders was investigated by means of an automated gravimetric vapour sorption analyser, DVS Advantage-1 (Surface Measurements Systems Ltd, UK). DVS is a well-established method for the gravimetric determination of vapour sorption isotherms. The DVS Advantage-1 uses a Cahn D200 recording ultra-microbalance with a mass resolution of ±0.1 µg; the vapour partial pressure around the sample is controlled by mixing saturated and dry carrier gas streams (N_2) using electronic mass flow controllers (Burnett et al., 2008).

Samples were equilibrated at 0% RH until dry and the reference mass was recorded. The samples were exposed to the following % of relative humidity (RH) profile: 0 % to 90 % in 10 % steps and the reverse for desorption at 25.0±0.1 °C. At each stage, the sample mass was allowed to reach equilibrium defined as dm/dt = 0.002 mg/min over 10 min, before the RH was changed.

The amount of water uptake for each RH stage was expressed as a % of the dry sample mass (m_0).

For data analysis the Young and Nelson model was fitted to the vapour sorption isotherm, using the software provided by SMS Ltd. This model, which establishes a quantitative correlation between the moisture content and the %RH, was fitted to profile the water uptake as water adsorbed in a monolayer and multilayer, and as water absorbed (Bravo-Osuna et al., 2005; Tewes et al., 2010):$M_s = A(\beta + \theta) + B\theta RH$ and $M_d = A(\beta + \theta) + B\theta RH_{max}$ where M_s and M_d are, respectively, the amount of water sorbed and desorbed at each RH (%), expressed as a fraction of the dry mass of the sample. *A* and *B* are constants characteristic of each material: $A = \frac{\rho_w Vol_M}{W_m}$ and $B = \frac{\rho_w Vol_A}{W_m}$ where ρ_w is the water density, Vol_M and Vol_A are, respectively, the adsorbed and absorbed water volumes and W_m is the weight of dry material. In this model, ϑ is the fraction of the material surface covered by at least one layer of water molecules, and $A\vartheta$ is the mass of water in a complete adsorbed monolayer expressed, like all masses in the model, as a fraction of the dry mass of the solid. $A(\beta+\vartheta)$ is the total amount of adsorbed water, and $A\beta$ is the mass of water which is adsorbed beyond the mass of the monolayer, that is, in multilayers. *B* is the mass of absorbed water at 100 % RH, and, hence, $B\vartheta RH$ is the mass of absorbed water when the monolayer coverage is ϑ and the relative humidity is RH.

2.2.11 High performance liquid chromatography (HPLC)

Salmon calcitonin (sCT) content was analysed by HPLC, as previously describe by Tewes et al. (2010). An LC-IOAT VP pump, FCV-10AL VP delivery module, DGU-14A degasser, SIL-10AD VP autosampler, SPD-10A VP UV–VIS-detector and CLASS-VP software (all Shimadzu, Japan) were used. The chromatographic system was set up with a Genesisass of the rbed in a monolapolar column (Jones Columns, Crawford scientific, UK). Measurement were conducted by injecting 50 µl of samples, standards or controls in the mobile phase running at 1.0 ml/min and composed of 66% v/v of aqueous phase (1.16 g/l of NaCl, 0.032 % v/v of TFA dissolved in H_2O) and 34 % v/v of acetonitrile. sCT were detected by measuring the absorbance at 214 nm. sCT concentration of the standards ranged from 0.1 mg/l to 0.003 mg/l and calibration curves were prepared in triplicate. Controls were performed to check for any interference on the assay by the excipents. No interference was found. Presented values are the average ± standard deviation of three measurements.

2.2.12 Solid state Fourier transform infrared spectroscopy (FTIR)

Infrared spectra of samples were evaluated in order to evaluate possible molecular modifications after processing of excipients and peptide (Ní Ógán et al, 2010). Spectras were recorded on a Nicolet Magna IR 560 E.S.P. (USA) spectrophotometer equipped with MCT/A detector, working under Omnic software version 4.1. A spectral range of 650-4000 cm^{-1}, resolution 2 cm^{-1}, and accumulation of 64 scans were used in order to obtain good quality spectra. A KBr disk was used. Samples were mixed with KBr at a ratio of 1:100 using an agate mortar and pestle. Disks were compressed at 8 tonnes pressure for 1 to 2 minutes using a 13 mm KBr die set (Apollo Scientific, U.K.). The raw absorption spectras were baseline corrected and smoothed. For samples containing peptide, the amide I band was truncated followed by area normalization using Originlab software to enable direct quantitative comparisons between spectra, as described by Van de Weer et al. (2001).

2.2.13 Circular dichroism (CD) (These studies were carried out by Fatma Faraq, UCC)

CD was carried out to evaluate sCT secondary structure using a Chirascan CD Spectrometer from Photophysics. A 0.1 mm pathlength cell was used for the Far UV spectra which were measured in the range 185-260 nm. Data was collected in millidegree units using the band width of 1 nm at a 0.5 nm step size and the time per point was 0.5 sec. Three replicates were performed. Stepped temperature ramping from 20 ^{o}C to 75 ^{o}C was used for the heating and cooling experiment with a 5^{o}C step size and equilibrium time 2 min/ temperature point. For the temperature ramping experiment a 0.5 mm pathlength cell was used. Data was analysed using the software CDNN for calculation of secondary structure ratios of the sCT molecule. The spectra of the blank solutions were subtracted from the protein solutions spectra.

2.2.14 Salmon calcitonin activity assay

The capacity of sCT formulations to increase intracellular cyclic adenosine monophosphate (cAMP) was assessed in accordance with a previously reported method (Ryan et al., 2009). T47D human breast cancer cells expressing calcitonin receptors were cultured in RPMI (Roswell Park Memorial Institute) 1640 with HEPES modification culture medium supplemented with 1 % v/v L-glutamine solution, 1 % v/v penicillin–streptomycin, 10 % v/v foetal bovine serum and 0.2 IU/mL insulin. Cells were seeded on 24-well plates, previously coated with 1.15 % v/v collagen solution, at an initial density of $1x10^{6}$ cells/well and incubated in air with 5 % of CO_2 at 37 ^{o}C for 2 days. Cells where then washed with PBS and serum free medium and pre-incubated with fresh serum free medium supplemented with the phosphodiesterase inhibitor, 3-isobutyl-1-methyl-xanthine

(IBMX, 0.2 mM) at 37 ºC for 30 min. sCT formulations (with sCT at a concentration of 10^{-8} M) dissolved in serum free RPMI 1640 plus IBMX was then added to the cells and incubated for 15 min. After removing the supernatant, cells were rinsed three times in cold PBS and resuspended in 1 ml of cell lysis buffer. Cells were frozen at −20 °C and thawed with gentle mixing. The freeze/thaw cycle was repeated once and the mixture was centrifuged at ~ 10,000 rpm for 5 min at 4 °C to remove cellular debris. The supernatant was collected and cAMP concentrations were measured by cAMP Enzyme immuno-assay (EIA) kit (RandD Systems, Abingdon, UK). All measurements were done in triplicate and responses expressed as average the blank solutions.

2.2.15 Pharmacokinetic studies (These studies were performed by Dr. Frederic Tewes and Dr. Oliviero Gobbo, TCD)

In vivo studies were performed using Male Wistar rats (BioResources, TCD, Ireland) weighing 350±50 g. The compliance of this study with EC Directive 86/609 was reviewed and approved by the Trinity College Dublin ethical committee. Rats were anesthetsed by an intraperitoneal (ip) injection of a mixture of ketamine and medetomidine hydrochloride at the doses of 60 mg/kg and 0.5 mg/kg body weight, respectively. After anaesthesia, in the case of intravenous (iv) administration of sCT, two heparinised permanent polyurethane intravascular tubings were implanted on the day of the experiment. The left femoral vein was cannulated for sCT solution administration, while the left femoral artery was cannulated for blood sampling. For pulmonary sCT administration, only one catheter was implanted in the left femoral artery for blood sampling. The iv bolus administration of sCT (100 periment. The left femoral vein was cannulated for sCT solutin 0.9 % w/v NaCl. Then the anesthetic reversal agent, atipamezole hydrochloride solution (Antisedan, Pfizer, Ireland), was injected ip at 5 mg/kg. The sCT dose for pulmonary administration was 100 µg/kg, which corresponded approximately to the insufflations of 1 mg of dry powder or to the nebulization of 100 µg of sCT solutions at 350 µt/mL in 0.9% w/v NaCl. Powder administration was performed using a dry powder Insufflator Model DP-4. (Penn-Century, Philadelphia, PA, USA). sCT solution nebulisation was performed using an AeroProbe intracorporeal nebulising catheter controlled by a LabNeb unit (Trudell Medical International, London, U.K.). Anesthetized rats were maintained by the upper incisors on a rodent work stand inclined at 45° angle. Vocal cords were visualised with the help of an otoscope, and then a plastic guide was inserted between them. The rat was put back to the horizontal position, followed by the introduction of the sprayer into the plastic tube and the formulation nebulized when the rat was breathing in. The tip was withdrawn and anesthetic reversal agent was injected ip. . Blood samples (200 µL) were collected in heparinized tubes at the following times: 0; 3; 10; 20; 30; 60;

90; 120; 180 min after sCT administration. In each case, blood was replaced by an equal volume of isotonic solution. Blood samples were centrifuged at 10000 rcf for 5 min. Plasma was withdrawn and kept frozen at -20 °C until sCT assay by ELISA kit (S1155, Bachem, U.K.). Pharmacokinetic parameters were determined for each individual rat using a non-compartmental model.In the latter model the change of drug concentration over time is usually regarded as a statistical distribution curve, for which the first two moments (zero and first) are defined as the area under the curve (AUC) and as mean residence time (MRT), a mean time interval during which a drug molecule resides in the body before being excreted (Gabrielsson and Weiner, 2000; Kwon, 2002; Cryan, et al., 2007). AUC can be calculated by the linear trapezoidal method and MRT as follows:= $\frac{AUMC_0^\infty}{AUC_0^\infty}$, where AUMC is the area under the first-moment curve of the plasma drug concentration vs. time curve from time 0 to infinity (Gabrielsson and Weiner, 2000; Kwon, 2002). Other pertinent pharmacokinetic estimates were: intra-venous clearance $Cl = \frac{D_{iv}}{AUC_0^\infty iv}$; pulmonary clearance $Cl_{pul} = \frac{Cl}{F}$; absolute bioavailability $F_a = \frac{AUC_{pul}}{AUC_{iv}} \times \frac{D_{iv}}{D_{pul}}$; relative bioavailability $F_r = \frac{AUC_{pul}}{AUC_{sol\,pul}} \times \frac{D_{sol\,pul}}{D_{pul}}$; steady state volume of distribution $V_{ss} = MRT \times Cl$; volume of distribution during the terminal phase $V_{d\beta} = \frac{Cl}{\beta}$; the half-life of the terminal β phase$t_{1/2\beta} = \frac{\ln(2)}{\beta}$; mean absorption time $MAT = MRT_{pul} - MRT_{iv}$; the constant of absorption $k_a = \frac{1}{MAT}$; and the constant of elimination $k_e = \frac{1}{MRT}$ (Gabrielsson and Weiner, 2000; Kwon, 2002).

2.2.16 Storage stability

Solid state stability studies of sCT composites were conducted using the conditions of temperature and relative humidity (RH) described by Ní Ógáin (2010) for a period of 24 weeks. Hence, conditions studied were: 4 °C/5 % RH and 25 °C/5 % RH using the conditions of temperature and relative humidity of Amebis Ltd (Ireland) stability products. Samples were placed in special powders containers that possess a mesh on the bottom and top to allow full contact with air, which were then placed in test chambers with humidity devices (containing saturated salt solutions) designed to achieve the required relative humidity. Test chambers were kept in an incubator or fridge according to tested conditions. Samples were removed at appropriate time intervals and analysed as outlined in Table 2.1.

Tabel 2.1 Outline of sample stability analysis by scanning electron microspcopy (SEM), differential scanning calorimetry (DSC), thermogravimetric analysis (TGA), X-ray diffraction (XRD), Fourier transform infrared spectroscopy (FITR), high performance liquid chromatography (HPLC) and bioactivity.

	SEM	DSC	TGA	XRD	FTIR	HPLC	Bioactivity
Day 0	X	X	X	X	X	X	X
Day 1		X	X	X			
Week 1		X	X	X			
Week 2		X	X	X			
Week 4		X	X	X	X	X	
Week 8		X	X	X			
Week 12		X	X	X	X	X	
Week 16		X	X	X			
Week 20		X	X	X			
Week 24	X	X	X	X	X	X	X

2.2.17 Statistical analysis

Statistical analysis of variance, ANOVA with Tukey´s, was performed to determine the significance (p-value) and impact (F-value) of an effect or difference between means, using Minitab™ software (version 13.32). Parameters found to be significant at at least the 95% confidence level were considered to have an effect or to be different.

Descriptive statistics (median and standard deviation) were determined using Microsoft® Office Excel®

CHAPTER 3

ONE-FACTOR-AT-A-TIME OPTIMISATION OF SPRAY DRYING OF NON-REDUCING SUGARS

3.1 INTRODUCTION

Powder presence or build-up on the drying chamber and/or cyclone wall surfaces is a regular occurrence in industrial spray drying operations, in particular with sugar-rich foods (Bhandari, 1997; Maa et al., 1998; Masters, 2002). Powder build-up is caused by numerous factors: insufficient droplet drying, thermoplastic/hygroscopic nature of the powder resulting in particles with sticky surfaces, electrostactic forces, deposition at positions of any distortion on the inner spray drier glassware surface and heat loss causing condensation on the glassware leading to powder stickiness (Masters, 2002).

Several studies have addressed this problem at a laboratory scale. Bhandari et al. (1997) studied problems associated with spray drying of sugar-rich foods, indicating stickiness inherent to sugar as the major reason limiting their suitability for spray drying. Properties such as high hygroscopicity of the amorphous counterpart, low melting point and glass transition temperature (T_g), were identified as the main causes of low powder collection on spray drying sugars. Bhandari et al. suggested different approaches to overcome such problems: the addition of "drying aids" (e.g., maltodextrins – to increase the T_g, allowing spray drying to be conducted at higher inlet temperatures, resulting in drier powders), modification of dryer design and the use of mild temperature conditions. Maury et al. (2005) evaluated the effects of spray drying process variables on the production yield of trehalose powders, reporting the formation of wet deposits on the cyclone wall. Maury et al. determined that the use of higher inlet temperatures could improve particle drying and reduce wall deposition. Ní Ógáin (2008) spray dried raffinose pentahydrate and trehalose dihydrate to produce nanoporous microparticles and highlighted problems with the process such as: low yields (< 50%), powder deposits on cyclone wall and high electrostatic charge of the collected powder.

Our aim was to optimise the spray drying conditions and feed solution concentration for the production of sugar nanoporous/nanoparticulate microparticles (NPMPs) by means of a one-factor-at-a-time (OFAT) study and, to investigate their physicochemical properties, in order to ensure their suitability for later incorporation of peptides and proteins, as a system designed for pulmonary delivery.

3.2 UNPROCESSED MATERIALS: RAFFINOSE PENTAHYDRATE AND TREHALOSE DIHYDRATE

Properties of raffinose pentahydrate (R5W) and trehalose dehydrate (T2W) as supplied materials were investigated. Raffinose crystals presented a prism shape and trehalose crystals a cubic shape (Figure 3.1), with a geometric median diameter of 123.7±4.36 μm and 173.4±13.96 μm, respectively, as measured by laser diffraction, and a true density of 1.50±0.00 g/cm^3 for raffinose and 1.51±0.00 g/cm^3 for trehalose. XRPD showed the characteristic peaks of the two sugars: at 10.75, 13.65 and 21.1° for raffinose (Leinen and Labuza, 2006; Ní Ógáin O., 2008) and at 8.7° and 23.8° for trehalose (Nagase H. et al., 2002; Pinto S. et al., 2006; Ohashi T. et al., 2007) (Figure 3.2).

Thermogravimetric analysis (TGA) of R5W showed a large step between 25 and 140 °C, corresponding to a mass loss of ~14 % due to dehydration, consistent with the theoretical mass of water in the pentahydrate of ~15 %. This water loss was also evident on the DSC scan, where a sharp endotherm was detected at ~90 °C. The latter scan presented a disordered pattern after the endothermic peak, which could be assigned to degradation of the sugar. No other thermal events were registered (Figure 3.3).

The TGA of T2W presented a large step between 25 and 200 °C, corresponding to a mass loss of ~9 % due to dehydration, once more consistent with the theoretical mass of water of ~9.5 %. The first sharp endotherm at ~100 °C in the DSC scan corresponds to the aforementioned water loss. A second sharp endotherm was found at ~200 °C that could be attributed to the melting of the anhydrous trehalose - polymorph β (Sussich et al., 1998; Sussich and Cesàro, 2008). A third small endothermic peak was detected at ~115 °C overlapping to some extent with the previous peak at ~100 °C. Taylor and York (1997) have also reported an endothermic peak over the temperature range 112-125 °C , that was attributed to the rapid rate of weight loss due to dehydration of trehalose dihydrate (Figure 3.4).

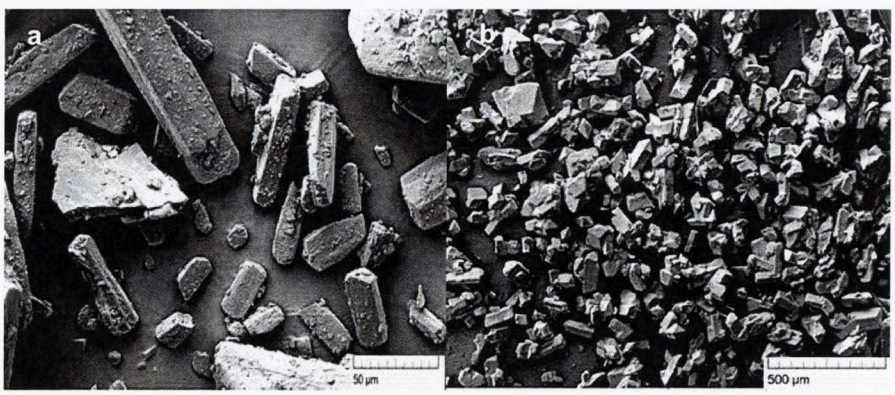

Figure 3.1 SE micrographs of (a) raffinose pentahydrate and (b) trehalose dihydrate

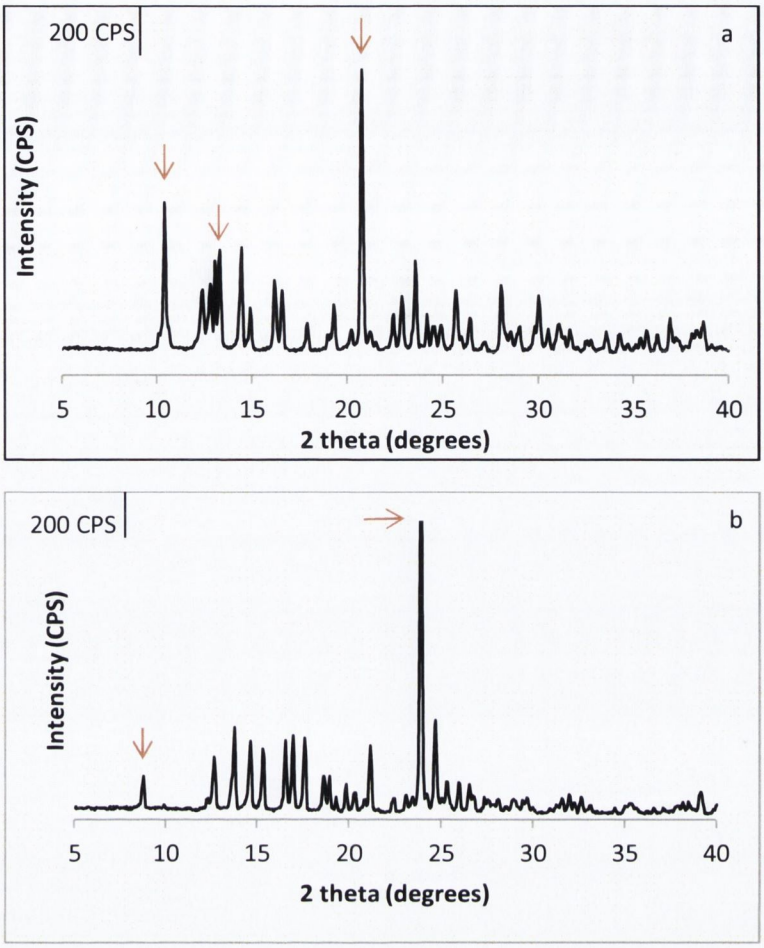

Figure 3.2 XRPD of (a) raffinose pentahydrate and (b) trehalose dihydrate. Red arrows indicate the characteristic peaks

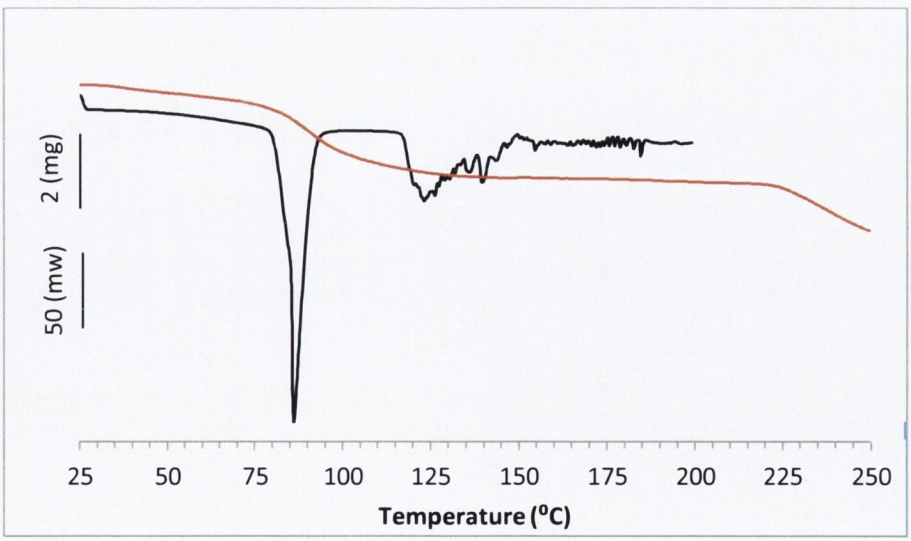

Figure 3.3 DSC (black) and TGA (red) scan of raffinose pentahydrate

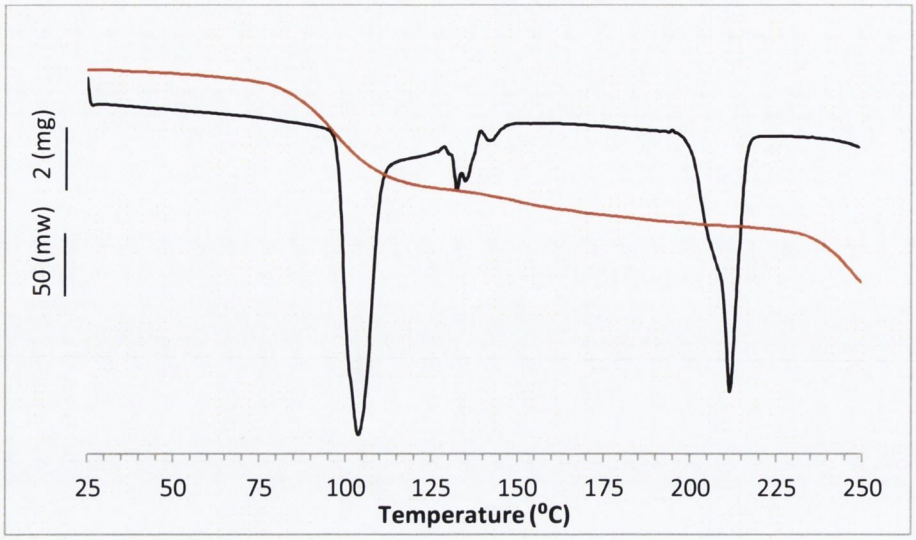

Figure 3.4 DSC (black) and TGA (red) scan of trehalose dihydrate

3.3 PREPARATION OF SUGAR NPMPs

Raffinose and trehalose were spray dried as solutions of 1 % and 0.5 % (w/v) respectively, from 80% methanol/20% n-butyl acetate (v/v). These solutions were previously successfully spray dried by Ní Ógáin (2008) to produce raffinose and trehalose NPMPs. In the current studies, nitrogen (at 6 bar) was used as the drying gas in a co-current mode with aspirator capacity set to maximum (100 %) and the airflow rate constant at 667 l/h, as was the case in the previous studies conducted by Ní Ógáin (2008). The remaining operating parameters were set according to the one-factor-at-a-time procedure (Table 3.1). This method consists of selecting a starting point, or baseline set of levels, for each factor, and then successively varying each factor over its range with the other factors held constant (Montgomery, 1997). The impact of feed solution concentration was also studied (Table 3.1). Spray dried particles were separated from the drying gas by a high-performance cyclone (Büchi, Switzerland), since previous studies have indicated an improved efficiency of this cyclone compared to a regular cyclone in collecting particles less than 2 µm in diameter (Brandenberger, 2003; Ní Ógáin, 2008). The effects of spray drying parameters on powder production yield, particle size and density, residual solvent content, glass transition temperature and process outlet temperature were assessed.

Table 3.1 Process variables evaluated in the one-factor-at-a-time study

		Setting	Units
Aspirator		100	%
Airflow		40	mm
Inlet temperature		90-140	°C
Pump (feed solution rate)		20-35	%
Feed Solution Concentration	**Raffinose**	1 - 3.5	% (w/v)
	Trehalose	0.5 -1.5	

3.4 EFFECT OF INLET TEMPERATURE

Inlet temperature (T_{inlet}) was varied between 90 and 140 °C, resulting in an outlet temperature (T_{outlet}) range of 54-79 °C for raffinose NPMPs and 48-81 °C for trehalose NPMPs, with a significant increase for the latter ($p=0.011$ for R and $p<0.05$ for T) as inlet temperature was set to higher temperatures. Increased inlet temperature leads to an incremental supply of heat energy, resulting in higher outlet temperatures (Tajber et al., 2009; Technical data Büchi B-290, 2009). Figure 3.5*a* and 3.5*b* represent the difference between the inlet and outlet temperature (heat usage) during spray drying as a function of inlet temperature, T_{inlet}. The greater the air temperature difference, the smaller the heat requirement to produce a unit weight of powder of constant residual moisture/solvent content, and the more efficient the process is (Masters, 2002). Spray drying at higher inlet temperatures resulted in a more efficient processing of both materials; the slope of the linear curve fitted (ratio $\frac{T_{inlet}-T_{outlet}}{T_{inlet}}$) was higher for raffinose than for trehalose, giving an indication that the heat usage was more efficient for raffinose drying.

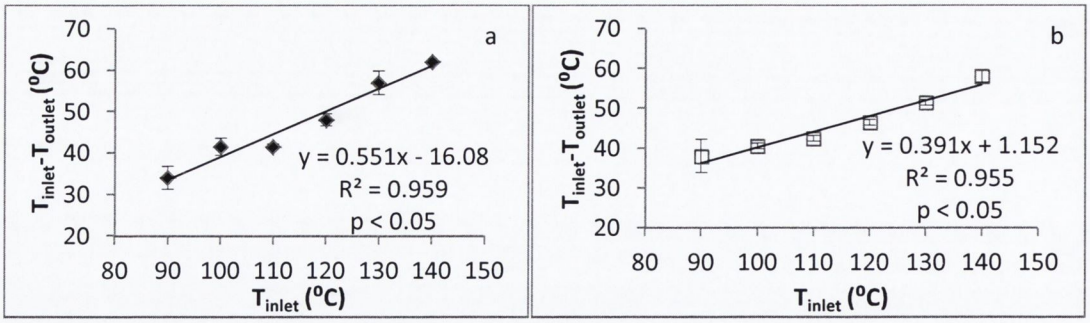

Figure 3.5 Process heat usage as function of inlet temperature of (a) spray dried raffinose NPMPs and (b) spray dried trehaoseNPMPs

XRPD of all spray dried samples presented a scattered diffractogram, known as the amorphous halo, characteristic of amorphous powders (Figure 3.6a and 3.6b). Therefore, by spray drying it is possible to modify the solid state of raffinose and trehalose from the crystalline state to the amorphous state.

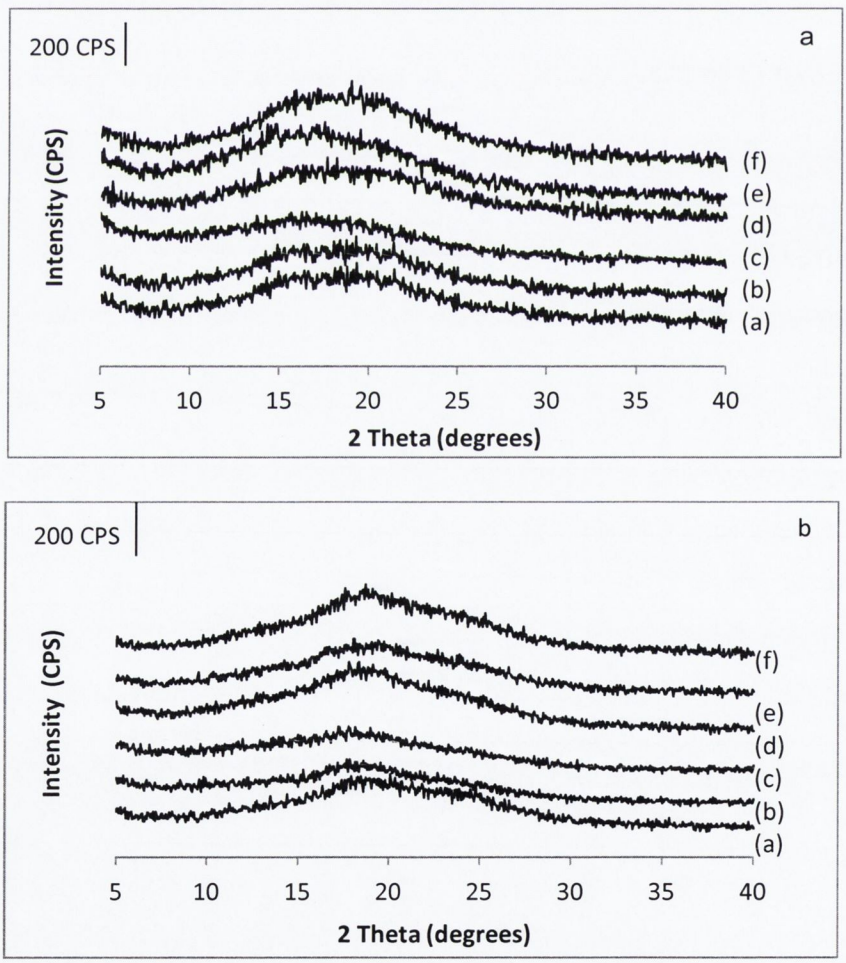

Figure 3.6 XRPD of (a) raffinose NPMPs and (b) trehalose NPMPs spray dried at different inlet temperatures: (a) 90 °C, (b) 100 °C, (c) 110 °C, (d) 120 °C, (e) 130 °C and (f) 140 °C.

Spray dried raffinose yields varied between 43.7 and 59.8% and spray dried trehalose between 37.3 and 55.7 %. The increase in yield was not directly proportional to inlet temperature increase; a maximum was achieved at T_{inlet} 120 °C with a yield of 60.4±0.8 % for raffinose and 52.6±0.5 % for trehalose (Figure 3.7a and b). All experimental runs presented powder build-up/sticking on the cyclone wall. According to Maury et al. (2005), insufficient droplet/particle drying leads to formation of a wet deposit resulting in a reduction in powder yield. Statistical analysis showed no significant differences between trehalose samples ($p>0.05$); in the case of raffinose, samples spray dried at T_{inlet} of 110 and 120 °C were different from all other samples ($p=0.021$).

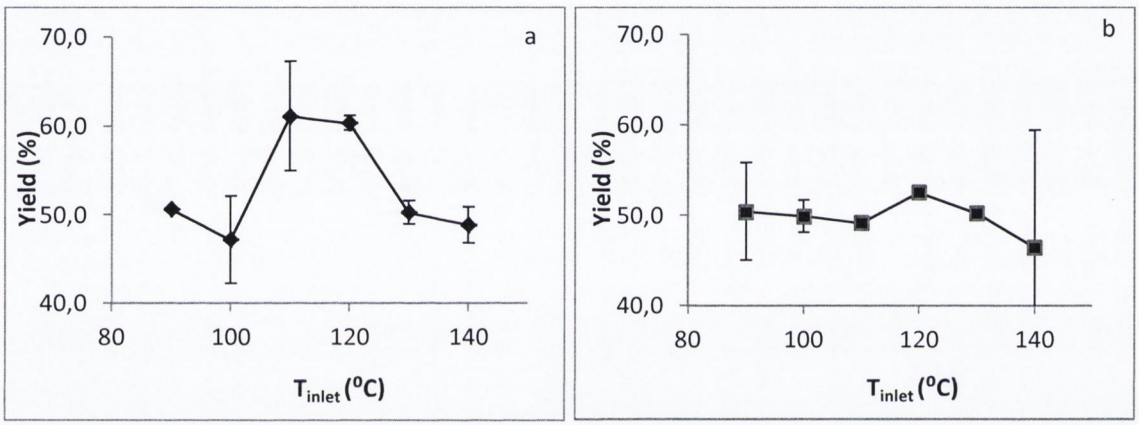

Figure 3.7 Spray dried (a) raffinose powders yield and (b) trehalose powders yield as function of inlet temperature

SE micrographs of all spray dried raffinose and trehalose powders showed these were constituted by porous, spherical particles (Figure 3.7 and 3.8); following the MSC system implemented by Paluch et al. (2012) spray dried particles of both sugars were type 1BIIIα.

Particle size volume distributions in all cases were narrow and monomodal with low span values (between 1.2 and 1.8 for raffinose and 1.1 and 2.2 for trehalose). The median particle size (d_{50}) for raffinose particles was in the range of 2.1–2.8 μm and for trehalose particles was in the range 1.7–2.1 μm (Table 3.2 and 3.3). No statistically significant differences were found between raffinose samples ($p=0.395$); in contrast, trehalose NPMPs when spray dried at T_{inlet} 120 °C and 130 °C presented a significantly higher geometric median particle diameter than when spray dried at T_{inlet} 90 °C ($p=0.019$). A correlation between d_{50} and powder yield was investigated for trehalose powders only, since raffinose powders presented no differences in particle size. A significant correlation ($r^2=0.556$, $p=0.013$) was found where, as particle size increases, higher yields are achieved (Figure 3.10); the outlier point results from a sample spray dried at 140 °C, powder stuck in cyclone walls might have led to the lower yield. Larger particles are easier to

capture in the cyclone and only particles with diameters above the cyclone's cut-off point will be collected; for this reason we calculated the cut-off point of the Büchi HP cyclone using Barth's model as described by Maury et al. (2005):$\bar{d}^2 = \frac{9\eta Q}{(\upsilon_t^{-p})\rho_p \pi h_i}$, where η is air viscosity, Q is the air flow rate, ρ_p particle density, and h_i vortex height, to exclude the influence of the cyclone on collected yields. The cut-off point was found to be 0.60 µm for raffinose particles and 0.61 µm for trehalose particles, smaller than the d_{10} calculated for both type of powders(Table 3.2 and 3.3). However, no particles with diameters equal to or less than 0.60 µm were found in the volumetric particle size distribution data of any of the analysed samples.

True, bulk and tap density measurements of spray dried powders are presented in Table 3.2 and 3.3. ANOVA analysis for all three outcomes showed significant differences ($p<0.05$) between spray dried samples for both types of sugars, with a decrease in true density and variation of bulk and tap density as inlet temperature was increased. Bulk and tap density presented values < 0.3 g/cm^3 making them suitable for pulmonary delivery (Bosquillon et al., 2004).

The aerodynamic diameter was calculated for all samples (Table 3.2 and 3.3). A diameter in the range of 1-3 µm is desirable for central and distal deposition in the lungs (Hickey, 1996). All trehalose spray dried powders complied with this diameter range. In the case of raffinose NPMPs only powders spray dried at higher inlet temperatures presented aerodynamic diameters below 3 µm.

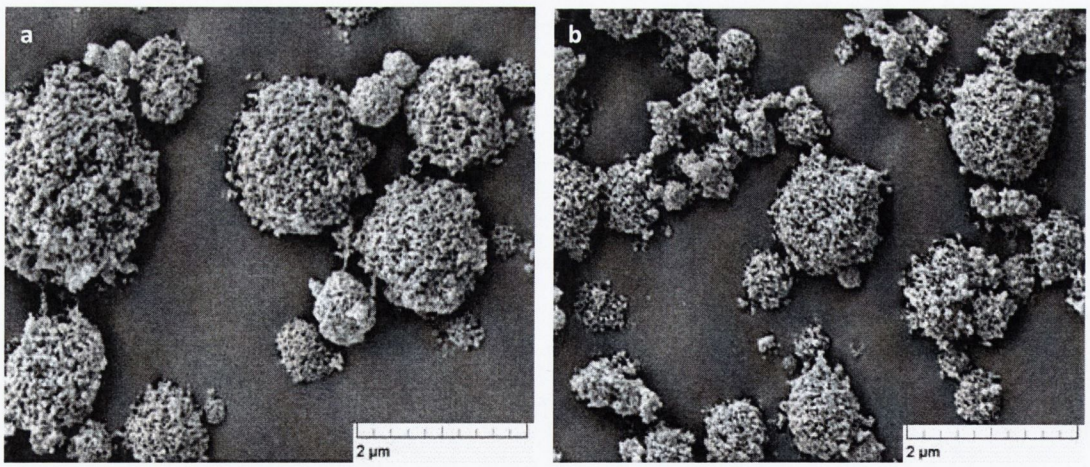

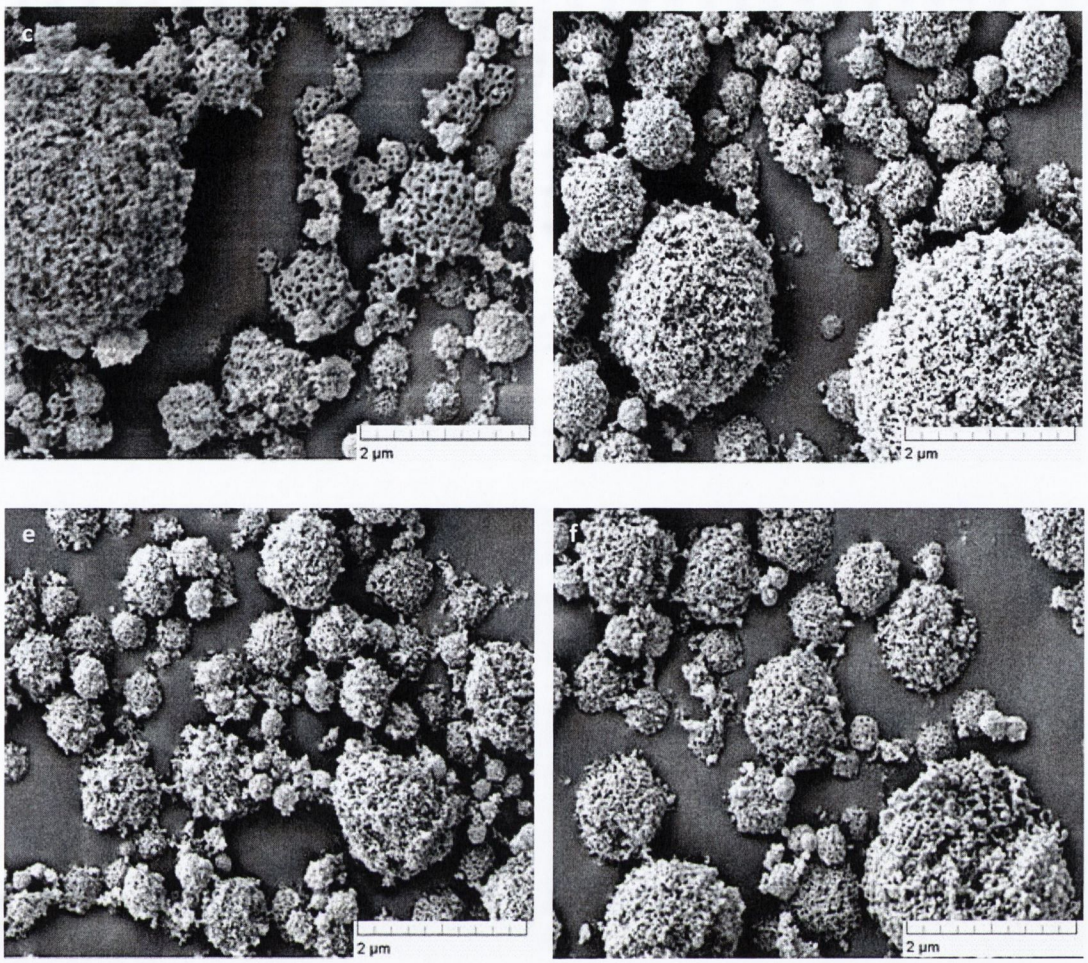

Figure 3.8 SE micrographs of raffinose NPMPs spray dried at different inlet temperatures: (a) 90 °C, (b) 100 °C, (c) 110 °C, (d) 120 °C, (e) 130 °C and (f) 140 °C.

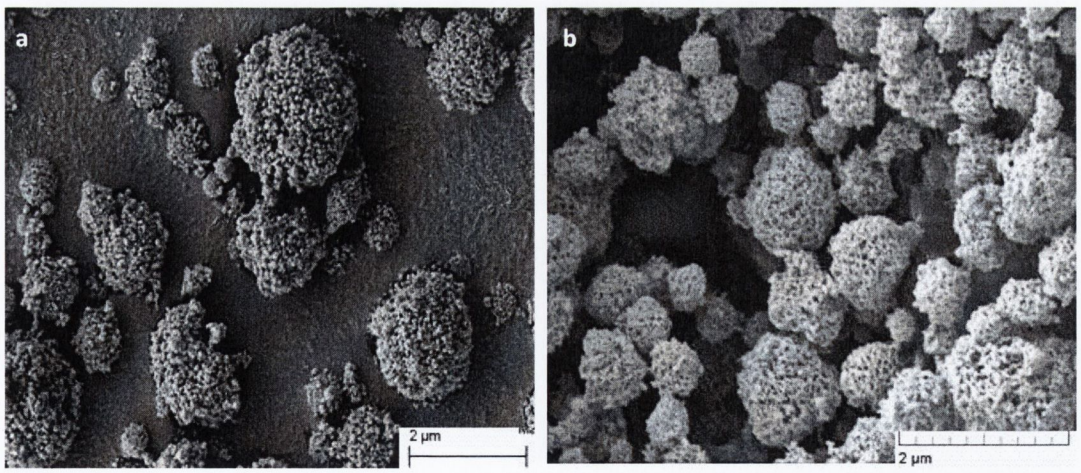

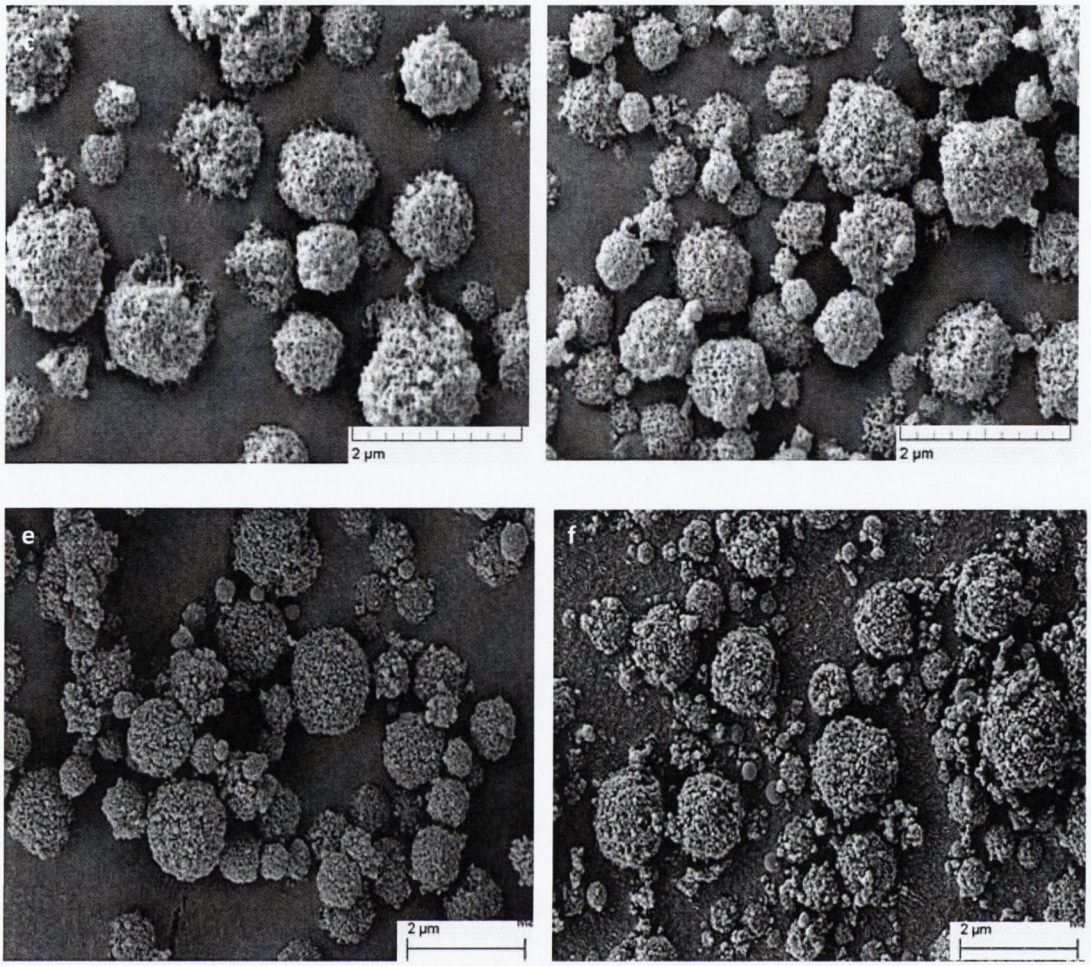

Figure 3.9 SE micrographs of spray dried trehalose NPMPs at different inlet temperatures:(a) 90 °C, (b) 100 °C, (c) 110 °C, (d) 120 °C, (e) 130 °C and (f) 140 °C.

Table 3.2 Particle size, true, bulk (bp) and tap (tp) density and calculated aerodynamic diameter (d_{aer}) of raffinose spray dried samples at different inlet temperatures

T_{inlet} (°C)	90	100	110	120	130	140
d_{10} (µm)	1.3±0.11	1.2±0.11	1.3±0.13	1.2±0.01	1.1±0.03	1.3±0.04
d_{50} (µm)	2.7±0.33	2.5±0.03	2.8±0.70	2.3±0.03	2.1±0.09	2.3±0.18
d_{90}(µm)	6.3±0.67	5.6±0.13	5.8±1.75	4.8±0.01	4.0±0.18	4.1±0.45
<1µm (%)	3.3±1.34	4.2±0.21	3.1±0.50	3.7±0.19	6.0±0.19	3.3±0.13
True density (g/cm^3)	2.05±0.07	2.08±0.02	1.66±0.02	1.65±0.01	1.80±0.07	1.67±0.02
bp (g/cm^3)	0.05±0.00	0.08±0.00	0.05±0.00	0.07±0.0	0.06±0.00	0.09±0.01
tp (g/cm^3)	0.09±0.01	0.14±0.01	0.11±0.00	0.14±0.01	0.10±0.00	0.17±0.00
d_{aer} (µm)	4.1±0.07	3.6±0.06	4.1±0.16	3.0±0.16	2.7±0.05	2.8±0.02

Table 3.3 Particle size, true, bulk (bp) and tap (tp) density and calculated aerodynamic diameter (d_{aer}) of trehalose spray dried samples at different inlet temperatures

T_{inlet} (°C)	90	100	110	120	130	140
d_{10} (µm)	1.0±0.02	1.0±0.01	1.0±0.04	1.1±0.11	1.1±0.10	1.0±0.01
d_{50} (µm)	1.7±0.08	2.0±0.05	1.9±0.14	2.1±0.05	2.0±0.05	1.8±0.06
d_{90}(µm)	3.6±0.79	5.3±0.72	4.1±1.20	4.4±0.74	4.7±0.37	3.2±0.33
<1µm (%)	11.4±0.74	10.7±0.56	7.4±1.70	9.8±1.30	9.9±1.15	9.0±0.54
True density (g/cm^3)	1.46±0.00	1.60±0.04	1.56±0.04	1.55±0.02	1.53±0,03	1.55±0.01
bp(g/cm^3)	0.07±0.02	0.04±0.00	0.06±0.00	0.09±0.01	0.11±0.00	0.14±0.01
tp (g/cm^3)	0.12±0.00	0.09±0.00	0.12±0.00	0.17±0.00	0.19±0.00	0.21±0.00
d_{aer} (µm)	2.1±0.00	2.5±0.03	2.4±0.03	2.6±0.03	2.5±0.02	2.2±0.00

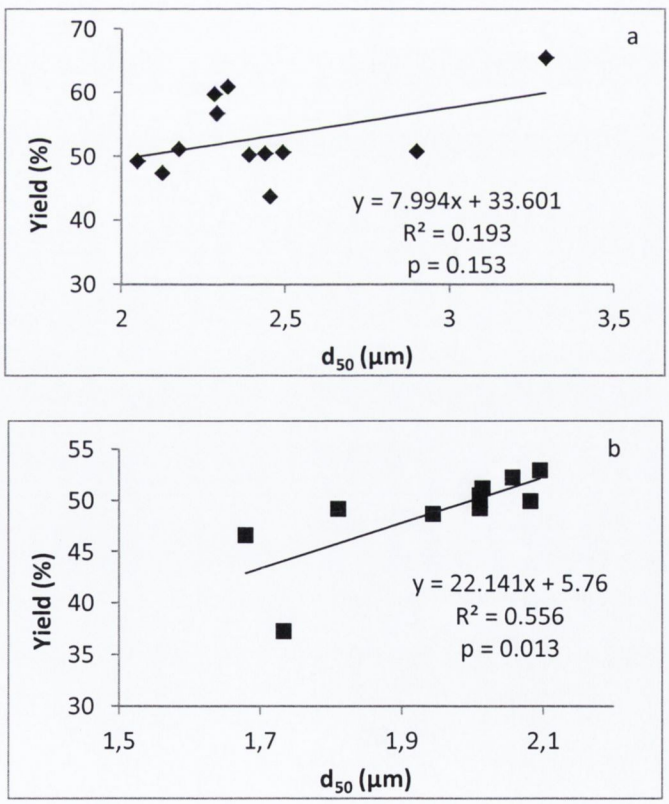

Figure 3.10 Influence of geometric median particle size on yield of (a) raffinose and (b) trehalose powders spray dried at different inlet temperatures

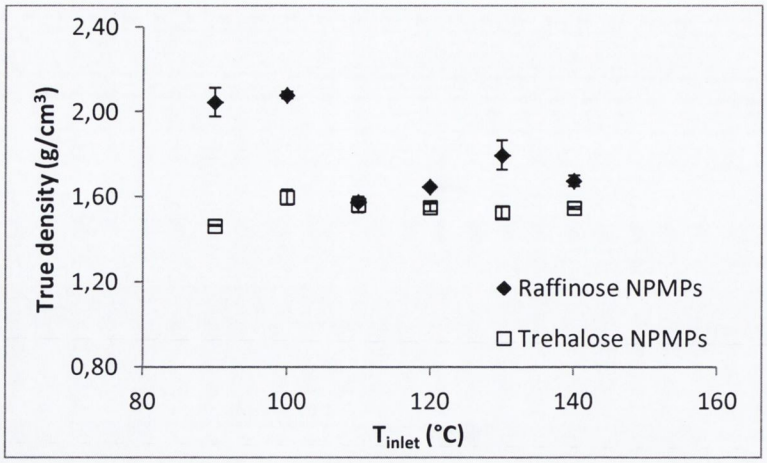

Figure 3.11 Effect of increasing inlet temperature on raffinose and trehalose powders true density

A residual solvent content (RSC) of 1.97-8.46 % and 1.69-6.12 % was determined for raffinose and trehalose NPMPs samples over the temperature range 25-130 ^{o}C from TGA, with a significant reduction in RSC as inlet/outlet temperature increased ($p<0.05$ for R and T) (Table 3.4, Figure 3.11). Studies by Billon et al. (2000), Goula and Adamopoulos (2005), Maury et al. (2005) and Maltesen et al. (2008) also verified a reduction in RSC of spray dried powders with a higher inlet temperature setting.

Studies by Goula and Adamopoulos (2005) reported a dependency of the powder bulk density on powder moisture content, where the higher the moisture content, the greater was the tendency of particles to stick together, leaving more interspaces between them and consequently resulting in a larger bulk volume and hence, lower bulk density. In our studies we have found the residual solvent content to be dependent on the inlet temperature; therefore, spray drying at elevated inlet temperatures results in powders with lower RSC and lower tendency to stick together, decreasing the bulk volume and consequently increasing the bulk density (Tables 3.2, 3.3 and 3.4).

DSC scans of spray dried raffinose NPMPs powders showed a single glass transition step with no evidence of other thermal events (Figure 3.14 and Table 3.5). The glass transition temperature (T_g) increased when powders were spray dried at $T_{inlet} \geq 110$ ^{o}C (Table 3.5). The increase was found not to be significant at a confidence level of 95 %, with $p=0.167$.

DSC scans of spray dried trehalose NPMP powders showed a single glass transition step followed by an exothermic peak, corresponding to the collapse of the amorphous state into the crystalline state – crystallisation, and finally an endothermic event correspondent to the melting of the material (Figure 3.14 and Table 3.5). In contrast to raffinose, spray drying trehalose at higher

temperatures has a significant effect on the glass transition resulting in an increase in same (p=0.013). No significant effects of an increase in inlet temperature on the crystallisation and melting temperature were found (p=0.265 and p=0.822, respectively). According to Hancock (2007) solvents have the ability to plasticise amorphous materials, leading to a depression of the glass transition temperature; therefore in our study powders with a lower RSC would be expected to present higher glass transitions temperatures. This was verified by DSC (Table 3.5).

Table 3.4 Residual solvent content of sugars NPMPs spray dried at different inlet temperatures.

Inlet temperature (°C)	Raffinose	Trehalose
	Residual solvent content (%, w/w)	
90	8.5±0.65	6.1±0.16
100	5.7±1.45	4.7±0.34
110	4.7±0.44	4.2±0.66
120	3.0±0.35	3.6±0.01
130	2.0±0.20	3.2±0.39
140	2.5±0.15	1.7±0.57

Table 3.5 Glass transition temperature (T_g), recrystallisation temperature and enthalpy (T_c, ΔH_c) and melting temperature and enthalpy (T_m, ΔH_m) of raffinose and trehalose NPMPs spray dried at different inlet temperatures

T_{inlet} (°C)	R NPMPs	T NPMPs				
	T_g (°C)		T_c (°C)	ΔH_c (J/g)	T_m(°C)	ΔH_m (J/g)
90	116.4±0.06	120.4±0.32	165.7±3.56	116.9±6.14	211.3±0.10	142.6±1.67
100	116.2±0.05	120.3±0.06	163.4±0.19	114.4±0.10	211.0±0.04	145.3±1.68
110	117.0±0.15	120.2±0.04	177.1±0.13	135.8±4.21	212.1±1.22	146.4±0.35
120	116.7±0.21	120.8±0.07	164.8±0.69	116.1±2.46	211.5±0.05	145.3±2.89
130	116.8±0.03	120.3±0.10	157.6±0.06	105.5±4.31	211.5±0.90	142.7±0.69
140	116.5±0.13	121.1±0.05	162.9±4.64	114.9±4.43	210.9±0.39	146.3±3.43

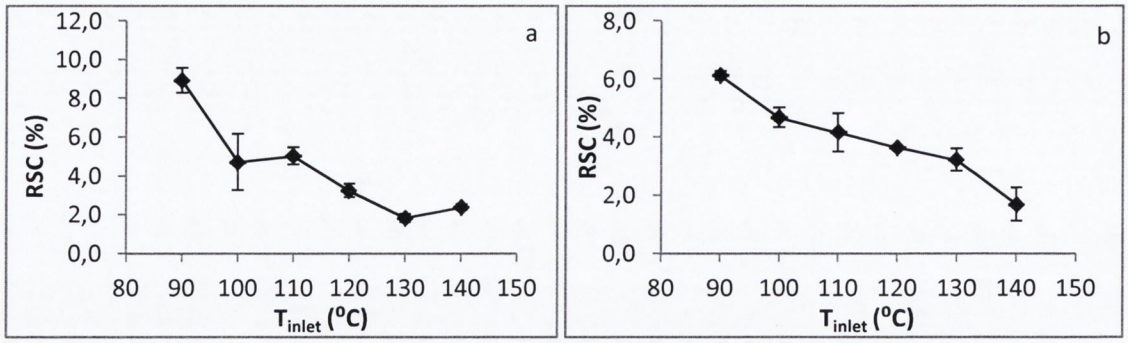

Figure 3.12 Effect of inlet temperature on (a) raffinose and (b) trehalose spray dried powders residual solvent content (RSC)

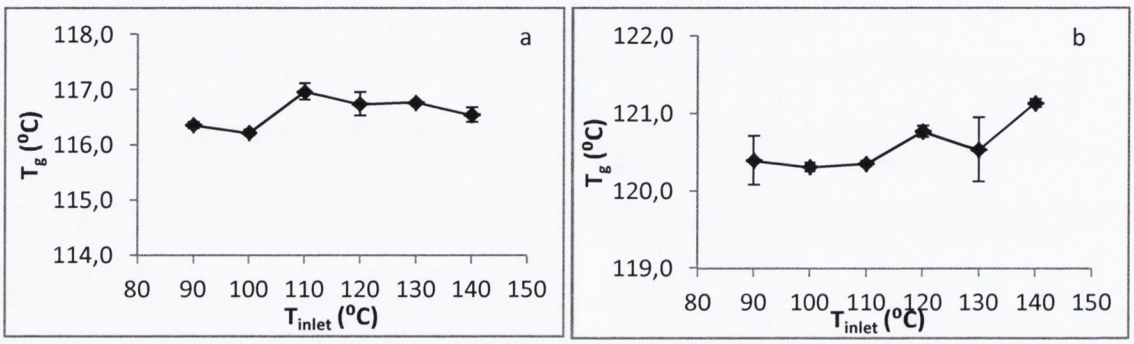

Figure 3.13 Effect of inlet temperature on the glass transition temperature (T_g) of spray dried (a) raffinose and (b) trehalose powders

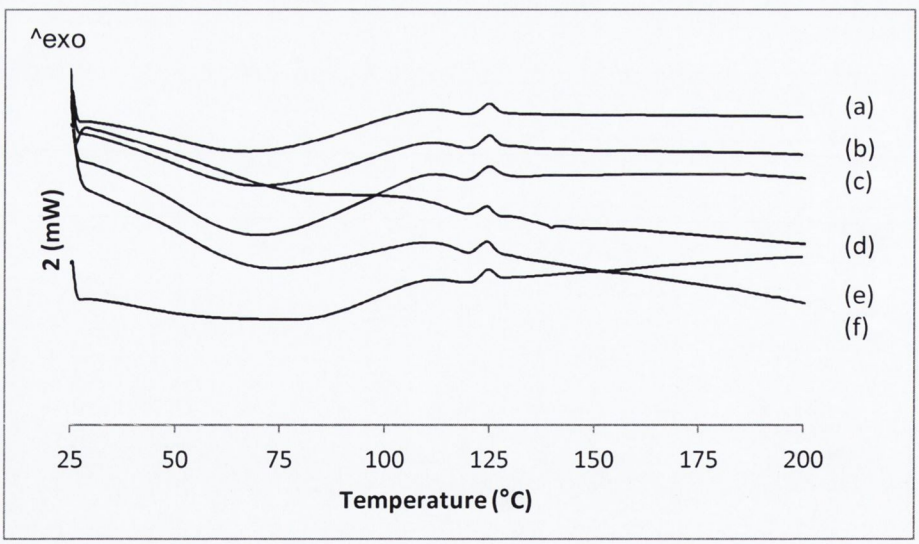

Figure 3.14 DSC scans of raffinose NPMPs spray dried at different inlet temperatures: (a) 90 °C, (b) 100 °C, (c) 110 °C, (d) 120 °C, (e) 130 °C and (f) 140 °C.

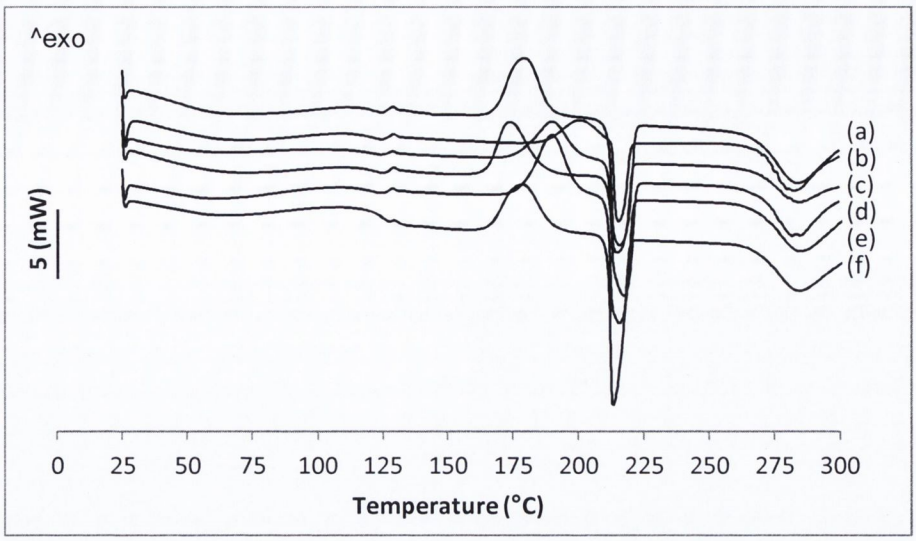

Figure 3.15 DSC scans of trehalose NPMPs spray dried at different inlet temperatures: (a) 90 °C, (b) 100 °C, (c) 110 °C, (d) 120 °C, (e) 130 °C and (f) 140 °C.

3.5 EFFECT OF LIQUID FEED FLOW RATE

In order to study the effect of liquid feed flow rate (pump setting) on raffinose and trehalose NPMPs powders, an inlet temperature 120 °C was selected, based on the previous studies.

Table 3.6 summarises the results for outlet temperature, yield and solid state for spray dried raffinose and trehalose powders processed with different pump setting. All powders were amorphous. Outlet temperature was found decrease significantly with increasing pump setting when spray drying both sugars (Figure 3.16). A higher pump setting translates into a higher throughput of solution to the atomizer, more droplets are produced, with more energy being required to dry same (when inlet temperature is constant), resulting in a decrease in the outlet temperature (Maury et al., 2005; Technical data Büchi B-290, 2009).

A correlation between yield and pump setting, for both sugars, was investigated in order to verify if yield increases or decreases when spray drying with a higher pump setting. There was an increase in powder yield with increased pump setting, but the correlations were found to be not significant ($p=0.080$, $r^2=0.424$ for raffinose; $p=0.259$, $r^2=0.301$ for trehalose), hence an effect of liquid feed flow rate on powder yield was not seen in this study. In contrast, Maury et al. (2005), when spray drying trehalose from aqueous solutions using a Büchi Model 191 laboratory spray-dryer, observed a variation in yield with a pump setting range between 3 and 5 ml/ml and, a decrease in yield when pump setting was in the range 5-9 ml/min. Residual solvent content was not affected by changes in pump setting and no significant differences were found between raffinose samples or trehalose samples ($p=0.835$ for raffinose and $p=0.089$ for trehalose).

SE micrographs showed all powders constituted spherical porous particles (Figure 3.17 and 3.18).

Table 3.6 Process outlet temperature (T_{outlet}), yield, solid state and residual solvent content (RSC) of spray dried raffinose and trehalose NPMPS at different pump settings. am - amorphous

	Raffinose NPMPs				Trehalose NPMPs			
Pump (%)/ (ml/min)	**T_{outlet} (°C)**	**Yield (%)**	**XRPD**	**RSC (%)**	**T_{outlet} (°C)**	**Yield (%)**	**XRPD**	**RSC (%)**
20/5.8	73±1.41	44.2±0.94	am	2.8±0.10	-	-	-	-
25/7.5	72.5±0.71	44.8±1.63	am	3.1±0.88	73.0± 1.00	48.8±6.04	am	4.8±0.89
30/8.3	72±1.41	60.4±0.83	am	3.0±0.35	73.5 ± 0.50	52.6± 0.34	am	3.6±0.01
35/10.0	69.5±0.71	51.8±0.91	am	3.2±0.08	69.0 ± 1.00	54.9± 2.45	am	3.2±0.12

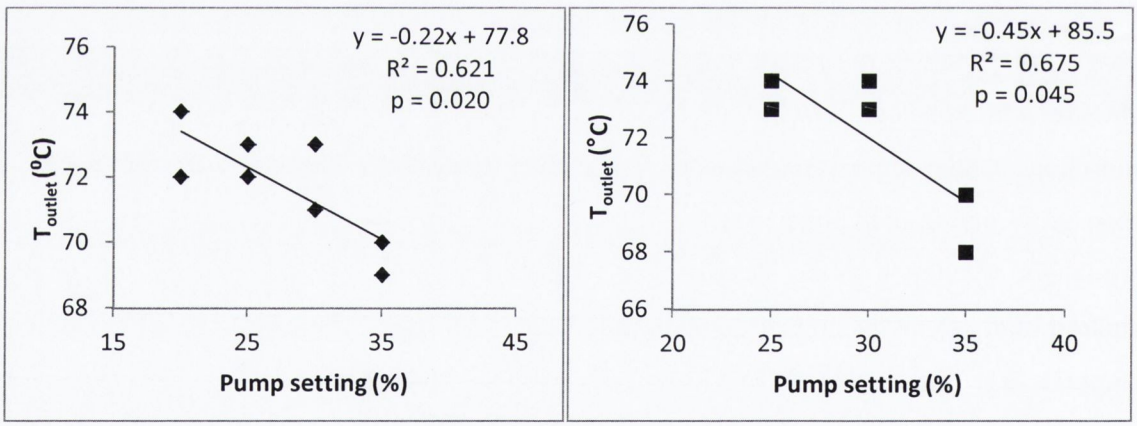

Figure 3.16 Process outlet temperature as a function of pump setting of spray dried (left) raffinose NPMPs and (right) trehalose NPMPs powders

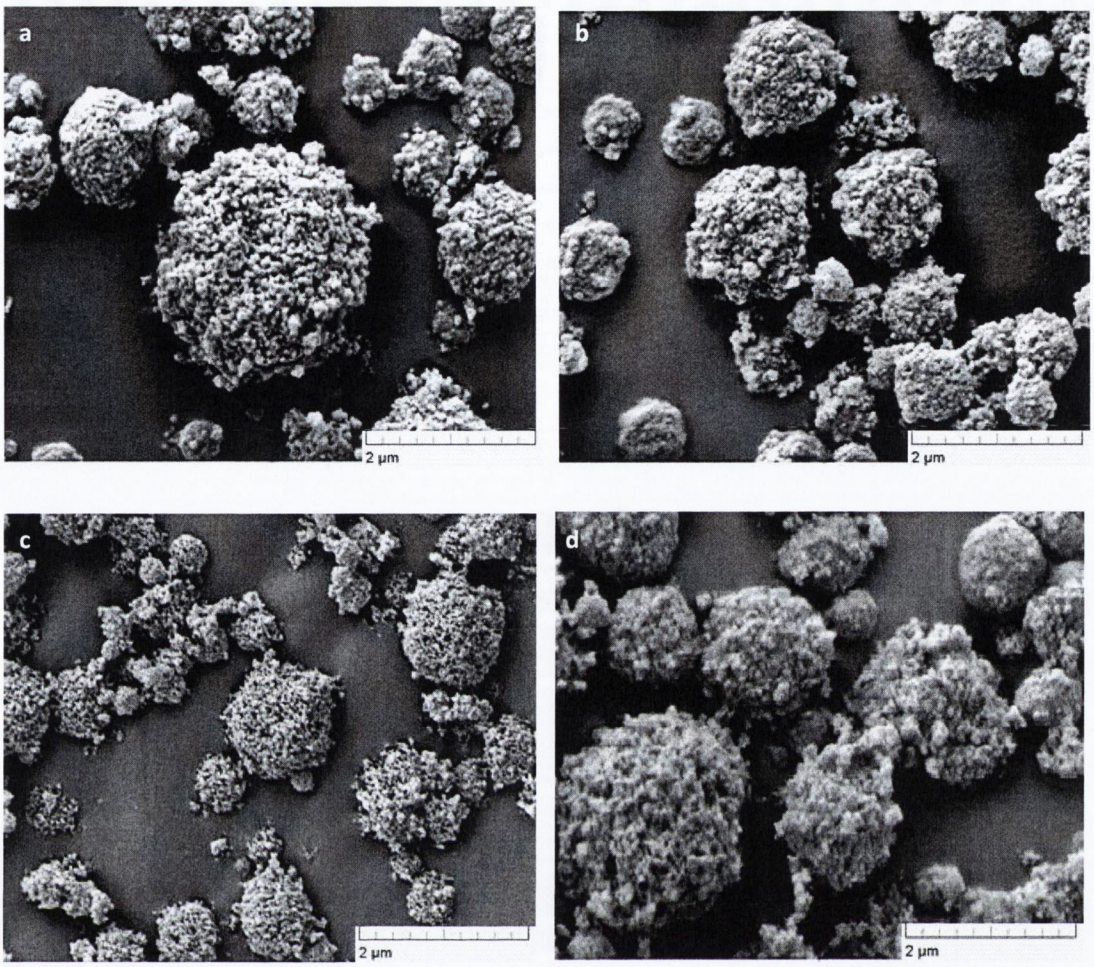

Figure 3.17 SE micrographs of spray dried raffinose NPMPs at different pump setting: (a) 20%, (b) 25%, (c) 30% and (d) 35%

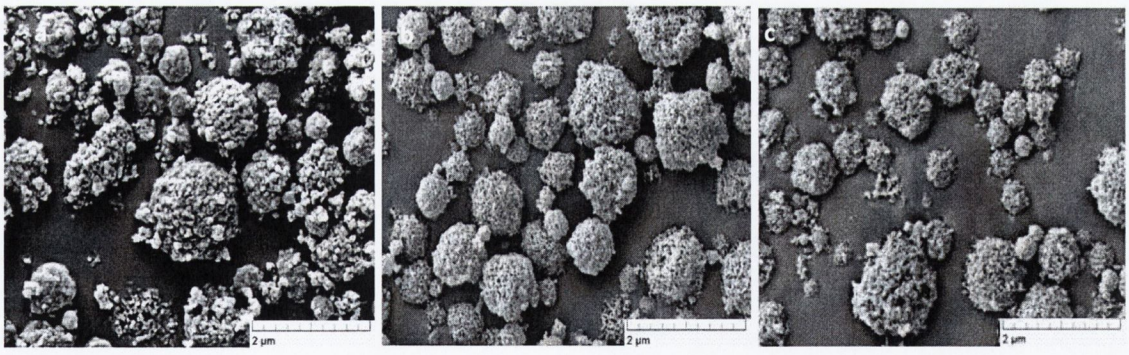

Figure 3.18 SE micrographs of spray dried trehalose NPMPs at different pump setting: (a) 25 %, (c) 30 % and (d) 35 %

Particle size volume distributions in all cases were narrow and monomodal with low span values (between 1.3 and 1.8 for raffinose and 1.1 and 2.0 for trehalose). The median particle size (d_{50}) for raffinose particles was in the range of 1.9–2.3 µm and for trehalose particles was in the range 2.0–2.1 µm (Table 3.7 and 3.8). No significant differences were found between raffinose samples ($p=0.136$) or trehalose samples ($p=0.426$).

True, bulk and tap density measurements of spray dried powders are presented in table 3.7 and 3.8. ANOVA analysis of true density and tap density showed significant differences ($p<0.05$) between spray dried samples for both types of sugars. Spray drying at a pump setting of 30% for raffinose and at 25 % for trehalose results in the production of powders with different true and tap density from spray drying at other pump settings. Bulk density of samples spray dried at pump setting of 25 % were significantly different ($p<0.05$) from samples spray dried at other pump settings. Bulk and tap densities were < 0.3 g/cm^3 making the powders suitable for pulmonary delivery (Bosquillon et al., 2004).

The aerodynamic diameter was calculated for all samples (Table 3.7 and 3.8). All spray dried powders complied with the diameter range of 1-3 μm which is desirable for central and distal deposition in the lungs (Hickey, 1996).

DSC scans of spray dried raffinose NPMPs powders showed a single glass transition step with no evidence of other thermal events (Figure 3.19 and Table 3.9). The T_g temperature ranged from 115.2 – 116.7 ^oC, with no statistically significant differences between samples ($p=0.123$).

DSC scans of spray dried trehalose NPMPs powders showed a single glass transition step followed by an exothermic peak and finally an endothermic event correspondent to the melting of the material (Figure 3.20 and table 3.9). As for raffinose powders, no significant differences were found between the glass transition temperatures ($p=0.098$). However, significant differences were found for the crystallisation and melting temperature onsets ($p=0.039$ and $p=0.002$ respectively).

Table 3.7 Particle size, true, bulk (bp) and tap (tp) density and calculated aerodynamic diameter (d_{aer}) of raffinose spray dried samples at different pump setting

Pump (%)	20	25	30	35
d_{10} (μm)	1.0±0.07	1.1±0.01	1.2±0.01	1.0±0.00
d_{50} (μm)	2.0±0.03	1.9±0.25	2.3±0.03	2.1±0.03
d_{90}(μm)	4.1±0.31	3.6±1.07	4.8±0.01	4.8±0.20
<1μm (%)	8.8±2.50	7.7±0.95	3.7±0.19	8.5±0.02
True density (g/cm^3)	1.54±0.01	1.54±0.00	1.65±0.01	1.55±0.01
bp (g/cm^3)	0.05±0.00	0.08±0.00	0.07±0.0	0.10±0.00
tp (g/cm^3)	0.09±0.00	0.14±0.01	0.14±0.01	0.16±0.00
d_{aer} (μm)	4.1±0.07	3.6±0.06	3.0±0.16	3.0±0.16

Table 3.8 Particle size, true, bulk (bp) and tap (tp) density and calculated aerodynamic diameter (d_{aer}) of trehalose spray dried samples at different pump setting

Pump (%)	25	30	35
d_{10} (µm)	1.1±0.00	1.1±0.11	1.2±0.05
d_{50} (µm)	2.1±0.11	2.1±0.05	2.0±0.20
d_{90}(µm)	5.4±0.62	4.4±0.74	5.0±2.52
<1µm (%)	6.6±0.20	9.8±1.30	9.1±1.94
True density (g/cm^3)	1.59±0.01	1.55±0.02	1.54±0.01
bp(g/cm^3)	0.05±0.00	0.09±0.01	0.10±0.00
tp (g/cm^3)	0.10±0.00	0.17±0.00	0.17±0.01
d_{aer} (µm)	2.5±0.01	2.6±0.03	2.6±0.01

Table 3.9 Glass transition temperature (T_g), recrystallisation temperature and enthalpy (T_c, ΔH_c) and melting temperature and enthalpy (T_m, ΔH_m) of raffinose and trehalose NPMPs spray dried at different pump setting

Pump (%)	**Raffinose NPMPs**	**Trehalose NPMPs**				
	T_g (°C)	**T_g (°C)**	**T_c (°C)**	**ΔH_c (J/g)**	**T_m(°C)**	**ΔH_m (J/g)**
20	115.6±0.76	-	-	-	-	-
25	115.2±0.23	120.8±0.26	174.5±0.58	119.1±0.43	211.0±0.01	145.4±1.51
30	116.7±0.21	120.8±0.07	164.8±0.69	116.1±2.46	211.5±0.05	145.3±2.89
35	115.2±0.71	121.1±0.05	180.4±8.47	119.5±11.50	211.3±0.01	144.7±1.32

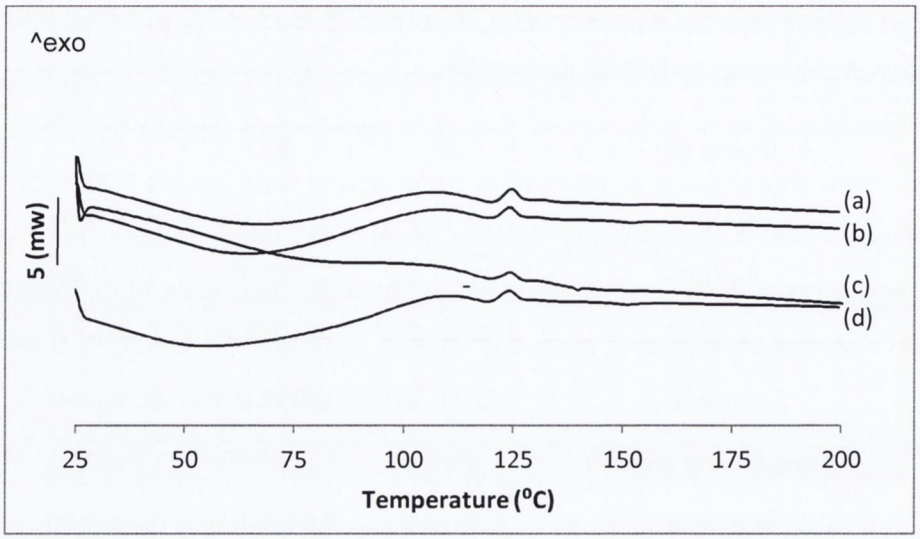

Figure 3.19 DSC scans of raffinose NPMPs spray dried at (a) 20 %, (b) 25 %, (c) 30 % and (d) 35 % pump setting

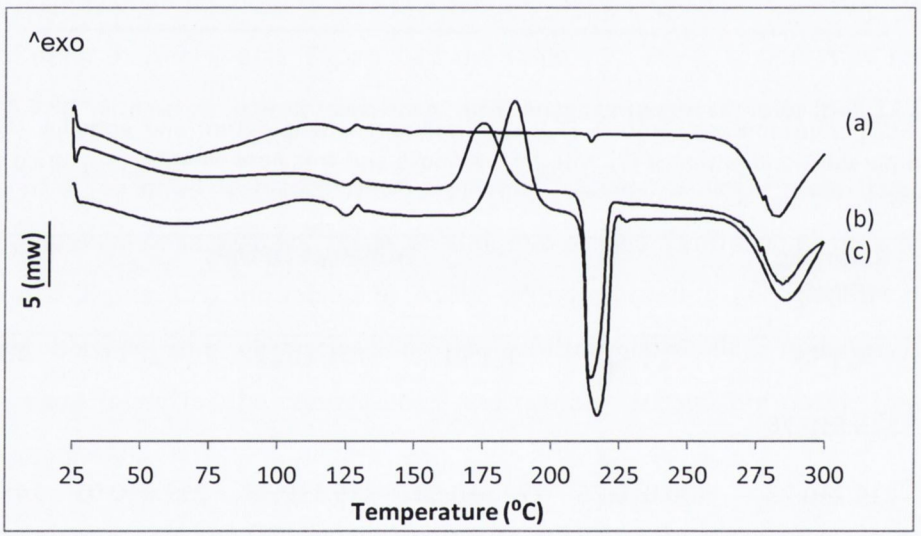

Figure 3.20 DSC scans of trehalose NPMPs spray dried at (a) 25 %, (b) 30 % and (c) 35 % pump setting

3.6 EFFECT OF FEED SOLUTION CONCENTRATION

Another relevant process condition studied was the feed solution concentration. The spray drying inlet temperature was kept constant at 120 °C and pump was set at 30% for raffinose and 35% for trehalose. The concentration range has been reported previously in Table 3.1.

The outlet temperature varied between 69.5 and 72 °C for raffinose and between 69 and 70.5 °C for trehalose with no statistically significant differences between samples of both sugars ($p=0.923$ for raffinose and $p=0.754$ for trehalose). Yields ranged from 57.7 to 61.9 % for raffinose and 54.9 to 61.1 % for trehalose. Figure 3.17*a* and 3.17*b* show an increase in powder yield when spray dying higher concentration solutions. This increase was not significant for raffinose

powder (p=0.263) nor for trehalose samples (p=0.187). Spray drying of more concentrated feed solutions results in the production of larger particles that are easier to separate and collect (Maury et al., 2005; Technical data Büchi B-290, 2009).

Particles produced were all spherical and porous (Figure 3.22 and 3.23) and all demonstrated amorphous halo patterns when analysed by XRPD.

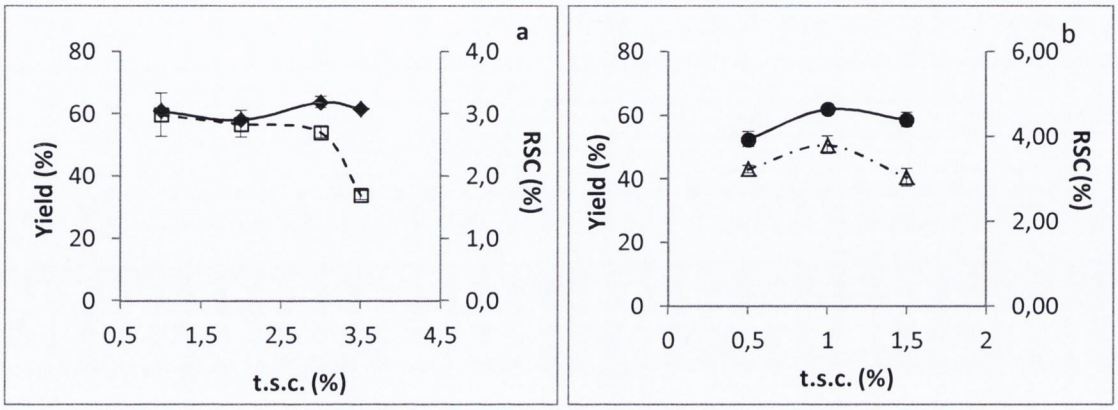

Figure 3.21 Powder yield (solid line) and residual solvent content (RSC) (dashed line) as function of total solid concentration (t.s.c.) of spray dried (a) raffinose NPMPs and (b) trehalose NPMPs.

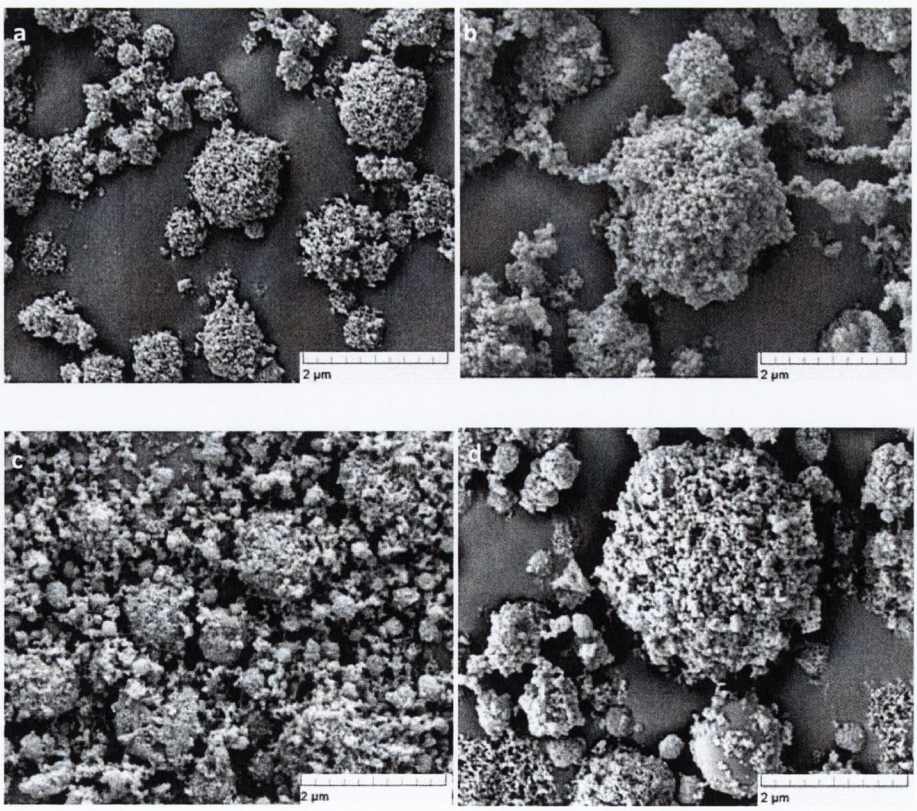

Figure 3.22 SE micrographs of raffinose NPMPs spray dried from (a) 1 %, (b) 2 %, (c) 3 % and (d) 3.5 % (w/v) feed solutions

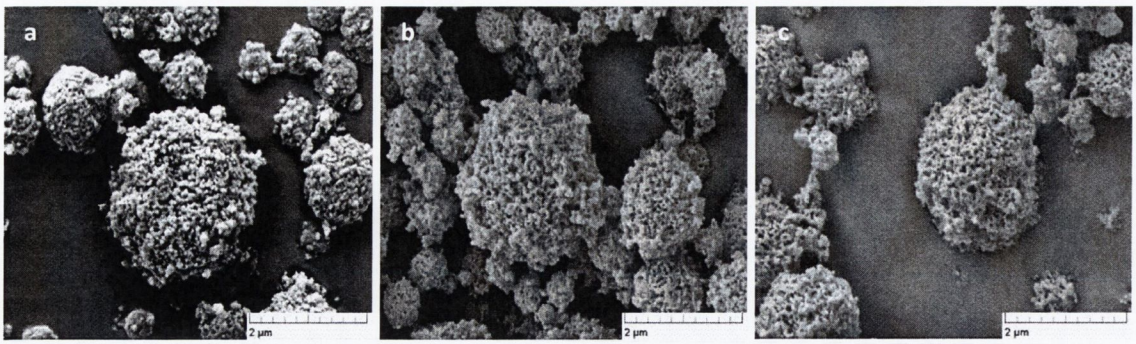

Figure 3.23 SE micrographs of trehalose NPMPs spray dried from (a) 0.5 %, (b) 1 % and (c) 1.5 % (w/v) feed solutions

Particle size data is presented in Tables 3.10 and 3.11. Spray drying of both sugars from concentrated feed solutions resulted in an increase in the geometric median particle size, as expected (Figure 3.24). The correlation between yield and d_{50} is represented in Figure 3.25; the expected result of increasing yield with increasing particle size was verified. Studies by Moran and Buckton (2007) on spray drying of different concentrations of trehalose aqueous solutions, also showed an increase in size with higher feed concentrations.

RSC was found to decrease with increasing solution solid content (Figure 3.21). The decrease was more significant for raffinose powders ($p=0.012$) with a reduction of ~1 % when increasing the t.s.c. from 3 to 3.5 %. As previously reported, larger droplets are formed with higher solid content; therefore less solvent is present to be removed. The non-existence of significant differences in outlet temperature of samples produced from variable solution concentration, results in a constant T_{inlet}-T_{outlet}, translating into an equal heat usage throughput in all experimental runs; consequently when the requirement of solvent evaporation is lower (i.e., less liquid is present) particles will be dryer.

The evaluation of bulk, tap and true densities of spray dried powders revealed an increase in these parameters when total solid concentration of spray dried solutions was increased (Table 3.10 and 3.11). Studies by Watson and Mumford (1999) have previously shown an increase in the bulk density of different spray dried products such as glucose, dextran, milk, among others, with increasing feed solution concentration.

Calculated aerodynamic diameter, being directly affected by particle size and density, increased when spray drying solutions with higher solid content (Table 3.10 and 3.11).

DSC scans of spray dried raffinose NPMPs powders showed a single glass transition step ranging from 115.1 -116.7 ^{o}C, with no evidence of other thermal events (Figure 3.27 and Table 3.12). Trehalose NPMPs DSC scans also presented a single glass transition step, 120.6 – 121.1 ^{o}C,

followed by an exothermic peak, 153.8 – 175.5 °C, corresponding to recrystallisation, the position of which shifted to lower temperatures as feed solution concentration increased (Figure 3.28 and Table 3.12). Lastly, an endothermic peak was recorded due to material melting at ~211 °C. In both spray dried products a trend was found of decreasing glass transition temperature with increasing material concentration in the feed solution (Figure 3.26).

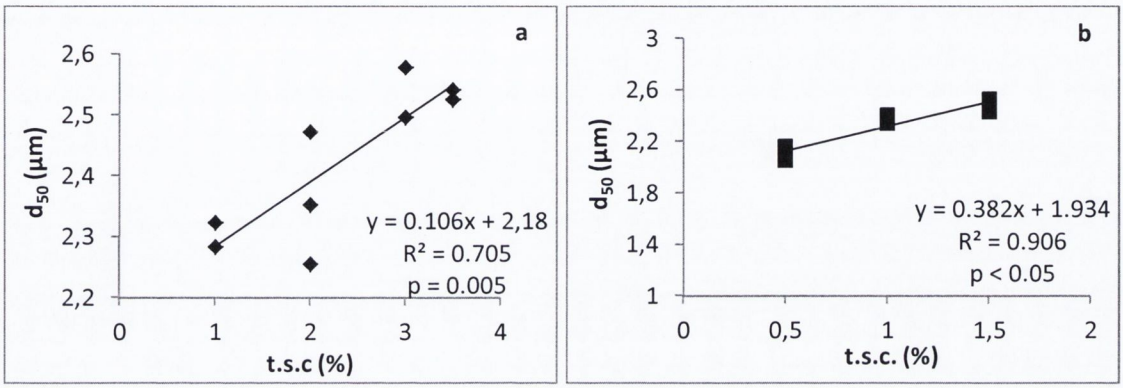

Figure 3.24 Geometric median particles size (d_{50}) as function of total solid concentration (t.s.c.) of (a) raffinose and (b) trehalose solutions

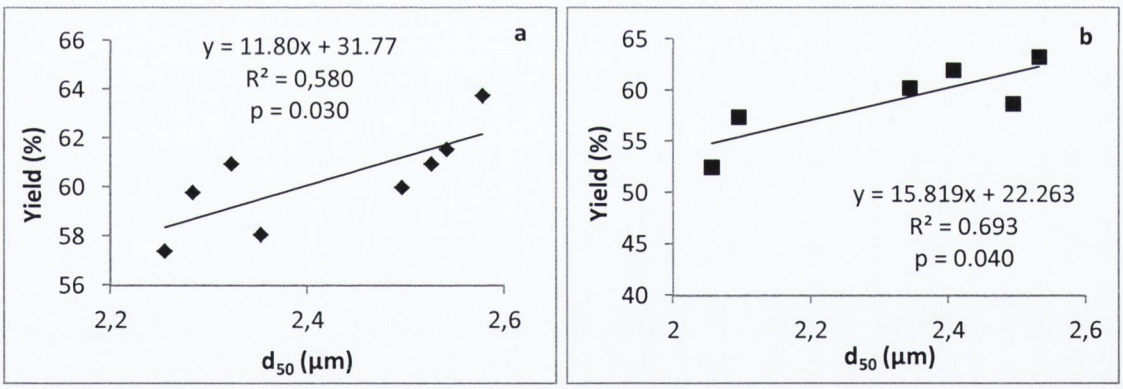

Figure 3.25 Spray dried powder yield of (a) raffinose and (b) trehalose as function of geometric median particle size (d_{50})

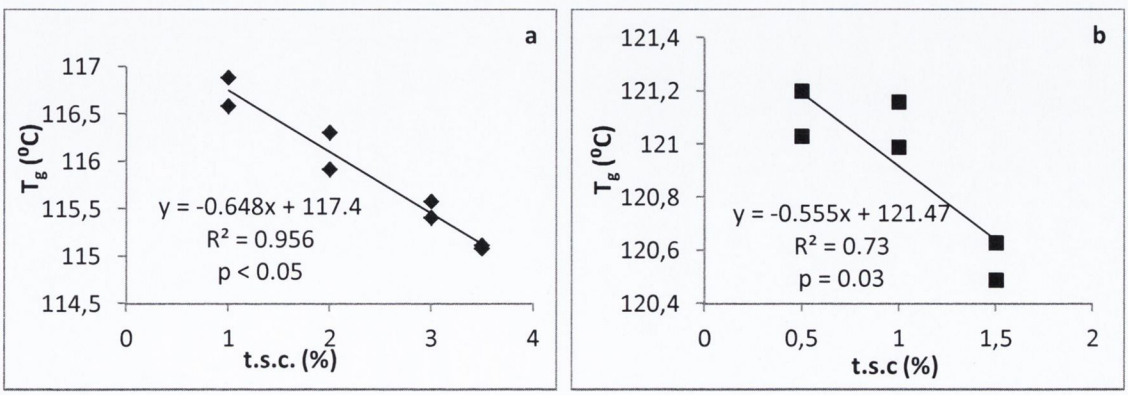

Figure 3.26 Glass transition temperatures (T_g) as function of total solid concentration (t.s.c.) of (a) raffinose and (b) trehalose solutions

Table 3.10 Particle size, true, bulk (bp) and tap (tp) density and calculated aerodynamic diameter (d_{aer}) of raffinose spray dried samples from different solid content solutions

t.s.c. (%)	1	2	3	3.5
d_{10} (µm)	1.2±0.01	1.3±0.01	1.2±0.01	0.8±0.08
d_{50} (µm)	2.3±0.03	2.4±0.01	2.5±0.06	2.5±0.01
d_{90}(µm)	4.8±0.01	4.6±0.04	5.4±0.12	5.3±0.03
<1µm (%)	3.7±0.19	3.6±0.26	5.5±0.08	5.0±0.05
True density (g/cm^3)	1.65±0.01	1.54±0.06	1.55±0.01	1.65±0.01
bp (g/cm^3)	0.07±0.0	0.11±0.00	0.13±0.01	0.13±0.01
tp (g/cm^3)	0.14±0.01	0.19±0.01	0.21±0.01	0.23±0.01
d_{aer} (µm)	3.0±0.16	2.9±0.06	3.2±0.01	2.8±0.10

Table 3.11 Particle size, true, bulk (bp) and tap (tp) density and calculated aerodynamic diameter (d_{aer}) of trehalose spray dried samples from different solid content solutions

t.s.c. (%)	0.5	1	1.5
d_{10} (µm)	1.2±0.05	1.3±0.02	1.2±0.05
d_{50} (µm)	2.0±0.20	2.4±0.05	2.5±0.05
d_{90}(µm)	5.0±2.52	4.6±0.30	5.5±0.15
<1µm (%)	9.1±1.94	5.2±0.11	5.6±1.99
True density (g/cm^3)	1.54±0.01	1.53±0.01	1.53±0.00
bp(g/cm^3)	0.10±0.00	0.11±0.00	0.10±0.00
tp (g/cm^3)	0.17±0.01	0.18±0.01	0.18±0.01
d_{aer} (µm)	2.6±0.01	2.9±0.01	3.1±0.00

Table 3.12 Glass transition temperature (T_g), recrystallisation temperature and enthalpy (T_c, ΔH_c) and melting temperature and enthalpy (T_m, ΔH_m) of raffinose and trehalose NPMPs spray dried at different feed concentrations.

	Raffinose NPMPs			Trehalose NPMPs		
t.s.c (%)	**T_g (°C)**	**T_g (°C)**	**T_c (°C)**	**ΔH_c (J/g)**	**T_m(°C)**	**ΔH_m (J/g)**
0.5	-	121.1±0.05	180.4±8.47	119.5±11.50	211.3±0.01	144.7±1.32
1	116.7±0.21	121.1±0.16	163.9±0.82	119.1±0.43	211.2±0.35	144.2±0.53
1.5	-	120.6±0.07	153.8±0.29	83.8±0.40	211.2±0.40	142.5±2.29
2	116.1±0.28	-	-	-	-	-
3	115.5±0.12	-	-	-	-	-
3.5	115.1±0.03	-	-	-	-	-

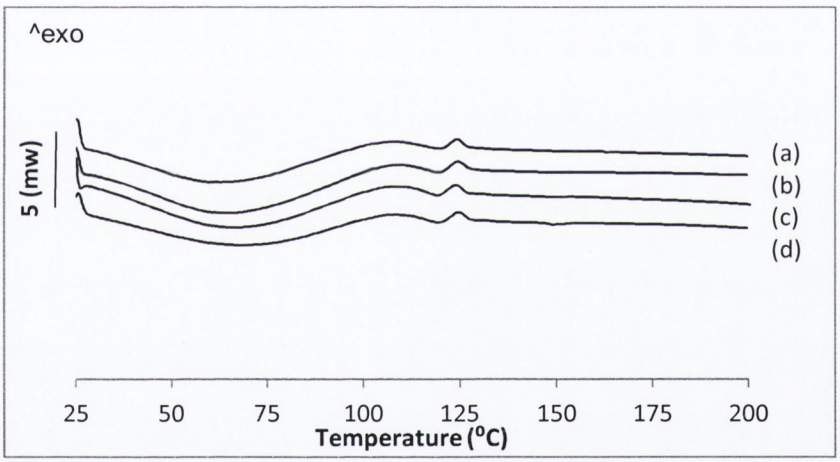

Figure 3.27 DSC scans of R NPMPs spray dried from solutions with different total solid concentration (t.s.c.): (a) 1 %, (b) 2 %, (c) 3 % and (d) 3.5 %.

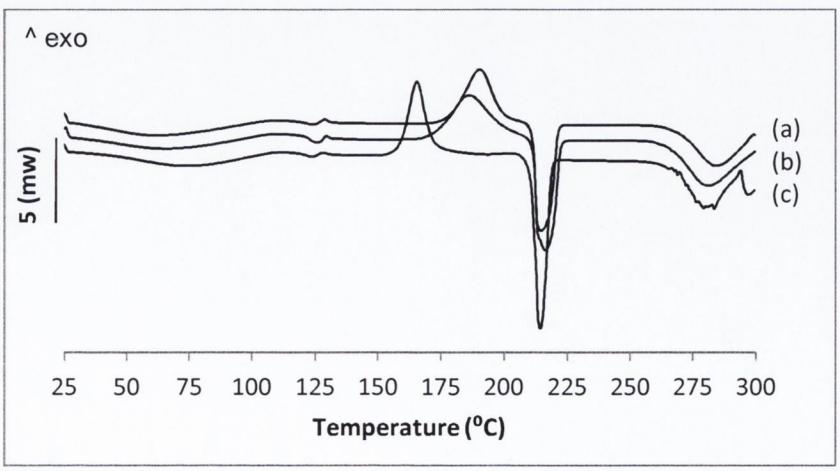

Figure 3.28 DSC scans of T NPMPs spray dried from solutions with different total solid concentration (t.s.c): (a) 0.5 %, (b) 1 % and (c) 1.5 %.

3.7 CONCLUSION

The one-factor-at-a-time study undertaken resulted in an enhancement of raffinose and trehalose NPMPs processing knowledge. Yield, particle size, true, bulk and tap density and residual solvent content were affected by the inlet temperature and feed solution concentration; outlet temperature and true, bulk and tap density by the inlet temperature and pump setting.

The best setting for spray drying sugar NPMPs was determined to be: inlet temperature at 120 ^{o}C, pump at 30 % for raffinose and 35 % for trehalose and a 2 % and 1 % (w/v) feed concentration solution for raffinose and trehalose respectively. These conditions result in powders with yields > 50 %, calculated aerodynamic diameter < 3 µm, low bulk and tap density and high glass transition, making them suitable to be used as carriers for pulmonary delivery.

Table 3.33 Effect of increasing spray drying process parameters on evaluated outcomes of raffinose NPMPs. T_{inlet} –inlet temperature; T_{oulet} –outlet temperature; RSC-residual solvent content; bp-bulk density

	T_{inlet}	Feed rate (pump)	Feed concentration
T_{outlet}	significantly increases	significantly decreases	no effect
Particle size	no effect	no effect	significantly increases
RSC	significantly decreases	no effect	significantly decreases
bp	variable	increases	increases
Yield	variable	increases	increases

Table 3.14 Effect of increasing spray drying process parameters on evaluated outcomes of trehalose NPMPs. T_{inlet} –inlet temperature; T_{oulet} –outlet temperature; RSC-residual solvent content; bp-bulk density

	T_{inlet}	Feed rate (pump)	Feed concentration
T_{outlet}	Significantly increases	Significantly decreases	no effect
Particle size	increases	no effect	significantly increases
RSC	significantly decreases	no effect	significantly decreases
bp	variable	increases	no effect
Yield	variable	increases	increases

CHAPTER 4

A 2^4 FACTORIAL DESIGN FOR THE OPTIMISATION OF RAFFINOSE AND TREHALOSE NPMPs SPRAY DRYING PROCESS

4.1 INTRODUCTION

Billon et al. (2000), Stähl et al. (2002), Al-Asheh et al. (2003) and Tajber et al. (2009) have used factorial design studies to optimise spray drying processes, proving the usefulness of such statistical tools in understanding the process, saving time and reducing material costs.

Maltesen et al. (2008) carried out a design of experiment on the spray drying of insulin intended for inhalation on a Büchi Mini spray dryer B-290 to understand the effects of process and formulation on powder/particle characteristics, such as yield, particle size, density, morphology and moisture content. Five variables were investigated: feed solution concentration, drying gas and feed flow rate, inlet air temperature and aspirator capacity. The variables with main effects on powder/particles characteristics were found to be feed concentration, inlet temperature and gas flow rate. A limited number of studies have investigated the effects of spray drying parameters on the production of trehalose and raffinose powders for inhalation. Maury et al. (2005) reported that the most important spray drying parameter to improve trehalose powder yield, for non-porous particles spray dried from aqueous solutions, was the inlet temperature, with the nozzle (a two-fluid nozzle with cap-orifice diameter of 0.7 mm) and aspirator setting have little influence. Ní Ógáin et al. (2011) studied the production of trehalose and raffinose nanoporous microparticles (NPMPs) for inhalation, evaluating different ratios of methanol:n-butyl acetate (MeOH:BA) solvent system, and concluded that NPMPs spray dried from 80:20 (v/v) MeOH:BA displayed favourable micromeritic characteristics suggesting potential suitability for pulmonary delivery. The porous morphology of the particles was found to improve the aerosolisation properties compared to equivalent non-porous spray dried particles. In the previous chapter a one-factor-at-a-time optimisation of the spray drying process of the work initiated by Ní Ógáin et al. (2011) was discussed. However, the study was limited in that it did not encompass the full complexity of the spray drying process and therefore may not have led to full optimisation of the production of powders intended for pulmonary delivery. Therefore, a 2^4 factorial design was undertaken with resulting powders characterised in terms of yield, particle size, thermogravimetric analysis and outlet temperature, as in studies by Tajber et al. (2009). An additional outcome evaluated was the specific surface area, as it is a reflection of porosity associated with porous particles such as the NPMPs (Healy et al., 2008).

Bosquillon et al. (2001) studied the effect of formulation excipients and physical characteristics of inhalation powders on their *in vitro* aerosolisation performance showing that fine particle fraction was affected by the excipient proportions and by the powder's tapped density. Ní Ógáin et al. (2011) showed that raffinose and trehalose NPMPs had higher fine particle fractions (FPF)

and higher specific surface areas (SSA) than the equivalent non-porous particle powders. Hence, a relation between SSA and the *in vitro* deposition of the sugar NPMPs powders was also investigated.

The European Pharmacopeia classifies methanol and butyl acetate as class 2 and class 3 residual solvents respectively (organic volatile chemicals that are used in the preparation of medicinal products and that have no therapeutic benefit (European Pharmacopoeia 7th Edition, 2012). Hence it is important to quantify their levels, in order to certify that these solvents are below the pharmacopoeial limits (5000 ppm for MeOH and 3000 ppm for BA), to explore methods for reduction of residual solvent content and to study possible alternatives to their use, such as replacement by another solvent. As such, a study on powder drying was performed and an attempt was made to produce raffinose and trehalose NPMPs by replacing butyl acetate with a solvent with a lower boiling point - propyl acetate.

4.2 Experimental design

A randomised 2^4 full factorial design with two replicates was devised to assess the effect of spray drying process parameters on powder production yield, particle size, specific surface area, residual solvent content and process outlet temperature. The parameters chosen to be studied were: (A) inlet temperature, (B) spray dryer airflow rate, (C) pump setting (feed solution flow rate) and (D) feed concentration. Each factor was studied at two levels: low and high (Table 4.1).

The setting for inlet temperature, pump setting and gas flow were based on preliminary one-factor-at-a-time studies where inlet temperature was varied between 90 and 140 °C and pump setting from 20 to 35%; practical work specifications were taken into account such as there being no condensation of the solution on the drying chamber during the process. The upper limit for feed concentration corresponds to the visually assessed limit of raffinose and trehalose solubility in the solvent mix used at room temperature.

The chosen factorial model was represented by:

$$Yi = \beta_0 + \beta_1 A + \beta_2 B + \beta_3 C + \beta_4 D + \beta_{12} AB + \beta_{13} AC + \ldots \quad \text{(Eq. 1)}$$

where β_n is the coefficient associated with factor, *n*, and the letters, *A*, *B*, *C*, etc., represent the factors (the spray drying parameters) in the model. Combinations of factors (such as *AB*) represent an interaction between the individual factors in that term. The equation coefficients were calculated using coded values, for purposes of direct comparison regardless of the factor

magnitude. A low response is coded as -1 and a high response as +1 (Montgomery, 1997; Tajber et al., 2009).

Statistical analysis of variance, ANOVA, was performed to determine the significance (p-value) and impact (F-value) of each main factor as well as their interactions. Parameters found to be significant at at least the 95% confidence level were included in the final prediction models.

Table 4.1 Process variables evaluated in the factorial study.

Parameters		Low (-)	High (+)	Units
A - Inlet temperature		90	150	°C
B – Gas flow		30	50	mm
C – Pump setting		15	40	%
D - Feed concentration	**Trehalose**	0.5	1.5	%
	Raffinose	1	3.5	

4.3 Evaluated outcomes

The design matrix and the data collected from the particle characteristics evaluated for each sugar are provided in Tables 4.2 and 4.3.

The coefficients of the final prediction models linking the spray drying and formulation parameters (in terms of coded factors) with responses are presented in Tables 4.4 and 4.5. To indicate the goodness of fit of these models the R^2 is also given in the latter tables.

To establish whether the model equations can estimate the response values well, the observed versus predicted values for each outcome evaluated were plotted. Figure 4.1a and 4.1b show a good linear relationship between observed and predicted particle size for raffinose (R^2=0.95) and trehalose (R^2=0.94) spray dried powders, where shown experimental points obtained by navigating the design space, are close to the regression line. A similar relationship was observed for the remaining outcomes.

In contrast to our results, studies by Baldinger et al. (2011) on the application of a two level full factorial design to the spray drying process of aqueous solutions with total solid concentration of 10% (w/v) containing a mixture of mannitol and trehalose in a mass ratio of 90:10 to produce inhalable dry powders, showed a poor linear relationship between the observed and predicted values obtained for the evaluated responses, using multivariate analysis as a statistical tool.

The latter study focused only on three parameters of the spray drying process: inlet temperature, atomisation air flow rate and feed solution flow rate. The full factorial design presented in the current study, also evaluates the effect of the drying gas flow rate and concentration of the feed solution on the physicochemical characteristics of the sugar nanoporous microparticles. The difference in parameters investigated and in the feed solution formulation may be the reason for the difference between the two studies.

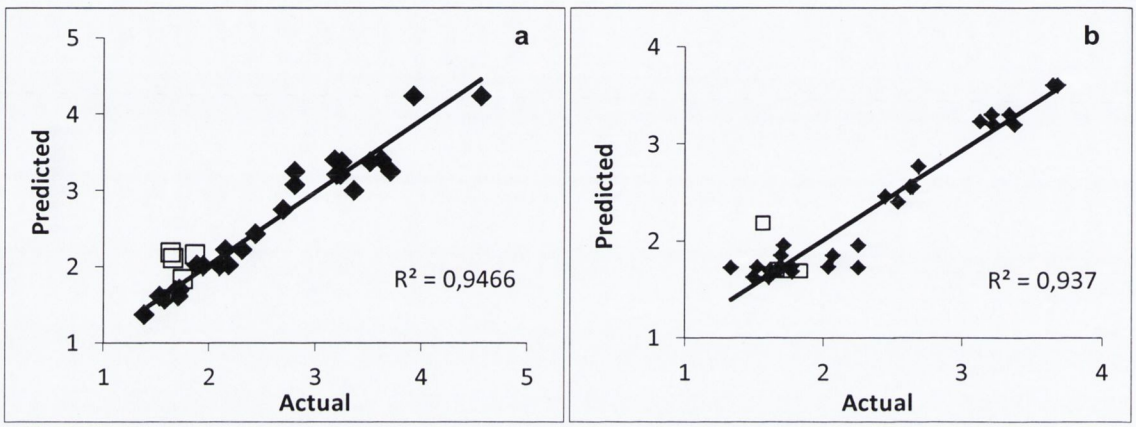

Figure 4.1 Correlation between actual versus predicted particle size (a) for raffinose NPMPs and (b) for trehalose NPMPs. Experimental points (squares) are also shown.

Table 4.2 Design matrix of raffinose spray drying and the data collected from the analyses.

Run	Inlet temp	Gas flow rate	Pump setting	Feed conc.	Yield (%)	PS (d_{50}) (μm)	Specific surface area (m^2/g)	Residual solvent content (%)	Outlet temp (°C)
1	+	+	-	-	30.2	1.4	61.51	3.4	96
2	-	+	-	+	49.4	1.9	67.58	2.7	58
3	-	-	+	+	63.7	3.9	28.02	4.6	52
4	+	+	+	-	45.4	1.7	67.63	2.3	84
5	-	-	+	-	57.2	3.2	25.53	2.4	90
6	+	+	+	+	59.8	1.9	51.86	2.7	89
7	+	-	+	-	65.9	3.4	31.22	1.7	90
8	+	+	-	+	51.6	1.7	51.73	1.6	92
9	-	-	+	+	59.8	4.6	30.27	4.4	52
10	+	-	+	-	57.9	2.8	45.03	3.2	89
11	-	+	+	-	42.6	1.7	74.59	3.2	49
12	+	+	+	+	58.3	2.1	28.91	2.1	85
13	-	-	-	+	59.6	3.5	30.00	1.6	62
14	+	-	+	+	65.6	3.6	27.06	2.6	89
15	+	-	-	-	61.9	2.4	38.79	2.4	99
16	-	-	-	-	52.0	2.7	26.76	4.0	60
17	-	+	+	+	57.4	2.3	48.88	3.0	48
18	-	-	+	-	56.3	3.2	30.22	2.7	51
19	+	+	+	-	41.2	1.7	51.66	2.5	82
20	+	-	-	-	63.1	2.4	32.96	3.1	99
21	-	+	+	+	55.6	2.2	62.16	2.6	48
22	+	+	-	-	37.0	1.4	59.85	3.3	94
23	+	-	-	+	64.6	3.7	26.53	2.8	94
24	-	-	-	+	43.0	3.3	43.21	1.6	60
25	+	+	-	+	37.6	1.5	61.15	1.7	93
26	-	+	-	-	38.4	1.6	80.34	2.5	58
27	-	-	-	-	53.8	2.8	53.21	2.7	61
28	-	+	-	+	49.0	2.2	67.20	3.3	56
29	-	+	+	-	39.3	1.7	61.08	3.1	50
30	+	-	-	+	44.0	3.7	28.69	2.5	101
31	-	+	-	-	38.5	1.6	72.96	2.5	57
32	+	-	+	+	71.6	3.6	30.99	2.6	89

Table 4.3 Design matrix of trehalose spray drying and the data collected from the analyses.

Run	Inlet temp	Airflow rate	Pump setting	Feed conc.	yield (%)	PS (d_{50}) (µm)	Specific surface area (m^2/g)	Residual solvent content (%)	Outlet temp (°C)
1	+	+	+	+	50.5	1.7	40.84	2.2	84
2	-	+	+	-	35.0	1.5	46.02	3.6	49
3	+	+	+	+	53.8	1.7	50.58	1.6	85
4	-	-	+	-	53.1	3.1	34.43	2.9	50
5	-	-	+	-	55.0	3.1	40.76	2.1	50
6	+	-	-	+	53.7	2.6	35.79	1.4	98
7	+	+	-	-	62.2	2.3	37.63	2.4	103
8	-	-	+	+	57.1	3.7	36.89	5.3	53
9	-	+	+	+	36.5	4.6	57.65	4.8	57
10	-	-	-	+	34.0	1.7	48.31	1.8	60
11	+	+	+	-	43.3	2.7	59.02	2.7	81
12	+	+	-	+	33.4	1.8	38.20	1.8	94
13	-	-	+	+	56.7	3.7	17.52	5.2	50
14	-	+	-	+	33.2	2.1	42.33	1.3	61
15	+	+	-	-	28.8	1.3	46.28	2.4	95
16	-	+	-	+	34.3	1.7	57.50	3.5	54
17	-	+	+	-	53.8	2.0	47.76	3.2	49
18	-	+	+	+	28.8	2.3	44.46	4.8	52
19	+	-	+	+	64.4	3.2	40.03	3.2	85
20	+	+	+	-	47.8	1.8	44.77	2.7	86
21	+	-	-	-	59.1	2.2	39.32	2.8	99
22	-	-	-	-	47.3	2.6	47.61	2.7	60
23	-	-	-	+	45.9	2.7	43.96	1.8	59
24	-	+	-	-	42.0	1.5	56.44	3.5	57
25	+	-	+	-	63.1	3.4	39.81	3.4	87
26	+	-	+	-	64.9	3.2	43.84	3.2	86
27	-	+	-	-	38.9	1.6	59.06	3.5	58
28	+	-	-	-	65.4	2.5	28.76	2.0	103
29	+	-	+	+	62.8	3.3	41.19	2.2	86
30	+	+	-	+	34.3	1.6	37.16	3.3	91
31	-	-	-	-	44.7	2.5	45.47	1.8	61
32	+	-	-	+	47.4	2.6	33.43	1.4	97

Table 4.4 Raffinose: Coefficients of the model equations linking the significant (at least $p < 0.05$) spray drying parameters (in terms of coded factors) with responses. I - intercept (β_0); A - inlet temperature; B - gas flow, C – pump setting; D – feed solution concentration; SSA – specific surface area; RSC - residual solvent content.

Term	Yield (%)	F-value	Term	PS (d_{50}) (µm)	F-value	Term	SSA (m^2/g)	F-value	Term	RSC (%)	F-value	Term	Outlet temp. (°C)	F-value
I	52.22		I	2.50		I	46.80		I	2.72		I	74.28	
B	-6.52	39.61	B	-0.72	267.39	A	-3.33	4.66	A	-0.19	6.66	A	17.28	190.30
C	3.87	13.95	C	0.20	20.58	B	13.77	79.79	AC	-0.18	6.26	B	-3.09	6.10
D	3.42	10.92	D	0.27	38.07	C	-3.36	4.74	CD	0.30	16.32	C	-3.22	6.60
BD	3.19	9.50				D	-4.03	6.85	BCD	-0.19	6.74			
									ABCD	0.37	25.35			
R^2	0.84		R^2	0.96		R^2	0.87		R^2	0.83		R^2	0.93	

Table 4.5 Trehalose: Coefficients of the model equations linking the significant (at least $p < 0.05$) spray drying parameters (in terms of coded factors) with responses. I - intercept (β_0); A - inlet temperature; B - gas flow, C – pump setting; D – feed solution concentration; SSA – specific surface area; RSC - residual solvent content.

Term	yield (%)	F-value	Term	PS (d_{50}) (µm)	F-value	Term	SSA (m^2/g)	F-value	Term	RSC (%)	F-value	Term	Outlet Temp. (°C)	F-value
I	47.98		I	2.35		I	43.21		I	2.85		I	73.13	
A	5.65	74.82	B	-0.59	229.24	A	-3.53	27.43	A	-0.45	31.19	A	18.13	1649.02
B	-6.67	104.24	C	0.21	28.87	B	4.64	47.35	C	0.54	46.10	C	-5.00	125.49
C	2.49	14.51	D	0.082	4.38	AC	4.34	44.15	AB	-0.21	6.71	AC	-1.25	7.84
D	-2.57	15.50	BC	-0.18	21.39	BC	1.73	6.59	AD	-0.14	13.33	AD	-1.00	5.02
BC	-2.47	14.32				BD	2.34	44.15	BC	-0.21	6.70	CD	1.13	6.35
CD	3.41	27.24				ABD	1.87	6.59	CD	0.44	29.77			
ABC	1.48	5.10							ACD	-0.34	18.02			
ACD	1.76	7.25												
ABCD	1.46	4.98												
R^2	0.94		R^2	0.93		R^2	0.91		R^2	0.91		R^2	0.98	

4.3.1 Production yield

Spray dried raffinose yields varied between 30.2 and 71.6%, and trehalose yields between 28.8 and 64.9 %. In both studies the yield increased with a decrease in gas flow rate (F-value 39.61 ($p<0.0001$) for raffinose and, F-value 104.24 ($p<0.0001$) for trehalose), with this variable having the greatest effect. Lower gas flow reduces atomisation energy producing larger particles, which are easier to capture in the cyclone (Technical data Büchi B-290, 2009; Stähl et al., 2002). Figure 4.2 supports this hypothesis showing a correlation between yield and particle size, where an increase in particle size results in an increase in yield.

Statistical analysis of the product yield values for raffinose powders demonstrated that among the main effects two have positive coefficients (an increase in the variable results in an increased response): pump setting and feed concentration, and one has a negative coefficient (an increase on the variable results in a decreased response): gas flow (Table 4.4). The inlet temperature was determined to be not significant ($p>0.05$). Stähl et al. (2002) and Tajber et al. (2009) also observed gas flow rate to have the largest effect on product yield, whereas Prinn et al. (2002) and Maltesen et al. (2008) demonstrated that feed solution concentration had the highest impact on yield, and that gas flow was a less impacting variable.

Studies in technical data Büchi B-290 (2009) on the characterisation of the effect of variable parameters on spray dried powders demonstrated that gas flow and feed solution concentration have a large influence on the resulting particle size.

Considering the existence of a correlation between yield and particle size (Figure 4.2), it is expected that particle size would have an influence on powder yield.

An interaction between gas flow and feed concentration (F-value 9.50) was found to be significant ($p=0.007$) in the present study for raffinose and positively correlated, reinforcing the importance of these parameters.

Statistical analysis of trehalose powder yield values revealed two positive main effects: inlet temperature and pump setting, and two negative main effects: gas flow and feed concentration (Table 4.5). The inlet temperature, as well as the gas flow, had a strong impact on production yields (F-value 74.82, $p<0.0001$), consistent with results reported by Maury et al. (2005) for trehalose spray dried from aqueous solution, where high T_{inlet} resulted in higher T_{outlet} leading to drier and less sticky powders, increasing the production yield. Several interactions among operating variables were detected for trehalose production yields: two factors, three factors and four factors (involving all main effects); showing how complex the spray drying process is and

how one parameter will affect the response from the remaining parameters (Table 4.5 and Figure 4.3). The strongest interaction was between pump setting and feed concentration (CD) (F-value 27.24, $p<0.0001$) with a positive coefficient.

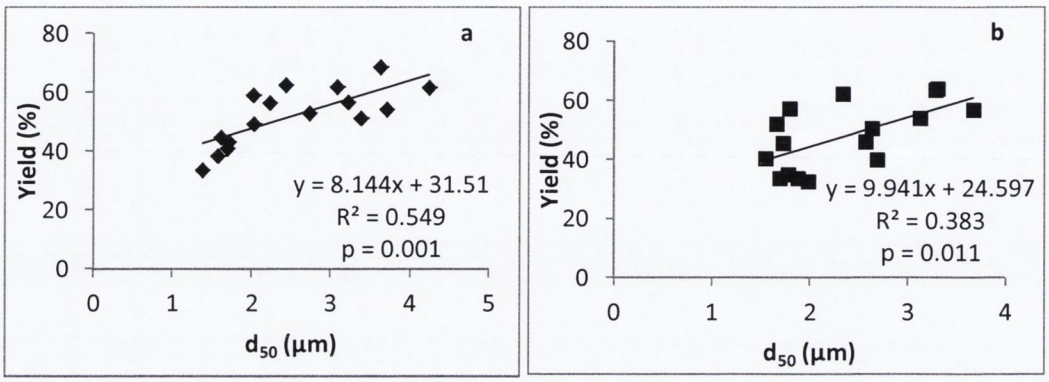

Figure 4.2 Influence of median particle size (d_{50}) on yield of (a) raffinose NPMPs (b) trehalose NPMPs.

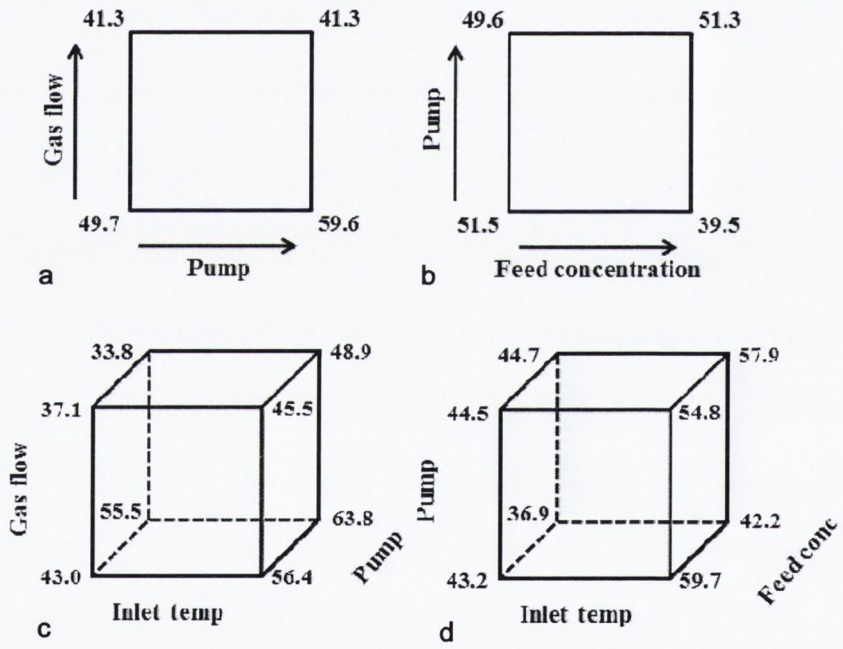

Figure 4.3. Impact of interactions between process variables on trehalose NPMPs yields: plot of interaction between (a) gas flow and pump setting and (b) feed concentration and pump setting; cube graph of interaction between (c) inlet temperature, gas flow and pump setting and (d) inlet temperature, pump setting and feed concentration

4.3.2 Particle size

Spray dried raffinose and trehalose powders consisted of small spherical and porous particles as shown by SEM (Figure 4.4). Particle size volume distributions in all cases were narrow and monomodal with low span values (between 1.2-2.3 for raffinose and 1.1-2.2 for trehalose). The

median particle size (d_{50}) for raffinose particles was in the range of 1.4-4.6 μm and for trehalose particles was in the range 1.3-4.6 μm.

In the case of raffinose powders, ANOVA indicated that only the main effects were significant at the 95% confidence level and can be regarded as impacting on the size of particles. The process parameter with the greatest influence was the gas flow (F-value 267.39, $p<0.0001$) followed by the feed concentration (F-Value 38.07, $p<0.0001$). There are a number of reports in the literature which indicate that the size of particles in spray drying is controlled by feed concentration, where larger particles are obtained from more concentrated solutions and lower atomisation levels (Elversson and Millqvist-Fureby, 2005; Technical data Büchi B-290, 2009). Lower gas flow reduces atomisation energy producing larger particles, which are easier to capture in the cyclone (Stähl et al., 2002; Technical data Büchi B-290, 2009). From the model equation, a negative coefficient for gas flow and positive coefficient for feed concentration was found, which means, as gas flow decreases and feed concentration increases larger particles are produced, which is consistent with previous reports (Stähl et al., 2002; Al-Asheh et al., 2003; Tajber et al., 2009).

Statistical analysis of trehalose powders showed only three main effects: gas flow, pump setting and feed concentration were statistically significant with regard to particle size. F-values for these parameters are 229.24 ($p<0.0001$), 28.87 ($p<0.0001$) and 4.38 ($p=0.048$), respectively. Maury et al. (2005) reported that an increase in pump setting at constant atomizing air flow rate resulted in larger spray droplets, hence larger particles. The coefficients of the model equation are negative for gas flow and positive for pump setting and feed concentration, i.e., as gas flow decreases and pump setting and feed concentration increases, particle size increases which is consistent with previous studies (Stähl et al., 2002; Al-Asheh et al., 2003; Maury et al., 2005; Tajber et al., 2009). ANOVA also revealed a significant (at the 95% confidence level) interaction between two main effects: gas flow and pump setting (BC) (F-value 21.39, $p=0.0001$) (Table 4.5).

In contrast to studies by Stähl et al. (2002), Al-Asheh et al. (2003) and Tajber et al. (2009), the inlet temperature had no significant effect on the particle size of raffinose or trehalose spray dried powders. The previous studies showed an increase in particle size with increasing inlet temperatures, due to agglomeration of particles at higher temperatures and to hardening of the droplet (Stähl et al., 2002; Al-Asheh et al., 2003).

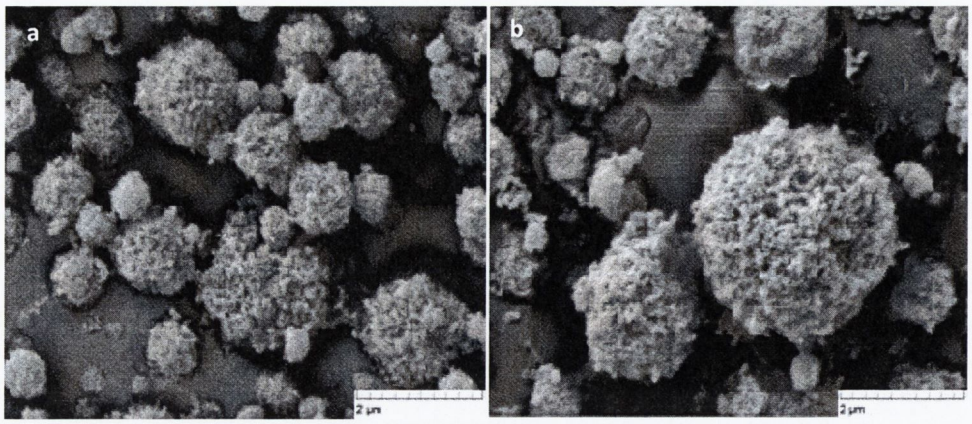

Figure 4.4 SEM micrographs for raffinose NPMPs (a) and trehalose NPMPs (b).

4.3.3 Residual solvent content

Residual solvent content ranged from 1.6 to 4.6 % for raffinose powders and from 1.3 to 5.3 % for trehalose powders.

ANOVA showed that the statistical model developed for the residual solvent content values of raffinose powders was significant (F-value 5.17, p=0.0011). The inlet temperature was the only statistically significant main effect impacting on the residual solvent content (F-value 6.66, p=0.0201) and it had a negative coefficient. With increasing inlet temperature, more energy is supplied to the drying chamber leading to more efficient solvent removal from the droplets. This results in powders with lower residual solvent content (Maury et al., 2005; Technical data Büchi B-290, 2009).

Also, several interactions were found below the established confidence level of 95% (Table 4.4 and Figure 4.6) and therefore deemed significant: a two-factor interaction between inlet temperature and pump setting (AC) (F-value 6.26, p=0.0201) and pump setting and feed concentration (CD) (F-value 16.32, p=0.0009), a three-factor interaction between gas flow, pump setting and feed concentration (BCD) (F-value 6.74, p=0.0195), and a four factor interaction between inlet temperature, gas flow, pump setting and feed concentration (ABCD) (F-value 25.35, p=0.0001).

The quantity of solvent to be evaporated is dependent on the inlet temperature and gas flow that affect the heat supply for droplet drying and on the pump setting and feed concentration that control the size and the solid and solvent content in the droplet. Raffinose NPMPs residual solvent content is the result of the effect of spray drying parameters on their own and of interactions between them.

ANOVA showed that the model established fitted the data obtained for trehalose powders well and was significant (F-value 10.86, $p<0.0001$). The main effects with major impacts were inlet air temperature (F-value 31.19, $p<0.0001$) and pump setting (F-value 46.10, $p<0.0001$). The impact of gas flow and feed concentration were not significant at the 95% confidence level. An increase in inlet air temperature will lead to a decrease in residual solvent content (negative coefficient, Table 4.5), in other words, an increased supply of heat energy will result in a more efficient drying. Pump setting is positively correlated with residual solvent content. When the pump speed is higher, more liquid is supplied to the drying chamber and more solvent vapour is generated, decreasing the exhaust temperature leading to a less efficient drying, hence higher residual solvent content (Maury et al., 2005; Technical data Büchi B-290, 2009). A lower pump setting should result in a higher outlet temperature and therefore more efficient drying, resulting in lower residual solvent contents (Figure 4.5).

Statistical analysis also revealed significant two-factor interactions between the following parameters: inlet temperature and gas flow (AB) (F-value 6.71, $p=0.0197$), inlet temperature and feed concentration (AD) (F-value 13.33, $p=0.0022$), gas flow and pump setting (BC) (F-value 6.70, $p=0.0198$) and pump setting and feed concentration (CD) (F-value 29.77, $p<0.0001$) and a three-factor interaction was determined between inlet temperature, pump setting and feed concentration (ACD) (F-value 18.02, $p=0.0006$) (Figure 4.7).

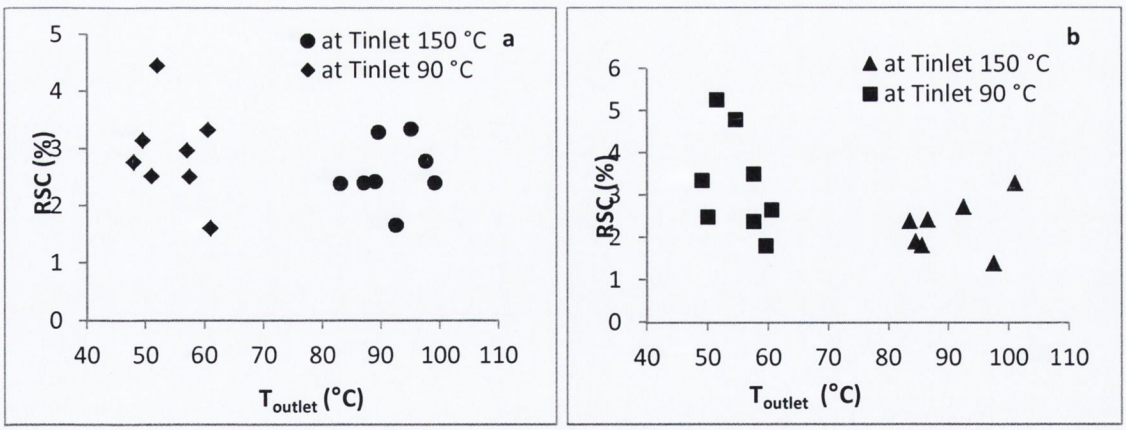

Figure 4.5 Influence of outlet temperature on residual solvent content (RSC) for (a) raffinose NPMPs and (b) trehalose NPMPs.

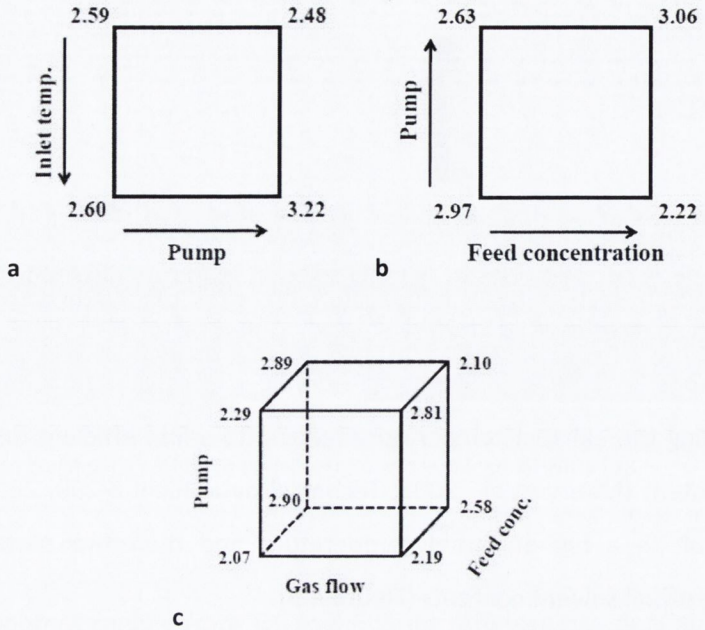

Figure 4.6 Impact of interactions between process variables on raffinose powder residual solvent content: plot of interaction between (a) inlet temperature and pump setting, (b) pump setting and feed concentration: (c) cube graph of interaction between pump setting, gas flow and feed concentration.

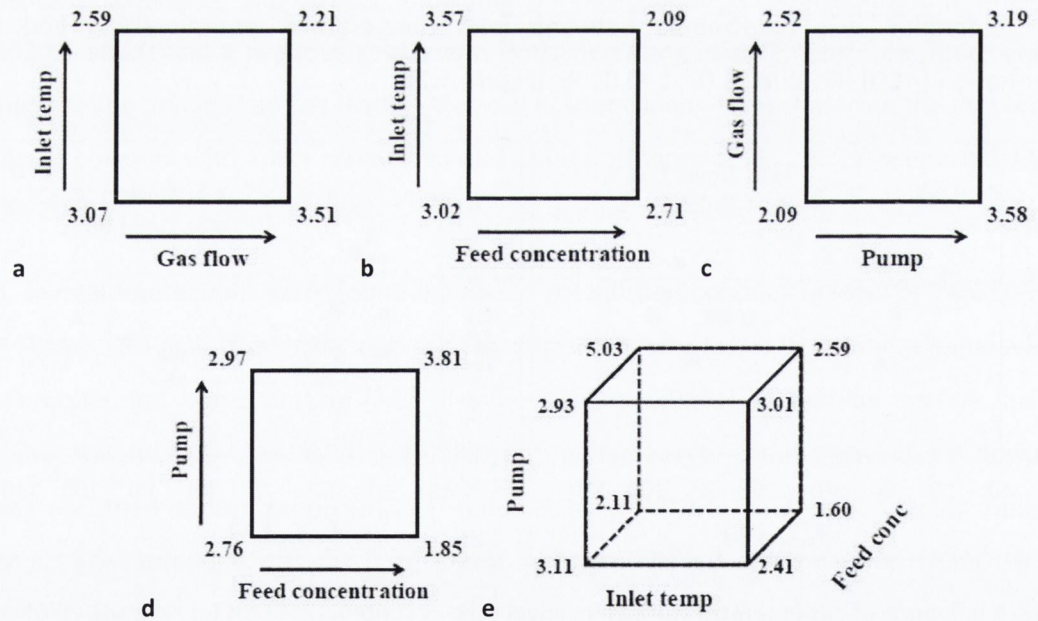

Figure 4.7 Impact of interactions between process variables on trehalose powder residual solvent content: plot of interaction between (a) inlet temperature and gas flow, (b) inlet temperature and feed concentration (c) gas flow and pump setting and (d) pump setting and feed concentration; (e) inlet temperature, pump setting and feed concentration.

4.3.4 Outlet temperature

The outlet temperature varied between 48 and 101 °C for raffinose spray drying, and between 49 and 103 °C for trehalose spray drying. This response was mainly affected by the inlet air temperature and pump setting, shown to be significant at the 95% confidence level, for both sugars (Table 4.4 and 4.5).

Increased inlet temperature leads to an increased supply of heat energy, leading to higher outlet temperatures (Tajber et al., 2009). Referring to the model equations for both sugars (Table 4.4 and 4.5), a positive correlation was found, i.e., higher setting of the inlet temperature resulted in higher outlet temperatures.

At a higher pump setting, more liquid is supplied to the drying chamber and more solvent vapour is generated, therefore decreasing the exhaust temperature (Maury et al., 2005; Büchi, 2009). The model equations, for raffinose and trehalose spray drying, showed negative coefficients for pump setting, i.e., as pump setting decreases, outlet temperature increases. Stähl et al. (2002) and Maltesen et al. (2008) reported the same effect for spray drying of insulin particles.

For the purpose of this study a high outlet temperature is desirable, leading to drier powders and higher yields. This can be seen on figure 4.5 which displays the relationship between the residual solvent content and the outlet temperature, where higher temperatures are observed to result in lower solvent residue content. A similar study by Billon et al. (2000) demonstrated the same relationship.

4.3.5 Specific surface area

Porous microparticles have potential advantages over non-porous materials as they have reduced interparticulate attractive forces and improved flow characteristics, low bulk densities and exhibit smaller aerodynamic diameters than their geometric diameters, facilitating greater deposition in the lower pulmonary region, with potential for improved efficiency of administration to the lungs in the dry form (Healy et al., 2008). The presence of porosity leads to high specific surface area (SSA) values (Papelis et al., 2003; Healy et al., 2008).

SSA values ranged from 25.53 to 80.34 m^2/g for raffinose particles and from 17.52 to 59.02 m^2/g for trehalose particles.

Evaluating results from raffinose powders, ANOVA calculations determined that the main effect with an impact on SSA was the gas flow (F-value 79.79, $p<0.0001$). The other main effects (inlet

temperature, pump setting and feed concentration) influenced the surface area at a lower level (12 to 17 fold less) with $p<0.05$. No interactions between factors were significant at $p<0.05$. The coefficients of the model equation are given in Table 4.4. Three of the main effects have a negative coefficient i.e. inlet temperature (A), pump (C) and feed concentration (D), indicating that when any of these factors decrease, particles with higher surface area are produced. One main effect has a positive coefficient i.e. gas flow (B), giving particles with higher surface area when at higher levels.

ANOVA evaluation of trehalose values showed that the main effects with a significant impact on SSA were inlet temperature (F-value 27.43, $p<0.0001$) and gas flow (F-value 47.35, $p<0.0001$). The strongest interaction was between inlet temperature and pump setting, with F-value of 44.15 ($p< 0.0001$).

According to Gregg and Sing (1982), when considering a non-porous particle, the surface area is inversely proportional to particle size; Figure 4.8a and 4.8b show this relationship for surface area estimated from particle size data, assuming non-porous spherical particles of raffinose and trehalose. Taking into account the porosity of our particles, a correlation between actual measured surface area and particle size was investigated (Figure 4.8c and 4.8e). The correlation was found to be strong for raffinose particles ($R^2=0.74$, $p<0.001$) and weak for trehalose particles ($R^2=0.28$, $p=0.0421$), where, as particle size increases surface area decreases.

In this study we have observed that the particle size decreases with increased gas flow, decreased feed concentration and reduced pump setting. The existing relationship between particle size and specific surface area would lead us to think that the same variables would have an impact on SSA. This hypothesis is valid for the studies on raffinose powders (Table 4.4), since the process parameters gas flow, pump setting and feed concentration impacted on SSA in the same way as on particle size.

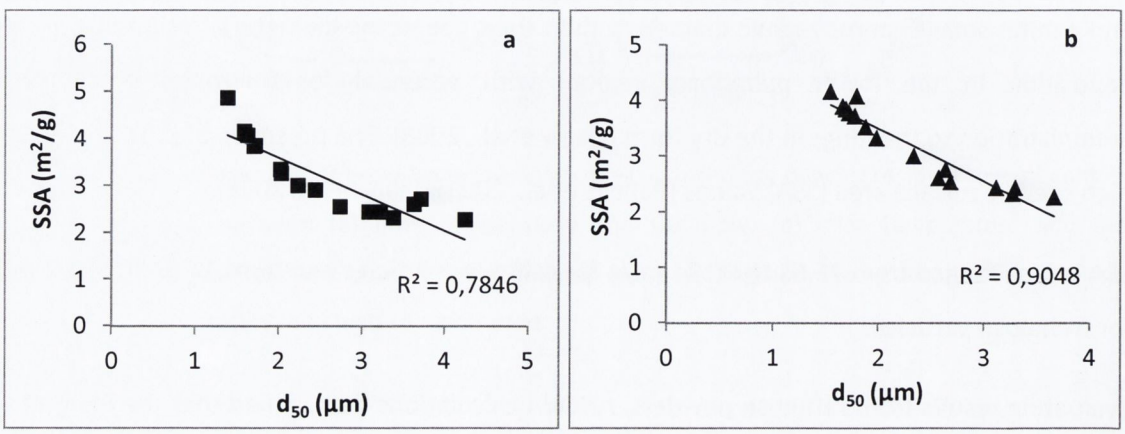

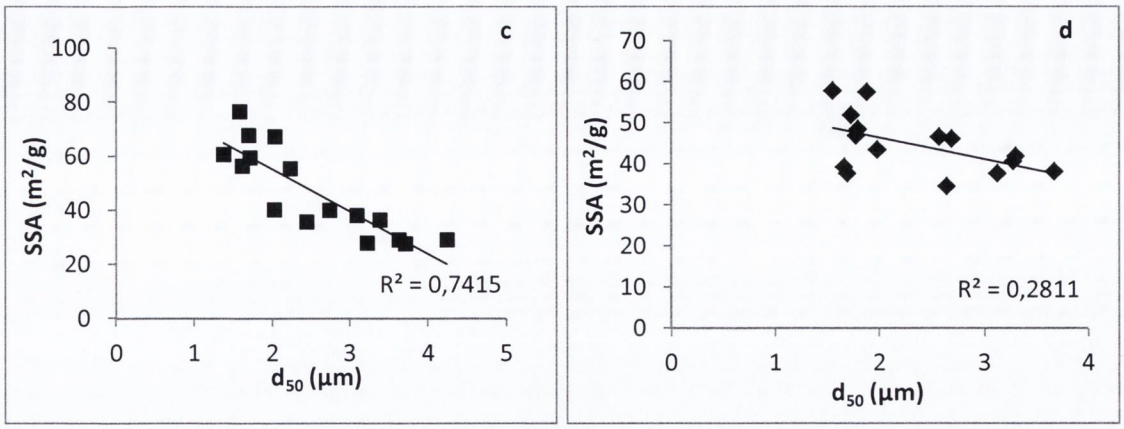

Figure 4.8 Relationship between particle size (d_{50}) and specific surface area (SSA) for (a) raffinose particles where particles are assumed non-porous and the SSA is derived from particle size data, (b) trehalose particles where particles are assumed non-porous and the SSA is derived from particle size data (c) raffinose NPMPs, taking the actual measured SSA and (d) trehalose NPMPs, taking the actual measured SSA.

4.3.5.1 Effect of particle specific surface area on aerosolisation properties

The effect of the specific surface area (SSA) of particles on the fine particle fraction below 5 µm (FPF) of powders was studied for powders produced with the same particle size (d_{50}) and different SSA. Preliminary aerodynamic studies on the NPMPs established that particles with a median particle size of ~1.7 µm had an aerodynamic diameter of ~2 µm. NPMPs of raffinose and trehalose were therefore spray dried using the process parameters determined by applying the model equations to yield powders with a d_{50} value of 1.7 µm but with SSA of minimum, average and maximum value in order to have three representative points within the design space.

For raffinose and trehalose NPMP powders a trend was observed where, as the SSA of porous particles increased a higher FPF could be achieved (Figure 4.9), reaching a FPF of more than 50% at the highest SSA values. Table 4.6 shows the obtained mass median aerodynamic diameter (MMAD) and geometric standard deviation (GSD) for raffinose and trehalose powders.

Ní Ógáin et al. (2011) showed that raffinose and trehalose NPMP powders had higher FPF than the non-porous particles powders as well as higher SSA, by ~40-fold.

The main difficulty associated with inhalation of fine particle powders and their efficient delivery is the strong interparticle forces (mainly van der Waals forces) which make the cohesive bulk powder agglomerate (Daniher et al. 2008). The cohesion between non-porous particles by contact surfaces is proportional to the specific surface area (Chew et al., 2000).

Studies by Tabor (1977) demonstrated that surface roughness can greatly reduce the adhesion between solids, due to the high surface asperities, which can prize the surfaces apart and break the adhesions occurring at the lower asperities.

Our results lead us to believe that the high surface area of NPMPs, due to high porosity, resulted in particles presenting fewer areas of contact, leading to lower cohesion and easier dispersion, resulting in high FPFs.

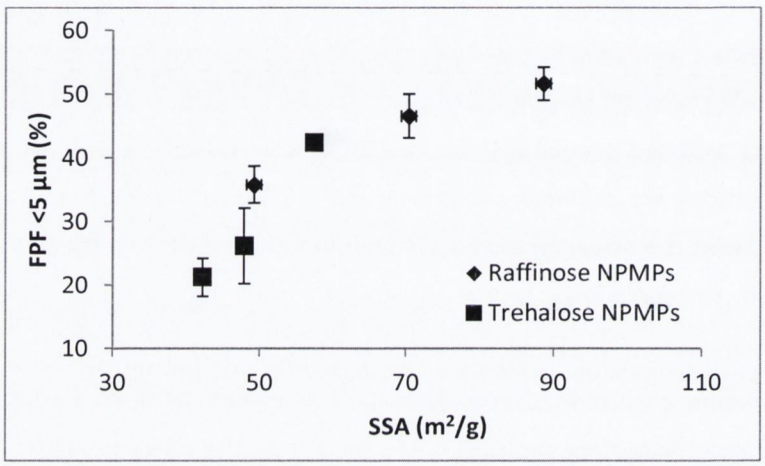

Figure 4.9 Effect of specific surface area (SSA) on the fine particle fraction of spray dried raffinose NPMPs (R^2=0.973, p=0.0004) and trehalose NPMPs (R^2=0.978, p=0.0007).

Table 4.6 Mass median aerodynamic diameter (MMAD), geometric standard deviation (GSD) and geometric median particle size (d_{50}) for raffinose and trehalose powders with increasing specific surface area (SSA).

	SSA (m^2/g)	MMAD (µm)	GSD	PS (d_{50}) (µm)
	49.26±0.42	3.3±0.14	2.1±0.09	1.7±0.02
Raffinose	70.39±0.68	3.4±0.33	2.4±0.14	1.6±0.01
	88.66±0.79	3.6±0.51	2.6±0.09	1.8±0.01
	42.28±0.30	8.4±1.37	3.4±0.53	1.7±0.07
Trehalose	47.89±0.13	7.4±0.13	3.4±0.77	1.7±0.04
	57.41±0.73	4.3±0.35	2.8±0.09	1.7±0.02

4.4 Prediction of optimal process conditions

A theoretical optimisation can be performed using the statistical models obtained to find the optimal settings of the spray drying parameters to achieve a product with desired properties. Raffinose and trehalose NPMP production was optimised in order to obtain powders with minimum residual solvent content (RSC), particle size (PS) < 3 μm, high specific surface area (SSA) and yield ≥ 50%. A higher importance was ascribed to minimising residual solvent content, followed by maximising SSA. The European Pharmacopeia classifies methanol as class 2 and butyl acetate as class 3 residual solvents (organic volatile chemicals that are used in the preparation of medicinal products and that have no therapeutic benefit (European Pharmacopoeia 7th Edition, 2012). Hence it is important to minimise their levels in the sugar NPMPs powders in order for these to be suitable for human use. Also, we have shown that a higher value of SSA will lead to higher fine particle fraction and should optimise pulmonary delivery.

Predicted optimal settings for raffinose NPMPs were as follows: T_{inlet} 150 °C, gas flow rate 50 mm (1052 l/h), pump rate 30 % (8.5 ml/min) and 2.9% total solid concentration in the feed solution. For trehalose NPMPs the process conditions should be: T_{inlet} 150 °C, gas flow rate 50 mm (988 l/h), pump rate 40 % (11.4 ml/min) and 1% total solid concentration in the feed solution. Using these suggested process variables the resulting outlet temperature was predicted to be 87 °C for raffinose and 86 °C for trehalose.Table 4.7 presents the predicted and actual results of the optimisation of the studied outcomes.

The results for outlet temperature, residual solvent and particle size were similar to the predicted values and within the standard deviation of the experimentally determined results. Yield and surface area values were higher than predicted. Thus, the outcome in terms of these latter parameters was even better than predicted by the model.

Table 4.7 Predicted and actual results of the optimisation of the studied outcomes for raffinose and trehalose NPMPs powders using the statistical models obtained by the applied DOE. PS –particle size SSA – specific surface area RSC- residual solvent content T_{outlet} – outlet temperarure

	Raffinose NPMPs		Trehalose NPMPs	
Outcome	**Predicted**	**Actual**	**Predicted**	**Actual**
Yield (%)	50	57.7±1.6	49	57.1±2.4
PS (d_{50}) (μm)	1.8	1.8±0.02	1.7	1.6±0.04
SSA (m^2/g)	49.97	58.16±0.51	45.53	51.44±0.49
RSC (%, w/w)	2.2	2.6±0.34	2.3	2.5±0.49
T_{outlet} (°C)	87	85±1.4	86	86±0.0

4.5 Residual solvent content of raffinose and trehalose NPMPs powders

Residual solvents have no therapeutic benefit, they are organic volatile chemicals that are used or produced in the manufacture of active substances or excipients, or in the preparation of medicinal products and, these should be removed to the extent possible, since some are known to cause unacceptable toxicities (European pharmacopoeia 7th Edition, 2012). The concentration limits for permitted daily exposure stated by the pharmacopoeia for methanol and butyl acetate are 3000 ppm and 5000 ppm respectively (European pharmacopoeia 7th Edition, 2012). These limits apply to the active principal ingredient, excipients and medicinal product.

GC-FID was used for quantifying the residual content of methanol and butyl acetate. Raffinose NPMPs were found to contain 0.3±0.01 % (w/w) (3122±129 ppm) of MeOH and 0.8±0.02 % (w/w) (7231±122 ppm) of BA while trehalose NPMPs were found to contain 0.4±0.06 % (w/w) (3731±437 ppm) of MeOH and 1.0±0.003 % (w/w) (9879±23 ppm)of BA. Therefore, 15 to 50 % of the residual solvent content was constituted by organic solvents, the remainder being attributed to bound and un-bound moisture.

Removal of the organic solvents was tested by subjecting two batches of freshly produced raffinose NPMPs powders to a nitrogen gas purge at 25 °C. The conditions used were those also used in the sample preparation for specific surface area analysis and that are known not to affect powder micromeritic properties (Ní Ógaín et al., 2008).

Figure 4.10 represents the percentage of residual solvent over the 24 hours of exposure to the nitrogen purge. After 2 to 6 hours it was no longer possible to detect methanol (LOD=305ppm=0.15 % (w/w)). Butyl acetate content was reduced to ~50 % in the first two hours of drying, after which it slowly reduced until a constant level of ~0.4 % (w/w) (4020±163 ppm) was achieved.

The levels of methanol and butyl acetate after raffinose and trehalose NPMPs spray drying were below the pharmacopoeial limits; reduction and elimination of these solvents is possible by storing the produced powders under a nitrogen purge at 25 °C for 24h.

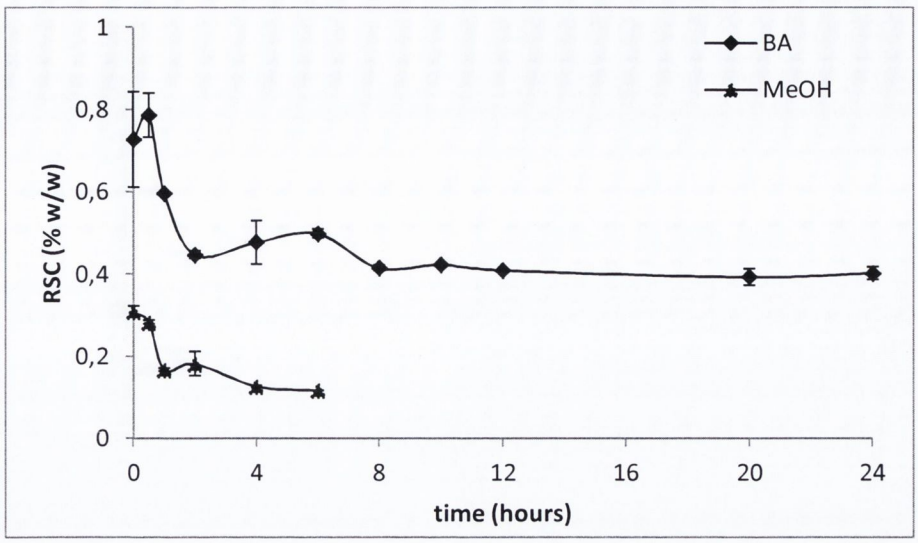

Figure 4.10 Residual solvent content (RSC) of spray dried raffinose NPMPs powders during exposure to a nitrogen purge over 24 hours.

4.6 Spray drying raffinose and trehalose NPMPs from a methanol:propyl acetate co-solvent system

Raffinose NPMPs were found to contain 0.3±0.01 % (w/w) (3122±129 ppm) of MeOH and 0.8±0.02 % (w/w) (7231±122 ppm) of BA while trehalose NPMPs were found to contain 0.4±0.06 % (w/w) (3731±437 ppm)of MeOH and 1.0±0.003 % (w/w) (9879±23 ppm)of BA. Therefore, the possibility of replacing BA with propyl acetate (PA) which has a lower boiling point (76.5 – 77.5 °C for PA and 124 - 126 °C for BA) was investigated, in order to produce powders with lower residual solvent content and similar physicochemical and aerodynamic characteristics.

4.6.1 Yield, solid-state, morphology and micromeritic properties

Spray drying settings followed the optimised conditions discused in section 4.4. Solutions of 2.9 % (w/w) raffinose and 1 % (w/w) trehalose were prepared in different MeOH:PA co-solvent system ratios: 65:35, 70:30 and 80:20. Outlet temperature varied between 86 - 89 °C for raffinose and 85 - 88 °C for trehalose. No statistically significant differences were found between spray drying outlet temperatures of the different samples ($p = 0.306$ for raffinose and $p = 0.081$ for trehalose).

Production yield varied from 37.1±2.2 to 49.6±3.4 % for raffinose and 36.7±5.2 to 50.7±3.9 % for trehalose. Highest yields were obtained when spray drying from solutions with 70:30 MeOH:PA ratio. In all runs, powder sticking to the cyclone walls was observed. No significant correlation was found for either of the non-reducing sugars between the influence of proportion of propyl acetate in the spray drying solution and the powder yield ($r^2=0.352$ and $p=0.214$ for raffinose

and, r^2=0.308 and p=0.252 for trehalose). Comparing with the resulting yields when spray drying from the MeOH:BA co-solvent system (57.7±1.6 % raffinose; 57.1±2.4 % trehalose) the attained yields when spray drying from MeOH:PA solutions were poorer. Therefore, in order to attain higher yields it may be necessary to adjust the process settings, by establishing a design of experiments such as the one described earlier in this chapter.

All raffinose powders produced were amorphous by XRPD analysis (Figure 4.11a). The same was not evident for trehalose (Figure 4.11b), though samples were predominantly amorphous, small peaks are visible (marked with arrow).

Particle morphology, assed by SEM, revealed these were porous, with improvement of particle shape from irregular shape to spherical with an increasing fraction of propyl acetate in the co-solvent system (Figure 4.13). Particles could be classified, according to the classification system developed by Paluch et al. (2012), as: type 1BIIIα for samples produced from solutions with 30 and 35 % (v/v) PA, type 2BIIIα and type 2BIIα (marked with red circle, Figure 4.13c) for raffinose samples spray dried from solution with 20 % (v/v) PA, and type 2BIIβ for trehalose samples spray dried from solution with 20 % (v/v) PA. Spray dried raffinose and trehalose powders from MeOH:BA 80:20 consisted of small spherical and porous particles, type 1BIIIα, as shown in figure 4.13.

Esposito et al. (2000) studied the impact of different co-solvents systems, ethanol (EtOH):Water, MeOH:Water, acetonitrile/water and pure acetonitrile on spray-dried eudragit particle morphology concluding that it was dependent on the material solubility in the studied solvent or co-solvent mixture and on how the evaporation of the solvent occurs during particle formation in the spray drying chamber. Ni Ógáin et al. (2010) spray-dried raffinose and trehalose from different co-solvent systems: EtOH:Water and MeOH:BA and reported different particle morphologies depending not only on the type of solvent but also on the ratio of the co-solvent system, as well as, the importance and impact of excipient/drug solubility in the solvent systems on particle morphology. The formation of raffinose and trehalose NPMPs was also fully described in this study. Therefore, the different morphologies attained when spray drying raffinose and trehalose from different co-solvent system ratios is probably due to differences in the evaporation of propyl acetate compared to butyl acetate, as well as to the solubility of sugars in propyl acetate. Additionally it was seen that trehalose systems are not fully amorphous; Vehring (2007) has reported that the solid state of materials can affect particle morphology by changing the solvent evaporation rate. Also, non-reducing sugars NPMPs can be produced when spray-dried from a MeOH:PA solution at ratios 70:30 and 65:35.

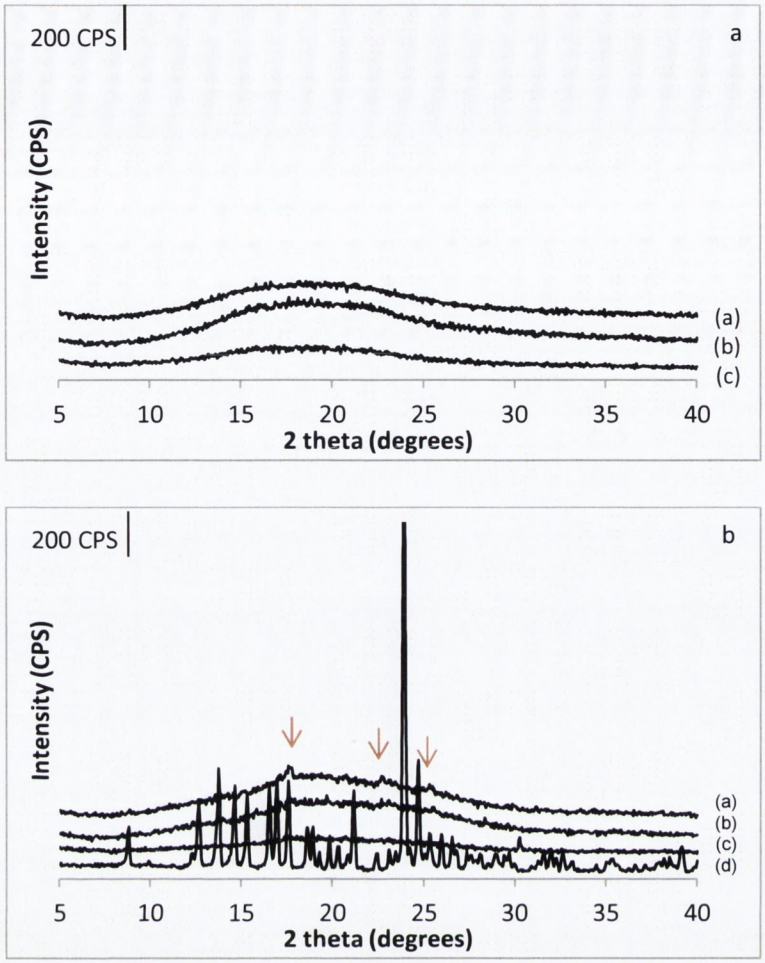

Figure 4.11 XRPD scans of spray dried (a) raffinose and (b) trehalose from different ratios of the cosolvent system MeOH:PA: (a) 65:35, (b) 70:30 and (c) 80:20. Crystalline trehalose is also represented in plot b as (d).

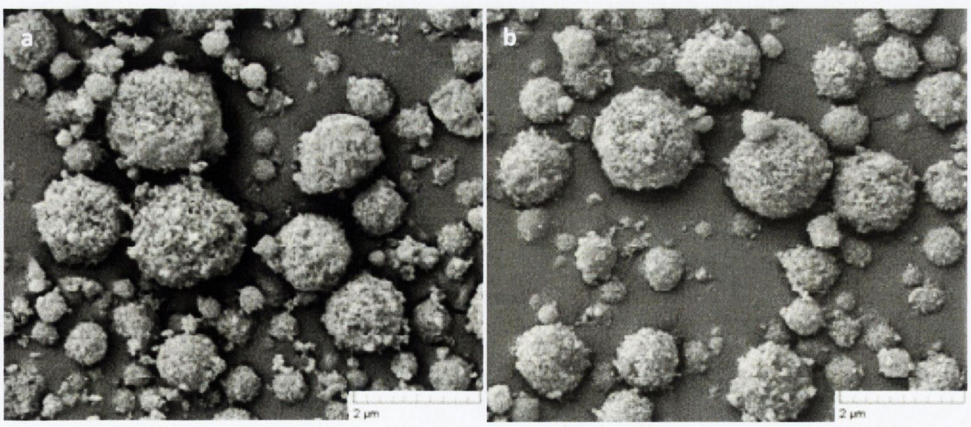

Figure 4.12 SEM micrographs of (a) raffinose and (b) trehalose spray dried from 80:20 (v/v) MeOH:BA using optimal process conditions.

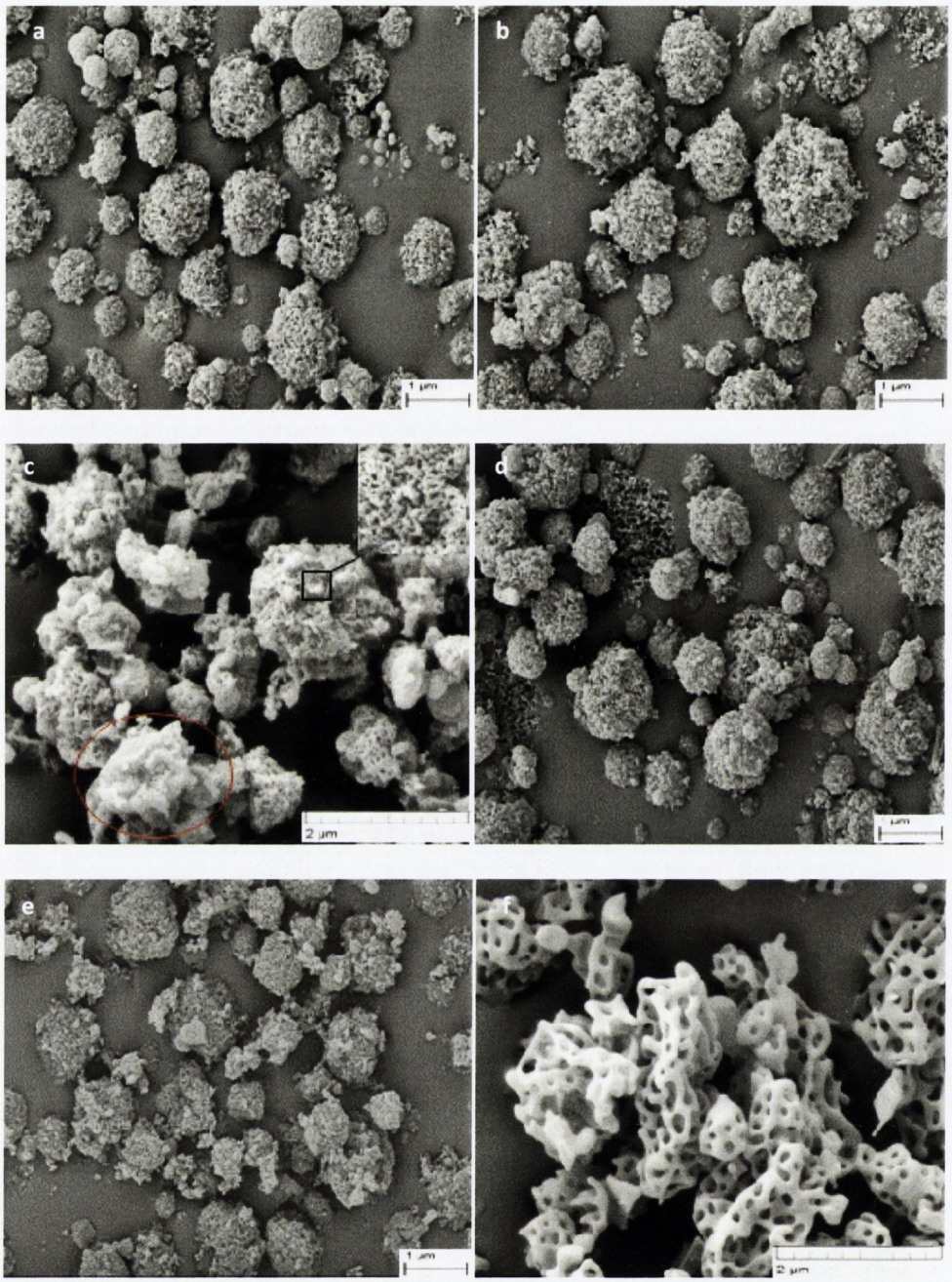

Figure 4.13 SEM micrographs of spray dried raffinose from different ratios of the cosolvent system MeOH:PA: (a) 65:35, (b) 70:30 and (c) 80:20; SEMD micrographs of spray dried trehalose from different ratios of the cosolvent system MeOH:PA: (d) 65:35, (e) 70:30 and (f) 80:20.

Particle size by laser diffraction, the results of which are summarised in table 4.7, showed the geometric median particle size varied between 1.6-2.0 µm for raffinose and 1.8-2.1 µm for trehalose. A correlation between geometric median particle size and yield was investigated for all samples spray dried from MeOH:PA in order to determine if the particle size had an influence on the obtained yields. No statistically significant correlation between variables for both sugars was found (Figure 4.14*a* and 4.14*b*).

The particle size of samples spray dried from MeOH:PA solutions were found to be larger than raffinose and trehalose spray dried from MeOH:BA 80:20 ($p < 0.05$), with the exception of raffinose spray dried from a solution of 65:35 MeOH:PA that presented similar particle size to MeOH:BA system.

Specific surface area ranged from 40.25 to 47.00 m^2/g and 43.34 to 47.98 m^2/g for raffinose and trehalose respectively. SSA of MeOH:PA systems was found to be smaller than systems spray dried from MEOH:BA (Table 4.8).

As described previously in this section the co-solvent system ratio will affect particle morphology and consequently powder specific surface area. According to Ní Ógáin et al. (2011), the NPMPs formation is dependent on the sugar solubility and the less volatile solvent content of the droplet. Upon atomisation, as the more volatile solvent evaporates the droplet becomes richer in the less volatile solvent, in which the sugar is less soluble. The fall in solubility of the sugar may be dramatic and it may condense out initially as a nanosized liquid phase within the droplet. As drying proceeds, the sugar phase droplets become less fluid and come closer together, and the sugar may precipitate out as primary nanoparticles which agglomerate together either at the particle surface (forming an outer shell) or within the particle, leading to nanoparticulate microparticle formation. Hence, the influence of co-solvent system composition, i.e. PA fraction, on powder SSA was investigated (Figure 4.15). It was found when increasing PA fraction the SSA of raffinose particles reduces and the SSA of trehalose particles increases, not being significant for the latter ($p=0.001$, $r^2=0.950$ for raffinose; $p=0.217$, $r^2=0.349$ for trehalose).

Table 4.8 presents the data obtained from density measurements of all spray-dried samples. Statistical evaluation, by ANOVA followed by Tukey's test, of density data for raffinose systems spray dried from MeOH:PA and MeOH:BA showed significant differences between tap density and true density for these two solvent systems ($p=0.001$ and $p=0.028$ respectively), with an increase in tap density and decrease in for MeOH:BA true density. It was also possible to determine that MeOH:PA 80:20 ratio system presented similar tap density to MeOH:BA system. No significant differences were found in powder bulk densities. Trehalose powders spray-dried from MeOH:PA presented bulk, tap and true densities which were statistically significantly different ($p=0.022$, $p=0.001$ and $p < 0.05$, respectively) from trehalose powders spray dried from MeOH:BA. Tukey's test revealed that powders spray dried from different MeOH:PA ratios all presented similar bulk densities; MeOH:PA 65:35 system had a tap density different from all other spray-dried ratios; and true density was different for all spray dried MeOH:PA ratios.

Correlations between tap and true density measurements and PA fraction in the spray drying solution were investigated to determine if there was an effect of the latter on powder density (Figure 4.16a, 4.16b, 4.16c and 4.16d). A trend was seen for raffinose and trehalose powders, where an increase in PA fraction led to the formation of powders with higher tap density. The tapped density is attained after mechanically tapping a receptacle containing the powder sample, its measurement includes the volumes of the solids in each particle, the voids within the particle (open and closed pores) and, excludes the voids between particles ("external void") (Webb, 2001; European Pharmacopoeia 7^{th} Edition, 2012). The morphology and particle size distribution will affect particle packing, enlarging or reducing the tap density (Howard, 2007). It was observed by SEM (Figure 4.13) that particle morphology was modified with increasing fraction of PA from irregular to spherical and, that the polydispersity (span) of particle size reduced (Table 4.8). Hence, it is believed that the irregular shaped particles and increased variability of particle size (larger span) will present poorer packing (lower tap density) by increase of the external void.

The trend found for true density differed depending on the sugar studied. For raffinose powders it was found that true density reduced when spray drying from solutions with higher fraction of PA. On the other hand, for trehalose powders true density increased with increasing fraction of PA. True density is known to be dependent on feed solution concentration, particle morphology (smooth surface versus irregular surface; hollow versus solid; porous versus non-porous) and gas permeability when using gas pycnometry (Elversson and Fureby, 2005; Vehring, 2007). Vehring (2007) described hollow, irregular surface and porous particles to present lower densities than their solid, smooth, non-porous counterparts. Raffinose and trehalose were spray dried from feed solutions with different concentration; therefore, any comparison between the true densities of these two sugars will be discarded. The presence of porosity leads to high specific surface area (SSA) values (Papelis et al., 2003; Healy et al., 2008). It was previously seen that with increasing PA fraction, SSA decreases for raffinose (lower porosity) and increases for trehalose (higher porosity), therefore it was expected to see a decrease in true density for raffinose and an increase for trehalose when spray drying from solutions with higher fraction of PA as shown in figure 4.16.

The aerodynamic diameter was calculated for all systems and found to be within the desirable particle size range for alveolar deposition in the lungs, that is, 1-3 μm (Table 4.7). The DPI aerosol cloud should consist of particles with aerodynamic diameters between 1 and 3 μm with

good dispersibility (good flow) to efficiently deliver the drug into the lower (alveolar) regions of the lungs (Hickey, 1996).

Table 4.8 Particle size, true, bulk and tap density and calculated aerodynamic diameter of raffinose and trehalose spray dried from MeOH:PA and MeOH:BA solutions.

	Raffinose				Trehalose			
	MeOH:PA (% v/v)			MeOH:BA (% v/v)	MeOH:PA (% v/v)			MeOH:BA (% v/v)
	65:35	70:30	80:20	80:20	65:35	70:30	80:20	80:20
d_{10} (µm)	0.9±0.00	1.0±0.07	1.0±0.06	1.1±0.02	1.0±0.04	0.9±0.00	0.9±0.03	0.9±0.02
d_{50} (µm)	1.6±0.02	2.0±0.05	2.0±0.09	1.7±0.01	1.8±0.04	1.9±0.00	2.1±0.28	1.6±0.02
d_{90} (µm)	3.1±0.12	3.7±0.08	4.2±0.30	2.9±0.04	6.0±1.30	4.3±0.35	3.6±0.14	2.7±0.03
<1µm (%)	15.3±0.26	11.7±2.79	10.8±2.26	7.2±0.71	12.6±1.47	13.2±0.04	11.7±1.84	13.0±10.1
Span	1.4±0.06	1.5±0.12	1.6±0.14	1.0±0.06	1.5±0.02	1.8±0.19	2.4±0.34	1.1±0.05
SSA (m^2/g)	44.27±0.28	40.25±0.27	47.00±0.22	58.16±0.51	47.44±0.27	47.98±0.56	43.34±.32	51.44±0.49
True density (g/cm^3)	1.55±0.01	1.57±0.01	1.57±0.003	1.58±0.01	1.60±0.01	1.53±0.005	1.45±0.05	1.43±0.06
bp(g/cm^3)	0.16±0.01	0.15±0.01	0.15±0.01	0.15±0.01	0.13±0.01	0.13±0.01	0.12±0.004	0.15±0.01
tp (g/cm^3)	0.29±0.02	0.29±0.01	0.26±0.01	0.24±0.00	0.26±0.01	0.22±0.001	0.21±0.01	0.22±0.01
d_{aer} (µm)	2.1±0.004	2.3±0.01	2.5±0.003	2.2±0.02	2.3±0.01	2.3±0.003	2.4±0.05	1.9±0.04

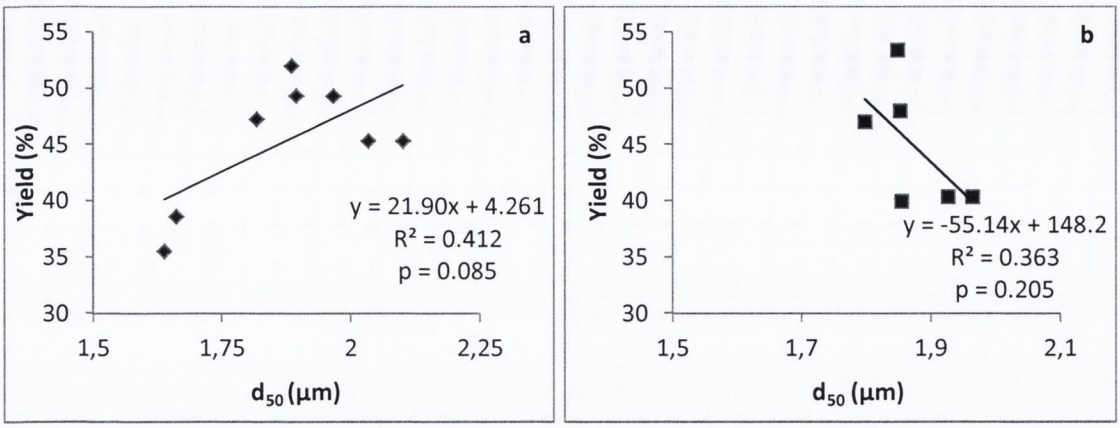

Figure 4.14 Influence of geometric median particle size (d_{50}) on (a) raffinose and (b) trehalose powders yield.

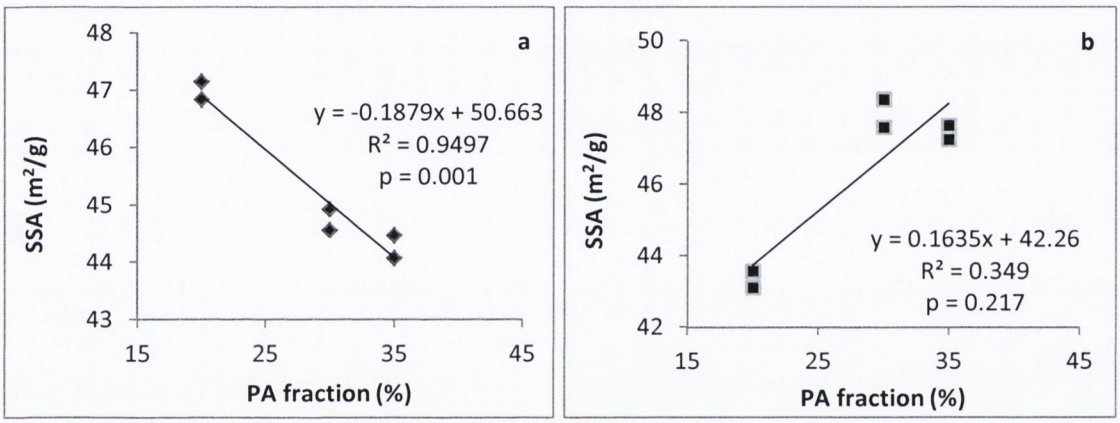

Figure 4.15 Influence of propyl acetate (PA) fraction on (a) raffinose powders specific surface area (SSA) and (b) trehalose powders specific surface area.

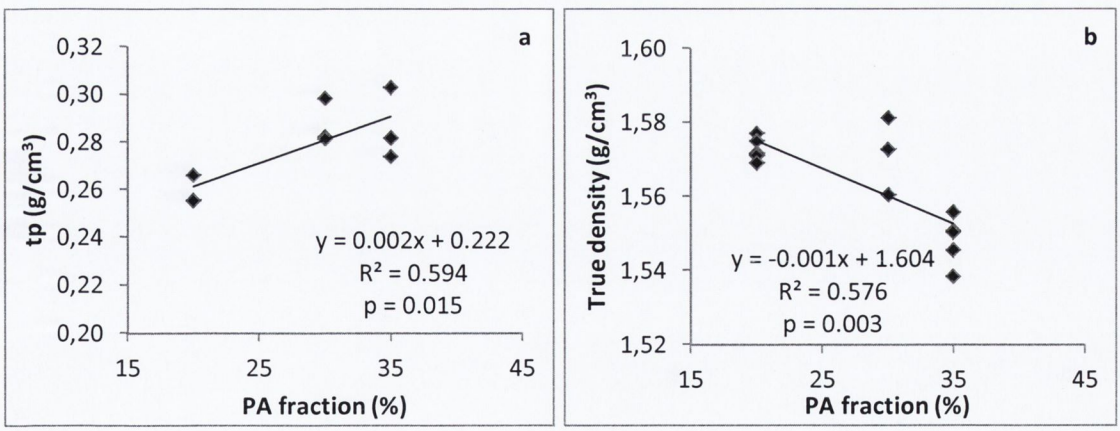

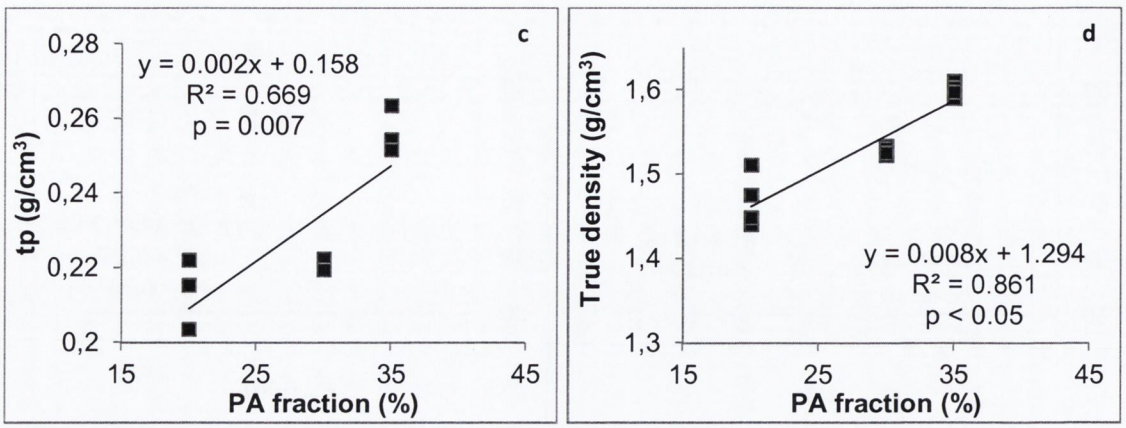

Figure 4.16 Influence of propyl acetate (PA) fraction in spray drying solution on raffinose powders (a) tap density and (b) true density and, on trehalose powders (c) tap density and (d) true density.

4.6.2 Thermal analysis and residual solvent content by GC-FID

DSC scans were similar for all raffinose (R) samples (Figure 4.17). The glass transition temperature was found to be ~116 °C for raffinose spray dried from MeOH:BA and 115-117 °C for raffinose spray dried from MeOH:PA (Table 4.9); a broad endotherm from 25 to ~115 °C due to residual solvent loss was also observed with large relaxation event after T_g; no other thermal events were recorded. ANOVA followed by Tukey's test showed the T_g of R:MeOH:PA 65:35 was significantly different from all other systems T_g ($p=0.036$). A correlation between co-solvent system composition, as PA fraction, and T_g was investigated (Figure 4.19), due to the existence of differences between MeOH:PA systems. It was found that the glass transition temperature increased when spray drying from solutions with higher PA fraction. The same effect was seen in studies by Paudel and Mooter (2012) on the miscibility and physical stability of naproxen/PVP solid dispersions spray dried from methanol and acetone mixtures (methanol boiling point 65 °C and acetone boiling point 56-57 °C), with diferent solvent ratio and equal total solid concentration, was evaluated. An increase in the glass transition temperature of the drug and excipient when spray dried from solutions with increased fraction of the solvent with higher boiling point, i.e. methanol in this study, was reported.

Trehalose systems also presented similar DSC scans; a broad endotherm, from 25 to ~115 °C, was recorded after which there was a glass transition event (Figure 4.18). The glass transition temperature was found to be ~121 °C for MeOH:BA system and 120-122 °C for MeOH:PA systems (Table 4.9). A recrystallisation exotherm was recorded at 153-158 °C, followed by a melting endotherm ~210/211 °C for all systems. ANOVA analysis showed no statistically significant differences between the T_g ($p = 0.098$), T_m ($p = 0.071$), ΔH_c ($p = 0.064$) and ΔH_m ($p = 0.277$) of all systems spray dried from MeOH:PA. The onset of recrystallisation (T_c) of MeOH:BA

system and MeOH:PA 80:20 ratio system were found to be different between each other and from the other MeOH:PA systems by ANOVA followed by Tukey's test (p=0.001). Ní Ógain (2008) also reported different onsets of recrystallisation for trehalose systems spray dried from different ratios of MeOH:BA.

A residual solvent content (RSC) of 2.60±0.31 % and 3.78-4.62 % was determined by TGA for raffinose MeOH:BA system and MeOH:PA systems respectively, over the temperature range 25-130 °C (Table 4.10). For trehalose MeOH:BA system and MeOH:PA systems a RSC of 2.49±0.50% and 2.78±0.32% were calculated by TGA. ANOVA with Tukey's test showed no significant differences for raffinose and trehalose systems (p=0.235 and p=0.268, respectively).

The RSC was further analysed by GC-FID with quantification of MeOH, butyl acetate and propyl acetate (Table 4.10). Water content was extrapolated from the difference between the values calculated RSC by TGA and GC-FID. It was found that water/moisture is the main component of the RSC followed by the acetates (BA or PA). At the spray drying conditions of this study the residual content of PA found in the systems was higher than for BA and, the European Pharmacopeia also classifies propyl acetate as a class 3 residual solvent (European Pharmacopoeia 7th Edition, 2012), the same as butyl acetate.

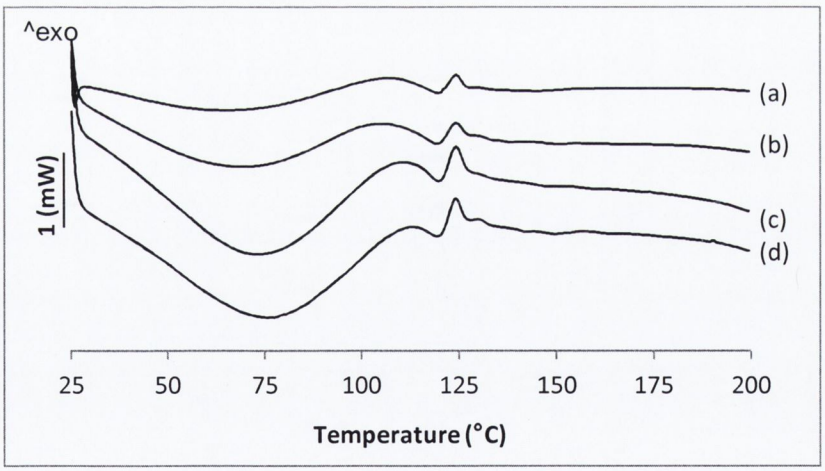

Figure 4.17 DSC scan of spray dried raffinose from (a) MeOH:BA, (b) MeOH:PA 80:20, (c) MeOH:PA 70:30 and (d) MeOH:PA 65:35 co-solvent systems.

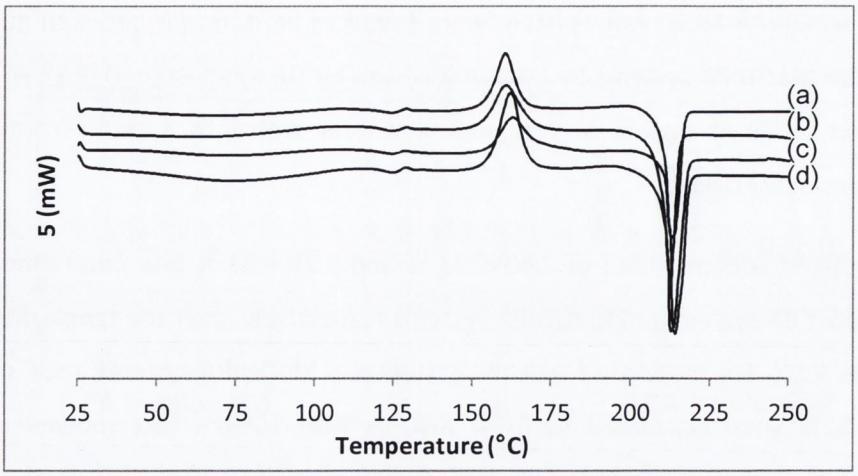

Figure 4.18 DSC scan of spray dried trehalose from (a) MeOH:BA, (b) MeOH:PA 80:20, (c) MeOH:PA 70:30 and (d) MeOH:PA 65:35 co-solvent system solutions.

Table 4.9 Glass transition temperature (T_g), recrystallisation temperature and enthalpy (T_c, ΔH_c) and melting temperature and enthalpy (T_m, ΔH_m) of raffinose and trehalose spray dried from MeOH:PA and MeOH:BA co-solvent system solutions.

		Raffinose	Trehalose				
		Tg (°C)	T_c (°C)	ΔH_c (J/g)	T_m(°C)	ΔH_m (J/g)	
MeOH:BA	80:20	115.6±0.21	121.0±0.30	158.7±0.54	99.2±6.10	210.4±0.42	138.6±8.32
MeOH:PA	80:20	114.6±0.15	120.6±0.22	153.3±0.57	88.5±0.95	209.9±1.89	132.9±2.88
	70:30	116.5±0.50	120.1±1.32	155.0±0.33	84.4±4.14	211.7±0.23	141.6±1.03
	65:35	117.0±0.27	121.6±0.25	155.4±0.11	88.1±1.42	211.0±0.13	143.3±2.23

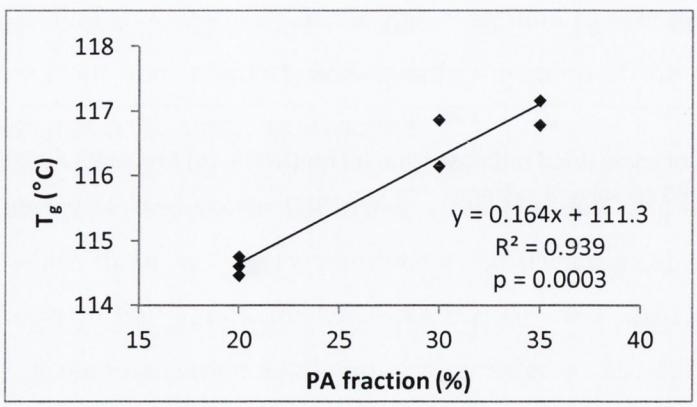

Figure 4.19 Influence of propyl acetate (PA) fraction in the co-solvent system on raffinose powders glass transition.

Table 4.10 Residual solvent content by TGA and GC-FID of raffinose and trehalose powders spray dried from MeOH:BA and MeOH:PA co-solvent system solutions.

				RSC by TGA (% w/w)	RSC by GC-FID (% w/w)		Extrapolated Water content (%)
					Methanol	Butyl/ Propyl Acetate	
Raffinose	MeOH:BA (% v/v)		80:20	2.60±0.34	0.30±0.01	0.81±0.02	2.24
	MeOH:PA (% v/v)		80:20	3.78±0.78	0.36±0.01	0.93±0.02	2.49
			70:30	3.87±0.99	0.22±0.03	0.87±0.01	2.78
			65:35	4.62±0.44	0.32±0.03	1.01±0.04	3.29
Trehalose	MeOH:BA (% v/v)		80:20	2.49±0.50	0.40±0.06	0.99±0.003	1.10
	MeOH:PA (% v/v)		80:20	4.32±0.22	0.15±0.02	1.32±0.13	2.85
			70:30	2.92±0.51	0.30±0.03	0.82±0.06	1.80
			65:35	2.78±0.81	0.21±0.02	1.23±0.05	1.34

4.6.3. *In vitro* deposition via next generation impactor

Powder pulmonary deposition was assessed *in vitro* using a next generation impactor. Deposition profiles and main deposition parameters are presented in Figures 4.20 and 4.21 and Tables 4.11 and 4.12. The greatest difference found in the deposition profiles, for raffinose powders, was the percentage of powder recovered from the mouthpiece adaptor and induction port. Raffinose NPMPs produced from MeOH:BA had less deposition than raffinose spray dried from the co-solvent mixture MeOH:PA. However, the dose emitted (as percentage recovered) showed no statistically significant difference between samples (p=0.203).

Spray drying raffinose from MeOH:PA 80:20 ratio resulted in powders with similar deposition parameters to the system spray dried from MeOH:BA 80:20 (Table 4.11). However, as the PA fraction was increased in the co-solvent mixture a reduction in the fine particle fraction and an increase in the MMAD was evident. The latter increased to ~ 5 and ~9.7 μm, indicating that most deposition occurred above stage 2 (cut off point of ~ 5 μm), resulting in the observed decrease in FPF. A larger MMAD than the geometric median particle size suggests the existence of aggregates that were not dispersed by the aerodynamic forces generated during the analysis (Bosquillon et al., 2001). ANOVA with Tukey's test showed significant differences in fine particle

fraction < 5 μm and < 3 μm ($p<0.05$ and $p=0.016$ respectively), mass median aerodynamic diameter and geometric standard deviation ($p=0.0002$ for MMAD and $p<0.05$ for GSD), where the system spray dried from 65:35 ratio MeOH:PA was different from other MeOH:PA systems and, the system spray dried from 80:20 ratio MeOH:PA was similar to the MeOH:BA system. The reduced FPF < 5 μm and < 3 μm for the system 65:35 MeOH:PA is due to its increased MMAD (Table 4.11) that was two times greater than the MMAD of the remaining MeOH:PA systems and MeOH:BA system.

Trehalose powder deposition profiles demonstrated that a large proportion of the emitted dose (36 to 74 %) was deposited in the mouthpiece adaptor/ induction port and stage 1 (cut off point ~9 μm). The dose emitted (as percentage recovered) varied between 45.7 and 81.0 %. The sample spray dried from 65:35 ratio MeOH:PA presented the lowest value and was statistically significant different ($p=0.013$) from all other systems (Table 4.12). Fine particle fraction < 5 μm and < 3 μm was similar for all samples, that is, no statistically significant differences were found ($p=0.458$ and $p=0.763$). The MMAD was found to be different for all samples ($p=0.025$) and 2 to 4 fold larger than the calculated aerodynamic diameter and geometric median particle size (Table 4.7). Trehalose NPMPs produced from MeOH:BA solutions presented the smallest MMAD, 4.4±0.35 μm, while all samples spray dried from MeOH:PA had a larger MMAD. Differences in particles morphology, size and density can result in formation of aggregates that lead to a larger MMAD (Bosquillon et al., 2001).

The GSD of all powders was significantly different ($p=0.039$); larger GSD were determined for powders with larger MMAD.

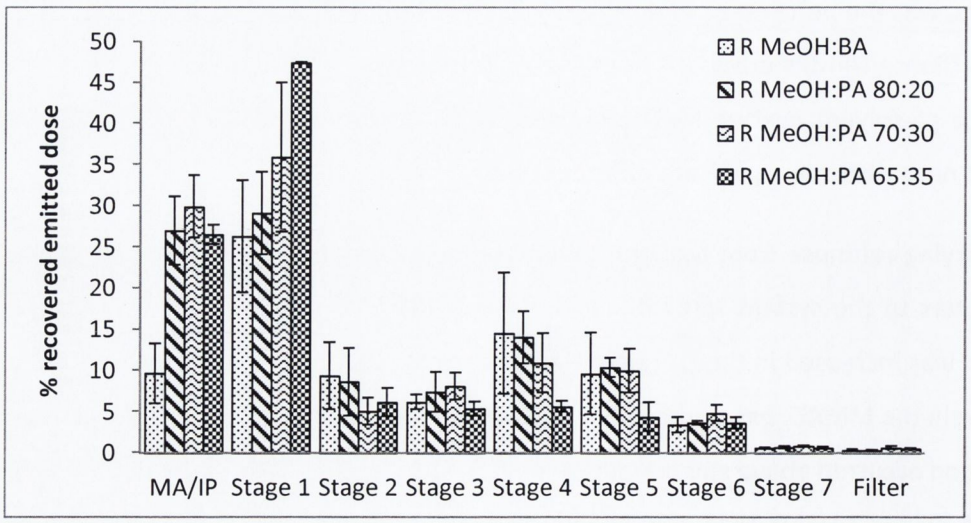

Figure 4.20 *In vitro* aerosol deposition profile by use of a NGI of raffinose MeOH:BA and MEOH:PA systems as calculated % of recovered emitted dose vs. NGI stages. MA – mouth adapter IP – induction port

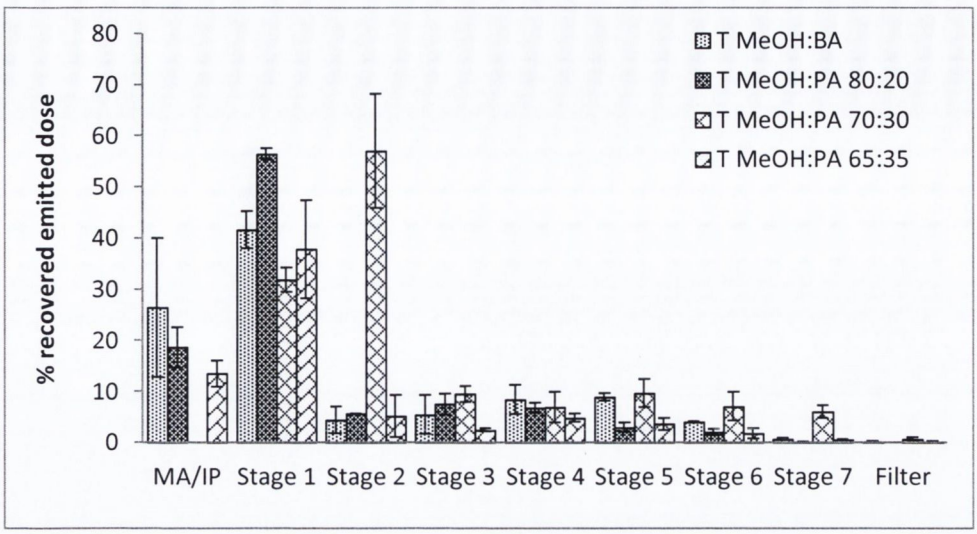

Figure 4.21 *In vitro* aerosol deposition profile by use of a NGI of trehalose MeOH:BA and MEOH:PA systems as calculated % of recovered emitted dose vs. NGI stages. MA – mouth adapter IP – induction port

Table 4.11 Recovered emitted dose, fine particle fraction (FPF), mass median aerodynamic diameter (MMAD) and geometric standard deviation (GSD) of *in vitro* aerosol deposition of raffinose MeOH:BA system and raffinose MEOH:PA systems.

	MeOH:BA	MeOH:PA 80:20	MeOH:PA 70:30	MeOH:PA 65:35
% recovered emitted dose	68.1±11.7	69.1±3.16	69.4±5.75	71.0±9.26
FPF < 5 µm	50.4±15.6	47.3±3.67	40.7±5.25	25.6±0.78
< 3 µm	26.4±10.0	33.4±2.99	33.8±5.03	19.6±1.21
MMAD	4.4±0.27	4.5±0.25	5.0±0.41	9.7±1.34
GSD	2.3±0.48	2.4±0.10	2.8±0.08	3.2±0.09

Table 4.12 Recovered emitted dose, fine particle fraction (FPF), mass median aerodynamic diameter (MMAD) and geometric standard deviation (GSD) of *in vitro* aerosol deposition of trehalose MeOH:BA system and trehalose MEOH:PA systems.

	MeOH:BA	MeOH:PA 80:20	MeOH:PA 70:30	MeOH:PA 65:35
% recovered emitted dose	81.0±12.1	65.9±8.86	78.5±4.70	45.7±1.68
FPF < 5 µm	27.4±7.6	31.9±5.96	33.1±4.84	26.1±7.25
< 3 µm	21.4±2.1	16.4±3.80	22.2±8.58	19.3±1.67
MMAD	4.4±0.35	6.6±1.45	8.4±0.97	8.2±1.30
GSD	2.6±0.02	2.2±0.20	3.1±0.39	3.0±0.12

4.7 CONCLUSION

The design of experiment study undertaken resulted in well fitted models which highlighted the process variables impacting on the sugar NPMPs characteristics. Yield was affected by the gas flow and pump setting; particle size and specific surface area by the gas flow; residual solvent content and outlet temperature via the inlet temperature. Interaction between the process parameters were also found, demonstrating the complexity of the spray drying process.

The factorial models constructed could be used to optimise the spray drying process for the production of powders with suitable characteristics for pulmonary delivery, i.e., high yield, small particle size and low residual solvent.

Previous studies on porous microparticles did not examine the effect of a change in surface area on the *in vitro* deposition for dry powders intended for pulmonary delivery. In this study we compared powders with similar particle sizes but differing SSA and demonstrated a trend of increasing FPF with increasing SSA, attributable to the porosity of the particles.

Raffinose NPMPs had better characteristics than trehalose NPMPs for use in dry powder inhalation, since particles with larger surface area, resulting in higher FPF, were produced.

Methanol and butyl acetate can be quantified by GC-FID. While the levels of methanol and butyl acetate in freshly prepared raffinose and trehalose NPMPs were below the pharmacopoeial limits, the content of both could be reduced by storing the produced powders under a nitrogen purge at 25 °C for 24 h.

Raffinose and trehalose NPMPs can also be produced by spray drying from methanol:propyl acetate co-solvent system at ratios 70:30 and 65:35. These NPMPs were amorphous for raffinose and predomintly amorphous for trehalose, as assessed by XRD. Micromeritic properties such as tap and true density and, specific surface area were found to be affected by the co-solvent system ratio, which impacted differently depending on the excipient used. The glass transition temperature of raffinose, assessed by DSC, was also found to depend on the co-solvent system ratio. This was not the case for trehalose, with similar glass transition temperatures found for trehalose spray-dried from solutions of MEOH:PA with different ratios. The residual solvent content was mainly constituted by water and propyl acetate. All spray-dried systems from MeOH:PA displayed favourable aerodynamic and micromeritic characteristics, suggesting potential suitability for pulmonary delivery, as was proven by the *in vitro* deposition studies by NGI, where the recovered emitted dose was above 65 % for most systems and the FPF < 5 μm was ~30 %.

Comparing with raffinose and trehalose NPMPs spray-dried from 80:20 MeOH:BA, no particular advantage can be achieved by replacing butyl acetate with propyl acetate when spray drying at the same conditions since micromeritic properties (particle size, specific surface area and tap density) were inferior and propyl acetate content in powders was higher than butyl acetate. However, this study shows that it is possible to produce non-reducing sugars NPMPs from other co-solvent systems and, there is the possibility, with future studies on spray drying conditions for MeOH:PA systems, to produce equivalent or better powders than those produced by spray-drying raffinose and trehalose from the 80:20 MeOH:BA co-solvent system.

Table 4.13 Effect of increasing spray drying process parameters on evaluated outcomes of raffinose NPMPs. T_{inlet} –inlet temperature; T_{oulet} –outlet temperature; PS-particle size; RSC-residual solvent content; SSA-specific surface area

	T_{inlet}	Gas Flow	Feed rate (pump)	Feed concentration
T_{outlet}	significantly increases	decreases	decreases	no effect
PS	no effect	significantly decreases	increases	increases
RSC	decreases	no effect	no effect	no effect
SSA	decreases	significantly increases	decreases	decreases
Yield	no effect	significantly decreases	increases	increases

Table 4.14 Effect of increasing spray drying process parameters on evaluated outcomes of trehalose NPMPs. T_{inlet} –inlet temperature; T_{oulet} –outlet temperature; PS-particle size; RSC-residual solvent content; SSA-specific surface area

	T_{inlet}	Gas Flow	Feed rate (pump)	Feed concentration
T_{outlet}	significantly increases	significantly decreases	no effect	no effect
PS	no effect	significantly decreases	increases	increases
RSC	decreases	no effect	increases	no effect
SSA	decreases	increases	no effect	no effect
Yield	significantly increases	significantly decreases	increases	decreases

CHAPTER 5
SPRAY DRYING OF SUGAR COMPOSITE SYSTEMS USING TREHALOSE, RAFFINOSE AND HYDROXYPROPYL-β-CYCLODEXTRIN

5.1 INTRODUCTION

Raffinose pentahydrate and trehalose dihydrate undergo a solid state modification during spray drying, resulting in amorphous powders. The amorphous solids are known to be less stable physically and chemically than the corresponding crystals (Yu, 2001; Newman et al., 2012). Amorphous sugar (glucose, lactose, raffinose, trehalose, sucrose) powders will spontaneously sorb (adsorb or absorb) a significant amount of water vapour from their surroundings unless stored under completely dry conditions; this sorbed water vapour can markedly change the physical and chemical properties of the sugars, accelerate hydrolytic degradation, isomerisation, and/or crystallisation processes and, thus, can have a significant impact upon their use and function in pharmaceutical dosage forms (Hancock and Shamblin, 1998). Different studies have determined a rapid water absorption and recrystallisation of amorphous raffinose and trehalose powders when exposed to ~75 % relative humidity (RH) for 24 hours (Hogan and Buckton, 2001; Charmathy et al., 2010; Shebor et al., 2010). Ní Ógáin et al. (2010) reported that exposure of trehalose or raffinose:lysozyme NPMP composites to 60 % RH for 24 hours resulted in particle morphology changes and amorphous state conversion into a crystalline state.

Solid dispersions incorporating a higher molecular weight compound can be used to enhance stability and prevent crystallisation of an excipient or drug by increasing the glass transition temperature, through molecular interactions between the drug/excipient and polymer and by the antiplasticisation effect of the polymer (Sinha et al., 2009).

Mazzobre et al. (1997) studied the effect of delaying crystallisation of trehalose in trehalose:lactase systems by the addition of maltodextrin in a ratio of 80:20 (maltodextrin:trehalose). Results showed an increase in the T_g of the system and a delay in trehalose recrystallisation, with improvement of lactase stability at relatively high RH (75 %).

Branchu et al. (1999) evaluated the inhibition of enzyme inactivation in sucrose:hydroxylpropyl-β-cyclodextrin (HPβCD) systems, concluding that the addition of HPβCD prevented enzyme degradation, being a useful stabilising excipient.

Different studies by Davidson and Sun (1998, 2001), Buera et al. (2005) and Leinen and Labuza (2006) have used raffinose and trehalose to delay and inhibit sucrose recrystallisation. These studies concluded that an increased ratio of raffinose or trehalose in the system increased the glass transition temperature and decreased the melting enthalpy, enhancing sucrose stability.

Based on the aforementioned studies we intended to spray dry composite systems of trehalose:raffinose, trehalose:HPβCD and raffinose:HPβCD, in order to improve trehalose and

raffinose stability, and to investigate if the composites have better properties for use as carriers in NPMPs for pulmonary delivery of peptides and proteins than raffinose or trehalose alone.

5.2. HYDROXYPROPYL-B-CYCLODEXTRIN – AS SUPPLIED

Properties of hydroxypropyl-β-cyclodextrin as supplied were investigated. SEM revealed that the material consists mainly of hollow spherical particles presenting collapsed surfaces (Figure 5.1), with a geometric median diameter of 7.3±0.05 μm, as measured by laser diffraction. XRPD showed HPβCD is an amorphous material. It has a glass transition temperature at 254.1±0.17 °C, as determined by DSC (Figure 5.3). TGA analysis revealed a residual moisture content of 5.8±0.27 % over the temperature range 25 ~325 °C (Figure 5.3).

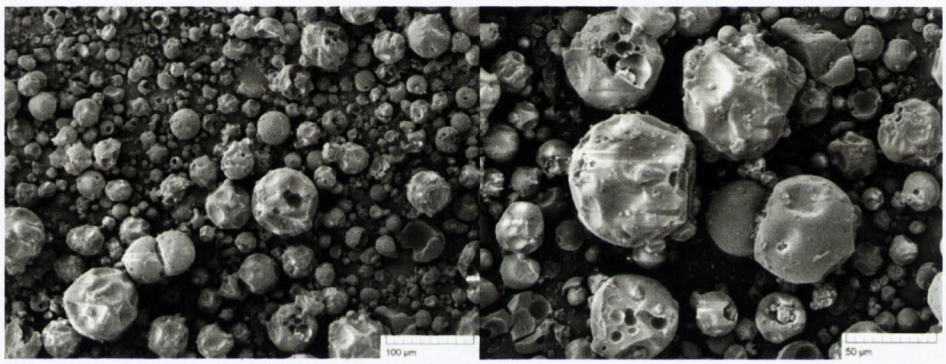

Figure 5.1 SE micrographs of unprocessed hydroxypropyl-β-cyclodextrin.

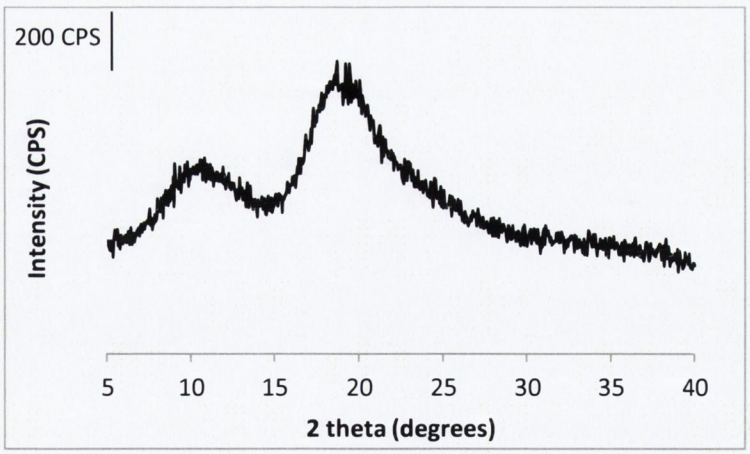

Figure 5.2 XRPD of unprocessed hydroxypropyl-β-cyclodextrin.

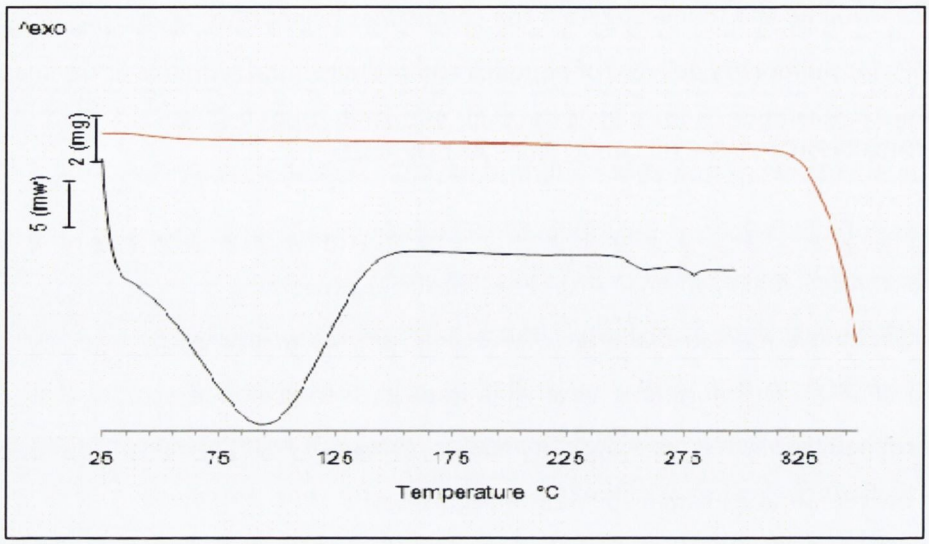

Figure 5.3 DSC (shown in black) and TGA (shown in red) of unprocessed hydroxypropyl-β-cyclodextrin.

5.3. SPRAY DRIED TREHALOSE COMPOSITE SYSTEMS

Spray drying conditions for the production of trehalose composite systems followed the conditions already described for optimised trehalose NPMPs (Chapter 4). Feed solutions of 1% (w/v) with 100:0, 80:20, 70:30, 60:40, 40:60, 30:70, 20:80 and 0:100 weight ratio of d-(+)-trehalose dihydrate:d-(+)-raffinose pentahydrate (T:R) or hydroxypropyl-β-cyclodextrin (T:HPβCD) in methanol:n-butyl acetate (4:1) (v/v) were spray dried. The outlet temperature of T:R samples varied between 83-86 ^{o}C and of T:HPβCD between 84-90 ^{o}C. Yields ranged from 51.6 to 63.9 % and 51.5 to 58.9 % for T:R and T:HPβCD, respectively. There was no statistically significant difference (T:R; p=0.481; T:HPβCD; p=0.301) between sample yields for both types of composites (trehalose:raffinose and trehalose:cyclodextrin).

5.3.1. Solid-state, morphology and micromeritic properties

All spray dried composites were amorphous (Figure 5.4 and 5.5). Diffractograms presented the typical diffuse halo pattern, characteristic of amorphous materials. Spray drying of T:R and T:HPβCD systems led to the conversion of the crystalline sugars into a disordered amorphous state.

The addition of an excipient to trehalose NPMPs did not affect the particle morphology; trehalose composite systems were all NPMPs. SE micrographs showed that T:R composite samples were composed of porous spherical particles, type 1AIIIα (Figure 5.6). Based on visual appearance no differences could be determined between samples. T:HPβCD composites were constituted by porous spherical particles, type 1AIIIα (Figure 5.7). Loss of spherical morphology could only be seen when HPβCD was spray dried alone (Figure 5.7h).

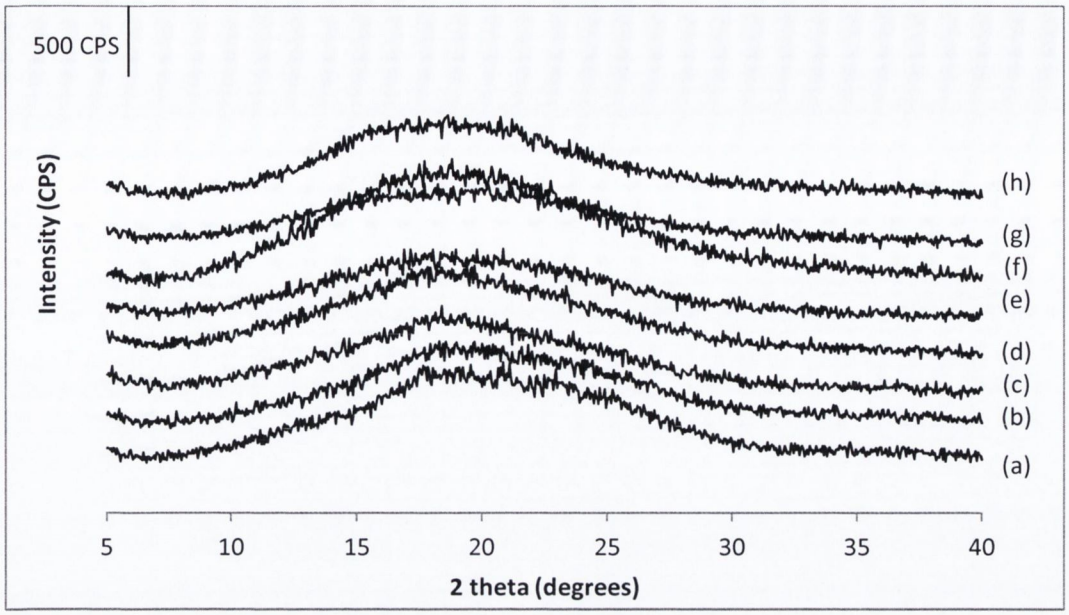

Figure 5.4 XRPD diffractograms of spray dried trehalose:raffinose at ratios: (a) 100:0, (b) 80:20 (c) 70:30, (d) 60:40, (e) 40:60, (f) 30:70, (g) 20:80 and (h) 0:100.

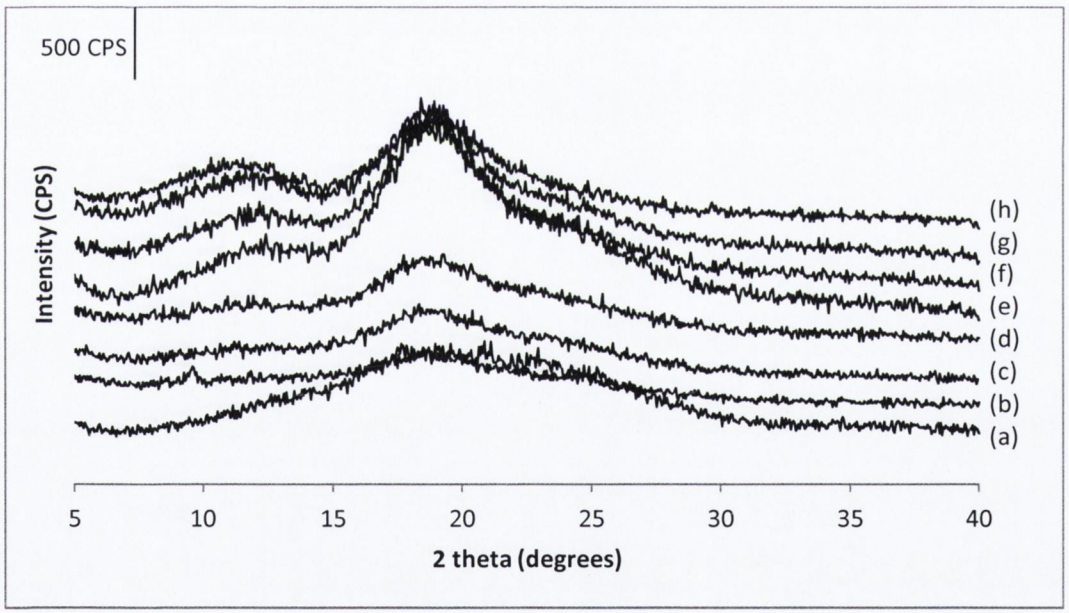

Figure 5.5 XRPD diffractograms of spray dried trehalose:HPβCD at ratios: (a) 100:0, (b) 80:20 (c) 70:30, (d) 60:40, (e) 40:60, (f) 30:70, (g) 20:80 and (h) 0:100.

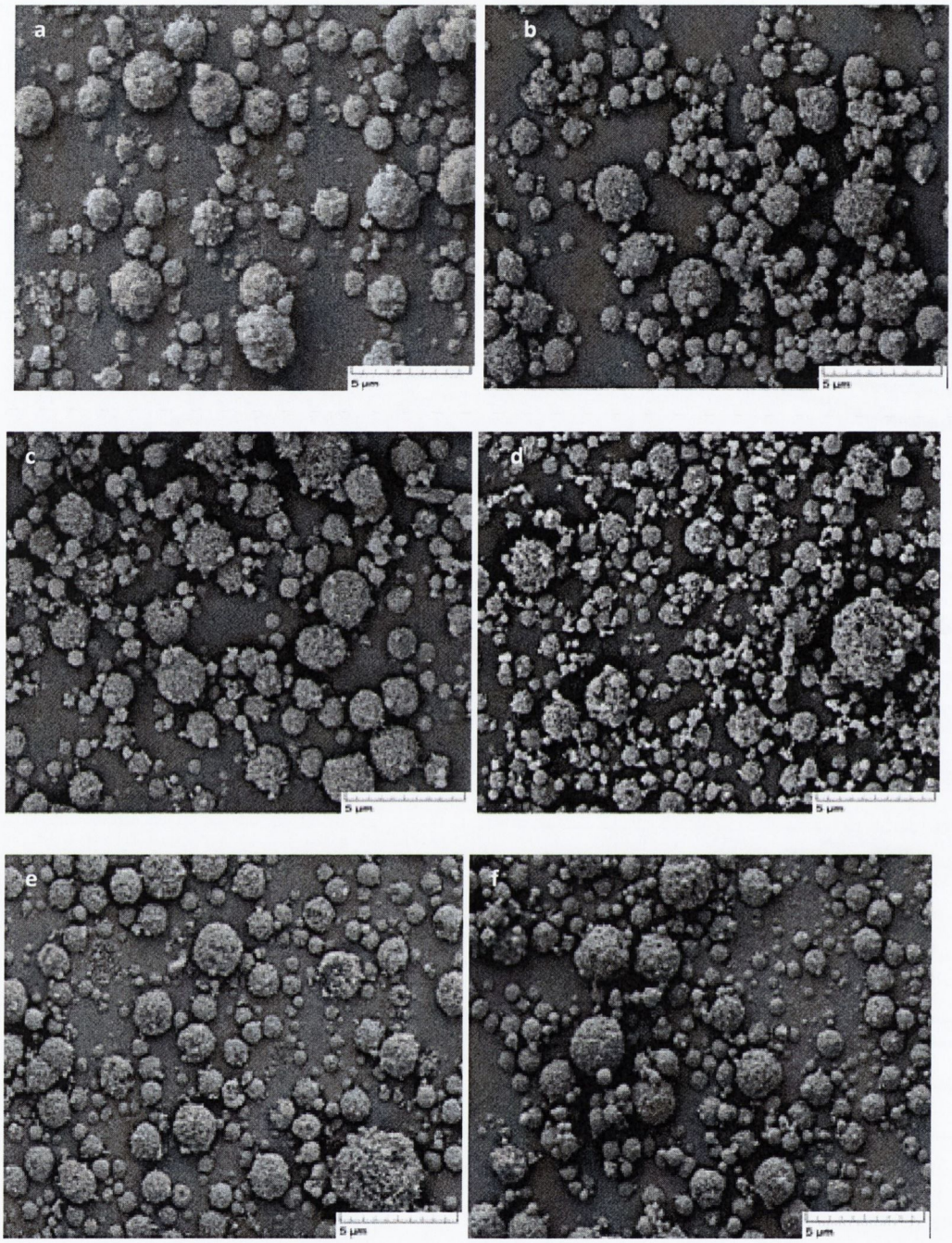
a
5 µm
b
5 µm
c
5 µm
d
5 µm
e
5 µm
f
5 µm

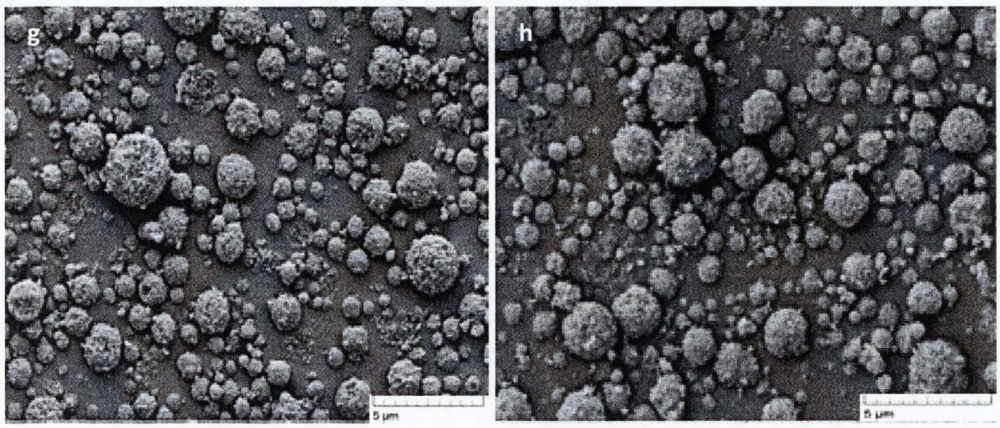

Figure 5.6 SE micrographs of (a) trehalose and trehalose with (b) 20%, (c) 30%, (d) 40%, (e) 60%, (f) 70%, (g) 80% of raffinose and (h) raffinose NPMPs.

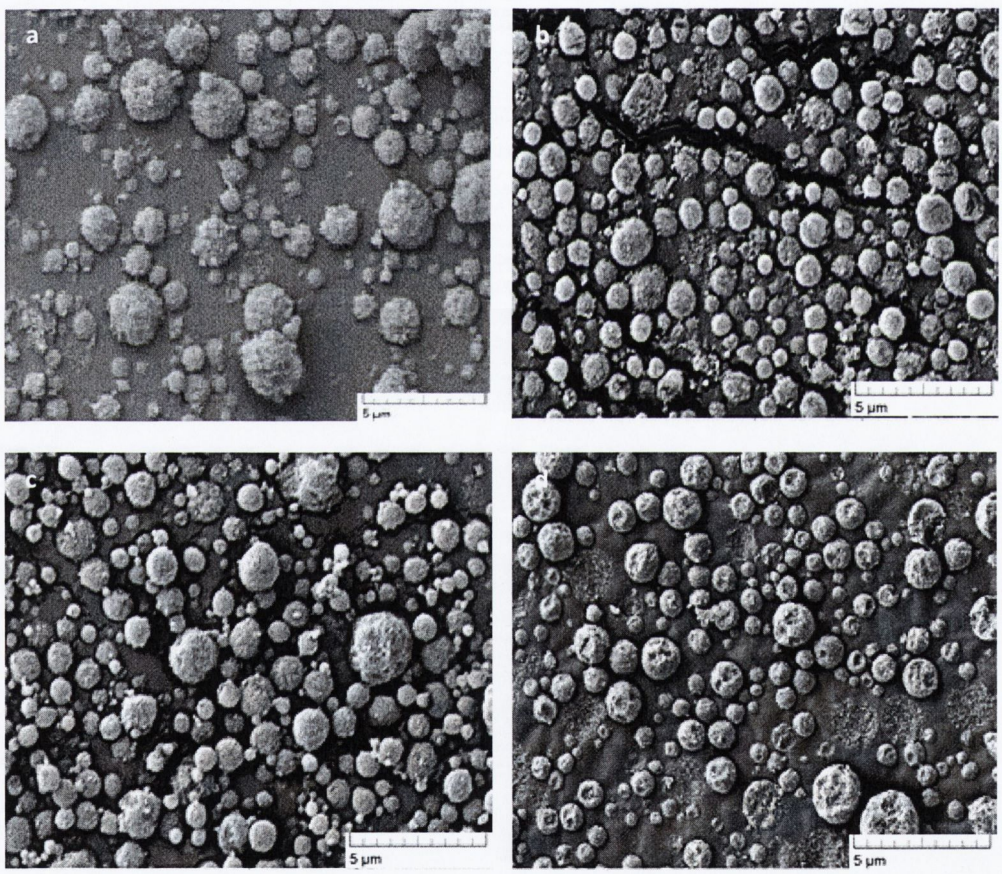

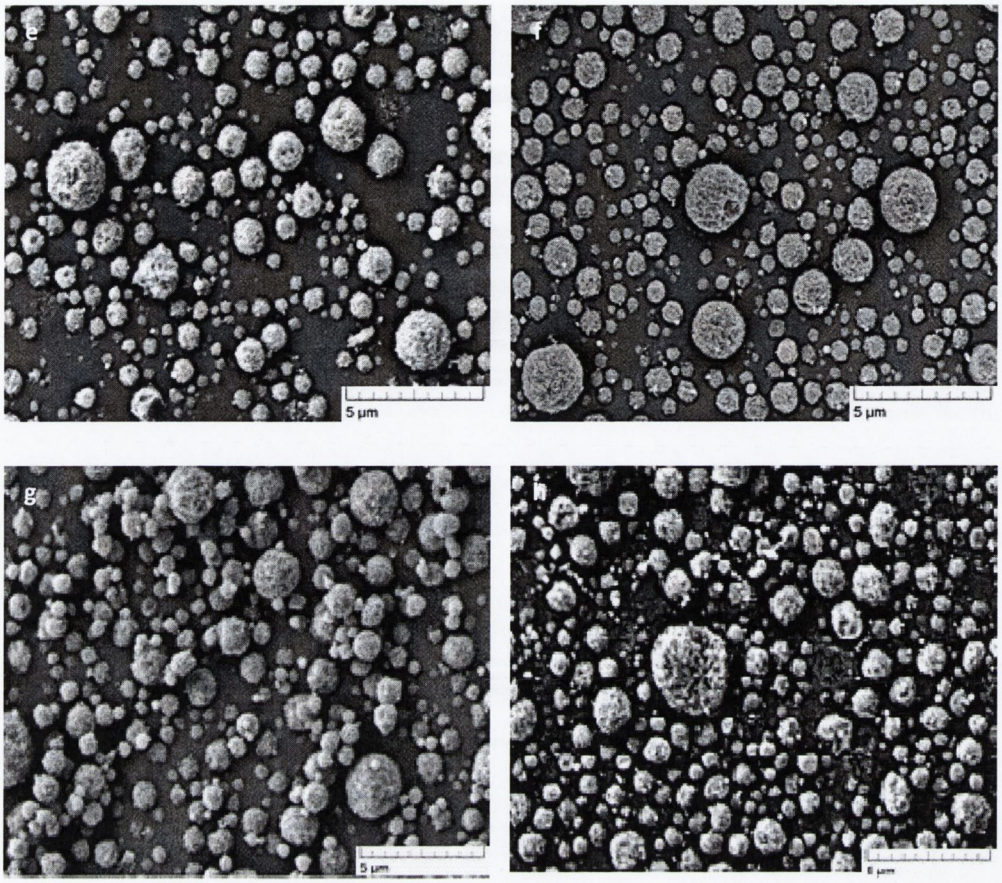

Figure 5.7 SE micrographs of (a) trehalose, trehalose with (b) 20%, (c) 30%, (d) 40%, (e) 60%, (f) 70%, (g) 80% of HPβCD and (h) HPβCD NPMPs.

Particle size volume distributions for all composites were narrow and monomodal with low span values (between 1.3 and 1.5 for T:R and between 1.0 and 1.2 for T:HPβCD). The geometric median particle size (d_{50}) for T:R particles was in the range of 1.6–1.8 µm and for T:HPβCD particles was in the range 1.5–1.6 µm. Tables 5.1 and 5.2 present the reported values of d_{10}, d_{50}, d_{90} and percentage of particles with size <1 µm as mean ± standard deviation.

ANOVA with additional Tukey's test ($p<0.05$) of T:R NPMP particle size distribution pointed out statistically significant differences between samples: the addition of 20-40 % of raffinose produced particles with larger particle size than particles of trehalose NPMPs.

The particle size distribution of T:HPβCD NPMPs suggested that the addition of cyclodextrin did not significantly affect the particle size, at a confidence level of 95 %. The percentage of particles with a diameter below 1 µm increased with higher weight fractions of cyclodextrin, that is, greater volumes of small particles were produced, but not enough to cause a statistically significant difference between samples, when this parameter is evaluated. In studies by Bosquillon et al. (2004) particles with submicrometre-size present better aerosol deposition in distal regions of the lungs. Thus, it may be possible to attain better aerosol deposition with

T:HPβCD NPMPs when compared to trehalose NPMPs. This subject will be further discussed later in this chapter.

Specific surface area (SSA) was also investigated as it is a reflection of porosity associated with porous particles such as NPMPs (Healy et al., 2008). A trend was seen with both types of composite systems - the addition of another excipient to trehalose NPMPs increased the surface area, hence the porosity (Figure 5.8 and Table 5.1). The porosity did not increase linearly with weight fraction; a maximum was achieved (59.11±0.58m^2/g for T:R and 102.79±0.17 m^2/g for T:HPβCD), after which SSA decreased to values closer to the surface area of the added excipient when spray dried alone. There was an optimum weight fraction of 40 % for both types of composite systems.

ANOVA with Tukey's test of the SSA data showed that T:R composite systems and T:HPβCD composite systems presented a significantly different surface area compared to trehalose NPMPs ($p=0.001$ for T:R and $p<0.05$ for T:HPβCD). The T:R composite system with a ratio of 60:40 was found to be different from all other T:R systems and similar to raffinose spray dried alone (T:R 0:100); the remaining T:R composite systems were similar to each other and similar to trehalose spray dried on its own (T:R 100:0). The composite systems T:HPβCD 60:40 and 40:60 were found to be different from remaining composite systems and raffinose spray dried on its own. The SSA of all T:HPβCD composite systems were different to trehalose spray dried alone.

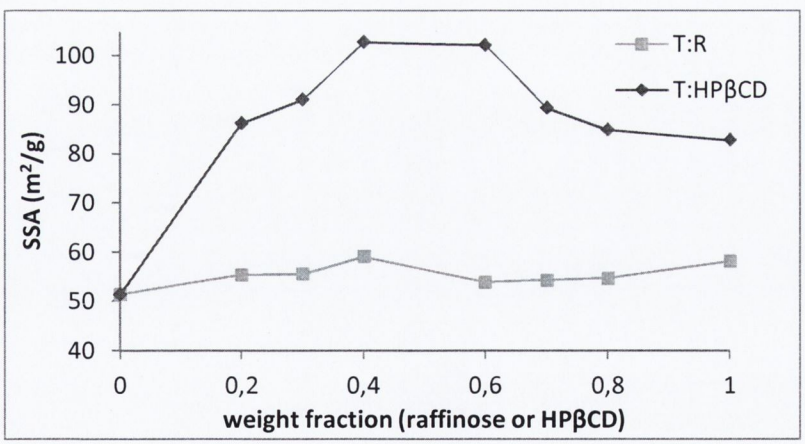

Figure 5.8 Specific surface area (SSA) of trehalose composite systems as function of the added excipient weight fraction.

True density measurements of T:R composite systems were higher than trehalose and lower than raffinose when spray dried alone (Tables 5.1 and 5.2). ANOVA analysis revealed there were differences between samples of the same composite type ($p<0.05$). Further Tukey's test showed

the composite system T:R 30:70 was different from all other composite systems including trehalose and raffinose spray dried alone.

T:HPβCD systems also presented significantly different true densities ($p<0.05$) compared to trehalose NPMPs. Composite systems T:HPβCD 80:20, 70:30 and 60:40 were also different from remaining T:HPβCD systems.

The aerodynamic diameter was calculated for all composites and found to be within the desirable particle size range for deposition in the deep lungs, that is, 1-3 μm (Tables 5.1 and 5.2). The DPI aerosol cloud should be constituted by particles with aerodynamic diameters between 1 and 3 μm with good dispersibility (good flow) to efficiently deliver the drug into the lower (alveolar) regions of the lungs (Hickey, 1996).

Bulk and tap density results for T:R and T:HPβCD are represented in tables 5.1 and 5.2. All samples presented values < 0.3 g/cm^3 making them suitable for pulmonary delivery (Bosquillon et al., 2004). ANOVA analysis of T:R composites showed there was no significant difference between samples (bulk density $p=0.549$; tap density $p=0.074$). In contrast, T:HPβCD composite systems presented significant differences ($p<0.05$): the bulk density of the cyclodextrin spray dried on its own was different from the composite systems with the ratios 80:20, 60:40 and 20:80; the tap density of the composite systems was different from cyclodextrin spray dried on its own and composite systems with ratios 70:30 and 20:80 had different tap density to trehalose spray dried alone.

Table 5.1 Particle size, specific surface area (SSA), true, bulk and tap density and calculated aerodynamic diameter of Trehalose:Raffinose composite systems. SSA-specific surface area; bp- bulk density; tp-tap density; d_{aer}- aerodynamic diameter

	100:0	80:20	70:30	60:40	40:60	30:70	20:80	0:100
d_{10} (μm)	0.9±0.02	0.9±0.03	1.0±0.01	1.0±0.01	0.8±0.04	0.8±0.02	0.9±0.01	1.1±0.02
d_{50} (μm)	1.6±0.02	1.8±0.06	1.8±0.01	1.8±0.02	1.7±0.06	1.6±0.02	1.5±0.01	1.7±0.01
d_{90}(μm)	2.7±0.03	3.7±0.55	3.3±0.03	3.3±0.05	3.5±0.10	2.4±0.54	2.7±0.01	2.9±0.04
<1μm (%)	13.0±10.1	13.0±1.24	11.5±0.33	11.4±0.37	16.6±1.15	18.1±0.45	17.3±0.43	7.2±0.71
SSA (m^2/g)	51.44±0.49	55.34±0.52	55.58±0.52	59.11±0.58	53.92±0.61	54.31±0.18	54.72±0.01	58.16±0.51
True density (g/cm^3)	1.43±0.06	1.57±0.01	1.56±0.00	1.57±0.01	1.56±0.01	1.52±0.02	1.56±0.01	1.58±0.01
bp (g/cm^3)	0.15±0.01	0.13±0.00	0.14±0.01	0.14±0.01	0.15±0.03	0.13±0.01	0.14±0.01	0.15±0.01
tp (g/cm^3)	0.22±0.01	0.22±0.01	0.23±0.01	0.24±0.01	0.25±0.02	0.23±0.02	0.25±0.00	0.24±0.00
d_{aer} (μm)	1.9±0.04	2.3±0.06	2.2±0.01	2.2±0.01	2.1±0.05	1.9±0.03	1.9±0.01	2.2±0.02

Table 5.2 Particle size, specific surface area (SSA), true, bulk and tap density and calculated aerodynamic diameter of Trehalose:HPβCD composite systems. SSA-specific surface area; bp- bulk density; tp-tap density; d_{aer}- aerodynamic diameter

	100:0	80:20	70:30	60:40	40:60	30:70	20:80	0:100
d_{10} (μm)	0.9±0.02	0.8±0.13	1.0±0.00	0.9±0.05	0.9±0.00	0.9±0.01	0.9±0.01	0.9±0.01
d_{50} (μm)	1.6±0.02	1.3±0.04	1.6±0.01	1.5±0.01	1.5±0.00	1.6±0.02	1.6±0.02	1.5±0.01
d_{90}(μm)	2.7±0.03	2.2±0.11	2.6±0.01	2.6±0.01	2.7±0.00	2.8±0.01	2.7±0.04	0.9±0.01
<1μm (%)	13.0±10.1	11.2±2.04	12.5±0.20	15.2±0.49	15.4±0.18	15.1±1.90	15.6±0.74	16.8±0.45
SSA (m^2/g)	51.44±0.49	86.24±0.22	91.06±0.14	102.79±0.17	102.20±0.01	89.39±0.10	84.92±0.02	82.82±0.04
True density (g/cm^3)	1.43±0.06	1.55±0.00	1.53±0.00	1.55±0.01	1.47±0,00	1.45±0.01	1.44±0.01	1.36±0.00
bp(g/cm^3)	0.15±0.01	0.15±0.002	0.10±0.001	0.14±0.003	0.12±0.004	0.11±0.004	0.14±0.003	0.17±0.003
tp (g/cm^3)	0.22±0.01	0.25±0.01	0.20±0.01	0.26±0.02	0.24±0.01	0.24±0.02	0.27±0.01	0.31±0.01
d_{aer} (μm)	1.9±0.04	1.6±0.04	2.2±0.01	2.1±0.01	2.1±0.00	2.2±0.02	1.9±0.02	1.8±0.01

5.3.2. FTIR analysis

Infrared absorption measurements were carried out to evaluate possible interactions between trehalose and raffinose or hydroxypropyl-β-cyclodextrin.

Figure 5.9 depicts the IR absorption spectrum of spray dried trehalose:raffinose (T:R) composite systems and crystalline trehalose and raffinose. The crystalline materials (raffinose pentahydrate and trehalose dehydrate) presented sharp absorption bands, whereas the amorphous trehalose, raffinose and T:R composite systems showed much broader absorption bands. Shoulder peaks in the OH stretching region between 3600 and 3000 cm^{-1} were detected in trehalose and raffinose crystalline spectra, indicative of hydrogen bonds of defined geometric positions (Wolkers et al., 1998; Wolkers et al., 2004). One sharp band around 3500 cm^{-1} was evident in the spectrum of crystalline trehalose, attributable to the stretching vibration of the two crystal water molecules in the trehalose dihydrate crystalline structure (Akao et al., 2001). The broad features of the OH band of amorphous trehalose, raffinose and T:R composite systems indicate a wide range of hydrogen bond lengths and orientations (Akao et al., 2001; Wolkers et al., 2004). Six peaks could be identified in the C–H stretching region, located between 3000 and 2800 cm^{-1} for crystalline trehalose and raffinose, whereas amorphous trehalose, raffinose and T:R composite systems showed only one broad band in this region (Wolkers et al., 1998; Wolkers et al., 2004).

The bands in the 1500–1200 cm^{-1} region arise mostly from C–H deformation vibrations, and the bands between 1200 and 900 cm^{-1} arise predominantly from a combination of CO (δC–O) stretching and OH bending (δC–O–H) vibrations (Wolkers et al., 2004; Cheng and Lin, 2006). The bands at 979 and 937 cm^{-1} for trehalose dihydrate and 980 and 948 cm^{-1} for raffinose pentahydrate, can be assigned to the asymmetric and symmetric stretching vibrations of the glycosidic bond. Different studies have reported peaks at 994 or 998 cm^{-1} and 956 or 954 cm^{-1} for trehalose dehydrate α-(1→1) glycosidic bond and peaks at 998 and 967 cm^{-1} for raffinose pentahydrate α-(1→6) glycosidic bond (Akao et al., 2001; Wolkers et al., 2004; Cheng and Lin, 2006).

In the 1500–1200 cm^{-1} region no differences in peaks positions were found between crystalline materials and spray dried ones, only a broadening of bands was observed. In contrast, bands between 1200 and 900 cm^{-1}showed broadening and a shift to higher wavenumbers after spray drying. Wolkers et al. (2004) attributed these shifts to a modification in the hydrogen bonding of the

C-O-H groups. These modifications are more evident in the composites with higher weight fractions of raffinose.

Modification of the asymmetric and symmetric stretch vibrations of the glycosidic bond was reported for all spray dried samples. According to Akao et al. (2001) this event is due to a conformation change of the molecules.

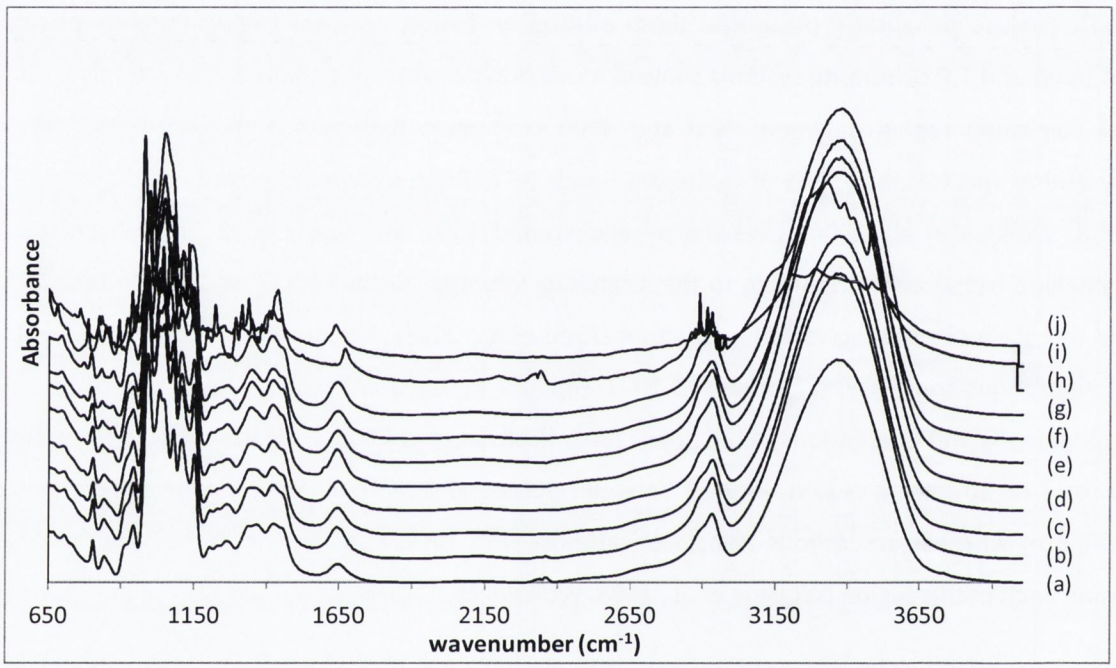

Figure 5.9 FTIR spectras of spray dried T:R composite systems (a) 100:0, (b) 80:20, (c) 70:30, (d) 60:40, (e) 40:60, (f) 30:70, (g) 20:80, (h) 0:100 (i) trehalose dihydrate and (j) raffinose pentahydrate.

Figure 5.10 shows the IR spectra for trehalose dihydrate, HPβCD as supplied and trehalose:hydroxypropyl-β-cyclodextrin (T:HPβCD) composite systems. The spectrum of HPβCD raw material presents a broad peak at 3413 cm^{-1} attributed to OH stretching vibrations; C-H stretching region was also evident with a broad peak; the bands in the range 500 to 1500 cm^{-1} cannot be attributed to a single type of molecular vibration since there is a strong coupling of vibrations from the macrocyclic, caused by neighbouring bonds vibrating with similar frequencies: bending C-H, C-O-H, C-C-H, and others (Misiuk and Zalewska, 2009). The peak corresponding to the α-1,4 glycosidic bond was detected at 966 cm^{-1} (Williams III et al., 1998; Misiuk and Zalewska, 2009; Wu et al., 2010).

As described previously for trehalose and T:R composite systems, a broad band in the OH stretching region between 3600 and 3000 cm^{-1} was detected for all spray dried samples indicative of a wide

range of hydrogen bond lengths and orientations (Akao et al., 2001; Wolkers et al., 2004) and, the C–H stretching region, located between 3000 and 2800 cm^{-1}, also showed one broad band (Williams III et al., 1998; Wolkers et al., 1998; Wolkers et al., 2004). In the 1500–1200 cm^{-1} region no differences in band positions were found between crystalline trehalose raw material, cyclodextrin raw material and spray dried composites, only a broadening of bands was observed. On the other hand, bands between 1200 and 900 cm^{-1} suffered broadening and a shift to higher wavenumbers after spray drying. Wolkers et al. (2004) attributed these shifts to a modification in the hydrogen bonding of the C-O-H groups. Modification of the asymmetric and symmetric stretch vibrations of the α-(1→1)-glycosidic bond was seen for spray dried samples, with an evident reduction of the absorbance as HPβCD weight fraction increased, with possible masking of trehalose bands by the cyclodextrin bands.

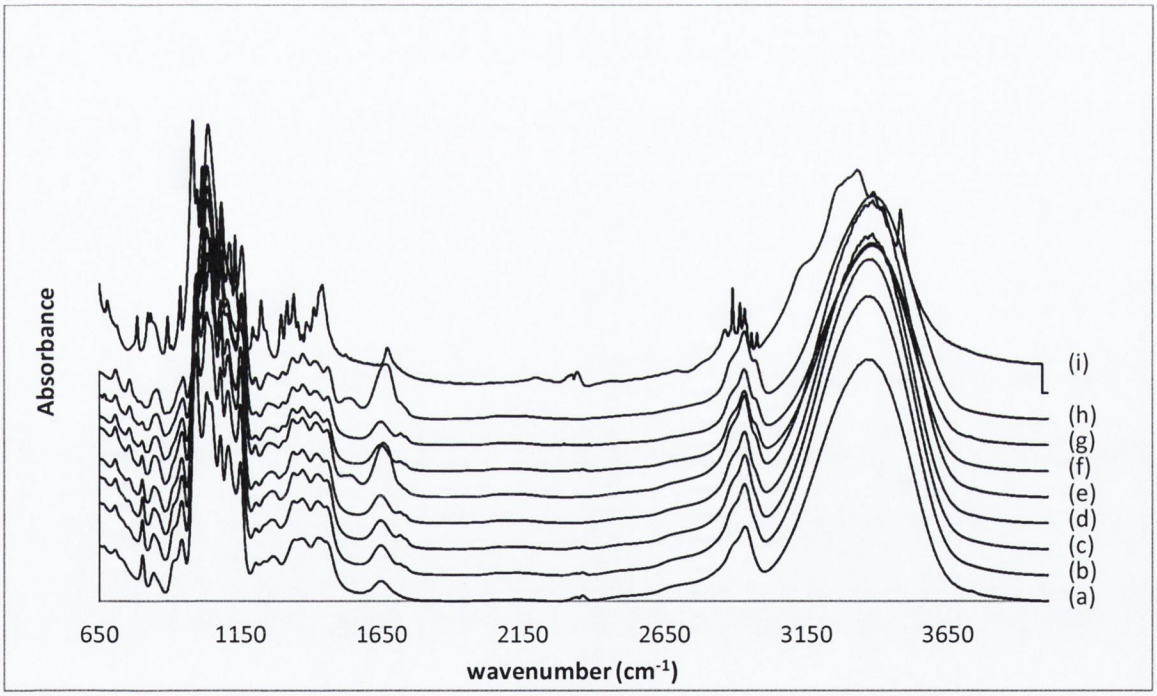

Figure 5.10 FTIR spectras of spray dried T:HPβCD composite systems (a) 100:0, (b) 80:20, (c) 70:30, (d) 60:40, (e) 40:60, (f) 30:70, (g) 20:80, (h) 0:100 and (i) trehalose dihydrate

5.3.3 Thermal analysis

DSC scans of spray dried composite systems showed a single glass transition that was intermediate between the glass transition temperature (T_g) values of the pure components. No evidence of further thermal events such as crystallisation or melting was found for T:R systems. On the other hand, T:HPβCD systems with higher content of cyclodextrin present delayed and reduced enthalpy crystallisation and melting events compared to spray dried trehalose alone (Figure 5.11 and 5.12 and Table 5.3), with total inhibition of both events when the cyclodextrin content was ≥60 %. When trehalose was spray dried with raffinose there was a significant decrease in T_g ($p=0.031$) at higher weight fractions of raffinose (>60 %) compared to trehalose alone; upon spray drying with HPβCD a significant increase in T_g ($p<0.05$) was observed when the content of the latter was increased. Clas et al. (1999) described the glass transition as a characteristic physical and energetic property of an amorphous compound. Hence, after spray drying crystalline trehalose and raffinose were in the amorphous state, as previously verified by XRPD. Another event of observed on the trehalose:raffinose composite systems was the inhibition of trehalose recrystallisation and melting.

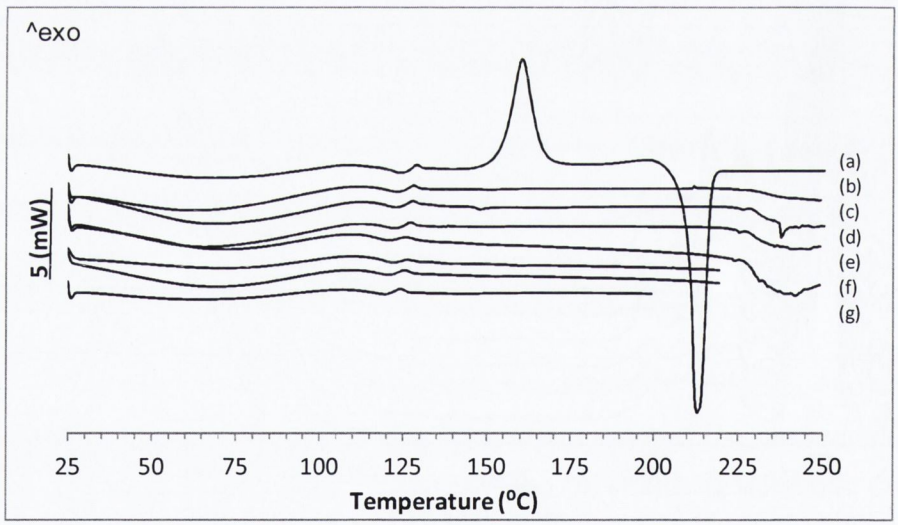

Figure 5.11 DSC scans of trehalose:raffinose composite systems with ratios: (a) 100:0, (b) 80:20, (c) 70:30, (d) 60:40, (e) 40:60, (f) 30:70, (g) 20:80 and (h) 0:100.

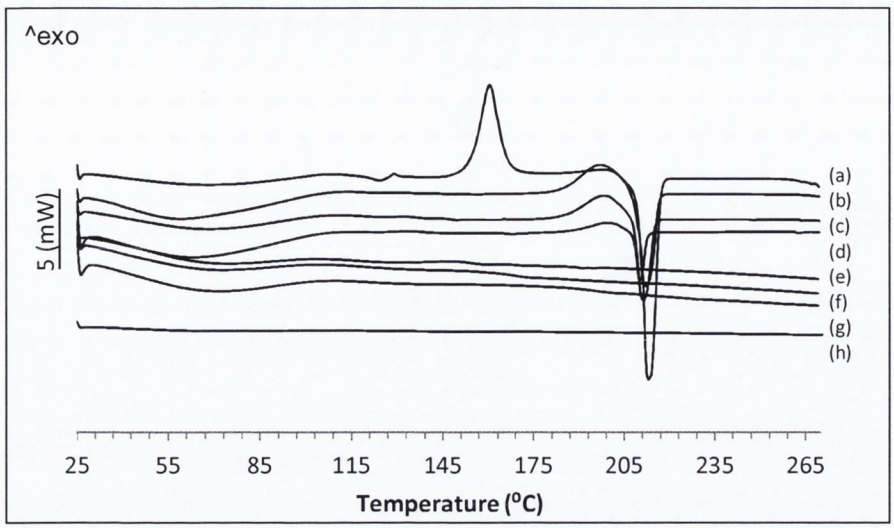

Figure 5.12 DSC scans of trehalose:hydroxypropyl-β-cyclodextrin composite systems with ratios: (a) 100:0, (b) 80:20, (c) 70:30, (d) 60:40, (e) 40:60, (f) 30:70, (g) 20:80 and (h) 0:100.

The delay and decrease in enthalpy of recrystallisation and melting events and their inhibition, suggests an enhancement of trehalose physical stability when mixed with raffinose or HPβCD. Leinen and Labuza (2006) studied the stability, in three different relative humidity conditions at ~23 °C, of a mixture of raffinose and sucrose (5:95) after spray drying and concluded that raffinose was able to inhibit sucrose recrystallisation at low RH and delay sucrose recrystallisation at high RH. Studies on HPβCD have shown that this oligossacharide is able to decrease the degree of crystallinity and inhibit recrystallisation of polymers and drugs, reducing the melting enthalpy and increasing their physical stability (Davies and Brewster, 2004; Yavuz et al., 2010; Tewes et al., 2011).

Table 5.3 Glass transition temperature (T_g), recrystallisation temperature and associated enthalpy (T_c, ΔH_c) and melting temperature and associated enthalpy (T_m, ΔH_m) of trehalose composite systems.

	T:R	T:HPβCD				
	T_g (°C)		T_c (°C)	ΔH_c (J/g)	T_m(°C)	ΔH_m (J/g)
100:0	121.8±0.45		158.7±0.54	99.2±6.10	210.4±0.42	138.6±8.62
80:20	119.6±0.10	120.3±1.75	197.6±0.00	91.0±0.57	211.5±0.40	70.2±3.49
70:30	119.5±0.06	119.3±0.40	198.6±0.06	69.9±4.97	211.3±0.06	55.6±1.86
60:40	119.3±0.03	120.6±0.76	197.4±1.10	33.8±9.59	210.7±0.75	24.2±8.95
40:60	118.7±0.47	153.7±1.03	-	-	-	-
30:70	118.2±0.06	166.5±1.04	-	-	-	-
20:80	117.1±0.73	193.4±0.37	-	-	-	-
0:100	115.6±0.21	225.4±0.32	-	-	-	-

For a thorough analysis of the composite system glass transition temperatures, in order to gain more knowledge on the physical properties of the systems, different model equations were used to predict the T_g and a comparison to the experimentally determined T_g was made:

- Gordon-Taylor (GT) equation with Simha-Boyer rule $T_g = \frac{w_1 Tg_1 + K_{GT} w_2 Tg_2}{w_1 + K_{GT} w_2}$ (Eq. 1) where $K_{GT} = \frac{d_1 Tg_1}{d_2 Tg_2}$, assuming ideal volume additivity of both materials at T_g, no specific interactions between the two components and the effect of density is accounted for; T_g, w and d are the glass transition temperature in degrees Kelvin, the weight fraction and density of the subscripts *1* (first component), *2* (second component) and mixture (no subscript), K_{GT} is related to a thermal expansion coefficient difference between glassy and liquid state (Kalichevsky at al., 1992; Chen et al., 2002; Tajber et al., 2005; Tewes et al., 2010);
- Fox equation $\frac{1}{Tg} = \frac{w_1}{Tg_1} + \frac{w_2}{Tg_2}$ (Eq. 2) assuming components have similar density (Kalichevsky et al., 1992; Chen et al., 2002; Tajber et al., 2005);

- Kwei equation is an extension of the GT equation, used in cases of strong interactions between components $Tg = \frac{w_1 Tg_1 + K_k w_2 Tg_2}{w_1 + K_k w_2} + q w_1 w_2$ (Eq. 3) where K_k and q are fitted values to experimental data (Kalichevsky et al., 1992; Tajber et al., 2005);

Figure 5.13 and Table 5.4 present the obtained results from the models fitting to trehalose composite systems. We could see for both type of systems (T:R and T:HPβCD) deviations to predictions by the Gordon-Taylor and Fox equations. In the case of T:R NPMPs, at low weight fractions of raffinose (0.2 – 0.4) the T_g was below predictions (negative deviations) and at high weight fractions (0.6 - 0.8) the T_g was above (positive deviations) predicted values. For T:HPβCD NPMPs all glass transitions presented a negative deviation from the calculated T_g. Gordon-Taylor and Fox model equations assume ideal behaviour between molecules, that is, there is ideal volume additivity and no interactions between components. Studies by Taylor and Zografi (1998) on sugar-polymer lyophilised systems also reported negative deviations from the predicted values by the Gordon-Taylor equation due to interaction between molecules as a result of the formation of hydrogen bonds. FTIR analysis, which is discussed later in this chapter, will investigate the existence of molecular interactions between trehalose and raffinose or hydroxypropyl-β-cyclodextrin, accounting for the deviations to the Gordon-Taylor equation. Given the observed deviations, there was the need to find a more suitable model for T_g prediction.

The Kwei equation presented a good fit to T:R data (r^2=0.917) and a very good fit for T:HPβCD data (R^2=0.983), hence there were interactions between molecules. Some data points presented very small deviations from predicted values; these might be due to plasticising effects of the residual solvent content in powders after spray drying (Kalichevsky et al., 1993). The constatnt q in equation 3, qw_1w_2, is proportional to the number of specific interactions existing in the mixture, with q as a measure of the efficacy of hydrogen bond formation; hence a larger magnitude of q, without regard to its sign, is indicative of a higher degree of hydrogen bonds between the mixture components (Kwei et al., 1984). Table 5.4 reports the q value for the spray dried systems, a high degree of hydrogen bonding is expected between trehalose and HPβCD than between trehalose and raffinose.

The best model equation to describe the T_g of the composite system was the Kwei equation, giving a strong suggestion of molecular interactions between the mixture components.

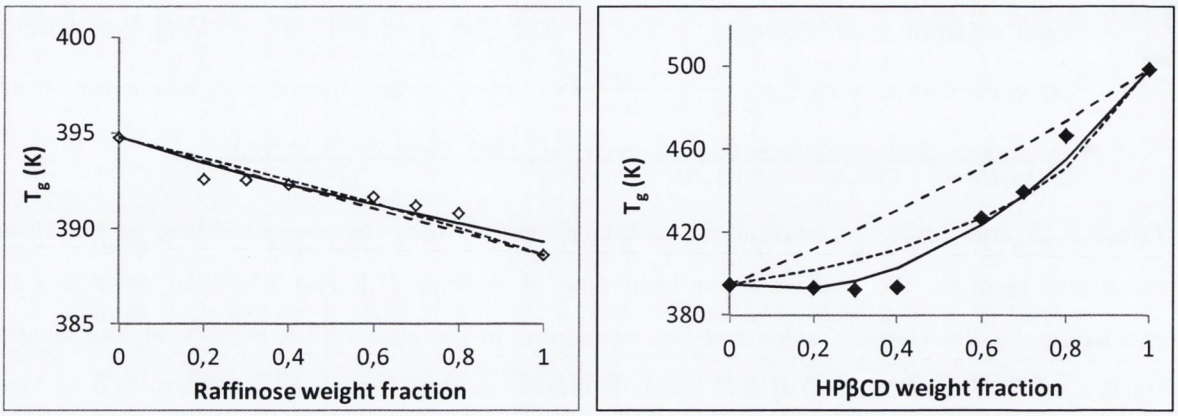

Figure 5.13 Glass transitions of (left) T:R and (right) T:HPβCD composite systems as function of the added excipient weight fraction. The dotted, dashed and solid lines represent the predictions based on the Gordon-Taylor, Fox and Kwei equations, respectively.

Table 5.4 The Gordon-Taylor parameter and the fitting coefficients by using the Kwei equation.

	Gordon-Taylor equation	Kwei equation
T:R	K_{GT} = 0.92	K_k = 1.75
		q = 1.75
		R^2 = 0.917
T:HPβCD	K_{GT} = 0.79	K_k =1
		q = -140.15
		R^2 = 0.983

A residual solvent content (RSC) of 2.49-3.67 % and 2.19-4.20 % was determined for T:R and T:HPβCD samples over the temperature range 25-130 °C from TGA (Table 5.5 and 5.6). ANOVA analysis revealed no significant difference between samples (p=0.199) for T:R data and, significant differences between samples (p=0.03) for T:HPβCD. For better comprehension of the RSC composition, GC-FID was used to quantify methanol and butyl acetate, assuming the difference between calculated values from the two techniques would correspond to bound and unbound water (i.e., $TGA - GC = water\ content$). Tables 5.5 and 5.6 present the values determined. RSC is constituted mainly by butyl acetate and water, methanol was not detected for most composite samples, that is to say it was below the limit of detection of the analysis method (305 ppm). The water content could be explained by the amorphous sugars' strong tendency to take up moisture by adsorption and desorption (Hancock and Shamblin, 1998). The presence of BA could be due to insufficient drying during processing or solvent entrapment in the particles matrix or by adsorption or capillary condensation in the pores (Gregg and Sing, 1982). A correlation between RSC and SSA

for T:HPβCD composites was investigated since the existence of significant differences between SSA of samples had previously been determined (Figure 5.14). A trend was found: as specific surface area increases, residual solvent content also increases. The assumption of entrapment of solvents/moisture in the porous structure of particles would appear to be valid for T:HPβCD composite systems.

Table 5.5 Residual solvent content by TGA and GC-FID for T:R composite systems. ND – not detectable.

T:R	RSC by TGA (% w/w)	RSC by GC-FID (% w/w)		Extrapolated
		Methanol	Butyl acetate	Water content (%)
100:0	2.49±0.50	0.4±0.06	0.99±0.003	1.1
80:20	3.09±0.37	ND	1.2±0.37	1.89
70:30	2.97±0.23	ND	0.3±0.01	2.67
60:40	3.58±0.05	ND	1.1±0.03	2.48
40:60	3.38±0.33	ND	1.8±0.13	1.58
30:70	3.67±0.13	ND	2.6±0.01	1.07
20:80	3.26±1.04	ND	1.6±0.04	1.66
0:100	2.60±0.31	ND	0.36±0.02	2.24

Table 5.6 Residual solvent content by TGA and GC-FID for T:HPβCD composite systems. ND – not detectable.

T:HPβCD	RSC by TGA (% w/w)	RSC by GC-FID (% w/w)		Extrapolated
		Methanol	Butyl acetate	Water content (%)
100:0	2.49±0.50	0.4±0.06	0.99±0.003	1.1
80:20	3.10±0.59	ND	1.0±0.05	2.1
70:30	3.51±0.30	ND	2.1±0.04	1.41
60:40	3.71±0.15	ND	1.4±0.04	2.31
40:60	3.85±0.15	ND	0.7±0.01	3.15
30:70	4.45±0.50	1.6±0.02	1.1±0.01	1.75
20:80	3.11±0.50	0.7±0.01	1.6±0.06	0.81
0:100	2.32±0.15	1.2±0.01	0.6±0.01	0.52

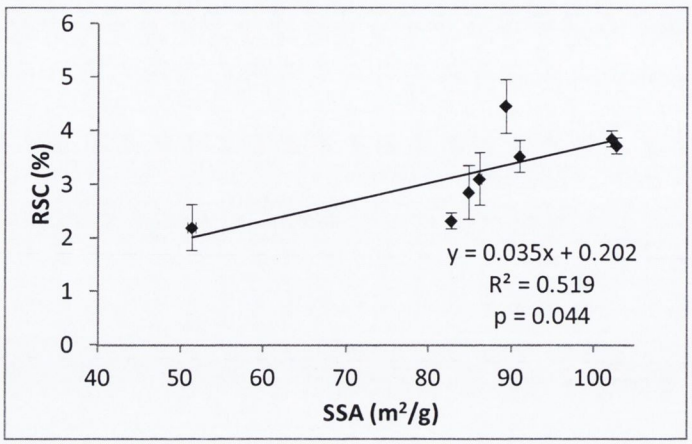

Figure 5.14 Residual solvent content (RSC) of spray dried T:HPβCD as a function of specific surface area (SSA).

5.3.4. Dynamic vapour sorption

DVS was used to evaluate the effect of moisture on the solid state stability of the different composites, in comparison to the constituents spray dried alone. Figure 5.15 shows the isotherms, i.e., percentage change in mass of the sample as a function of relative humidity, for excipients spray dried alone.

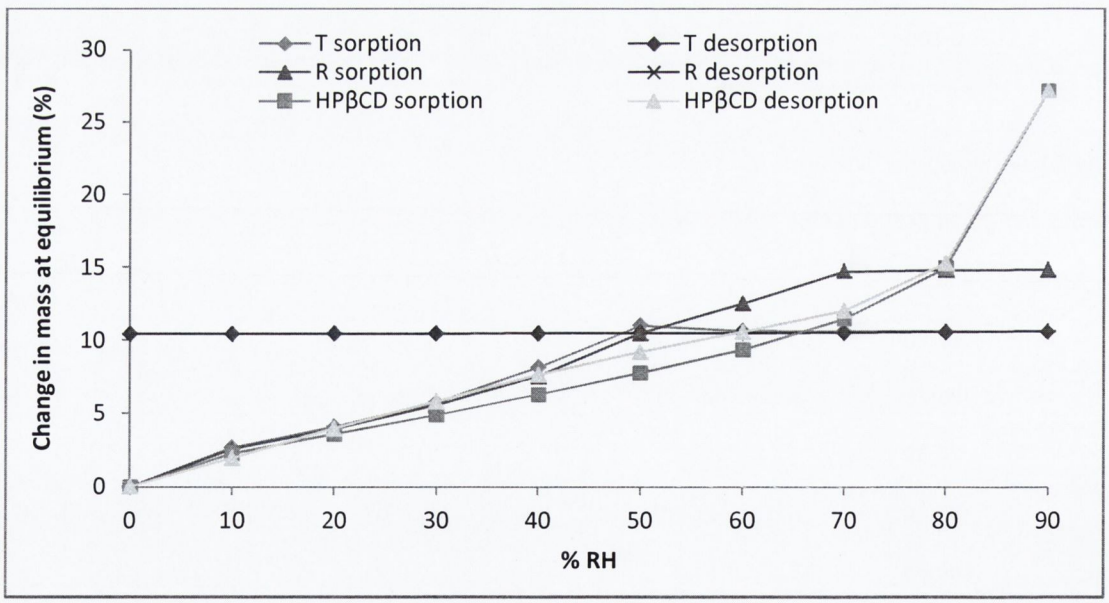

Figure 5.15 Water vapour sorption and desorption isotherms of trehalose, raffinose and hydroxypropyl-β-cylcodextrin spray dried alone.

Spray dried trehalose takes up ~11 % by mass of moisture below 50 % RH, however above 50 % RH there is a sudden loss in mass to approximately 10.6 % moisture content (2 moles of water per 1 mole of trehalose) with no water uptake at higher RH. The desorption isotherm shows no further water loss or gain, resulting in an open hysteresis.

The Young-Nelson model that establishes a quantitative correlation between the moisture content and the % RH, was fitted to profile the water uptake as water adsorbed in a monolayer and multilayer, and as water absorbed (Bravo-Osuna et al., 2005; Tewes et al., 2010):

$$M_s = A(\beta + \theta) + B\theta RH \text{ (Eq. 1)}$$

$$M_d = A(\beta + \theta) + B\theta RH_{max} \text{ (Eq.2)}$$

where M_s and M_d are, respectively, the amount of water sorbed and desorbed at each RH (used as per unit), expressed as a fraction of the dry mass of the material. A and B are constants characteristic of each material: $A = \frac{\rho_w Vol_M}{W_m}$ and $B = \frac{\rho_w Vol_A}{W_m}$ where ρ_w is the water density, Vol_M and Vol_A are, respectively, the adsorbed and absorbed water volumes and W_m is the weight of dry material. In this model, ϑ is the fraction of the material surface covered by at least one layer of water molecules, and $A\vartheta$ is the mass of water in a complete adsorbed monolayer expressed, like all masses in the model, as a fraction of the dry mass of the material. $A(\beta+\vartheta)$ is the total amount of adsorbed water, and $A\beta$ is the mass of water which is adsorbed beyond the mass of the monolayer, that is, in multilayer. B is the mass of absorbed water at 100 % RH, and hence, $B\vartheta RH$ is the mass of absorbed water when the monolayer coverage is ϑ and the relative humidity is RH.

Initial water uptake (10% RH) leads to the formation of a monolayer; at 20 % RH the presence of a multilayer and small amount of water absorption begins to be evident; as RH increases water is mainly absorbed; water desorption did not occur, water stayed in the bulk of the material, resulting in the open hysteresis (Appendix 3).

The type of hysteresis observed and the sudden mass loss with no further change is believed to occur as a result of amorphous trehalose collapse into its crystalline stable form. XRPD confirmed this assumption, since the two characteristic peaks of crystalline trehalose dihydrate (at 8.7 ^{o} and 23.8 ^{o}) were identified in the sample after DVS analysis (Figure 5.16A) (Nagase et al., 2002; Pinto et al., 2006; Ohashi et al., 2007). Hancock and Shamblin (1998) described that the maximum amount of

water absorbed by amorphous sugars is usually limited by crystallisation of the sugar at high relative humidities. Therefore the critical RH for trehalose NPMPs was 50 % RH.

Amorphous raffinose, also a highly hygroscopic sugar, was able to sorb ~14 % of its weight in moisture below 70 % RH (4 moles of water per 1 mole of raffinose), after which no water uptake was registered. Further weight loss, ~4 %, was only seen in the desorption isotherm at 10 % RH. The final water uptake was 10 % (w/w) (3 moles of water per 1 mole of raffinose) and an open hysteresis was recorded. Fitting of the Young-Nelson model, led to similar results as described for trehalose NPMPs: water uptake was mainly absorbed into the powder bulk, a small fraction formed a mono and multilayer with no evidence of water desorption (Appendix 3). XRPD showed there was recrystallisation to some extent, since the characteristic peaks of raffinose pentahydrate were identified (Figure 5.16B); raffinose trihydrate formation was hypothesised, but never confirmed, in studies by Cheng and Lin (2006) to explain the hydration of raffinose when exposed to high relative humidities suggesting the formation a hydrate form that was different to the pentahydrate. Previous studies by Hogan and Buckton (2001) and Charmathy et al. (2010) have shown that raffinose was able to absorb 4 moles of water per 1 mole of raffinose when exposed to 75 % RH, collapsing into its crystalline pentahydrate form. The critical RH for raffinose was determined here to be 70 %.

Hydroxypropyl-β-cyclodextrin presented high capacity for moisture uptake; ~27 % (13.6 moles of water to 1 mole of HPβCD) change in mass was observed at the end of the cycle, that is, at 90 % RH. On desorption only a small hysteresis loop was observed, and all moisture was released. Hence, the sorption/desorption isotherm presented the characteristic type IV shape (Gregg and Sing, 1982; IUPAC, 1986). This type of isotherm is usually attributed to porous materials and its hysteresis is caused by capillary condensation (Gregg and Sing, 1982). On the other hand, the hysteresis can also be due to bulk absorption, since we have an amorphous material (Hancock and Shamblin, 1998). Capillary condensation can occur, since our powder was constituted by porous particles with high surface area indicative of elevated degree of porosity. The Young-Nelson model was fitted to profile the water. There was no bulk absorption (Appendix 3); moisture uptake was only by mono and multilayer adsorption onto the solid. Therefore the hysteresis was attributed to capillary condensation. The XRPD showed the cyclodextrin to be amorphous after DVS analysis (Figure 5.16C).

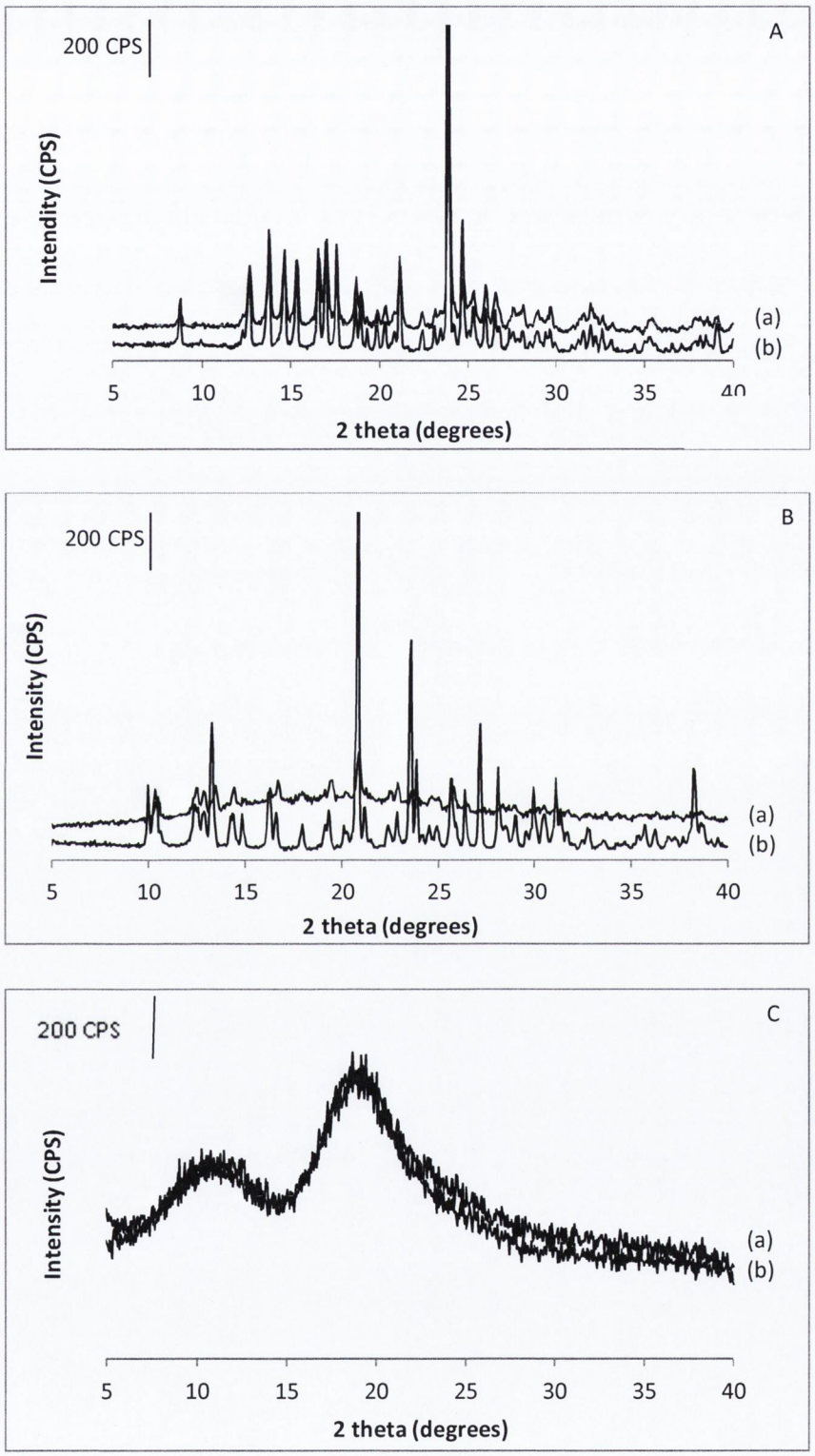

Figure 5.16 XRPD of spray dried excipients alone (a) after DVS analysis and (b) as supplied (A) trehalose, (B) raffinose and (C) HPβCD.

Sorption and desorption isotherms of T:R composite systems are represented in figure 5.17a and figure 5.17b. Composite systems with 20 % and 30 % raffinose weight showed a change in the critical RH compared to trehalose or raffinose spray dried alone, to 60% with water uptake of ~13 %. Above this RH there was ~2 % mass loss. The desorption isotherms showed no further gain or loss of moisture. XRPD demonstrated the collapse of the amorphous solid dispersion into a crystalline mixture of trehalose dihydrate and raffinose pentahydrate (Fig 5.18).

Higher percentages of raffinose (60 %, 70 % and 80 %) elevated the critical RH to 70 % with a moisture uptake of 18 to 19 %. Above 70% RH a mass loss of ~3 % and no further moisture uptake was registered. Desorption isotherms demonstrated no loss of moisture until 10 % RH, below which an additional mass loss of ~5 % was registered. X-ray diffractograms revealed trehalose dihydrate main characteristic peaks, hence trehalose did recrystallise but at a higher relative humidity. Raffinose was partially recrystallised, since there was evidence of amorphous material and only the peak at 21.1°, typical of the pentahydrate form, was identified.

Trehalose:raffinose composite systems presented an increase in the solid state stability compared to trehalose spray dried alone since a maximum critical RH of 70 % can be achieved with composites with ≥ 60% weight of raffinose.

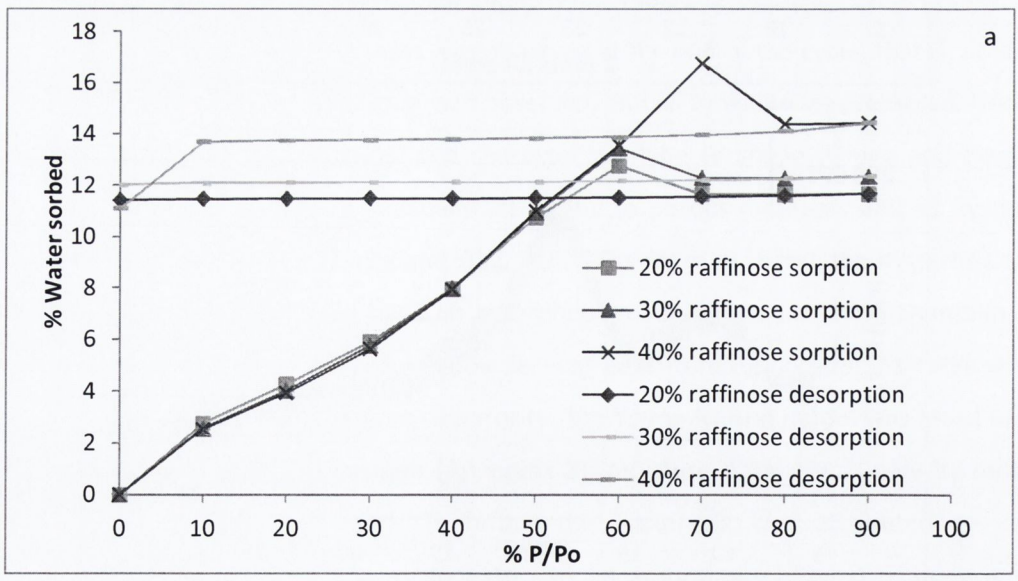

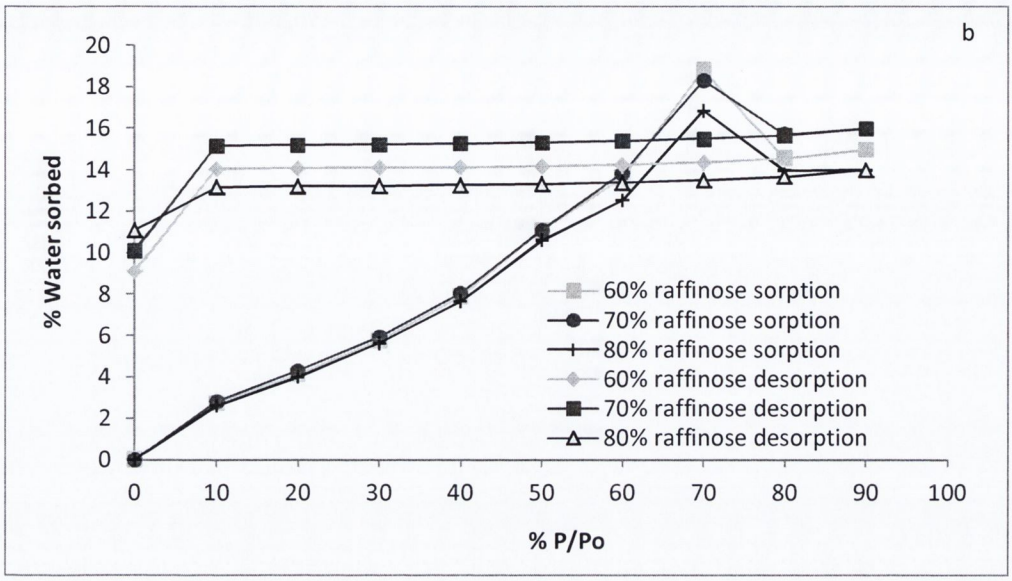

Figure 5.17 Water vapour sorption and desorption isotherms of trehalose:raffinose composite systems.

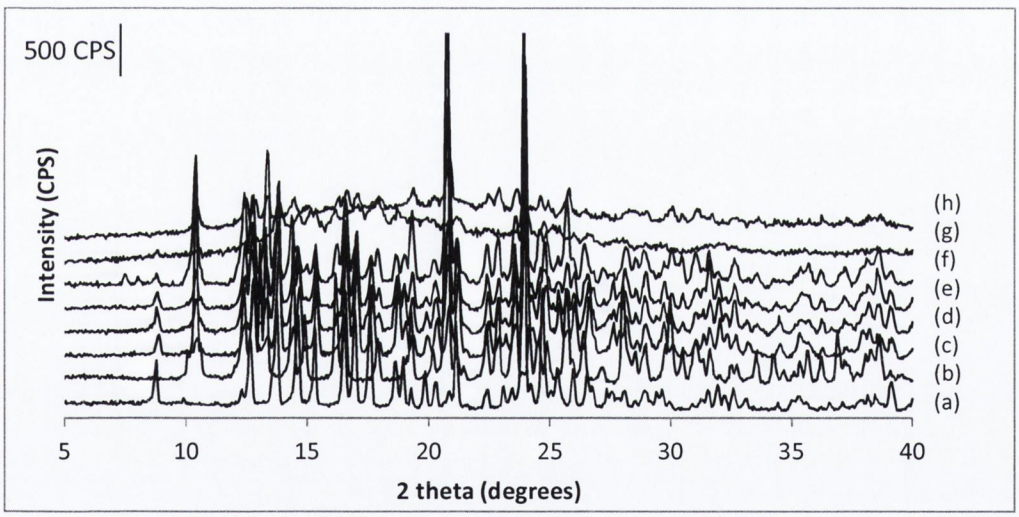

Figure 5.18 XRPD of T:R composite systems (a) 100:0, (b) 0:100, (c) 80:20, (d) 70:30, (e) 60:40, (f) 40:60, (g) 30:70, and (h) 20:80 after water vapour sorption and desorption analysis.

Sorption and desorption isotherms for T:HPβCD are represented in Figure 5.19. As different weights of HPβCD (20 %, 30 % and 40 %) were spray dried with trehalose we could see an immediate increase in the critical relative humidity to 60% RH with a water uptake of ~12 %. Above 60 % RH there was a small mass loss of ~2 % followed by water uptake. Desorption isotherms showed an initial mass loss at higher RH; a constant mass from 60 % to 40 % and a continuous mass loss from 40 % to 0 % RH. Final moisture uptake was ~5 %. The inflection point at 60 % RH was due to

trehalose recrystallisation, evident by XRPD analysis (Figure 5.20). The remaining water sorption and desorption was due to the cyclodextrin-water interactions.

When trehalose was spray dried with weights ≥60 % of HPβCD, moisture uptake was greatly enhanced. A maximum of 30 % mass gain could be achieved, similar to moisture uptake by HPβCD when spray dried alone. The sorption/desorption isotherms could be described as type IV. Different hysteresis loops were seen: 60 % and 70 % HPβCD composites presented a loop between 70 and 90 % RH and a second one between 0/10 and 70 % RH. Young-Nelson model was fitted to better comprehend these events. At high RH it was observed that moisture uptake was due to multilayer adsorption onto the solid surface; below 70% RH moisture uptake was not only due to the mono and multilayer adsorption but also to bulk absorption. The latter was due to the trehalose fraction, since there was no evidence of this event with cyclodextrin alone and water uptake by trehalose is primarily due to its absorption (Appendix 3).

XRPD after DVS revealed systems were still amorphous and that possible recrystallisation of trehalose was not evident. Hence the addition of ≥ 60 % weight of HPβCD to trehalose inhibits the recrystallisation of the latter, improving physical stability of trehalose NPMPs.

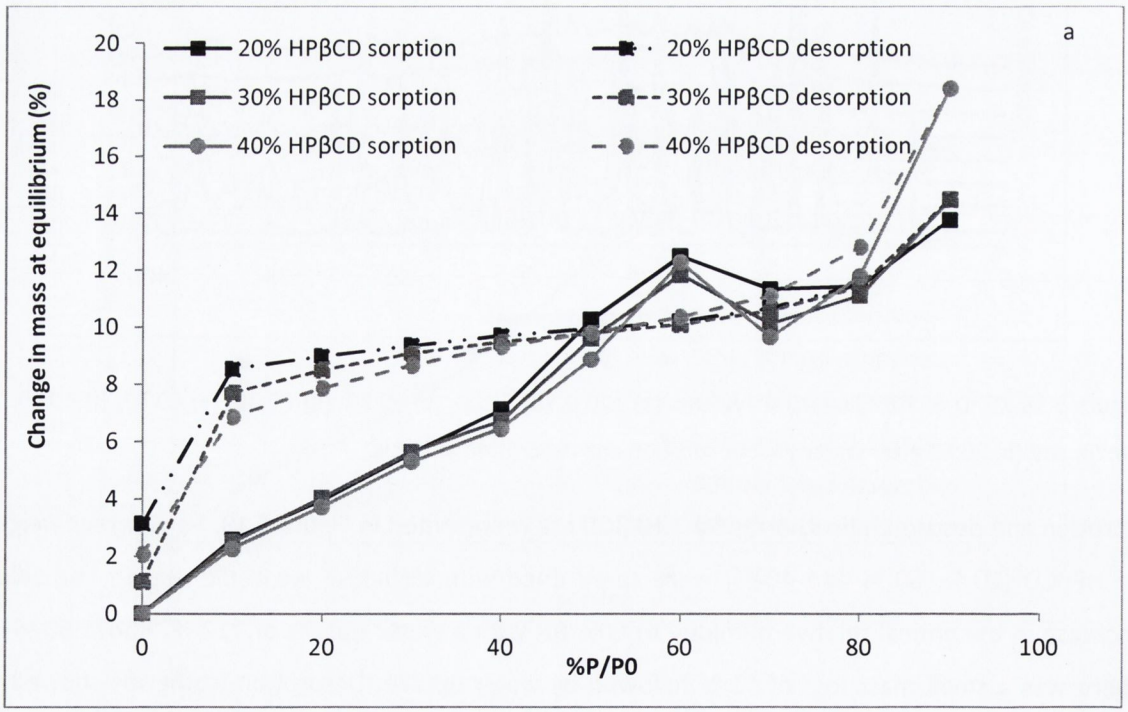

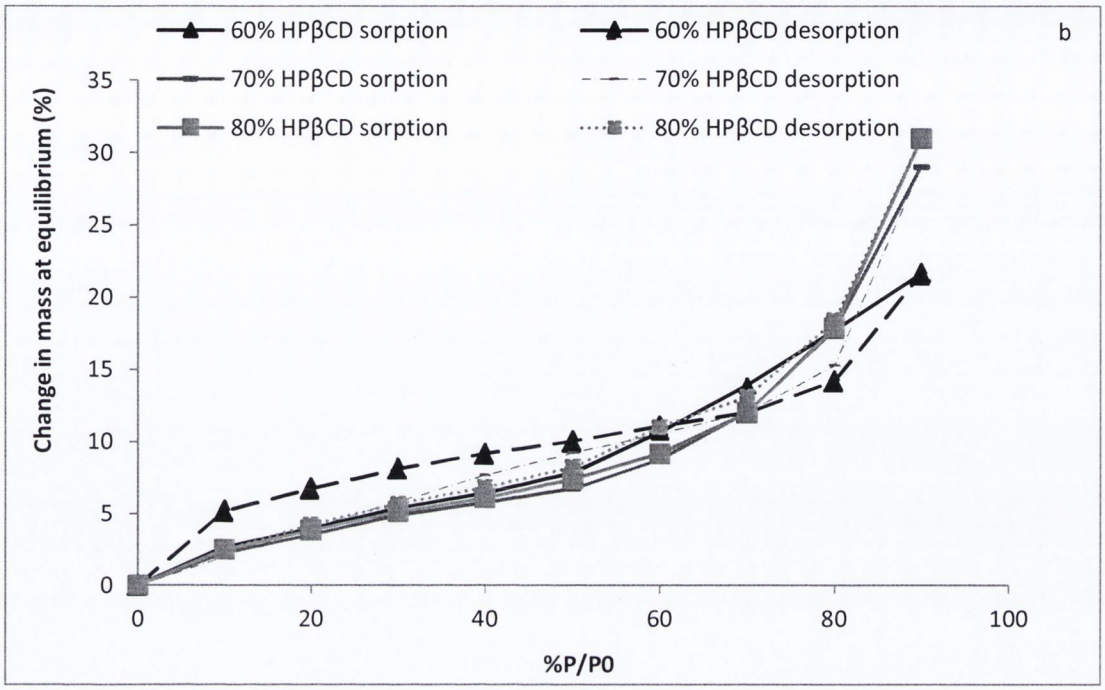

Figure 5.19 Water vapour sorption and desorption isotherms of trehalose:hydroxypropyl-β-cylcodextrin composite systems.

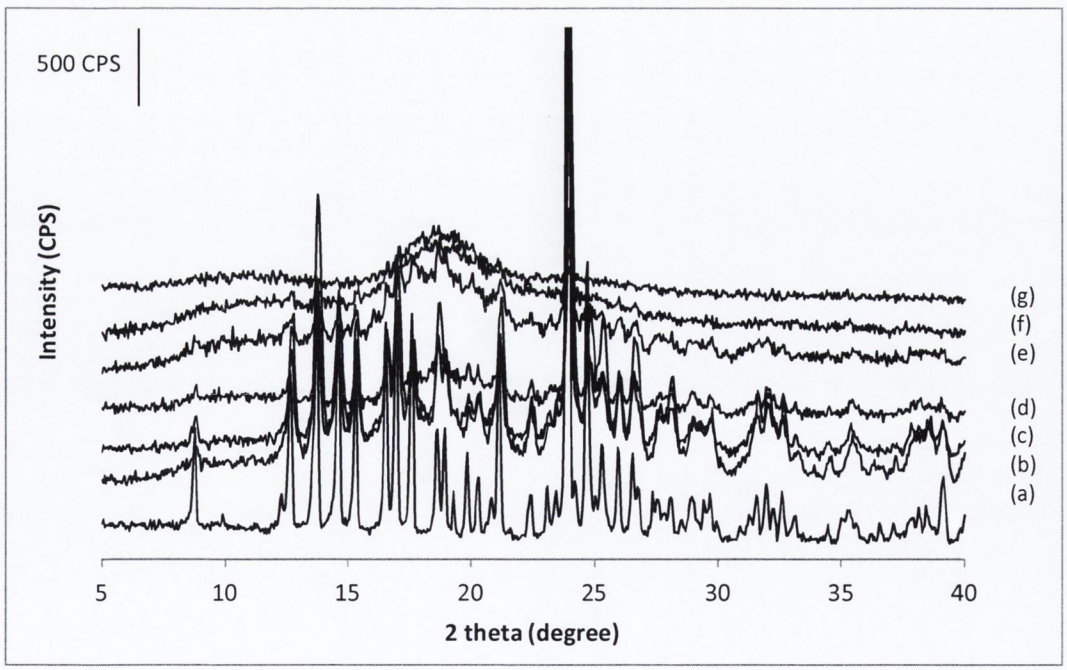

Figure 5.20 XRPD of T:HPβCD composite systems (a) 100:0, (b) 80:20, (c) 70:30, (d) 60:40, (e) 40:60, (f) 30:70 and (g) 20:80 after water vapour sorption and desorption analysis.

5.3.5. *In-vitro* deposition via next generation impactor analysis

In-vitro deposition analysis was performed on composites that presented the best characteristics: aerodynamic diameter < 3 μm, high specific surface area, high T_g and low RSC. Therefore, samples chosen to assay were: T:R 70:30 and 60:40; T:HPβCD 70:30, 60:40, 40:60 and 30:70.

Deposition profiles of T:R composites were similar to the deposition profile of trehalose when spray dried alone (Figure 5.21). The fine particle fraction < 3 and < 5 μm increased with increasing weight fraction of raffinose (Table 5.7). Due to the large variability however, there was not a statistically significant difference between composite systems and trehalose NPMPs (< 3 μm p=0.074; < 5 μm p=0.073). Mass median aerodynamic diameters of T:R NPMPs were smaller but once more not significantly different (p=0.081) compared to trehalose spray dried alone. Comparing the calculated d_{aer} with the MMAD, the latter was higher suggesting the presence of particle aggregates that were not broken/dispersed by the aerodynamic forces generated during the analysis. The main difficulty associated with inhalation of fine particle powders and their efficient delivery is the strong interparticle forces (mainly van der Waals forces) which make the cohesive bulk powder agglomerate (Daniher and Zhu, 2008).

Figure 5.22 represents the aerosol deposition of T:HPβCD composite systems. There was an evident improvement in the aerosol delivery with the addition of cyclodextrin to trehalose NPMPs, with less deposition in the mouthpiece adaptor and induction port and higher deposition on stages with lower cut-off points (≤ 2 μm, stage 4 to 7) for the composite NPMPs. Fine particle fraction < 3 and 5 μm of T:HPβCD composites was ~4 fold higher (Table 5.8) than for trehalose spray dried alone. As previously concluded in Chapter 4, for powders of similar particle size but differing SSA, a trend of increasing FPF with increasing SSA, attributable to the porosity of the particles is evident. This relationship between SSA and FPF was verified with T:HPβCD composite systems, that presented similar particle size to trehalose NPMPs and SSA ~2 fold higher.

The MMAD values calculated for the T:HPβCD composite systems were similar to the calculated aerodynamic diameters. Hence, any aggregates present are easily dispersed. This can be also attributed to the high SSA (high porosity), since these particles present fewer areas of contact, leading to lower cohesion and easier dispersion (Tabor, 1977).

Statistical analysis of emitted dose, FPF, MMAD and GSD by ANOVA showed all composite samples were significantly different ($p < 0.05$) to trehalose spray dried alone and additional analysis by the Tukey's test showed that all composite systems were similar in terms of these parameters.

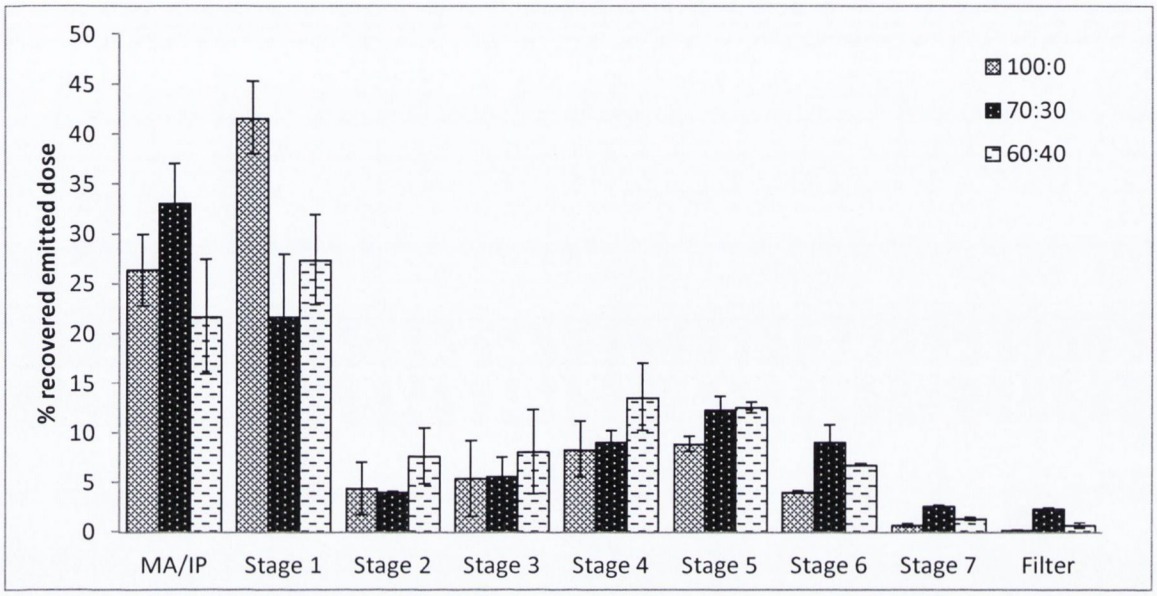

Figure 5.21 *In vitro* aerosol deposition profile by use of a NGI of T (ratio 100:0) and T:R NPMPs ratios 70:30 and 60:40 as calculated % of recovered emitted dose vs. NGI stages. MA – mouth adapter IP – induction port

Table 5.7 Recovered emitted dose, fine particle fraction (FPF), mass median aerodynamic diameter (MMAD) and geometric standard deviation (GSD) of *in vitro* aerosol deposition of T and T:R NPMPs.

	T:R 0:100	T:R 70:30	T:R 60:40
% recovered emitted dose	81.0±12.1	72.8±4.7	60.5±17.7
FPF < 5 µm	27.4±7.6	46.7±0.9	53.8±10.9
< 3 µm	21.4±2.1	36.1±3.2	40.2±8.3
MMAD	4.4±0.35	2.7±0.62	3.3±0.45
GSD	2.6±0.02	2.9±0.33	2.4±0.16

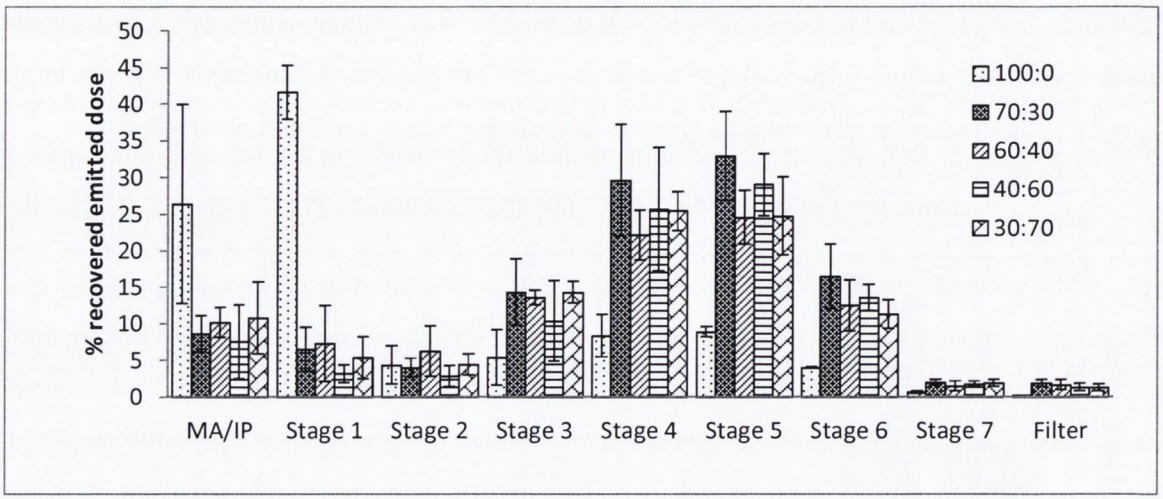

Figure 5.22 *In vitro* aerosol deposition profile by use of a NGI of T (ratio 100:0) and T:HPβCD NPMPs ratios 70:30, 60:40, 40:60 and 30:70 as calculated % of recovered emitted dose vs. NGI stages. MA – mouth adapter IP – induction port

Table 5.8 Recovered emitted dose, fine particle fraction (FPF), mass median aerodynamic diameter (MMAD) and geometric standard deviation (GSD) of *in vitro* aerosol deposition of T and T:HPβCD NPMPs.

	T:HPβCD 0:100	**T:HPβCD 70:30**	**T:HPβCD 60:40**	**T:HPβCD 40:60**	**T:HPβCD 30:70**
% recovered emitted dose	81.0±12.1	90.1±0.6	90.9±0.7	88.9±2.9	91.1±1.6
FPF < 5 μm	27.4±7.6	84.2±3.4	80.3±6.5	83.8±6.3	86.2±2.7
< 3 μm	21.4±2.1	81.8±1.5	74.6±9.9	79.9±8.1	83.0±3.4
MMAD	4.4±0.35	2.0±0.68	2.3±0.52	2.0±0.24	2.2±0.29
GSD	2.6±0.02	2.0±0.34	2.1±0.11	2.0±0.11	2.0±0.07

5.4. SPRAY DRIED RAFFINOSE:HYDROXYPROPYL-β-CYCLODEXTRIN COMPOSITE SYSTEMS

Raffinose composites were spray dried using the conditions described for optimised raffinose NPMPs. Feed solutions of 2.9% (w/v) of d-(+)-raffinose pentahydrate with 20%, 30%, 40%, 60%, 70% and 80 % weight hydroxypropyl-β-cyclodextrin in methanol:n-butyl acetate (4:1) (v/v) were spray dried. The outlet temperature of raffinose: hydroxypropyl-β-cyclodextrin (R:HPβCD) samples varied between 86-90 ^{o}C. Yields ranged from 57.5 to 62.8%, with no statistically significant difference (p=0.184) between samples.

5.4.1. Solid-state, morphology and micromeritic properties

R:HPβCD spray dried composites were amorphous (Figure 5.23). Diffractograms presented the typical diffuse halo pattern, characteristic of amorphous materials, with conversion of raffinose from crystalline state to the amorphous state.

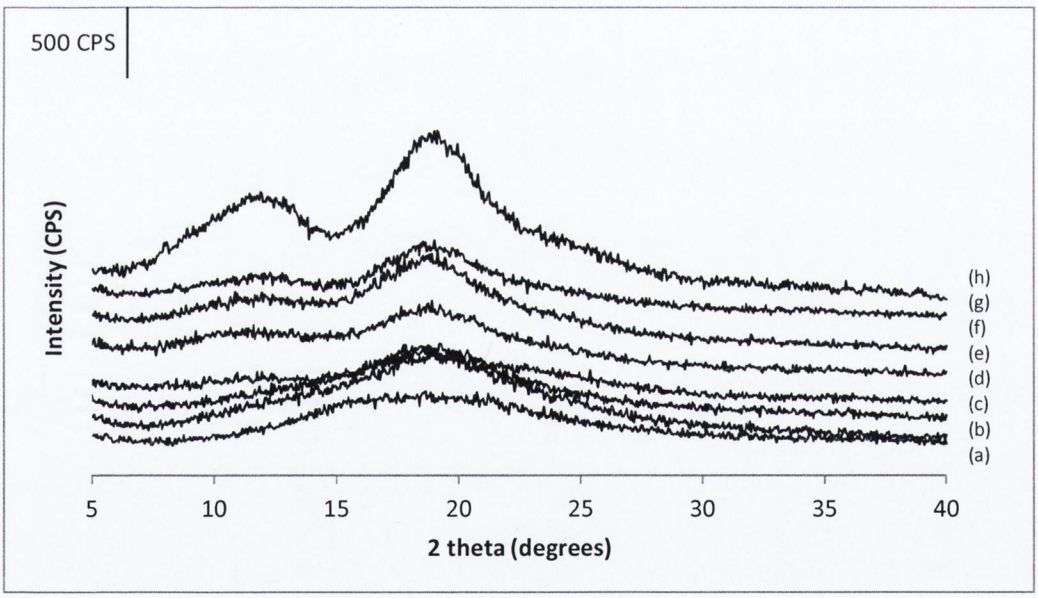

Figure 5.23 XRPD of spray dried raffinose, raffinose:HPβCD composite systems and HPβCD.

SE micrographs showed all samples were composed of porous particles (Figure 5.28). Loss of spherical morphology was seen with an increased weight fraction of HPβCD and irregular shaped porous particles were produced (Figure 5.24d-h).

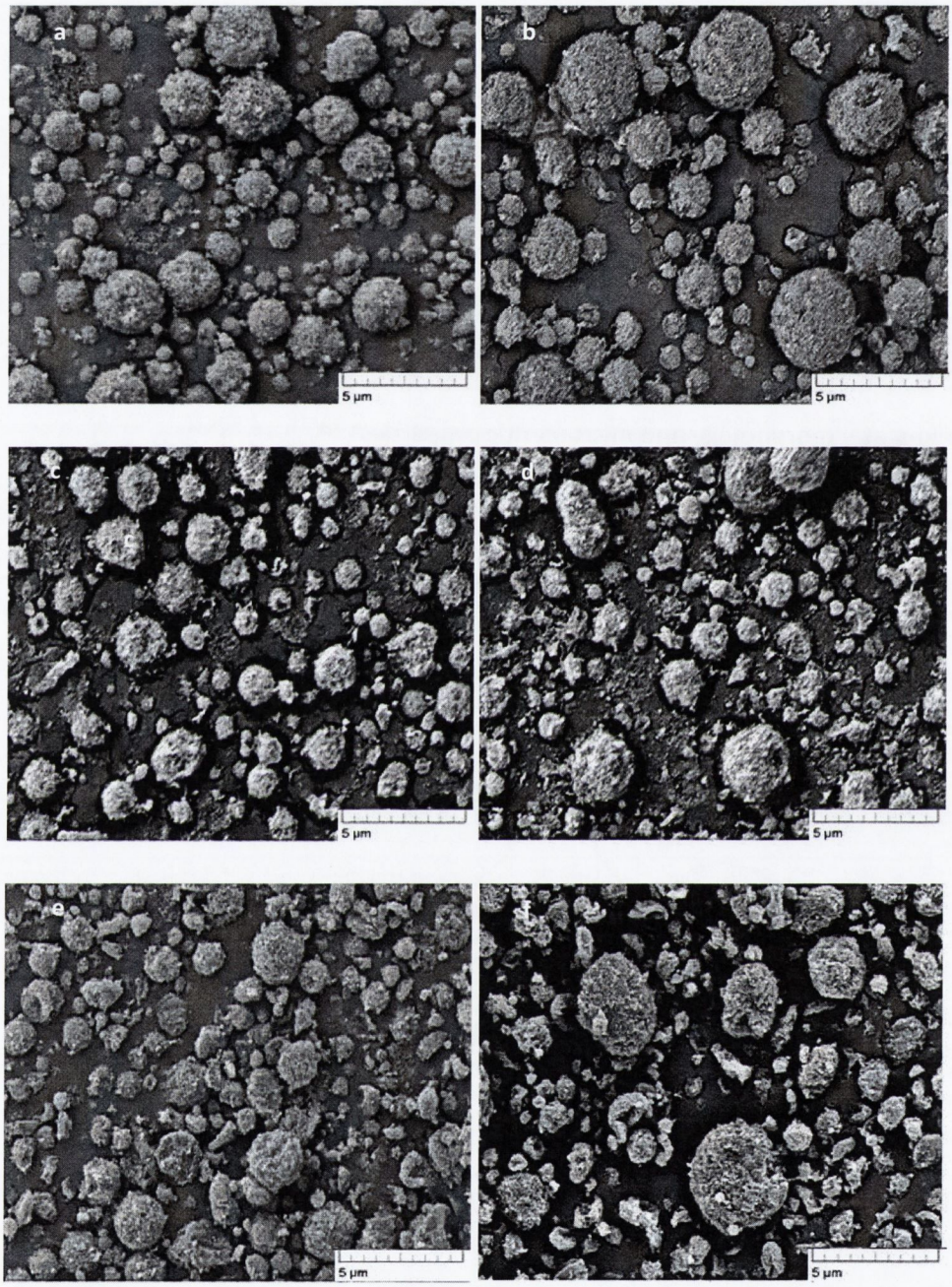
a
5 µm
b
5 µm
c
5 µm
d
5 µm
e
5 µm
f
5 µm

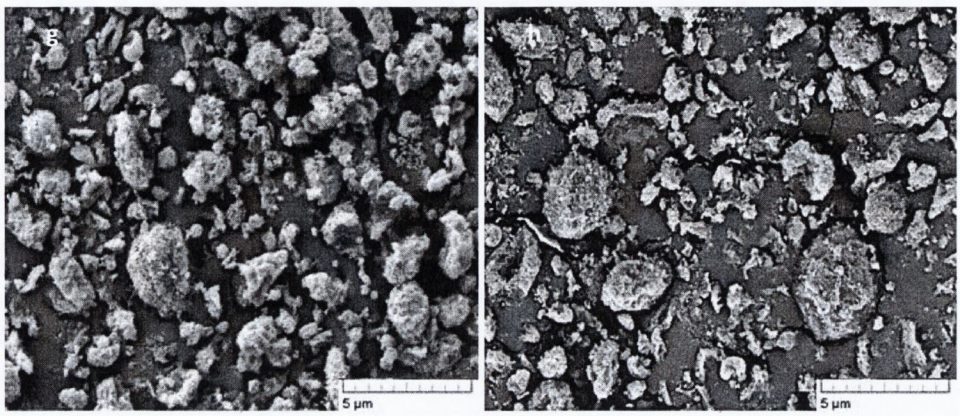

Figure 5.24 SE micrographs of raffinose:HPβCD composite systems (a) 100:0 (b) 80:20, (c)70:30, (d) 60:40, (e) 40:60, (f) 30:70, (g) 20:80 and (h) 0:100.

Particle size volume distributions of all R:HPβCD composite system were narrow and monomodal with low span values (between 1.1 and 1.2) and the median particle size (d_{50}) was in the range of 1.7–2.0 µm. Table 5.9 presents the determined values of d_{10}, d_{50}, d_{90} and percentage of particles with size < 1 µm as mean ± standard deviation.

ANOVA with additional Tukey method of analysis of the particle size distributions pointed out statistically significant differences between d_{50}, d_{90} and the percentage of particles with diameter below 1 µm ($p<0.05$): the d_{50} and d_{90} of R:HPβCD NPMPs were different from R NPMPs; the system comprising 40 % cyclodextrin showed a significant increase in submicron-size particles, distinguishing it from the remaining samples. The d_{10} was not significantly different ($p = 0.056$).

Specific surface area was also investigated as it is a reflection of porosity associated with porous particles such as the NPMPs (Healy et al., 2008).

As previously seen for trehalose composite systems, the addition of hydroxypropyl-β-cyclodextrin increases the surface area, and hence porosity (Figure 5.25 and Table 5.9). This increase is not linear with the increase of weight fraction, a maximum of 106.96±0.07 m^2/g is achieved at 40 % weight of cyclodextrin, after which SSA decreases to values closer to the surface area of the added excipient when spray dried alone.

ANOVA with Tuckey's test showed signifficant differences between R:HPβCD composites ($p < 0.05$): all systems were different form raffinose spray dried alone; sytems with 20 % weight of HPβCD was different from remaining composite systems; and system with 40 % weight HPβCD was different from systems with 30% and 60% weight HPβCD.

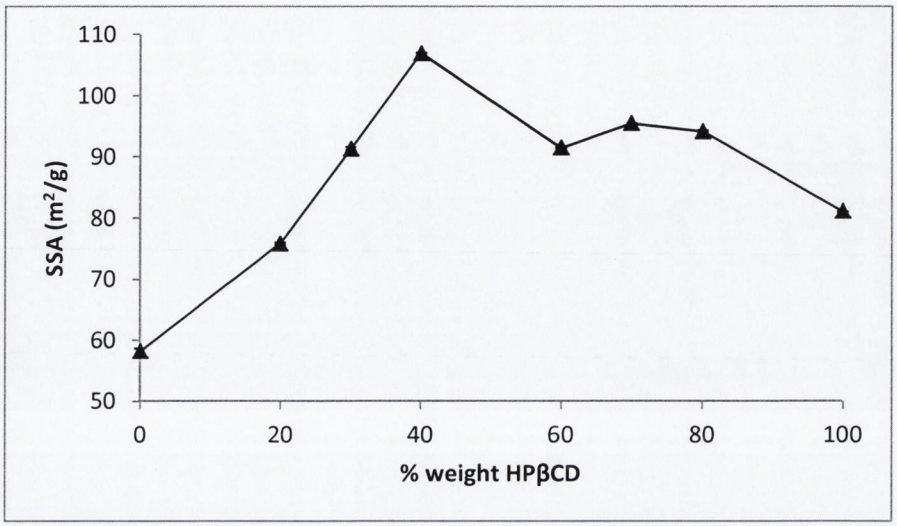

Figure 5.25 Specific surface area (SSA) of raffinose composite systems as function of the added excipient weight fraction.

True density data showed a decrease with an increase in % weight of HPβCD (Figure 5.30 and Table 5.9). ANOVA analysis with Tukey's test revealed that all samples were different to each other ($p < 0.05$), with the exception of samples 60 % and 70 % weight cyclodextrin.

The aerodynamic diameter was calculated and found to be within the desirable particle size range, 1-3 μm, for central and distal deposition in the lungs (Hickey 1996) (Table 5.9).

Bulk and tap density results for R:HPβCD are represented in table 5.9. All samples presented values < 0.3 g/cm^3 making them suitable for pulmonary delivery (Bosquillon et al., 2004). ANOVA with Tukey's test demonstrated significant differences ($p<0.05$), with systems comprising 80% weight of cyclodextrin resulting in powders with bulk and tap densities different from all other composites. Bulk density analysis also revealed additional differences: 40 and 60 % weight cyclodextrin were different from the systems comprising 30 % by weight cyclodextrin.

Table 5.9 Particle size, specific surface area (SSA), true, bulk and tap density and calculated aerodynamic diameter of Raffinose:HPβCD composite systems. SSA-specific surface area; bp- bulk density; tp-tap density; d_{aer}- aerodynamic diameter

	100:0	80:20	70:30	60:40	40:60	30:70	20:80	0:100
PS (µm)								
d_{10}	1.1±0.02	1.1±0.01	1.1±0.00	1.1±0.00	1.1±0.04	1.1±0.00	1.1±0.00	1.1±0.00
d_{50}	1.7±0.01	1.9±0.01	1.9±0.01	1.9±0.00	1.9±0.01	1.9±0.00	1.9±0.01	2.0±0.00
d_{90}	2.9±0.04	3.4±0.02	3.2±0.01	3.3±0.01	3.3±0.16	3.2±0.01	3.5±0.03	3.5±0.14
<1µm (%)	7.2±0.71	7.0±0.23	5.7±0.25	8.4±0.01	7.0±1.48	5.8±0.07	6.6±0.12	6.6±0.12
SSA (m^2/g)	58.16±0.51	75.84±0.12	91.32±0.27	106.96±0.07	91.52±0.01	95.48±0.08	94.21±0.12	81.08±0.03
True density (g/cm^3)	1.58±0.01	1.55±0.01	1.51±0.01	1.50±0.01	1.47±0.00	1.46±0.00	1.43±0.01	1.42±0.01
bp(g/cm^3)	0.15±0.01	0.14±0.01	0.15±0.01	0.13±0.00	0.13±0.01	0.14±0.00	0.10±0.00	0.16±0.00
tp (g/cm^3)	0.24±0.00	0.24±0.03	0.26±0.02	0.22±0.01	0.22±0.01	0.26±0.01	0.19±0.00	0.29±0.00
d_{aer} (µm)	2.2±0.02	2.4±0.01	2.3±0.00	2.3±0.01	2.3±0.01	2.4±0.01	2.3±0.00	2.4±0.00

5.4.2 FTIR analysis

Figure 5.26 shows the IR spectra for raffinose pentahydrate and raffinose:HPβCD composite systems.

Raffinose pentahydrate presented sharp absorption bands, whereas HPβCD raw material, amorphous R and R:HPβCD composites showed much broader absorption bands. The detected shoulder peaks in the OH stretching region between 3600 and 3000 cm^{-1} of crystalline raffinose are due to hydrogen bonds of defined geometric positions (Wolkers et al., 1998; Cheng and Lin, 2006). The broad features of the OH band of HPβCD raw material, amorphous R and R:HPβCD composites, at the same wavenumber range, indicate a wide range of hydrogen bond lengths and orientations (Wolkers et al., 1998; Williams III et al., 1998; Misiuk and Zalewska, 2009). Six bands could be identified in the C–H stretching region, located between 3000 and 2800 cm^{-1}, for crystalline raffinose, whereas HPβCD raw material, amorphous R and R:HPβCD composites showed only one broad band in this region (Wolkers et al., 1998; Williams III, et al., 1998).

The bands in the 1500–1200 cm^{-1} region in raffinose pentahydrate spectra arise mostly from C–H deformation vibrations, and the bands between 1200 and 900 cm^{-1} arise predominantly from a combination of CO (υC–O) stretching and OH bending (δC–O–H) vibrations (Wolkers et al., 1998; Cheng and Lin, 2006). The bands at 980 and 948 cm^{-1} for raffinose pentahydrate, can be assigned to the asymmetric and symmetric stretching vibrations of the α-(1→6)-glycosidic bond. Different studies have reported the glycosidic bond to present peaks at 998 and 967 cm^{-1} for raffinose pentahydrate (Cheng and Lin, 2006).

Bands in the range 500 to 1500 cm^{-1} of the spectrum of the HPβCD raw material cannot be attributed to a single type of molecular vibration since there is a strong coupling of vibrations from the macrocyclic, caused by neighbouring bonds vibrating with similar frequencies: bending C-H, C-O-H, C-C-H, and others (Williams III et al., 1998; Misiuk and Zalewska, 2009). The peak corresponding to the α-1,4 linkage was detected at 966 cm^{-1} (Williams III et al., 1998; Misiuk and Zalewska, 2009; Wu et al., 2010). In the 1500–1200 cm^{-1} region no differences in peak positions were found between crystalline raffinose, cyclodextrin raw material and spray dried composites, but a transition from raffinose fingerprint to the cyclodextrin fingerprint was seen, possibly due to an overlapping of bands (Misiuk and Zalewksa, 2009).

As the weight fraction of HPβCD increased a change in the bands between 1200 and 900 cm^{-1} was evident. Such modification can be due to entrapment of raffinose molecules in the cyclodextrin cavity, suppressing the characteristic signal bands and resulting in a modification in

the hydrogen bonding of the C-O-H groups (Williams III et al., 1998; Wolkers et al., 2004; Wu et al., 2010); hence the absence of the peak at 993 cm^{-1} of raffinose's α-(1→6)-glycosidic bond.

FTIR analysis verified the full miscibility predicted by XRD and DSC of raffinose:HPβCD, since interaction between molecules was evident by hydrogen bonding and molecular conformation changes.

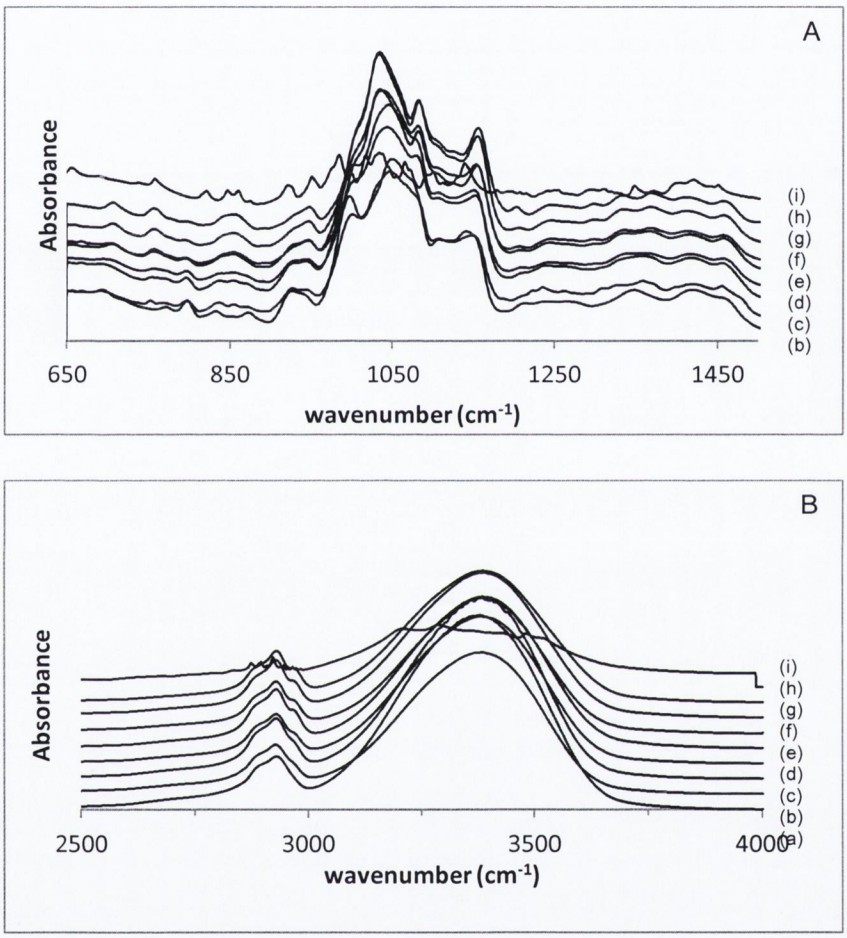

Figure 5.26 FTIR spectras (A- 6500-1450 wavenumber and B- 2500-4000 wavenumber) of spray dried R:HPβCD composite systems(a) 100:0, (b) 80:20, (c) 70:30, (d) 60:40, (e) 40:60, (f) 30:70, (g) 20:80 (h) 0:100 and (i) crystalline raffinose.

5.4.3. Thermal analysis

DSC scans of spray dried composite systems demonstrated the occurrence of one thermal event - glass transition step, which was intermediate to the T_g values of the pure components (Figure 5.27 and Table 5.10), indicative of amorphous solid solutions. The addition of cyclodextrin to raffinose caused a significant increase of the T_g ($p<0.05$).

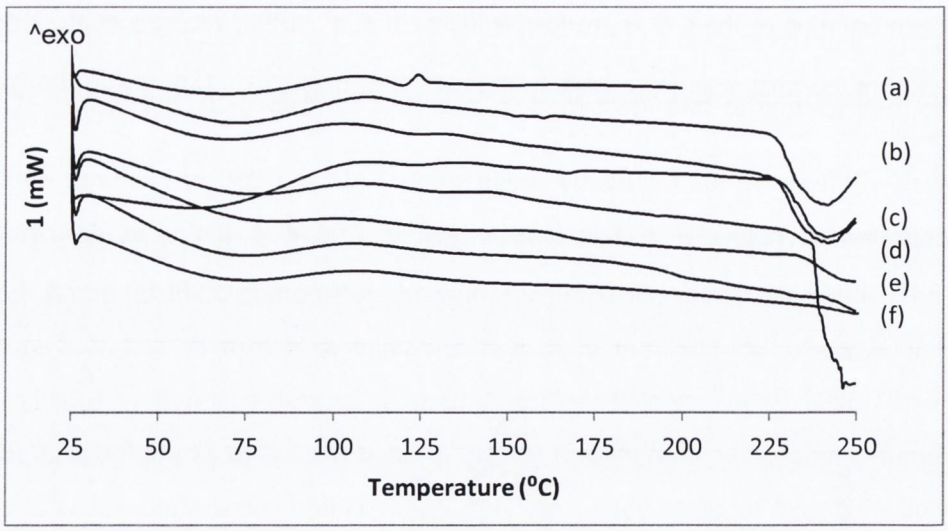

Figure 5.27 DSC scans of raffinose:hydroxypropyl-β-cyclodextrin, composite systems

Table 5.10 Glass transition temperature (T_g) of raffinose:HPβCD composite systems.

R:HPβCD	100:0	80:20	70:30	60:40	40:60	30:70	20:80	0:100
T_g (°C)	115.6± 0.21	115.0± 0.35	117.1± 0.11	117.5± 0.27	120.8± 0.26	165.6± 0.85	192.9± 0.88	225.4± 0.32

Different equations for prediction of T_g were fitted to our data as was previously done for trehalose composite systems. Therefore, Gordon-Taylor with Simha-Boyer rule, Fox and Kwei equations were used.

Figure 5.28 presents the results of the fit to the various models for R:HPβCD composites. It can be seen that only one experimental point was fitted by the Gordon-Taylor and Fox equations, with the remaining points falling below the predicted curve. The model equations assume ideal volume additivity and neglects any kind of interaction between components. FTIR analysis, indicated the existence of molecular interactions between raffinose and hydroxypropyl-β-cyclodextrin, which led to the deviations to Gordon-Taylor equation predictions.

The Kwei equation presented a good fit to the experimental data (R^2=0.902), therefore the assumption of interactions between molecules and a real mixture (as opposed to Gordon Taylor ideal mixture) between excipients was valid. Some data points presented very small deviations from predicted value; these might be due to plasticising effects of the residual solvents present in powders after spray drying (Kalichevsky et al., 1993). Previously we have discussed that *q* is a measure of the efficacy of hydrogen bond formation; hence a larger magnitude of *q,* without regard to its sign, is indicative of a higher extent of hydrogen bonding between the mixture

components (Kwei et al., 1984). The calculated q value for raffinose composite systems was -165.66 suggesting a high interaction between molecules due to hydrogen bonding.

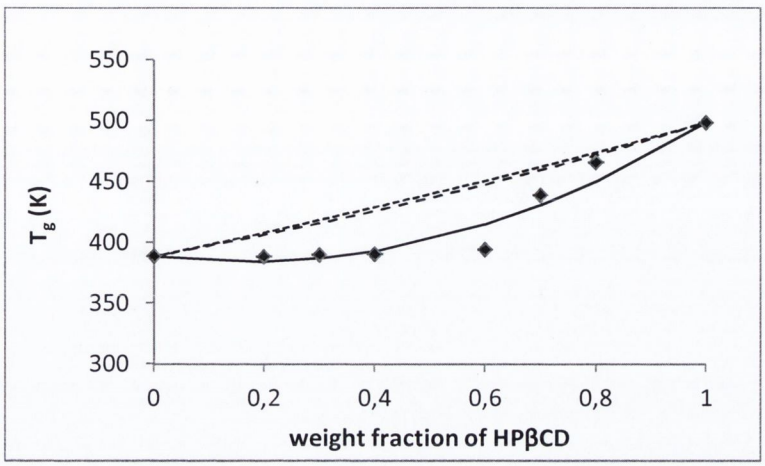

Figure 5.28 Glass transitions of R:HPβCD composite systems as a function of the added excipient weight fraction. The dotted, dashed and solid lines represent the predictions based on the Gordon-Taylor and Fox and Kwei equations, respectively.

Table 5.11 The Gordon-Taylor parameter and the fitting coefficients by using the Kwei and Schneider equations.

	Gordon-Taylor equation	Kwei equation
R:HPβCD	K_{GT} = 0.87	K_k =0.25
		q = -165.66
		R^2 = 0.902

A residual solvent content of 2.31-4.81 % was determined by TGA for R:HPβCD samples over the temperature range 25-130 °C. The RSC increased with increasing weight fraction of cyclodextrin. ANOVA analysis revealed a significant difference between composite systems and raffinose spray dried alone (p = 0.001). In order to gain more information about the RSC composition, GC-FID was used to quantify methanol and butyl acetate, assuming the difference between calculated values from the two techniques would correspond to moisture, i.e. $TGA - GC = water\ content$. Table 5.11 presents the determined values. RSC is constituted mainly of butyl acetate and water; a small content of methanol was found for most samples. The water content could be explained by the amorphous sugars' strong tendency to take-up moisture by adsorption and desorption (Hancock and Shamblin, 1998).

Table 5.11 Residual solvent content by TGA and GC-FID for R:HPβCD composite systems. ND – not determined.

R:HPβCD	RSC by TGA (% w/w)	RSC by GC-FID (% w/w)		Extrapolated Water content (%)
		Methanol	Butyl acetate	
100:0	2.60±0.31	ND	0.36±0.02	2.24
80:20	3.70±0.24	0.16±0.00	1.15±0.04	1.39
70:30	3.54±0.02	0.13±0.01	1.30±0.01	2.11
60:40	3.77±0.30	ND	1.24±0.05	2.53
40:60	3.80±0.27	0.13±0.01	1.29±0.01	2.38
30:70	4.12±0.01	0.11±0.00	1.23±0.91	2.78
20:80	4.64±0.03	0.07±0.07	1.75±0.02	2.82
0:100	4.67±0.20	0.14±0.01	2.35±0.01	2.18

5.4.4. Dynamic vapour sorption

Water vapour sorption and desorption studies were performed on raffinose:hydroxyl-β-cyclodextrin composites (Figure 5.29).

We have previously reported that spray dried raffinose when exposed to increasing relative humidities crystallises at 70% RH, retaining water (~10 %) pertaining to the hydrate crystal upon collapse of the amorphous form. The sorption isotherms corresponding to systems containing HPβCD in a weight fraction of 30% and 40% showed an inflection point at 70 % RH, after which water uptake continued, resulting in an increase of 5 % to 7 % of total water sorption by these composite systems when compared to raffinose alone (~15 % water sorption). The respective desorption isotherms showed an initial mass loss at higher RH followed by a constant mass loss until 10% RH after which there is a greater mass loss, resulting in an open hysteresis. Final moisture uptake was ~6 % and ~3 %. The inflection point at 70 % RH was due to raffinose recrystallisation for 30% weight fraction of HPβCD, as confirmed by XRPD analysis (Figure 5.36). The remaining water sorption and desorption was due to the cyclodextrin-water interactions.

The possible crystallisation of raffinose was not clear for 40 % weight fraction of HPβCD, since XRPD analysis showed the typical amorphous halo with no trace of peaks. Only 1 mole of water per mole of raffinose was present at the end of the analysis. Studies have reported the dehydration of crystalline raffinose pentahydrate to be a three step process: first, loss of one

water molecule, second and third loss of two water molecules, and the rehydration leads to the formation of raffinose pentahydrate and raffinose trihydrate (Cheng and Lin, 2006; Chamarthy et al., 2010). Therefore there is a possibility that crystallisation to the pentahydrate form did not occur due to insufficient availability of water molecules per raffinose molecule.

Spray drying of raffinose with HPβCD at a weight fraction ≥40 % produced powders with high capacity for moisture uptake; a maximum of 30 % mass gain could be achieved, similar to the moisture uptake of HPβCD when spray dried alone. The sorption isotherm of powder with 60% HPβCD presented an inflection point at RH 80 % with no mass loss and continuous water uptake. Desorption isotherms showed complete water desorption. Two hysteresis loops were seen: a loop between 70 and 90 % RH and a second one between 0 and 70 % RH. The Young-Nelson model was fitted to the absorption profiles to better comprehend these events (Appendix 3)indicating that, for the system comprising 60 % HPβCD, most water uptake was due to bulk absorption and multilayer adsorption whereas, for the system comprising 70% HPβCD, a small fraction of water was absorbed and most water was adsorbed forming a multilayer on the solid. The absorption events can be attributed to the raffinose fraction, since the interaction of hydroxypropyl-β-cyclodextrin with water vapour results only in the formation of adsorption multilayers. XRPD revealed systems were still amorphous post DVS analysis (Figure 5.36).

Solid dispersions of R:HPβCD NPMPs present enhanced physical stability when compared to raffinose NPMPs.

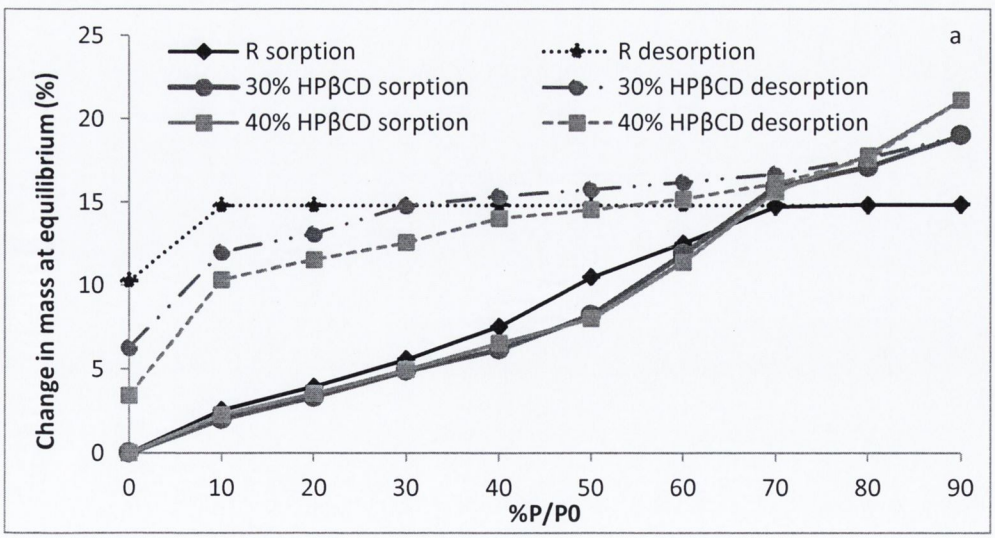

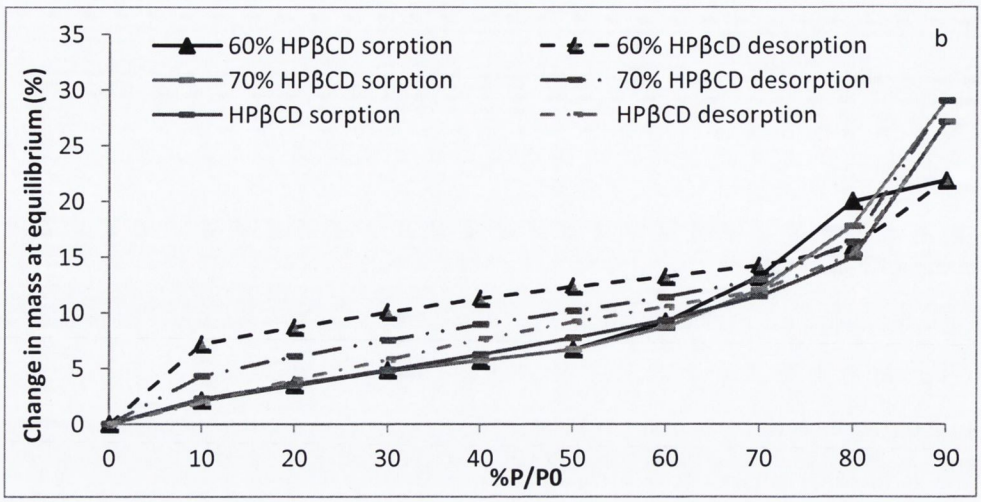

Figure 5.29 Water vapour sorption and desorption isotherms (a and b) of raffinose: hydroxypropyl-β-cylcodextrin composite systems

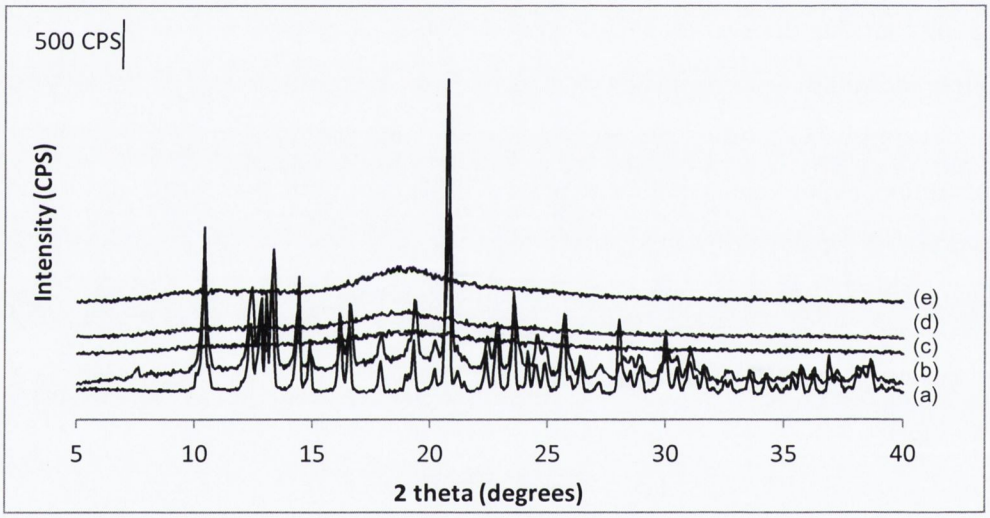

Figure 5.30 XRPD of R:HPβCD composite systems after water vapour sorption and desorption analysis (a) raffinose pentahydrate, (b)70:30, (c) 60:40, (d) 40:60 and (e) 30:70.

5.4.5. *In vitro* deposition via next generation impactor analysis

In vitro deposition analysis was performed on composites that presented the best characteristics: aerodynamic diameter < 3 μm, high specific surface area, high T_g and low RSC. Therefore samples chosen to assay were composite systems with 40 %, 60 % and 70 % weight of hydroxypropyl-β-cyclodextrin.

Deposition profiles of R:HPβCD composites are represented in figure 5.31, with evident improvement of the aerosol deposition with the addition of cyclodextrin compared to NPMPs comprised of raffinose alone. The composite systems showed less deposition in the mouthpiece adaptor and induction port, and higher deposition on stages with lower cut-off points (≤ 2 μm, stage) than raffinose NPMPs. Fine particle fraction < 3 and < 5 μm of R:HPβCD NPMPS was ~2

fold higher and significantly different to the FPF < 3 and < 5 µm for raffinose NPMPs (< 3 µm p=0.001; < 5 µm p=0.001) (Table 5.12). The % of recovered emitted dose also increased for HPβCD-containing systems and was significantly different (p=0.02) to NPMPs comprised of raffinose alone.

Statistical analysis of the mass median aerodynamic diameters of R:HPβCD showed a significant difference (p<0.05) to the MMAD determined for raffinose NPMPS. The MMAD was halved with the addition of cyclodextrin (Table 5.12) and was similar (values within standard deviation) to the calculated aerodynamic diameter. A possible explanation is the dispersion of possible aggregates due to the high SSA (high porosity), since these particles present fewer areas of contact, leading to lower cohesion and easier dispersion (Tabor, 1977).

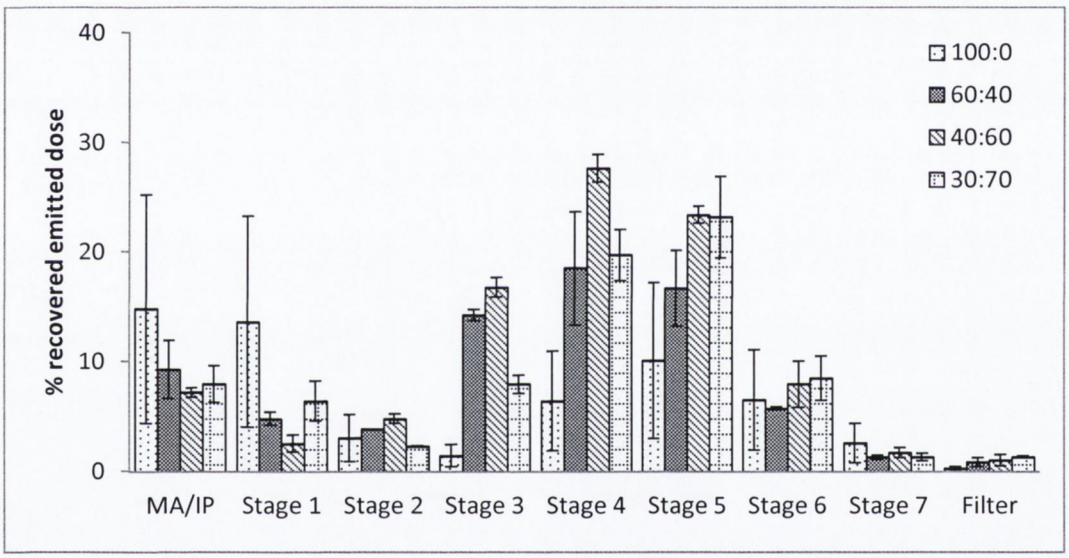

Figure 5.31 *In vitro* aerosol deposition profile by use of a NGI of R (ratio 100:0) and R:HPβCD NPMPa ratio 60:40, 40:60 and 30:70 as calculated % of recovered emitted dose vs. NGI stages. MA – mouth adapter IP – induction port

Table 5.12 Recovered emitted dose, fine particle fraction (FPF), mass median aerodynamic diameter (MMAD) and geometric standard deviation (GSD) of *in vitro* aerosol deposition of R and R:HPβCD NPMPs.

	R:HPβCD 0:100	R:HPβCD 60:40	R:HPβCD 40:60	R:HPβCD 30:70
% recovered emitted powder	68.1±11.7	91.4±1.2	92.7±10.5	88.0±1.7
FPF < 5 µm	31.8±9.9	69.5±7.1	87.3±0,5	81.0±4.6
< 3 µm	26.4±10.0	58.0±8.3	83.8±0.9	76.0±6.1
MMAD	4.4±0.27	2.4±0.07	2.2±0.18	2.1±0.16
GSD	2.3±0.48	2.1±0.04	2.0±0.04	2.1±0.09

5.5 CONCLUSION

NPMPs of composite systems of trehalose:raffinose, trehalose:HPβCD and raffinose:HPβCD were produced by spray drying. Particles were spherical and porous, with median geometric particle size < 2 μm, higher surface area than the excipients spray dried alone and low bulk and tap density. Thermal, FTIR and XRPD analyses indicated that spray dried composites were amorphous solid solutions, characterised by a single T_g and molecular interactions such as hydrogen bonding and conformational changes indicative of a homogeneous mixture.

Analysis of the glass transition temperature composition relationships for composite systems revealed deviations from the Gordon-Taylor and Fox equations, attributable to interactions between components, as was evident by FTIR analysis. However, good fitting was achieved with the Kwei equation, which takes into account the possibility of interactions between components.

Composite systems presented better physical stability than trehalose and raffinose NPMPs; glass transition temperatures were higher and the capacity for water sorption increased with no crystallisation in systems with higher contents of HPβCD.

An improvement in the aerosol deposition characteristics, illustrated by increases in the FPF and emitted recovered dose and reduction of the MMAD, was also achieved with NPMPs prepared by co-spray drying of trehalose or raffinose with HPβCD compared to trehalose or raffinose alone.

To conclude, the co-spray drying of trehalose with raffinose or hydroxypropyl-β-cyclodextrin and raffinose with HPβCD results in powders with improved physicochemical characteristics, physical stability and aerodynamic behaviour, suggesting their promise as drug-carriers for pulmonary delivery.

CHAPTER 6

SCALE-UP OF NPMPs

6.1 INTRODUCTION

To date, there has been very few published investigations into the scale-up of the spray drying process from laboratory scale to industrial production. In this chapter, the transfer and scale-up of spray ngdrying for the production of NPMPs from the Büchi Mini spray dryer B-290 to the Niro SDMicro™ (small scale/laboratory spray drying) and to the Niro Mobile Minor™ (pilot scale spray dryer) will be discussed. The study will give an indication of the nanoporous/nanoparticulate microparticle (NPMP) process robustness for potential industrial scale production.

6.2 SPRAY DRYING WITH THE NIRO SDMICRO™ SPRAY DRYER

Solutions with a concentration of 2.9 % w/v raffinose pentahydrate were prepared in a solvent composition of 80:20 MeOH:BA, as previously used for spray drying using the Büchi Mini spray dryer B-290 with the DOE optimised settings. Spray drying was carried out in a co-current mode with a two-fluid nozzle with 0.5 mm diameter, using nitrogen as the drying gas and a flow rate of 275 l/min (20.6 kg/h). All samples were produced in duplicate.

In order to produce raffinose NPMP powders with similar characteristics to those obtained from the Büchi spray dryer, the effects of nozzle gas and process gas pressure, feed solution rate (pump rate) on: outlet temperature, yield, residual solvent content, particle morphology, geometric median particle size and specific surface area, were investigated (Table 6.1). By increasing the nozzle gas flow pressure, it was envisaged that a smaller particle size would be obtained. This postulated effect was tested with runs SDM2 and 3. The process gas flow pressure was kept at 0.8 bar for both samples. The effect of pump rate on the raffinose NPMP production was also examined: run SDM4 employed a pump rate of 10 % (~6 ml/min), while run SDM5 employed a pump rate of 20 % (~12.5 ml/min); all other samples were produced with a pump setting of 15 % (~9.8 ml/min). The inlet temperature was kept constant at 180 °C, except for run SDM7, in order to achieve an outlet temperature of 85 °C, which was the outlet temperature in the Büchi spray dryer (Chapter 4).

Table 6.1 Summary of Niro SDMicro™ spray dryer settings. ALR: atomisation-gas-liquid-mass-ratio.

Run	Inlet temperature (°C)	Pump	Run	Inlet temperature (°C)	Pump
SDM1	180	0.6 (15)	1	1 (20%)	1.3
SDM2	180	0.6 (15)	0.8	1.2 (24%)	1.6
SDM3	180	0.6 (15)	0.8	1.4 (28%)	1.9
SDM4	180	0.4 (10)	1	1 (20%)	2
SDM5	180	0.8 (20)	1	1 (20%)	1
SDM6	180	0.8 (20)	0.8	1.4 (28%)	1.4
SDM7	170	0.4	(10)	1	1 (20%)

6.2.1 Characterisation of spray dried powders

The experimental design study on raffinose NPMP production using a Büchi Mini spray dryer B-290, discussed in Chapter 4, highlighted the process parameters affecting the raffinose NPMP production. Based on the DOE study, optimised raffinose NPMPs prepared using the Büchi Mini spray dryer B-290 presented the following characteristics: PS (d_{50}) 1.8±0.02 µm, SSA 58.16±0.51 m^2/g, RSC 2.6±0.34 % and process T_{outlet}85±1.4 °C.

All spray dried powders were amorphous by XRPD analysis, presenting the characteristic amorphous 'halo' (Appendix 3), as seen for spray dried powders using the Büchi Mini Spray Dryer.

Particle morphology was evaluated by SEM. Figure 6.1 shows the SE micrographs of the samples produced using the Niro SDMicro. Samples SDM1 and SDM7 were porous, spherical and were comprised of irregular shaped particles. Spherical and porous particles were found in samples SDM2, 3 and 6. Small spherical particles with smooth surfaces were also seen in samples SDM3 and SDM7 (marked with a red circle on Figure 6.2c and 6.2g). Samples SDM4 and SDM5 where comprised of spherical particles with smooth and crumpled surfaces. According to the Paluch et al. (2012) classification system, particles could be classified as 1BIIIα (SDM1, 6 and 7), 1BIIα (SDM2 and 3), 2BIIIα (SMD1 and 7), 1AIβ and 1BIβ (SDM4 and 5). Only SDM1, SDM6 and SDM7 presented the spherical and porous microparticles formed by conglomerates of nanoparticles that define the NPMPs (nanoporous/nanoparticulate micropartices) prepared with the Büchi Mini Spray Dryer.

The reduction of the inlet temperature from 180 to 170 °C, with the remaining parameters held constant (SDM4 and SDM7, respectively), resulted in a modification of particle morphology from non-porous to porous microparticles (Figure 6.5d – non-porous and Figure 6.5g - porous). It is thought that the reduction of inlet temperature and consequently outlet temperature allowed a slower solvent evaporation, resulting in the formation of porous particles. At high temperatures, when the droplet contacts the drying air, if the solid precipitation in the droplet is very quick it may results in the formation of a shell that becomes rigid, resulting in a non-porous and smooth/irregular particles (Vehring, 2007), as seen when spray drying at 180°C.

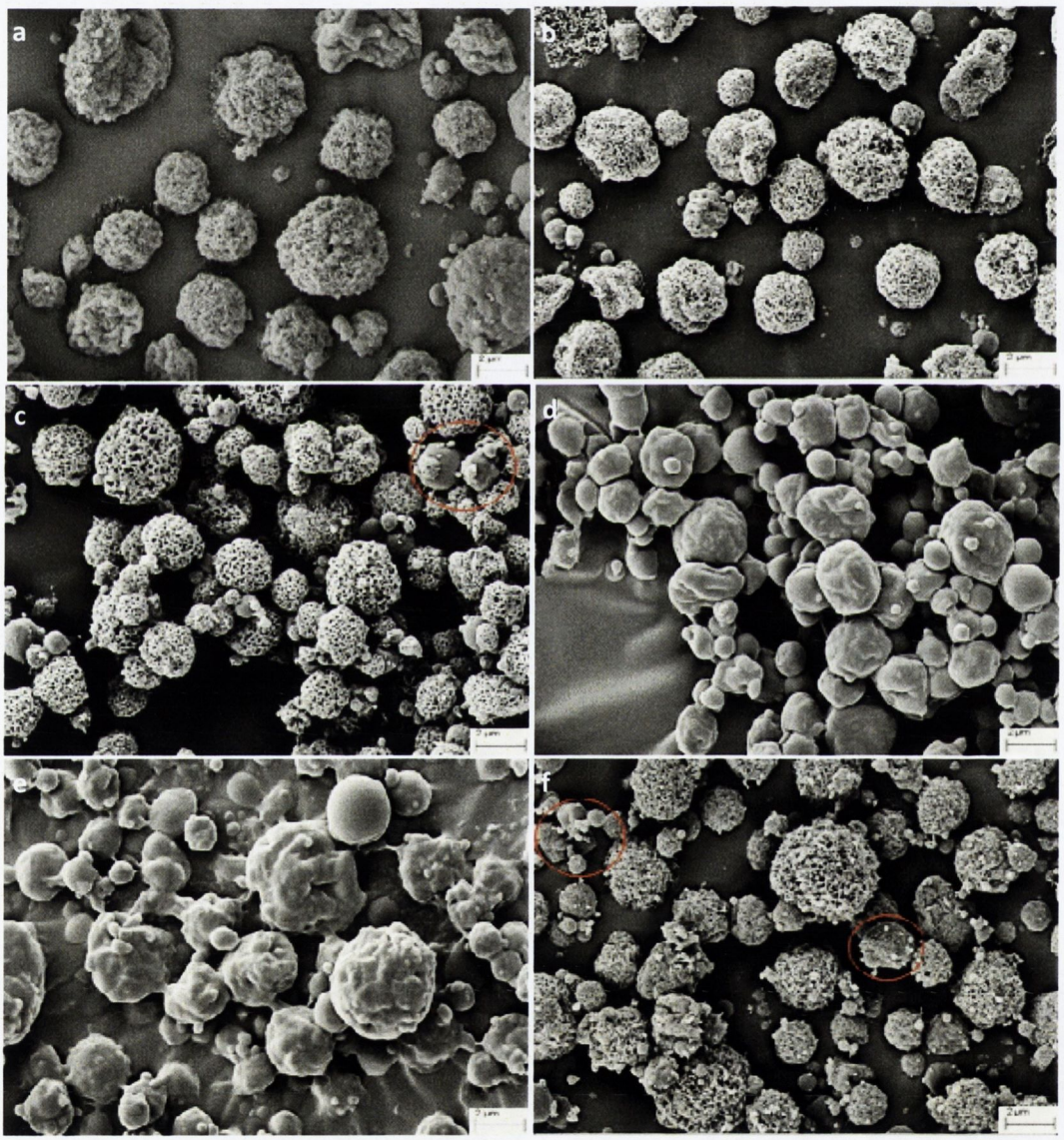

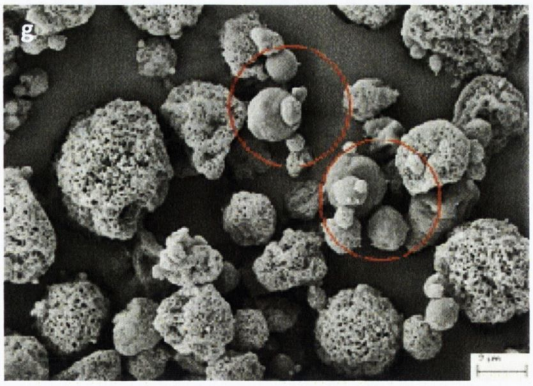

Figure 6.2 SE micrographs of spray dried raffinose using the Niro SD Micro: (a) SDM1, (b) SDM2, (c) SDM3, (d) SDM4, (e) SDM5, (f) SDM6 and (g) SDM7.

Table 6.2 presents the process outlet temperature and powder residual solvent content for each sample prepared with the Niro SDMicro. Process outlet temperature varied between 77±2.8 and 85±0.0 °C. A reduction in the T_{outlet} was observed with increased pump setting (feed flow rate) (p=0.015) (Table 7.2 - SDM1, SDM4 and SDM5, SDM3 and SDM7). When more liquid is supplied to the drying chamber, more solvent vapour is generated, decreasing the exhaust temperature (Maury et al., 2005). An effect of the inlet temperature on process T_{outlet} was also evident, where the latter increased with increasing heat energy supplied (higher T_{inlet}) (runs SDM5 and SDM7 with p=0.012).

The residual solvent content (RSC) was determined by TGA over the temperature range 25-130 °C. Values varied between 2.5±0.1 and 3.8±0.6 % (Table 6.2). Figure 6.3 shows how the RSC varied with the inlet temperature and pump setting. The RSC fluctuated mainly with the pump setting, since all samples were spray dried with the same inlet temperature, with the exception of sample SDM7. However, ANOVA showed no statistically significant differences between samples (p=0.089).

The residual solvent content of raffinose NPMPs spray dried from a Büchi Mini spray dryer B-290 under optimised conditions was 2.6±0.34 % (w/w) and was mainly affected by the inlet temperature and interactions between different spray drying parameters such as pump and gas flow. Similar results were found for samples SDM1, SDM6 and SDM7, which were spray dried at the same outlet temperature as that used in the Büchi Mini spray dryer.

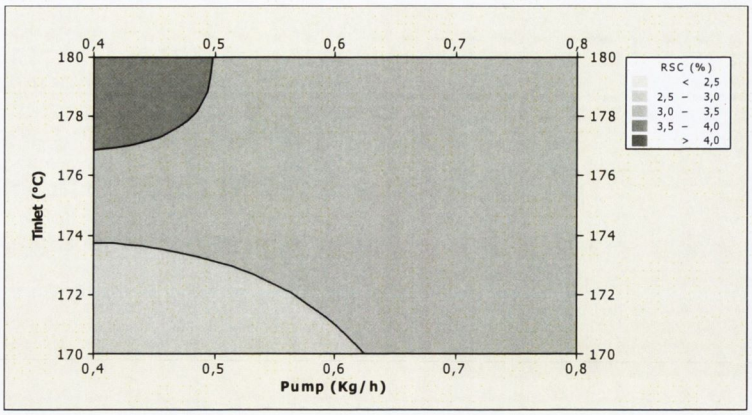

Figure 6.3 Contour plot of the effect of process variables inlet temperature (T_{inlet}) and pump setting on the residual solvent content of raffinose powders produced using the Niro SDMicro.

Geometric median particle size (d_{50}) and specific surface area (SSA) of raffinose spray dried samples are presented in Table 6.2. Particle size volume distributions were narrow and monomodal with low span values (between 1.3-1.7). The d_{50} was in the range of 3.2-4.1 µm. An effect on particle size of varying the pump setting and atomisation gas pressure was observed (Figure 6.4). The contour plot of d_{50} showed that the particle size was reduced when spray drying was conducted with a pump rate below ~0.55 kg/h, independent of the atomisation pressure setting within the range 0.8-1.0 bar. Large particles (> 4 µm) were produced when the pump rate was operated at >0.75 kg/h and at the extreme of the atomisation pressure (0.8 or 1 bar).

Masters (2002) has discussed that the droplet size, and thereby the particle size, for spray drying using a two-fluid nozzle, varies with the air/liquid mass ratio (ALR), where an increase in the ratio leads to a decrease in the droplet size. Figure 6.5 represents the relationship between d_{50} and the ALR. In these spray drying studies, a reduction in particle size with increasing ALR was observed.

Upon comparison of the results produced when using the Niro SDMicro with the particle size attained when using the Büchi Mini spray dryer, it was noted that larger particles are produced in the Niro SDMicro instrument. The deposition studies shown later in this section will determine if this increase in geometrical particle size affected the powder's deposition properties.

Specific surface area (SSA) varied between 15.90-48.66 m^2/g. SSA values were lower than those attained when using the Büchi Mini spray dryer. SSA of SDM samples was higher when the pump was set to 0.6 kg/h and the atomisation pressure was set of 1.2 bar, while all the remaining variables were held constant. No significant trends were found between SSA and pump setting or nozzle pressure. ANOVA followed by Tukey's test showed sample SDM2 to be different from

all other samples produced and no differences were determined among samples SDM1, SDM3, SDM6 and SDM7, with no trends being found. Samples SDM4 and SDM5, which consisted of non-porous particles and so, were expected to present lower SSA, as was the case.

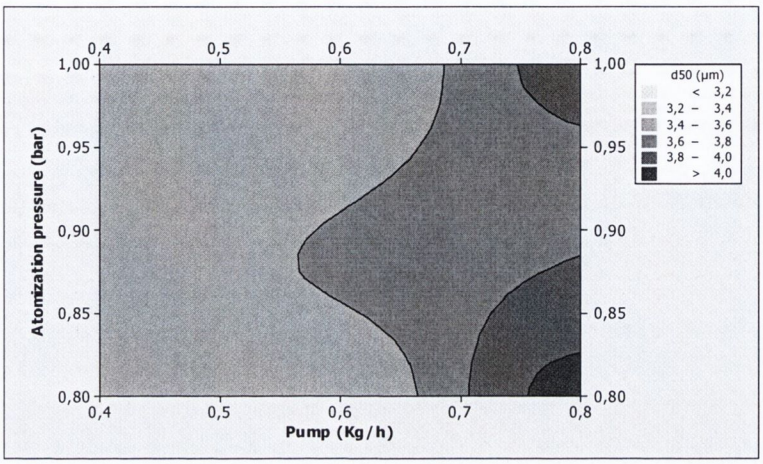

Figure 6.4 Contour plot of the effect of process variables atomisation pressure and pump setting on the geometric mean particle size (d_{50}) of raffinose powders produced using the Niro SDMicro.

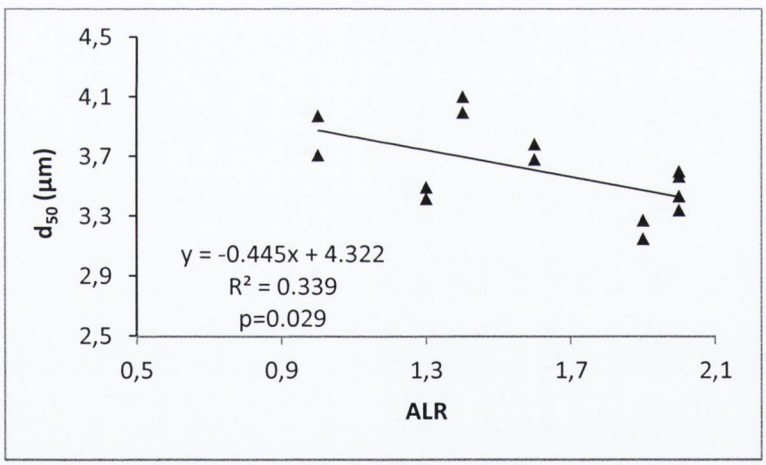

Figure 6.5 Effect of the air/liquid ration (ALR) on the geometric mean particle size (d_{50}) of raffinose powders spray dried using the Niro SDMicro.

Bulk and tap densities of powders were evaluated. All values were found to be lower than 0.3 g/cm^3, making them suitable for pulmonary delivery (Bosquillon et al., 2004) (Table 6.2). ANOVA followed by Tukey's test of SDM samples showed the existence of differences between samples' bulk and tap densities ($p<0.05$ and $p=0.012$, respectively): the bulk densities of SDM1 and SDM7 were higher than, and significantly different to, the remaining samples; the tap densities of SDM2 and SDM4 were distinct from each other, with no differences between remaining samples.

Table 6.2 Evaluated outcomes of raffinose samples spray dried using the Niro SDMicro™.

Run	T_{outlet} (°C)	ΔT (°C)	d_{50} (μm) (span)	SSA (m^2/g)	RSC (% w/w)	bp (g/cm^3)	tp (g/cm^3)
SDM1	831.4	42	3.5±0.06 (1.5±0.01)	33.71±0.07	2.5±0.1	0.14±0.01	0.25±0.02
SDM2	77±2.8	48	3.7±0.07 (1.5±0.01)	48.66±3.06	3.7±0.7	0.09±0.01	0.22±0.01
SDM3	82±1.4	43	3.2±0.09 (1.5±0.02)	38.16±0.28	3.8±0.6	0.11±0.003	0.24±0.01
SDM4	93	32	3.4±0.06 (1.3±0.12)	14.29±0.07	3.7±0.9	0.10±0.01	0.28±0.003
SDM5	82	43	3.8±0.18 (1.6±0.08)	17.99±0.66	4.2±0.3	0.10±0.003	0.26±0.02
SDM6	83±0.0	42	4.1±0.07 (1.7±0.20)	24.55±4.50	2.6±0.6	0.11±0.01	0.24±0.02
SDM7	85±0.0	40	3.6±0.02 (1.6±0.11)	31.86±0.26	2.6±0.3	0.13±0.004	0.26±0.02

Thermal analysis was performed on all samples from the Niro SDMicro that presented porous particles (exclusion of samples SDM4 and SDM5).

DSC scans were similar for all raffinose samples (Appendix 3). A broad endotherm in the interval 25 - 100 °C was observed and attributed to residual solvent loss; it was followed by a base line shift, the glass transition step, with no other thermal events registered. The glass transition temperature varied between 15.8±0.57 °C and 118.5±0.03 °C. ANOVA showed no statistically significant differences between SDM samples (p=0.091). Most samples presented a T_g value close to that found for raffinose NPMPs spray dried using the Büchi Mini spray dryer, i.e., 115.6±0.21 °C.

The residual solvent content of powders was further analysed by GC-FID, for quantification of butyl acetate and methanol. Water content was extrapolated from the difference between the RSC determined by TGA and the GC-FID-determined solvent content. With the exception of sample SDM6, Niro SDMicro samples presented lower or similar MeOH and BA content to the raffinose NPMPs prepared with the Büchi spray dryer (MeOH 0.30±0.01 % (w/w) and BA 0.81±0.02 % (w/w)) (Table 6.3).

Table 6.3 Glass transition temperature (T_g) and residual solvent content (RSC) by TGA and GC-FID of raffinose powders spray-dried using the Niro SD Micro.

	T_g (°C)	RCS by TGA (% (w/w))	RSC by GC-FID (% (w/w))		Extrapolated water content (%)
			MeOH	BA	
SDM1	115.8±0.57	2.5±0.1	0.20±0.01	0.84±0.01	1.46
SDM2	117.0±0.2	3.7±0.7	0.34±0.01	0.66±0.01	2.7
SDM3	118.5±0.03	3.8±0.6	0.11±0.03	0.74±0.04	2.95
SDM6	115.8±0.62	2.6±0.6	0.58±0.08	1.23±0.01	0.79
SDM7	116.7±0.71	2.6±0.3	0.17±0.04	1.01±0.14	1.42

6.3 A 2^2 FACTORIAL DESIGN TO STUDY THE EFFECT OF THE PROCESS AND NOZZLE PRESSURE ON THE PRODUCTION OF RAFFINOSE NPMPS USING THE NIRO SDMICRO™

A modification in the supply of nitrogen gas to the Niro SD Micro increased its flow rate to 340 l/min (27.7 kg/h). Hence, a randomised 2^2 full factorial design with two replicates was devised to assess the effect of the spray dryer process and nozzle gas flow (pressure) on raffinose NPMP particle size, specific surface area, residual solvent content and process outlet temperature, to facilitate the adjustment of the production of raffinose NPMPs to the machine's new conditions. The remaining parameters were held constant and set based on the previous results shown in section 6.3, i.e., inlet temperature was set at 180°C and pump rate at 15%.

The chosen factorial model was represented by: $Y_i = \beta_0 + \beta_1 A + \beta_2 B + \beta_{12} AB$ where β_n is the coefficient associated with factor n, and the letters A and B represent the factors (process and nozzle gas pressure) in the model. Combination of the factors, AB, represents an interaction between the individual factors.

Statistical analysis of variance, ANOVA, was performed to determine the significance (p-value) and impact (F-value) of each main factor as well as their interactions. Parameters found to be significant at at least the 5 % confidence level were included in the final prediction models.

Table 6.4 Process parameters evaluated in the factorial design.

Parameter	Low (-)	High (+)	Unit
Process gas pressure	0.8	1.2	Bar
Nozzle gas pressure	0.8	1.4	Bar

6.3.1 Evaluated outcomes

The design matrix and the data collected from the particle characteristics evaluated for raffinose powders are presented in Table 6.5. The coefficients of the final prediction models linking the spray drying parameters with responses are presented in Table 6.6. To indicate the goodness of fit of these models the R^2 is also given in the latter table.

Table 6.5 Design matrix of raffinose spray drying and the data collected from the analysis.

Run	Process gas pressure	Nozzle gas pressure	PS (d_{50}) (μm)	SSA (m^2/g)	RSC (%)	T_{out} (°C)	T_g (°C)
1	1	1	2.7	46.58	2.69	83	115.53
2	-1	-1	3.5	50.74	2.53	78	114.69
3	1	-1	3.2	13.00	3.33	98	113.56
4	-1	-1	3.5	44.57	2.8	82	116.78
5	-1	1	3.0	56.89	2.63	69	114.54
6	1	1	2.4	41.18	2.58	90	116.67
7	-1	1	3.0	52.34	2.84	73	114.7
8	1	-1	3.4	23.37	3.62	98	115.91

All spray-dried powders were amorphous as assessed by XRPD (Appendix 3).

The process outlet temperature ranged from 69 to 98 °C. This outcome was mainly affected by the process gas pressure (F-value 55.42, p=0.002), for which the model equation coefficient was positive. A higher flow into the drying chamber will increase the drying energy and therefore the outlet temperature. The nozzle gas pressure (F-value 20.75, p=0.01) presented a negative coefficient; that is, as the pressure increases the outlet temperature decreases, since the spray cloud is bigger, with more liquid entering the drying chamber (higher pump setting) increasing

the solvent vapour and, therefore, increasing the heat requirement for droplet drying. Since the inlet temperature was constant at 180 °C, when the nozzle pressure increased more liquid was in the drying chamber (higher atomisation cloud, more droplets) and consequently more solvent vapour, lowering the outlet temperature.

The median particle size (d_{50}) for spray dried powders was in the range of 2.4 - 3.5 μm and the volume distributions for all samples were narrow and monomodal with spans between 1.2 - 1.6.

SE micrographs of samples (Figure 6.6) showed that all were constituted by porous and spherical particles (morphology type 1BIIIα) with particles of small size presenting smooth surfaces (morphology type 1AIβ). Samples obtained from run 2/4 and run 3/8 also contained irregular shape porous particles (morphology type 2BIIIα). Masters (2002) reported that different particle shapes can exist in the same powder sample, due to individual atomized droplets of various sizes being subjected to different temperature and humidity gradients during passage through the drying chamber.

The nozzle gas pressure had a larger effect on particle size than the process gas pressure (F-value 33.36, p=0.005 and F-value 8.82, p=0,041 respectively). The droplet size is dependent on the air liquid ratio. An increase in the nozzle gas pressure increases the air liquid ratio which translates into a higher atomisation energy, resulting in droplets of smaller size and therefore smaller particle size (Masters, 2002; Maury et al., 2005). The model equation coefficient was negative for this parameter, that is, smaller particles are produced when setting a higher nozzle pressure, in accordance with the reported studies.

Specific surface area varied between 13.00-56.89 m^2/g. Both parameters (process gas and nozzle gas pressure) presented high F-values (strong effect), 33.08 for process gas pressure (p=0.005) and 21.82 (p=0.010) for nozzle gas pressure. The model equation coefficients were negative for process gas pressure and positive for nozzle gas pressure. The SSA of raffinose NPMPs prepared with a Büchi Mini spray dryer B-290 was affected by the atomizing gas; when the latter was increased so did the SSA.

Thermal analysis by DSC was also performed on spray dried samples (Appendix 3). All DSC scans were similar; a broad endotherm between 25 and 100 °C was initially detected, followed by a deviation of the base line, attributed to the glass transition temperature, at ~115 °C. No other thermal effects were registered. Statistical analysis by ANOVA showed no significant differences between samples, with p=0.570.

Using the statistical model equations obtained, it is possible to theoretically optimise the spray drying parameters to achieve a product with desired properties. Raffinose NPMP production was optimised in order to obtain powders with a minimum residual solvent content, particle size ≤3 µm, high specific surface area and yield. A higher importance was ascribed to minimising the RSC and maximising the SSA, as was previously carried out for the optimisation of raffinose NPMPs produced using the Büchi Mini spray dryer B-290. Predicted optimal settings for raffinose NPMPs were: process gas pressure of 1.2 bar and a nozzle gas pressure of 1.4 bar. The optimised settings were as runs 1 and 6 from the DOE space. Predicted outcomes were: PS 2.6 µm, SSA 43.88 m^2/g, RSC 2.6 % and T_{outlet} 86.5°C. The actual batch characteristics were: PS (d_{50}) 2.3±0.03 µm, SSA 43.88±3.82 m^2/g, RSC 2.6±0.08 % and process outlet temperature 86.5±4.9 °C. All outcomes, with the exception of PS, were as for predicted (no significant differences were found, $p>0.05$). Particle size was lower than predicted and significantly different $p=0.009$. Compared with the Büchi Mini spray dryer sample, the residual solvent content and outlet temperature were within the average ± standard deviation. However as seen in the preceding studies (Section 6.2), particle size was larger and SSA was lower for SDMicro samples.

Table 6.6 Coefficients of the model equations linking the significant (at least $p < 0.05$) spray drying parameters (in terms of coded factors) with responses. I - intercept (β_0); A – process gas pressure; B – nozzle gas pressure; PS - particle size; SSA – specific surface area; RSC - residual solvent content; Toutlet – outlet temperature.

Term	Yield (%)	F-value	Term	PS (d_{50}) (µm)	F-value	Term	SSA (m^2/g)	F-value	Term	RSC (%)	F-value	Term	T_{outlet} (°C)	F-value
I	20.00		I	3.09		I	41.08		I	2.88		I	83.88	
A	3.44	7.86	A	-0.17	8.82	A	-10.05	33.08	A	0.18	9.46	A	8.38	55.42
B	-4.97	16.35	B	-0.30	33.36	B	4.68	21.82	B	-0.19	11.12	B	-5.12	20.75
									AB	-0.23	15.54			
R^2	0.86		R^2	0.93		R^2	0.94		R^2	0.90		R^2	0.95	

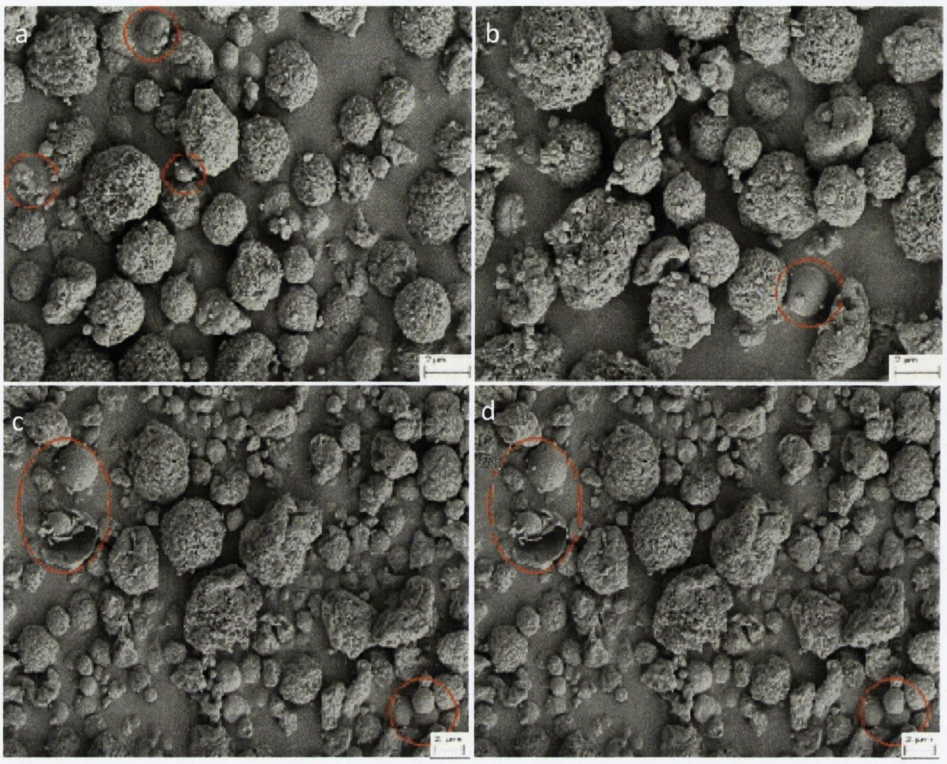

Figure 6.6 SE micrographs of spray-dried raffinose using the Niro SD Micro: (a) run 5/7, (b) run 1/6, (c) run 2/4 and (d) run 3/8.

6.4 *IN VITRO* DEPOSITION VIA NEXT GENERATION IMPACTOR FOR SAMPLES SPRAY DRIED USING THE NIRO SDMICRO™

The *in vitro* deposition properties of spray dried powders were studied for samples that presented high specific surface area and low residual solvent content. Samples studied were: SDM2, SDM3, SDM7 and the optimised sample (OSDM) when using the Niro SDMicro (as determined by the DOE outlined in Section 6.3). Samples were compared to the samples prepared using the Büchi Mini Spray dryer operated with the optimized settings by the DOE study.

Deposition profiles of Niro SDMicro raffinose NPMPs are presented in Figure 6.7. Deposition in the MA/IP and Stage 1 (cut-off point ~9 µm) was similar for all SDM samples. SDM samples presented higher deposition in stages 2 to 4 (cut-off point between 5 and 2 µm) than the Büchi sample. The recovered emitted dose varied between 68.1±11.7 % and 78.3±4.7 % with no significant differences between samples (SDM, OSDM and Büchi) ($p=0.303$) (Table 6.7). ANOVA with Tukey's test of FPF <5 µm showed the Büchi sample and OSDM to be significantly different from the remaining samples ($p=0.002$). FPF <3 µm of the Büchi sample and sample SMD7 were also significantly different ($p=0.002$). Samples SDM2 and SDM7 presented similar MMAD to the

Büchi NPMP sample. ANOVA proved the absence of significant differences between the MMAD and GSD values (p=0.115 and p=0.360, respectively) for all samples (SDM, OSDM and Büchi).

Previously, the differences in the micromeritic properties (SSA and PS) of samples spray dried using the Büchi Mini Spray dryer and the Niro SDMicro have been discussed, resulting in Niro samples to have lower SSA and higher d_{50}. A higher MMAD would be expected for the Niro samples since their geometric mediam particle size was higher and specific surface area was lower, existing more points of contacts between particles making them more cohesive forming aggregates harder to disperse. However ANOVA showed no significant difference between Büchi and Niro samples MMAD. If MMAD was similar it would be expected to see the same deposition profile, which was not true. Particle morphology was not the same between particles, although all porous, some were formed by conglomerates of nanoparticles (Büchi, SDM7 and OSDM) and others by fused nanoparticles (SDM2 and SDM3), which could impair on powder deposition.

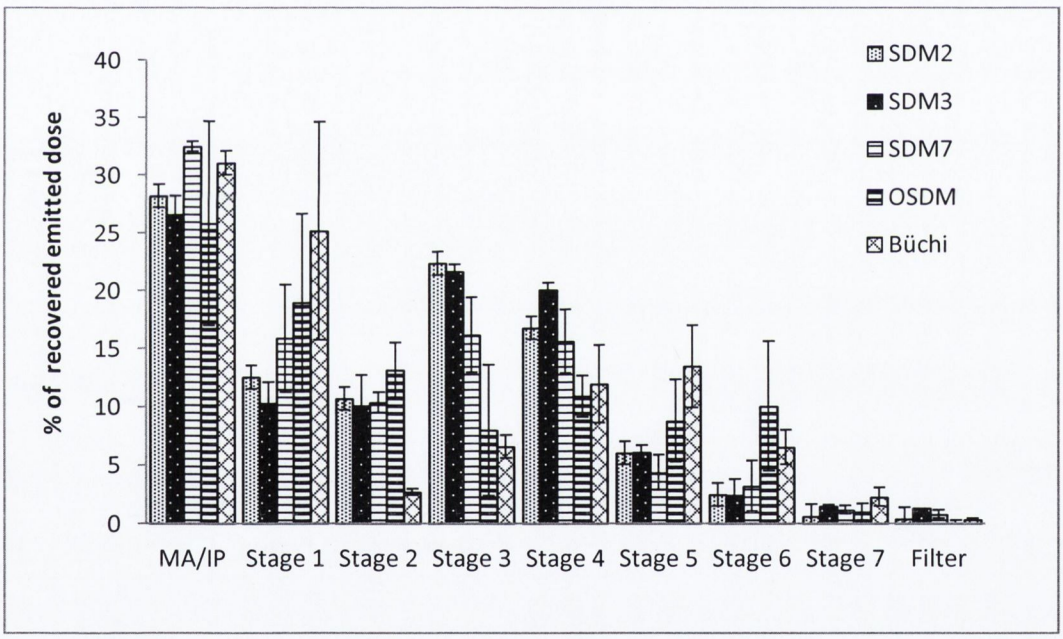

Figure 6.7 *In vitro* aerosol deposition profile determined using an NGI of raffinose NPMPS spray dried using the Niro SD Micro and optimised raffinose NPMPs spray dried using the Büchi Mini spray dryer, calculated as % of recovered emitted dose vs. NGI stages. MA – mouth adapter IP – induction port

Table 6.7 Recovered emitted dose, fine particle fraction (FPF), mass median aerodynamic diameter (MMAD) and geometric standard deviation (GSD) of *in vitro* aerosol deposition of raffinose NPMPS, spray dried using the Niro SDMicro.

	SDM2	SDM3	SDM7	OSDM	Büchi
% recovered emitted dose	69.8±5.8	78.3±4.7	75.3±5.2	71.9±6.16	68.1±11.7
FPF < 5 μm	61.3±2.8	60.1±3.9	54.4±5.1	69.7±6.67	50.4±15.6
< 3 μm	52.3±2.7	52.2±3.7	43.8±2.1	55.2±1.64	26.4±10.0
MMAD	4.0±0.28	3.6±0.08	4.4±0.67	3.4±0.28	4.4±0.27
GSD	2.1±0.25	2.5±0.03	2.4±0.23	2.3±0.09	2.3±0.48

6.5 SPRAY DRYING RAFFINOSE:HYDROXYPROPYL-B-CYCLODEXTRIN COMPOSITE SYSTEMS USING THE NIRO SDMICRO™

Raffinose:hydroxypropyl-β-cyclodextrin composite systems were spray dried using the optimised conditions defined for the Niro SD Micro (in section 6.4): T_{inlet} 180°C, Pump 0.6 kg/h, Process gas pressure 1.2 bar and nozzle gas (atomisation) pressure 1.4 bar. Feed solutions of 2.9 % (w/v) containing raffinose and hydroxypropyl-β-cyclodextrin (40 % and 60 % weight fraction) in methanol:n-butyl acetate (4:1) (v/v) were spray dried. Two replicates were produced.

The outlet temperature varied between 78-87 °C. Powders were amorphous by XRPD analysis (Appendix 3). Particle morphology by SEM showed spherical and irregular shape, porous particles, type 1BIIIα and 2BIIIα (Paluch et al., 2012) (Figure 6.8). The morphology of the samples was similar to that attained when using the Büchi spray dryer (Chapter 5, figure 5.28). Process outlet temperature was within the same range as seen with the Büchi (81-86 °C for Büchi).

Particle size volume distributions of R:HPβCD composite systems were narrow and monomodal with low span values (1.1±0.01 for both systems) and the median particle size (d_{50}) was 2.7±0.05 μm and 2.8±0.07 μm for R:HPβCD 60:40 and 40:60, respectively. Table 6.8 presents the reported values of d_{10}, d_{50}, d_{90} and percentage of particles with size < 1 μm as mean ± standard deviation. Statistical analysis by student's t-test, proved the existence of no significant differences between Niro samples; however when compared to their counterparts produced using the Büchi Mini spray dryer B-290 it was found that samples were different with $p<0.05$, since the latter samples presented a d_{50} of 1.9 μm, approximately one micrometer smaller than the Niro samples.

Specific surface area results are presented in Table 6.8. As seen in Chapter 5, section 5.4, the addition of HPβCD to the raffinose formulation resulted in an increase in the specific surface area. Student's t-test showed no significant difference between Niro composite systems ($p=0.135$) and between Niro R:HPβCD 40:60 and Büchi R:HPβCD 40:60 ($p=0.667$). The SSA of R:HPβCD 60:40 spray dried using the Niro SDMicro was significantly lower than that of R:HPβCD 60:40 spray dried using the Büchi Mini spray dryer B-290 ($p=0.008$; 86.15±2.64 vs. 106.96±0.07).

Bulk and tap density results for both powders spray dried on the Niro SD Micro were identical, 0.13 and 0.23 g/cm^3 (Table 6.8), values which, at < 0.3 g/cm^3 make them suitable for pulmonary delivery (Bosquillon et al., 2004) and, similar to samples produced using the Büchi Mini spray dryer B-290 (bp=0.13 g/cm^3 and tp=0.22 g/cm^3).

DSC scans of spray dried composite systems demonstrated the occurrence of one thermal event – the glass transition step, which was intermediate to the T_g values of the pure components (Appendix 3; raffinose T_g = 116.1±0.81 °C and HPβCD T_g = 225.4±0.32 °C). The addition of cyclodextrin to raffinose caused a significant increase in the T_g ($p<0.05$). Student's t-test show a significant difference between the T_g of R: HPβCD spray dried using the Niro SDMicro and the Büchi Mini spray dryer B-290, with an increase in T_g temperature when using the Niro machine.

A residual solvent content of 4.6±0.35% for R:HPβCD 60:40 and 4.1 ±0.32% for R:HPβCD 40:60 was determined over the temperature range 25-130 °C from TGA scans. Student's t-test showed no significant difference in RSC between the spray dried composite systems and between these and the systems spray dried using the Büchi spray dryer. For better comprehension of the RSC composition, GC-FID was used to quantify methanol and butyl acetate, assuming the difference between calculated values from the two techniques would correspond to moisture ($TGA - GC = water\ content$). Table 6.9 shows the calculated values. RSC was constituted mainly by butyl acetate and water, with methanol not being detected. The water content could be explained by the amorphous sugars strong tendency to take up moisture by adsorption and desorption (Hancock and Shamblin, 1998).

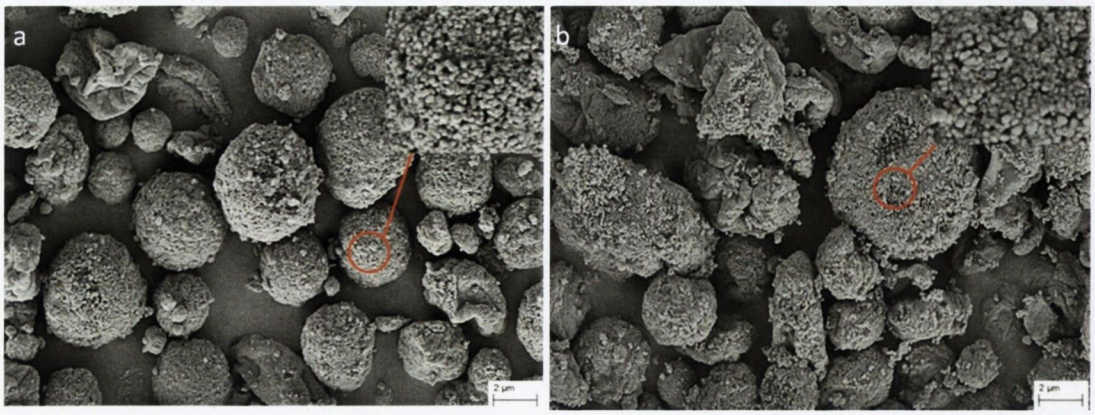

Figure 6.8 SE micrographs of spray dried raffinose:HPβCD composite systems with ratios (a) 60:40 and (b) 40:60.

Table 6.8 Particle size, specific surface area (SSA), true, bulk and tap density and calculated aerodynamic diameter of Raffinose:HPβCD composite systems spray dried using the Niro SD Micro.

	R:HPβCD 60:40 Niro SD Micro	**R:HPβCD 40:60 Niro SD Micro**
d_{10} (µm)	1.5±0.03	1.7±0.06
d_{50} (µm)	2.7±0.05	2.8±0.07
d_{90}(µm)	4.7±0.03	4.5±0.02
span	1.1±0.01	1.1±0.01
<1µm (%)	1.2±0.14	0.5±0.10
SSA (m^2/g)	86.15±2.64	94.28±3.91
bp(g/cm^3)	0.13±0.01	0.13±0.01
tp (g/cm^3)	0.21±0.002	0.21±0.002

Table 6.9 Residual solvent content by TGA and GC-FID for R:HPβCD composite systems. ND – not detected

R:HPβCD Niro SD Micro	**RSC by TGA (% w/w)**	**RSC by GC-FID (% w/w)**		**Extrapolated**
		Methanol	Butyl Acetate	**Water content (%)**
60:40	4.6±0.35	ND	0.72±0.01	3.9
40:60	4.1±0.32	ND	1.23±0.02	2.9

In vitro deposition analysis was also performed on spray-dried composite systems.

Deposition profiles of R:HPβCD systems spray dried using the Niro SDMicro and the Büchi Mini spray dryer B-290 are represented in Figure 6.9. Higher deposition in the mouthpiece adaptor and induction port was found for the Niro SDMicro systems. Statistically significant differences between the two composite systems spray dried using the Niro SD Micro were found for the fine particle fraction < 5 and 3 μm, with R:HPβCD 60:40 presenting the higher FPF <5 μm and the lower FPF <3 μm. R:HPβCD 40:60 SD Micro, presented smaller MMAD and GSD, hence the higher deposition in stages with cut-off < 3 μm (Table 6.10).

No significant differences were found for *in vitro* deposition parameters between R:HPβCD 60:40 SDMicro and R:HPβCD 60:40 Büchi. However, R:HPβCD 40:60 SD Micro and R:HPβCD 40:60 Büchi presented significantly different FPF <5 and 3 μm and GSD, with R:HPβCD 40:60 Büchi presenting higher fine particle fraction and smaller geometric standard deviation (Table 6.10), which is resulting from the powders micromeritic properties: smaller d_{50} and higher SSA.

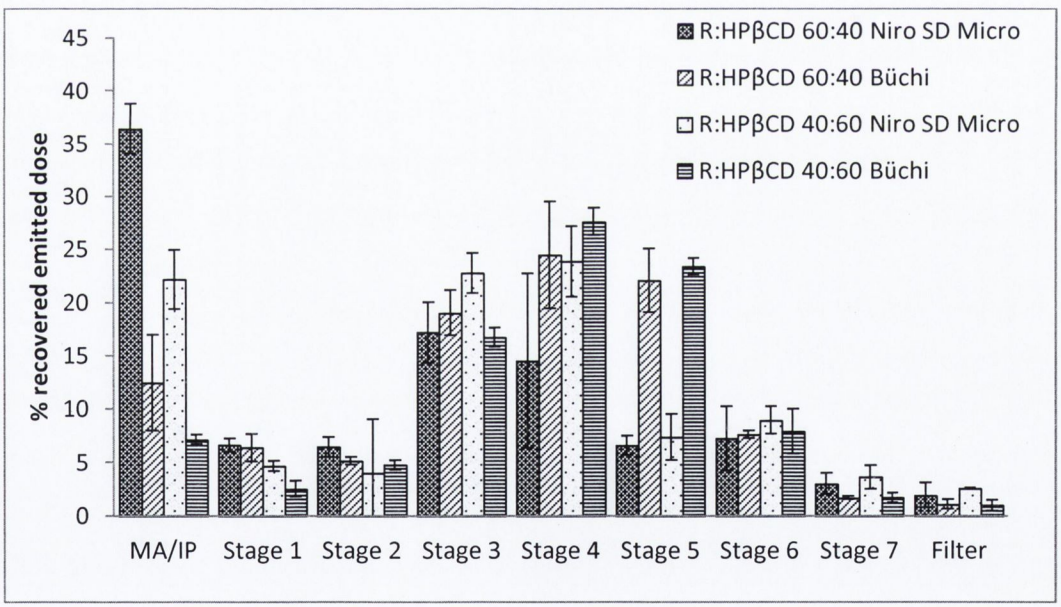

Figure 6.9 *In vitro* aerosol deposition profile by use of a NGI of R:HPβCD composite systems as calculated % of recovered emitted dose vs. NGI stages. MA – mouth adapter IP – induction port

Table 6.10 Recovered emitted dose, fine particle fraction (FPF), mass median aerodynamic diameter (MMAD) and geometric standard deviation (GSD) of *in vitro* aerosol deposition of R:HPβCD composite systems.

	R:HPβCD 60:40 Niro SD Micro	R:HPβCD 60:40 Büchi	R:HPβCD 40:60 Niro SD Micro	R:HPβCD 40:60 Büchi
% recovered emitted dose	87.2±5.5	91.4±1.2	89.1±2.6	92.7±10.5
FPF < 5 µm	54.5±2.9	69.5±7.1	70.5±2.5	87.3±0.5
< 3 µm	49.0±3.1	58.0±8.3	66.5±0.3	83.8±0.9
MMAD	2.7±0.15	2.4±0.07	2.3±0.19	2.2±0.18
GSD	2.6±0.36	2.1±0.04	2.4±0.04	2.0±0.09

6.6 SPRAY DRYING WITH THE NIRO MOBILE MINOR™ SPRAY DRYER

Solutions with a concentration of 2.0 % w/v of raffinose pentahydrate were prepared in a solvent composition of 80:20 MeOH:BA, 2.5 % w/v in 90:10 MeOH:BA (run 11) and 1.5 % w/v in 70:30 MeOH:BA (run 12). The spray drying was carried out in a co-current mode with a two-fluid nozzle, using nitrogen as drying gas at a flow rate of 80 kg/h. Parameter settings are presented in Table 7.11. The parameter settings and the feed solution concentration were based on the OFAT studies on the Büchi 290-B Mini Spray Dryer presented in Chapter 3, since this was the data available at the time the scale-up study on the Mobile Minor was undertaken.

This study aimed not only to produce raffinose NPMPs using a pilot scale facility but also, to compare the powder characteristics with raffinose NPMPs produced using the Büchi Mini spray dryer B-290. Single runs were performed due to short availability of the instrument. Evaluated outcomes were: outlet temperature, yield, residual solvent content, particle morphology, geometric median particle size and specific surface area. Thermal characterisation and *in vitro* deposition were also performed on selected samples.

Table 6.11 Summary of spray dryer settings for the Niro Mobile Minor™. ALR: atomisation-gas-liquid-mass-ratio

Run	Inlet temperature (°C)	Pump (kg/h)	Atomisation gas flow rate (kg/h) (atomisation pressure (bar))	ALR
MM1	125	0.8	6.5 (1)	8.1
MM2	110	0.8	6.5 (1)	8.1
MM3	90	0.8	6.5 (1)	8.1
MM4	125	1.4	11.5 (2)	8.2
MM5	125	1.2	15 (3)	12.5
MM6	125	1.8	6.5 (1)	3.6
MM7	150	2.0	6.5 (1)	3.8

6.6.1 Characterisation of spray dried powders

Data resulting from raffinose spray dried with the Büchi spray dryer with the parameters set to the optimised settings as predicted by the OFAT studies (rather than the DOE) were used for comparison between the Niro Mobile Minor and the Büchi Mini Spray Dryer, since these were the basis for selection of parameters to evaluate spray drying on the Niro Mobile Minor. The DOE study had not been completed in advance of scale up studies on the Mobile Minor being undertaken. The outcomes for the Büchi Mini Spray Dryer sample were: PS 2.4±0.01 µm, RSC 2.8±0.15 %, SSA 45.50 m^2/g and T_{outlet} 72 °C.

All spray dried powders were amorphous by XRPD analysis, presenting the characteristic amorphous 'halo' (Appendix 3), as seen for spray dried powders using the Büchi Mini spray dryer.

Particle morphology was evaluated by SEM. Figure 6.10 shows the SE micrographs of the samples produced using the Niro Mobile Minor. All samples, with the exception of sample MM11, were comprised of porous spherical particles, of type 1BIIIα according to the classification system developed by Paluch et al. (2012), and differing in particle size. Sample MM11 consisted of spherical particles with smooth surfaces, type 1AIβ and, irregularly shaped fragments of spray dried material. Small smooth spherical particles were also present in samples MM8 and MM12 (marked with a red circle on Figure 6.10h and 6.10l).

The different morphology of sample MM11 was probably due to the feed solution composition, where the ratio of the co-solvent system and solid content were changed, such that these new proportions were not effective for the production of raffinose NPMPs. Studies by Ní Ógáin et al. (2010) on spray-dried raffinose and trehalose from different co-solvent systems, EtOH:Water and MeOH:BA (using the Büchi Mini spray dryer B-290) reported different particle morphologies depending not only on the type of solvent, but also on the ratio of the co-solvent system, as well as, the importance and impact of excipient/drug solubility in the solvent systems on particle morphology.

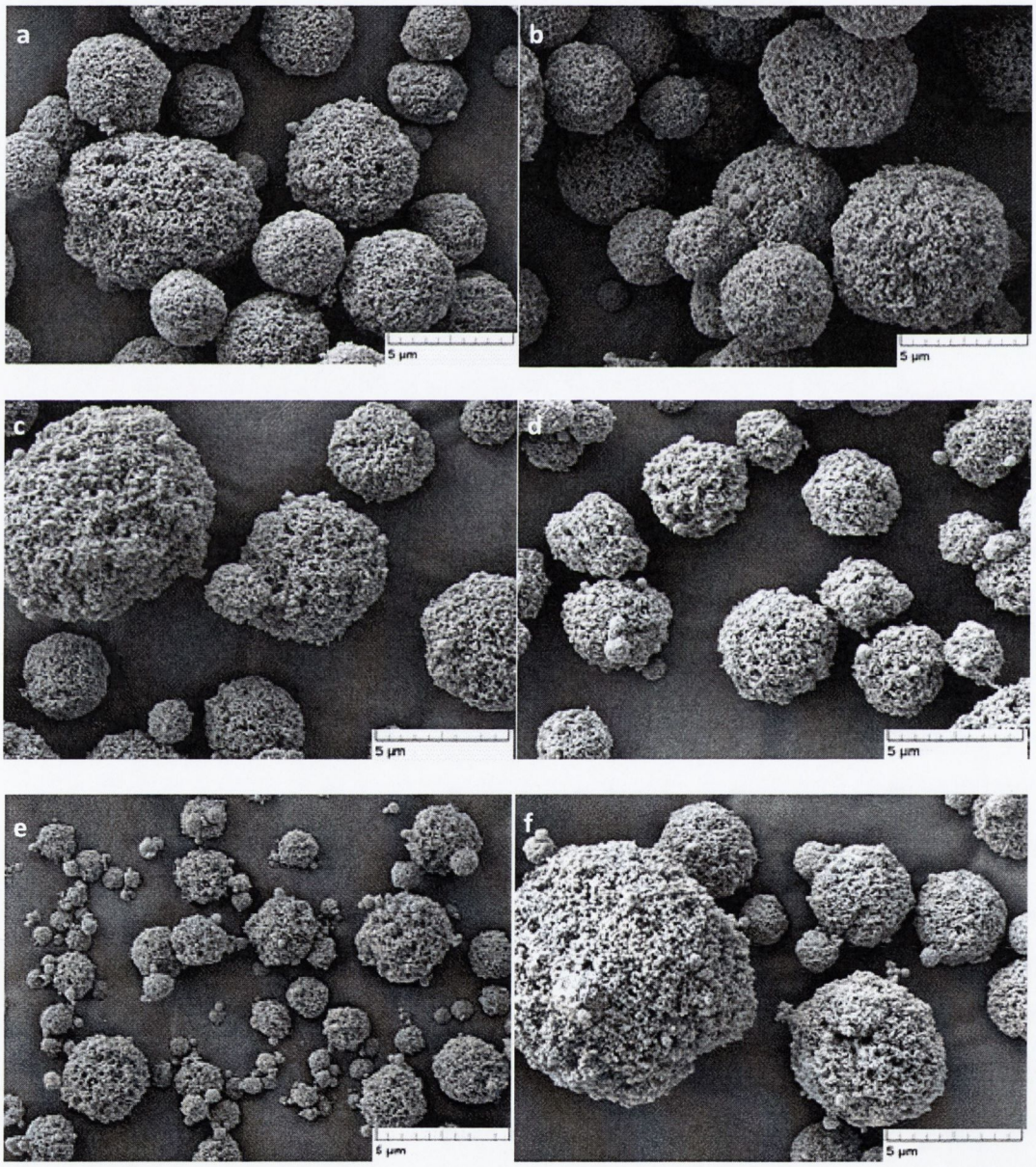

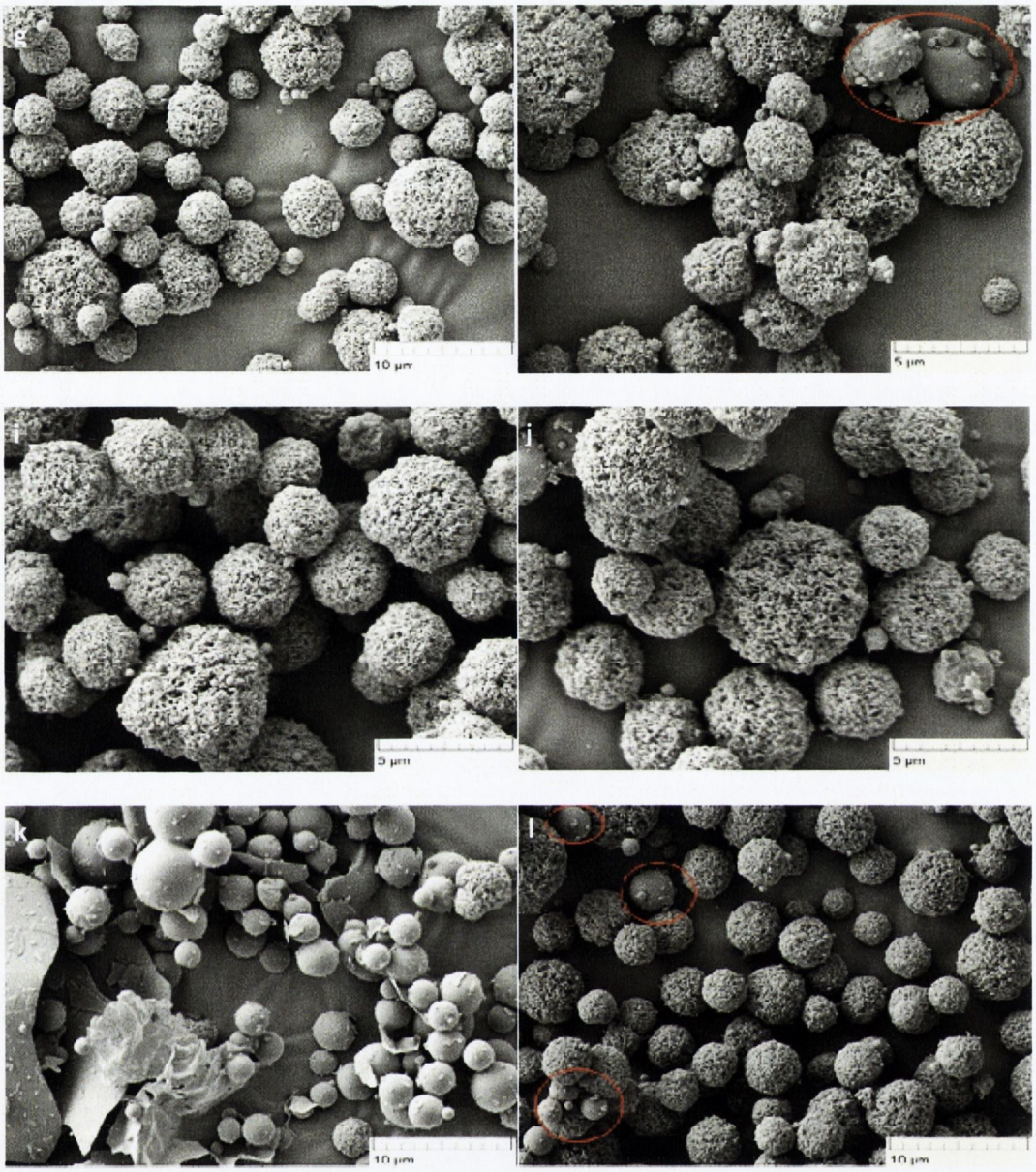

Figure 6.10 SE micrographs of spray dried raffinose using the Niro Mobile Minor: (a) MM1, (b) MM2, (c) MM3, (d) MM4, (e) MM5, (f) MM6, (g) MM7, (h) MM8, (i) MM9, (j) MM10, (k) MM11, (l) MM12

Tables 6.12 presents process outlet temperature and powder residual solvent content for each run in the Niro Mobile Minor respectively.

Process outlet temperature varied between 60 and 80 °C. Reduction in the T_{outlet} was observed with increased setting of pump (feed flow rate) (MM1 and MM6). When more liquid is supplied to the drying chamber, more solvent vapour is generated, decreasing the exhaust temperature (Maury et al., 2005). An effect of the inlet temperature on process T_{outlet} was also evident, where the latter increased with increasing heat energy supplied (higher T_{inlet}) (runs SDM5 and SDM7 for Niro SDMicro with p=0.012 and, MM1, MM2 and MM3 for Niro Mobile Minor).

The outlet temperature for raffinose NPMP production when using a Büchi Mini spray dryer B-290 at the OFAT optimised setting was 85 °C. This outlet temperature was attained when working with the Niro SDMicro by setting the inlet temperature to a higher value (180 °C) compared to the setting of the Büchi spray dryer. The Niro Mobile Minor presented a similar outlet temperature to that obtained when operating the Büchi Mini Spray Dryer at the OFAT optimised conditions for samples MM2, MM4, MM5 and MM6. The remaining samples were spray dried at a higher outlet temperature, due to variation in inlet temperature and pump setting, which are known to affect this outcome.

The residual solvent content (RSC) was determined by TGA over the temperature range 25-130 °C. Values varied between 1.1 and 3.5 % for the Niro Mobile Minor samples (Table 6.13). Figure 6.13 shows how the RSC varied with the inlet temperature and pump setting. Samples presented lower RSC when spray drying was conducted at higher inlet temperatures and an interaction between the inlet temperature and pump can be inferred, since RSC increased with reduction of both settings and an increase in the pump setting was always accompanied by an increase in the inlet temperature. It is postulated that there is an increase in solvent vapour generated when spray drying at high pump settings; thisis known to reduce the exhaust temperature, consequently decreasing solvent evaporation, resulting in powders with higher RSC. However, the effect of increasing the pump setting can be compensated for by increasing drying energy supplied, by elevating the inlet temperature.

Masters (2002) reported that the greater the air/gas temperature difference ($T_{inlet} - T_{outlet}$), the smaller the heat requirement to produce a unit weight of powder of constant residual moisture/solvent content, and the more efficient the process is. Figure 6.12 shows the effect of the gas temperature difference (ΔT) on the residual solvent content of powders. It was possible to see a significant reduction in the RSC when the ΔT was increased.

Samples MM2, MM5, MM6 and MM8 also presented similar RSCs to that obtained when operating the Büchi Mini Spray dryer at the OFAT optimised conditions. The remaining MM samples presented lower and higher RSC; the lower values resulted from spray drying at high inlet temperatures and low feed rate.

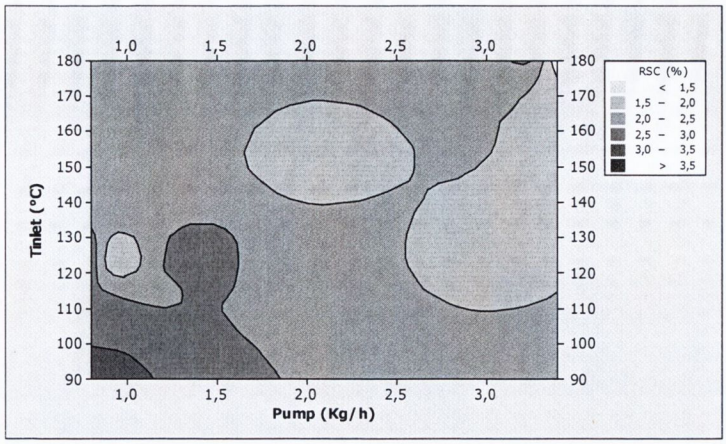

Figure 6.11 Contour plot of the effect of process variables inlet temperature (T_{inlet}) and pump setting on the residual solvent content of raffinose powders produced using (a) the Niro SDMicro and (b) the Niro Mobile Minor.

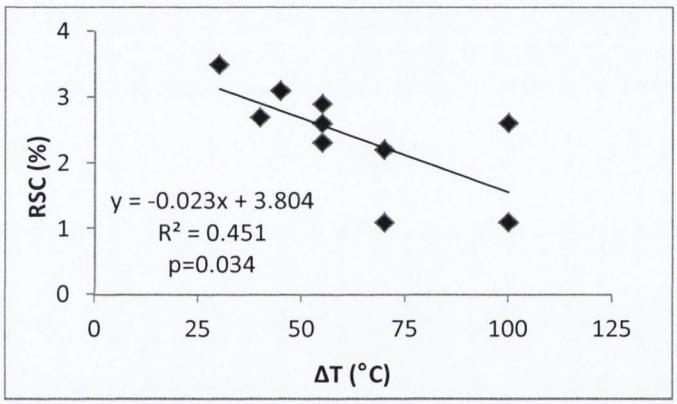

Figure 6.12 Influence of the air/gas temperature difference on raffinose powders residual solvent content spray dried using (a) the Niro SDMicro and (b) the Niro Mobile Minor.

Geometric median particle size (d_{50}) and specific surface area (SSA) of raffinose spray dried samples are presented in Table 6.12. Particle size volume distributions were narrow and monomodal with low span values (1.7-2.7). The d_{50} was in the range of 2.8-5.4 µm. It was possible to see an effect on particle size of varying the pump setting and atomisation gas pressure (Figure 6.13). The contour plot of d_{50} showed that particles of small size (< 3.0 µm) were produced when operating at low pump setting and high atomisation pressure. Nevertheless, a discrete domain could be seen, where small particles are also produced when operating at a medium atomisation pressure (within the range 1-3 bar) and high pump rate. Hence, an interaction between pump rate and atomisation pressure is evident.

Figure 6.14 represents the relationship between d_{50} and the ALR. A reduction in particle size with increasing ALR was observed. Studies by Thybo et al. (2008) also reported a decrease in particle size with increasing ALR when spray drying acetaminophen and PVP from water and ethanol solutions using a Niro Mobile Minor.

When the process was scaled up to the Niro Mobile Minor the particle size was also found to increase. The deposition studies shown later in this section will determine if this increase in geometric particle size affected the powders' deposition properties.

Specific surface area varied between 3.67-58.96 m^2/g. SSA of powders was affected by different parameters and was found to increase as follows: with an increase in inlet temperature, when the remaining parameters were constant (MM1, MM2 and MM3); when atomisation gas flow was increased, independently of pump setting (MM4, MM5, MM8 and MM10); with increasing concentration and reduction in pump setting (MM1, MM6, MM11 and MM12); with a decrease of pump setting (MM1 and MM6); and decrease in both inlet temperature and pump setting (MM1, MM6, MM7, MM9 and MM10). Figure 6.15 shows the effect of inlet temperature and pump setting on SSA (MM1, MM6, MM7, MM9 and MM10); higher surface areas are achieved when spray drying was conducted with T_{inlet} between 120 and 130 °C and pump setting range from 1 to 1.5 kg/h. The effect of total solid concentration and pump setting on SSA is demonstrated in Figure 6.16 (MM1, MM6, MM11 and MM12), with high SSA attained if concentration is ~2 % and pump rate is low.

The SSA of raffinose NPMPs spray dried using the Büchi Mini spray dryer B-290 set with the optimised conditions taken from the OFAT was 45.50 m^2/g; sample MM8 presented a similar value. When the DOE was performed it was found that the SSA was mainly affected by the gas flow, where, as the gas flow was increased, the SSA increased. This effect was also seen for the Niro Mobile Minor samples MM4 and MM5, and MM8 and MM10. The study indicates that, in relation to SSA, the spray drying variables impact is similar at the laboratory and pilot scale.

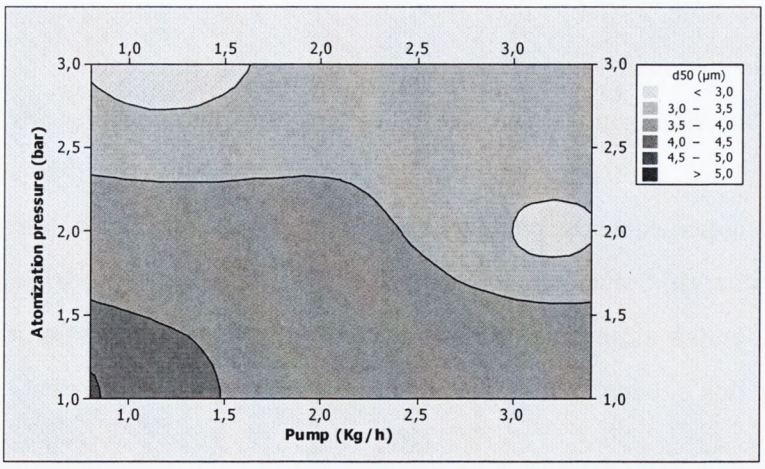

Figure 6.13 Contour plot of the effect of process variables atomisation pressure and pump setting on the geometric mean particle size (d_{50}) of raffinose powders produced using the Niro Mobile Minor.

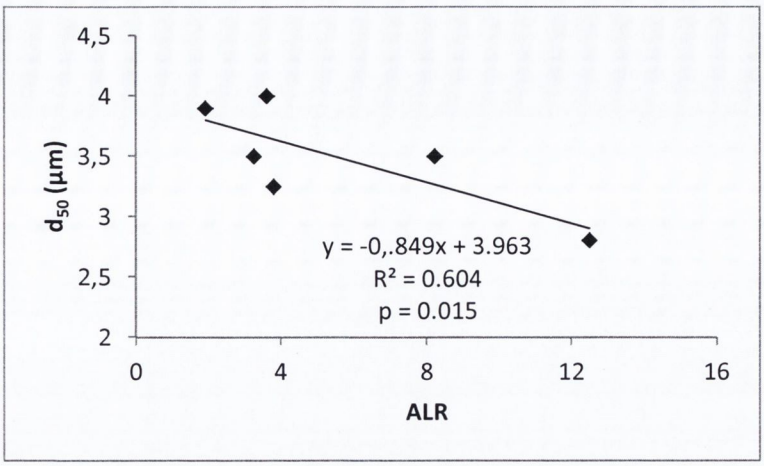

Figure 6.14 Effect of the air/liquid ration (ALR) on the geometric mean particle size (d_{50}) of raffinose powders spray dried using the Niro Mobile Minor.

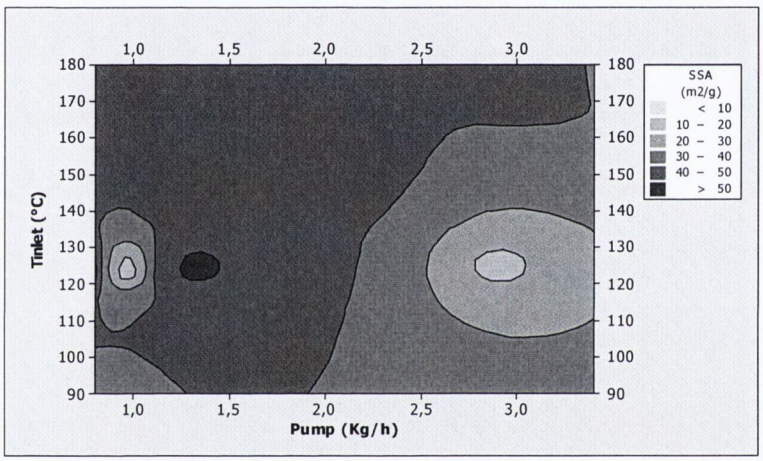

Figure 6.15 Contour plot of the effect of process variables atomisation pressure and pump setting on the specific surface area (SSA) of raffinose powders produced using the Niro Mobile Minor.

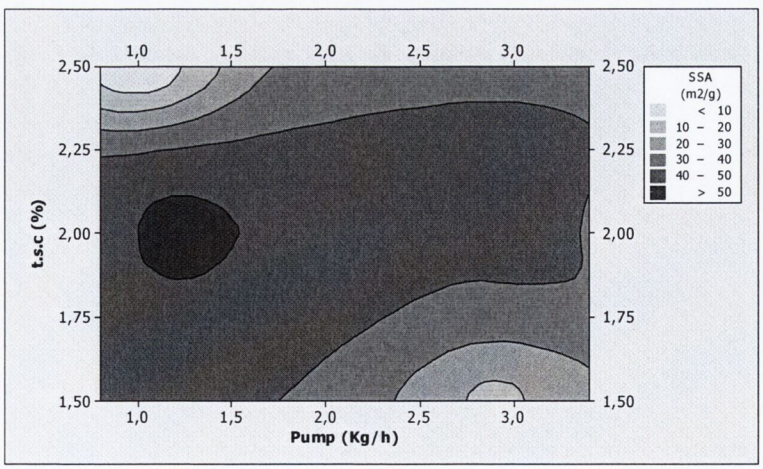

Figure 6.16 Contour plot of the effect of process variables total solid concentration (t.s.c.) and pump setting on the specific surface area (SSA) of raffinose powders produced using the Niro Mobile Minor.

Bulk and tap densities of powders were evaluated. All values were found to be lower than 0.3 g/cm^3, making them suitable for pulmonary delivery (Bosquillon et al., 2004) (Table 6.12). All

powders produced using the Niro Mobile Minor presented similar bulk and tap density with the exception of sample MM5. The latter had a lower bulk density than all other samples.

Table 6.12 Evaluated outcomes of raffinose samples spray dried using the Niro Mobile Minor. N/A – data not available

Run	T_{outlet} (°C)	ΔT (°C)	d_{50} (μm) (span)	SSA (m^2/g)	RSC (% w/w)	bp (g/cm^3)	tp (g/cm^3)
MM 1	80	45	4.9 (1.7)	58.96±0.75	3.1	0.11	0.19
MM 2	70	40	5.4 (1.8)	40.16±0.85	2.7	0.10	0.18
MM 3	60	55	4.3 (1.9)	38.42±0.11	3.5	0.11	0.18
MM 4	70	55	3.4 (2.7)	53.09±0.10	2.9	0.10	0.18
MM 5	70	55	2.8 (2.6)	56.12±0.17	2.6	0.06	0.21
MM 6	70	55	4.0 (2.1)	40.66±0.08	2.3	0.10	0.20
MM 7	80	70	3.8 (1.9)	39.88±0.12	2.2	0.11	0.18
MM 8	80	100	2.9 (1.9)	44.77±0.24	2.6	0.10	0.18
MM 9	80	70	3.5 (1.9)	49.58±0.09	1.1	0.11	0.19
MM 10	80	100	3.9 (1.9)	37.01±0.17	1.1	N/A	N/A
MM 11	80	45	4.0 (2.1)	3.67±0.05	1.2	N/A	N/A
MM 12	80	45	4.0 (2.0)	18.50±0.16	1.8	N/A	N/A

Thermal analysis was only performed on selected samples from the Niro Mobile Minor. The criteria for selection were low residual solvent content and high specific surface area. Hence, samples MM1, MM4, MM5, MM8 and MM9 were selected.

DSC scans were similar for all raffinose samples (Appendix 3). A broad endotherm in the interval 25-100 °C was seen and attributed to residual solvent loss; it was followed by a base line shift, the glass transition step, with no other thermal events registered. The glass transition temperature varied between 114.5±0.67 °C and 116.6±0.04 °C. ANOVA with Tukey's test showed statistically significant differences in the T_g between sample MM4 and MM5 ($p=0.033$). Sample MM4 had a higher residual solvent content than MM5 (Table 6.13) that can act as a plasticiser, reducing the glass transition temperature. Most samples presented a T_g value close to the value found for raffinose NPMPs spray dried using the Büchi Mini spray dryer, i.e., 116.7±0.28 °C.

The residual solvent content of powders was further analysed by GC-MS, for quantification of butyl acetate and methanol. Quantification of BA with GC-MS was not possible. MM samples presented higher methanol content than the raffinose NPMPs from the Büchi Mini spray dryer (0.30 ± 0.01% (w/w)) (Table 6.13).

Table 6.13 Glass transition temperature (Tg) and residual solvent content (RSC) by TGA and MeOH content GC-MS of raffinose powders spray-dried using the Niro Mobile Minor.

	Tg (°C)	RCS by TGA (% (w/w))	MeOH by GC-MS (% (w/w))
MM1	115.3±0.25	3.1	0.90
MM4	114.5±0.67	2.9	1.10
MM5	116.6±0.04	2.6	0.90
MM8	114.9±0.57	2.6	0.91
MM9	115.2±0.33	1.1	-

6.6.2 *In vitro* deposition via next generation impactor for samples spray dried using the Niro Mobile Minor

The *in vitro* deposition properties of spray dried powders were studied for samples that presented high specific surface area and low residual solvent content: MM1, MM4, MM5, MM8 and MM9. Samples were compared to the sample prepared using the Büchi Mini spray dryer operated with the optimised settings by the OFAT study.

Figure 6.17 presents the deposition studies for the Niro Mobile Minor raffinose NPMP samples and the Büchi raffinose NPMPs. A higher deposition on stage 1 (cut-off point ~9 µm) was obtained for the Büchi sample. All MM samples presented a high fraction of powder (30 to 60% of recovered emitted dose) retained in the mouthpiece adaptor/induction port (MA/IP). Fine particle fraction < 5 µm for MM samples varied between 29.7±1.8 % and 59.7±15.8 % and, FPF < 3 µm between 22.3±4.1 % and 40.0±11.6 %, with higher values pertaining to sample MM5 (Table 6.14). Statistical analysis by ANOVA of recovered emitted dose, fine particle fraction < 5 µm and FPF < 3 µm was not significant, p=0.424, that is, no differences were found among MM samples and between MM samples and the Büchi sample. However, the Büchi sample presented the lowest MMAD (p=0.016). Differences in the GSD were also found, p=0.007. ANOVA with Tukey's test showed samples MM4 and MM9 had a GSD different and higher from samples MM8 and

Büchi. The higher MMAD and GSD of the MM samples is thought to be the reason of the increased deposition of these powders in the higher cut-off stages such as the MA/IP.

The obtained results showed the differences seen on the micromeritic properties between raffinose NPMPs produced using the Niro Mobile Minor and the Büchi Mini spray drier did not affect, in general, the powder *in vitro* deposition. Sample MM5 and MM9 presented higher SSA than the Büchi sample. It is postulated that the large surface area that reduces the interparticle contact promoting easier particle dispertion, overcomes the increase in the particles geometric median diameter, since these samples presented higher d_{50}. Samples MM4 and MM8 had a SSA similar and lower than the Büchi sample; however, the differences were only reflected in the MMAD and GSD, possible particle cohesion may have lead to these results.

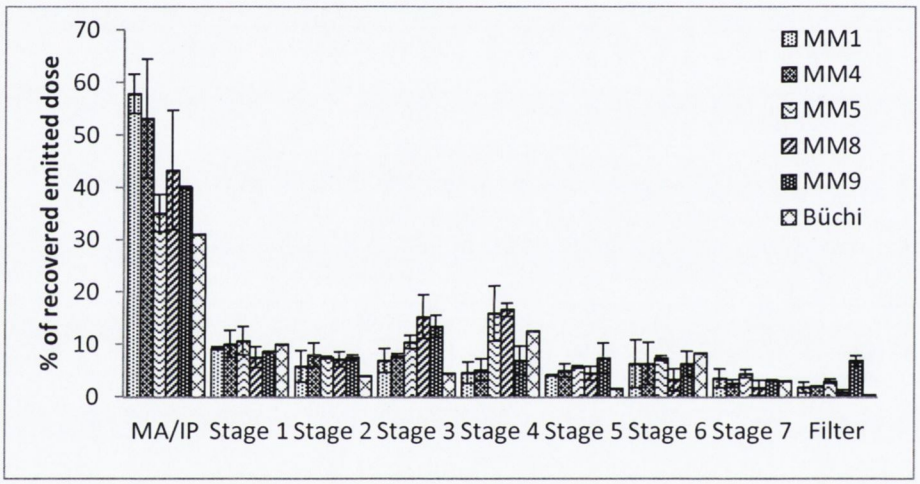

Figure 6.17 *In vitro* aerosol deposition profile determined using an NGI of raffinose NPMPs, spray dried using the Niro Mobile Minor and optimised OFAT raffinose NPMPs spray dried using the Büchi Mini spray dryer, calculated as % of recovered emitted dose vs. NGI stages. MA – mouth adapter, IP – induction port.

Table 6.14 Recovered emitted dose, fine particle fraction (FPF), mass median aerodynamic diameter (MMAD) and geometric standard deviation (GSD) of *in vitro* aerosol deposition of raffinose NPMPS, spray dried using the Niro Mobile Minor. Note: only one data point was available for the OFAT Büchi sample

	MM1	MM4	MM5	MM8	MM9	Büchi
% recovered emitted dose	83.0±12.1	51.8±5.7	76.7±1.6	84.9±4.3	85.4±6.9	74.49
FPF < 5 µm	29.7±1.8	31.7±8.7	59.7±15.8	56.2±4.8	49.5±2.9	35.0
< 3 µm	23.7±3.2	22.3±4.1	40.0±11.6	31.7±0.9	34.4±0.1	29.4
MMAD	3.2±1.50	3.3±0.18	2.7±0.40	3.2±0.42	2.4±0.14	2.6
GSD	3.5±0.28	3.7±0.46	3.2±0.24	2.4±0.14	4.1±0.24	2.4

6.7 CONCLUSION

NPMPs can be produced by spray drying in laboratory scale spray dryers of larger dimensions (Niro SDMicro) and at the pilot scale (Niro Mobile Minor). The studies presented identified the way process parameters impact on raffinose powders characteristics for both processing scales (laboratory and pilot). Residual solvent content was affected by the gas flow/pressure, pump setting and inlet temperature; particle size and specific surface area by the gas flow/pressure and pump setting; outlet temperature by the inlet temperature and pump setting; in a similar way as described for the Büchi Mini spray dryer B-290.

The additional factorial design on the raffinose NPMPs production using the Niro SDMicro resulted in well fitted models which highlighted how process and nozzle gas pressure impact on powder characteristics. Process gas pressure had a great impact on outlet temperature; nozzle gas pressure impacted on yield and particle size; both parameters strongly impacted on powder specific surface area.

Raffinose NPMPs produced in the Niro spray dryers presented, in general, higher geometric median particle size and RSC and smaller SSA than those produced using the Büchi Mini spray dryer B-290. However, the *in vitro* deposition studies showed powders produced in the Niro Mobile Minor (pilot scale) presented similar profiles and deposition parameters to Büchi raffinose NPMPs (laboratory scale) and, Niro SDMicro powders to have higher fine particle fraction than those prepared on the Büchi instrument.

Raffinose:hydroxypropyl-β-cyclodextrin composite systems can also be produced in a larger dimension laboratory scale spray dryer. The resulting powders presented the same morphology as those produced using the Büchi Mini spray dryer B-290. From the two ratios of excipients used, it was seen that powders with a ratio of 60:40 presented similar characteristics (only particle size was increased) and *in vitro* deposition to those obtained with the Büchi spray dryer.

In conclusion, the production of NPMPs can be transferred into a larger dimensions laboratory spray dryer as well as to a pilot scale spray dryer. Previous knowledge acquired using the Büchi Mini Spray dryer was crucial to inform the adjustment of settings in a different spray dryer. Even though the operating mode of the spray dryers was different (e.g., blow mode for the Niro SDMicro versus suction for the Büchi) the impact and trends of the spray drying parameters was almost identical and powders with suitable characteristics for pulmonary delivery were produced.

CHAPTER 7
SPRAY DRYING OF SALMON CALCITONIN: SUGAR COMPOSITE SYSTEMS

7.1 INTRODUCTION

Pulmonary drug delivery using dry powder inhalers in recent years has become an alternative for systemic delivery of peptides and proteins, improving their bioavailability and effectiveness (Daniher and Zhu, 2008).

Studies by Chan et al. (2004) focused on the spray drying of 1% (w/v) salmon calcitonin (sCT) solutions as binary mixtures with different ratios of mannitol to produce microparticles for pulmonary delivery. It was found that spray dried sCT alone was amorphous and its physical stability was unaffected by processing. The amorphous content of the binary mixtures was dependent on the mannitol fraction The aggregation stability of sCT and the physical stability of the dry powders were optimal when stored in a low humidity environment and, moisture content was the main factor affecting powder stability.

Yang et al. (2007) spray dried sCT powders suitable for inhalation, containing chitosan and mannitol as absorption enhancer and protection agent (against process stress - avoids aggregation and water scavenger), respectively. The addition of chitosan resulted in a decrease in sCT recovery and an alteration of the structure of sCT, probably due to a strong interaction between the two compounds.

A comparative study on the pulmonary bioavailability of powder and liquid aerosol formulations of sCT in healthy volunteers was performed by Clark et al. (2008). A sCT subcutaneous injection was used as control. Lung bioavailability, relative to the subcutaneous injection, ranged from 11 to 18%. It was concluded that there were the no statistically significant differences between area under the curve (AUC) for all formulations.

The reported studies indicate the main challenge in peptide lung delivery to be the development of a stable formulation with suitable physicochemical characteristics and biological activity. Previously (Chapters 4 and 5) we discussed different stabilising excipient formulations to be used as carriers for peptides. In this chapter it will be discussed if these formulations possess the physicochemical properties, the aerodynamic behaviour and the required stability to be suitable for sCT pulmonary delivery. *In vivo* studies to evaluate the pharmacokinetic profiles of the sugar salmon calcitonin formulations after pulmonary administration are also presented.

7.2 PREPARATION OF SALMON CALCITONIN:SUGAR COMPOSITE SYSTEMS

Production of powders was carried out on a laboratory scale spray dryer (Büchi Mini spray dryer B-290) set-up as discussed in Chapter 4 for optimised sugar NPMPs production. Solutions with 5:95 (w/w) ratio of salmon calcitonin:sugar (single excipient composite system) and sCT:sugar:oligosaccharide (two excipients composite system) in methanol:n-butyl acetate (4:1) were spray dried. The peptide load was chosen based on previous studies by Yang et al. (2007), Clark et al. (2008) and Ní Ógáin (2008) who spray dried powders with a salmon calcitonin loading of 5 % w/w using different excipients such as mannitol, citric acid and trehalose. Table 7.1 describes in detail the composition of the spray dried solutions.

For the purpose of evaluation, composite systems were grouped according to the non-reducing sugar present in their formulation: sCT:Raffinose(:oligosaccharide) and sCT:Trehalose(:oligosaccharide) composite systems.

Table 7.1 Salmon calcitonin solutions composition intended for spray drying. t.s.c.–total solid concentration

Sugar	Peptide:sugar ratio (w/w)	t.s.c. (%)	Abbreviation
d-(+)-raffinose pentahydrate	5:95	2.9	sCT:R
d-(+)-raffinose pentahydrate:hydroxypropyl-β-cyclodextrin	5:57:38	2.9	sCT:R:HPβCD
	5:38:57		
d-(+)-trehalose dihydrate	5:95	1	sCT:T
d-(+)-trehalose dihydrate:d-(+)-raffinose pentahydrate	5:57:38	1	sCT:T:R
d-(+)-trehalose dihydrate:hydroxypropyl-β-cyclodextrin	5:67:28	1	sCT:T:HPβCD
	5:57:38		
	5:38:57		
	5:28:67		

7.3 PHYSICOCHEMICAL CHARACTERISATION OF SPRAY DRIED POWDERS

7.3.1 Solid-state, morphology and micromeritic properties

All spray dried composite systems were amorphous (Figure 7.1). Diffractograms presented the typical diffuse halo pattern, characteristic of amorphous materials.

SE micrographs showed all spray-dried powders without HPβCD were constituted of spherical porous particles, type 1BIIIα as classified by Paluch et al. (2012) (Figure 7.2). The sCT:R:HPβCD

composite system also presented porous irregular-shaped particles, type 2BIIIα (Paluch et al, 2012). This change in morphology was previously observed in the unloaded composite system.

Particle size volume distributions in all sCT composite systems were narrow and monomodal with low span values (between 1.2 and 1.5) and the geometric median particle size (d_{50}) was in the range of 1.5–1.9 μm. Table 6.2 presents the reported values of d_{10}, d_{50}, d_{90} and percentage particles with size < 1 μm as mean ± standard deviation. Statistically significant differences were found in both types of composite systems ($p=0.026$ for raffinose and $p<0.05$ for trehalose). By means of Tukey's test it was found that: sample sCT:R:HPβCD 5:57:38 was different from sample sCT:R:HPβCD 5:38:57; sample sCT:T presented higher median particle size than all other calcitonin:trehalose:raffinose/HPβCD composite systems.

Specific surface area by BET was investigated as well as an estimation of the pore diameter distribution and pore diameter by BJH (Table 7.2 and Figure 7.3). Systems with HPβCD in their composition had higher surface areas and their respective pore diameter distributions were shifted to lower values. ANOVA followed by Tukey's test, demonstrated significant differences between samples in both type of composites ($p<0.05$). The sCT:R:HPβCD composite systems presented increasing SSA with higher fractions of cyclodextrin; with the sCT:R systems presenting the smallest SSA value. The sCT:T and sCT:T:R system had similar SSA, however the composites with cyclodextrin presented higher SSA.

Gregg and Sing (1982) classified pores as micropores (d<2 nm), mesopores (d=2-50 nm) and macropores (d>50 nm). The spray-dried particles presented mainly mesopores. Previously, in Chapter 4, the effect of SSA on fine particle fraction of sugar NPMPs powders was discussed. Here, a possible correlation between SSA and pore diameter was investigated. Figure 6.4 shows a decrease of the average pore diameter with increasing SSA (Figure 7.4). Ní Ógáin et al. (2010) and Paluch et al. (2012) have claimed that the solid dissolved in the solvent/antisolvent mixture (MeOH:BA) starts to precipitate out in the liquid environment due to solvent evaporation, with preferential evaporation of MeOH (the solvent with the higher vapour pressure) resulting in spontaneous phase separation of nanoparticlulates suspended in the solvent mixture that grow until separation of the solid from the solvent mix is complete. Finally, due to evaporation of excess solvents, the NPMPs particles are formed. The size of the nanoparticulates suspended in the solvent mixture will determine the pore diameter and SSA of the final particles. It is inferred that the solubility of the solid and its concentration in the co-solvent mixture will be determinant for the nanoparticulate size. From the excipients used it was seen that SSA increased with increasing weight fraction of HPβCD, hence it is possible that this excipient

presents higher solubility in the MeOH:BA mixture, resulting in small nanoparticulates, that in turn result in NPMPs with high surface area and smaller average pore diameter. It should be noted that the cyclodextrin as supplied is already in the amorphous state, which presents higher solubility when compared to the equivalent crystalline state.

True density measurements showed the addition of the sCT affected powder density. An increase in true density was recorded for sCT:T and sCT:T:R and a decrease was registered in all SCT:T or R:HPβCD composite systems when compared to the unloaded systems. All of the spray dried samples had true density values which were significantly different from one another ($p<0.05$ for the difference between raffinose and trehalose composite systems). A correlation was investigated between powder specific surface area and true density. A strong and significant correlation was found (Figure 7.5).

Bulk and tap density increased with the addition of peptide to the formulation when compared to the unloaded particles (Table 7.2). Statistically significant differences ($p<0.05$), were found between bp and tp of raffinose and trehalose composite systems. Using Tukey analysis: sCT:R was distinct from sCT:R:HPβCD composite systems; sCT:T:HPβCD 5:28:67 presented different values from all other samples, which could be paired by similarity (sCT:T:R and sCT:T:HPβCD 5:67:28; sCT:T and sCT:T:HPβCD 5:38:57).

The aerodynamic diameter was calculated and found to be within the desirable particle size range, 1-3 μm, for central and distal deposition in the lungs (Hickey 1996) for all spray dried composite systems (Table 7.2). The aerodynamic diameter of all samples were statistically significantly different from one another ($p<0.05$).

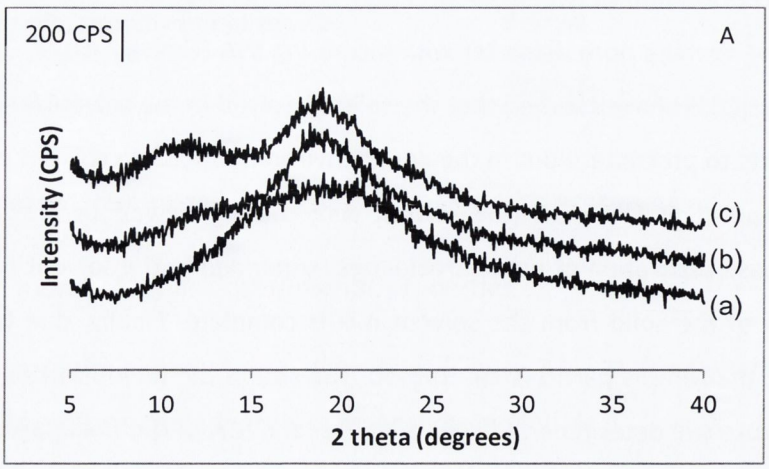

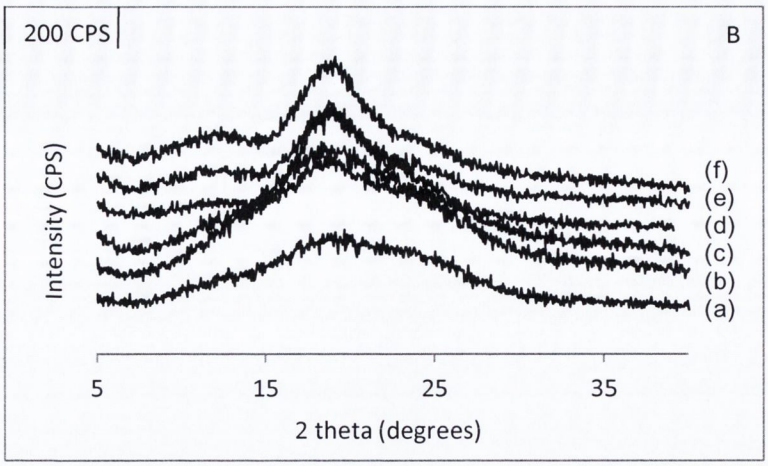

Figure 7.1 XRPD diffractograms of spray dried (A) sCT:raffinose composites: (a) sCT:R, (b) sCT:R:HPβCD 5:57:38 and (c) sCT:R:HPβCD 5:38:57 and (B) sCT:trehalose composite systems: (a) sCT:T, (b) sCT:T:R, (c) sCT:T:HPβCD 5:67:28, (d) sCT:T:HPβCD 5:57:38, (e) sCT:T:HPβCD 5:38:57 and (f) sCT:T:HPβCD 5:28:67.

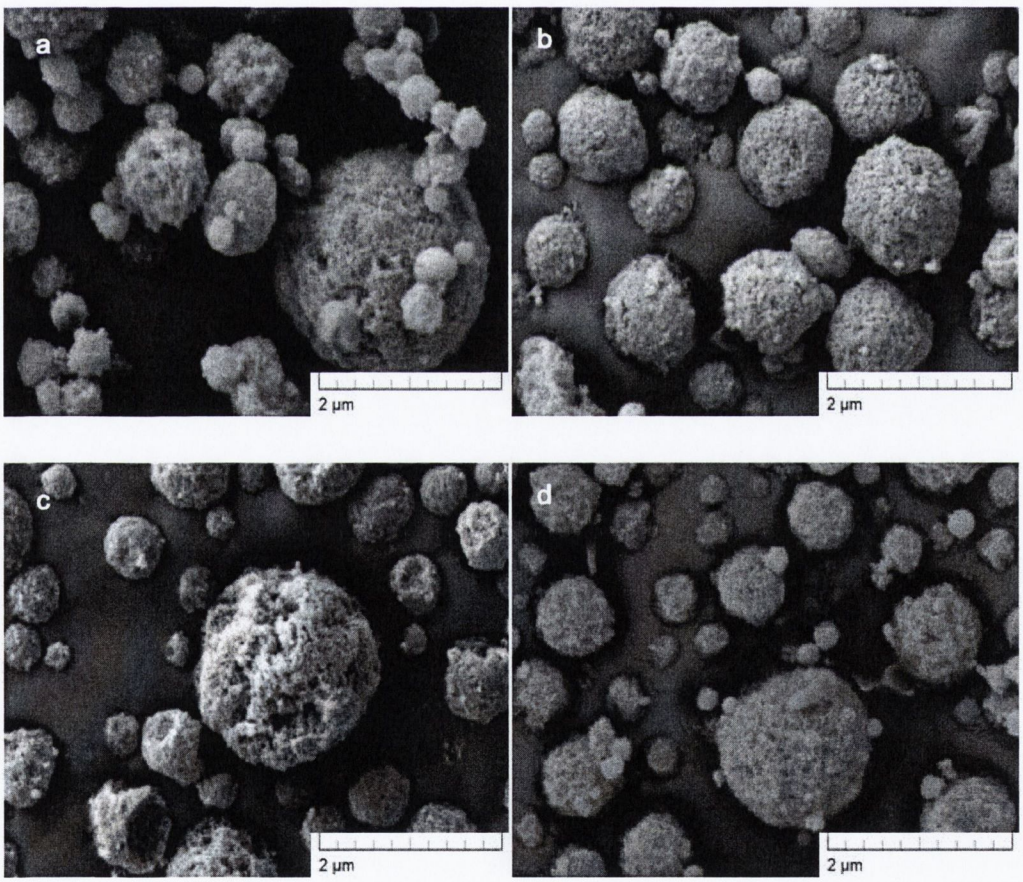

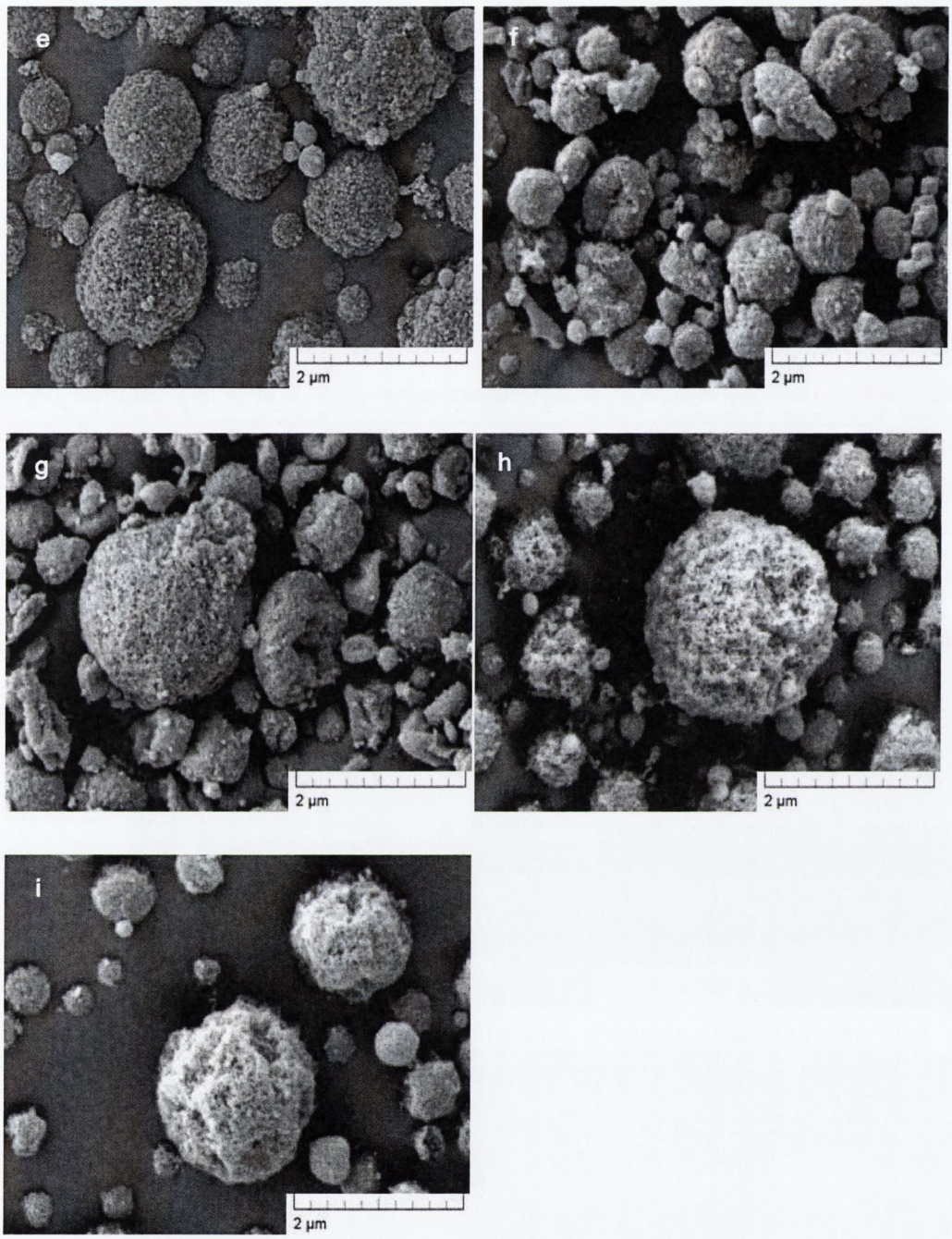

Figure 7.2 SE micrographs of spray dried (a) sCT:R, (b) sCT:R:HPβCD 5:57:38, (c) sCT:R:HPβCD 5:38:57, (d) sCT:T, (e) sCT:T:R, (f) sCT:T:HPβCD 5:67:28, (g) sCT:T:HPβCD 5:57:38, (h) sCT:T:HPβCD 5:38:57 and (i) sCT:T:HPβCD 5:28:67.

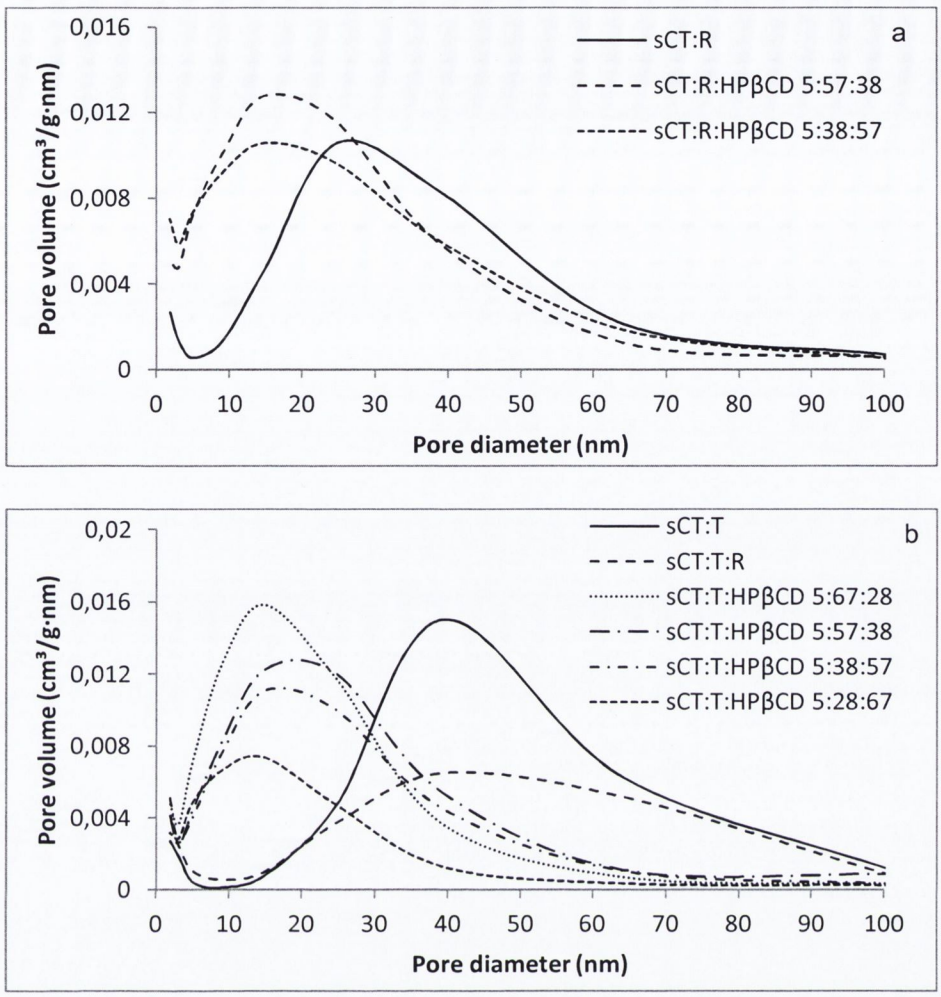

Figure 7.3 Particles pore diameter distribution by BJH adsorption of (a) sCT:R composite systems and (b) sCT:T composite systems. BJH – Barret-Jovner-Halenda

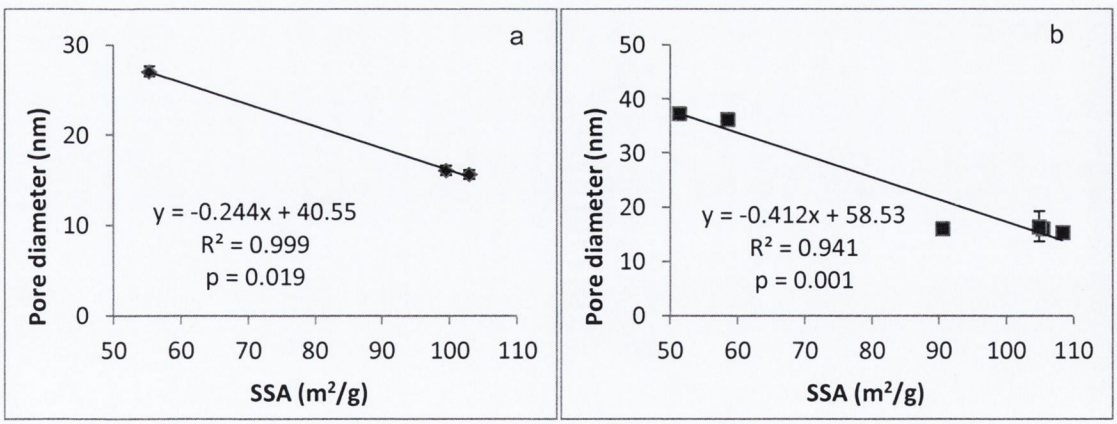

Figure 7.4 Average pore diameter as a function of specific surface area (SSA) of spray dried (a) sCT:raffinose composite systems and (b) sCT:trehalose composite systems.

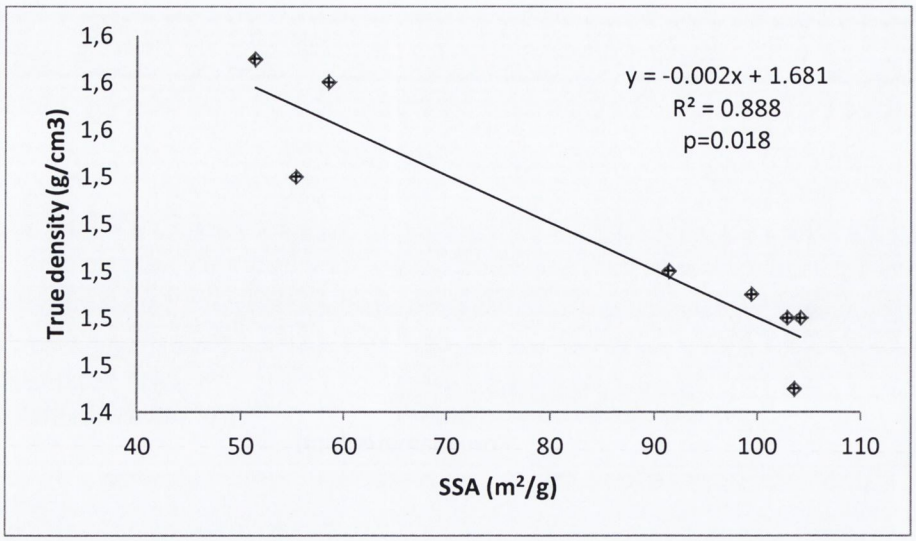

Figure 7.5 Effect of specific surface area (SSA) on powders true density.

Table 7.2 Particle size, specific surface area (SSA), true density (true den.), bulk density (bp), tap density (tp), and calculated aerodynamic diameter (d_{aer}) of sCT: sugar composite systems.

	sCT:R	sCT:R:HPβCD 5:57:38	sCT:R:HPβCD 5:38:57	sCT:T	sCT:T:R	sCT:T:HPβCD 5:67:28	sCT:T:HPβCD 5:57:38	sCT:T:HPβCD 5:38:57	sCT:T:HPβCD 5:28:67
PS (μm)									
d_{10}	1.0±0.00	1.0±0.01	1.0±0.05	1.0±0.01	0.88±0.01	0.9±0.02	0.9±0.00	0.9±0.00	0.9±0.00
d_{50}	1.8±0.05	1.7±0.01	1.9±0.04	1.8±0.01	1.6±0.00	1.5±0.02	1.6±0.00	1.6±0.00	1.6±0.00
d_{90}	3.4±0.04	3.0±0.00	3.4±0.12	3.3±0.05	2.75±0.01	2.7±0.00	2.7±0.00	2.7±0.00	2.7±0.01
<1μm (%)	12.2±0.18	12.0±0.36	9.8±1.76	11.7±0.35	16.45±0.28	17.8±1.39	16.11±0.21	15.9±0.16	16.4±0.04
SSA (m^2/g)	55.34±0.15	99.45±0.74	102.84±0.06	58.47±0.04	51.33±3.22	91.37±1.17	104.1±1.85	103.53±1.88	98.87±9.48
True den. (g/cm^3)	1.54±0.00	1.49±0.00	1.48±0.00	1.58±0.00	1.59±0.00	1.50±0.00	1.48±0.02	1.45±0.00	1.34±0.01
bp(g/cm^3)	0.22±0.00	0.19±0.01	0.20±0.00	0.17±0.00	0.20±0.01	0.20±0.01	0.18±0.01	0.16±0.01	0.23±0.00
tp (g/cm^3)	0.37±0.01	0.34±0.01	0.33±0.01	0.29±0.00	0.36±0.02	0.34±0.01	0.33±0.02	0.29±0.01	0.39±0.01
d_{aer} (μm)	2.2±0.02	1.4±0.00	1.6±0.00	2.2±0.01	2.0±0.00	1.9±0.00	1.9±0.01	1.9±0.00	1.8±0.01

7.3.2 Thermal analysis

The DSC profiles of spray dried samples are presented in Figures 7.6 and 7.7. Calcitonin:raffinose composite systems profiles was characterised by a broad endotherm attributed to residual solvent loss, followed by a glass transition step. No other thermal events were recorded. Similar profiles were found for sCT:trehalose composite systems with the exception of sCT:T system. The latter also presented an exothermic event due to crystallisation of trehalose followed by its melting endotherm. Samples containing cyclodextrin presented higher glass transition temperatures that increased with increasing ratio of HPβCD, as previously seen for the unloaded systems (Table 7.3).

A residual solvent content (RSC) of 2.7-3.5 % and 3.4-5.0 % was determined by TGA for sCT:raffinose and sCT:trehalose composite systems over the temperature range 25-130 °C from TGA (Table 7.4). ANOVA analysis revealed no significant difference between raffinose samples (p=0.543) or between trehalose samples (p=0.07). GC-FID was used to quantify methanol and butyl acetate, assuming the difference between calculated values from the two techniques would correspond to moisture ($TGA - GC = water\ content$). Table 7.4 presents the values determined. RSC is constituted mainly by butyl acetate and water. The water content could be explained by the amorphous sugars strong tendency to sorb moisture (Hancock and Shamblin, 1998). The presence of BA could be due to insufficient drying during processing or solvent entrapment in the particles' matrix or by adsorption or capillary condensation in the pores (Gregg and Sing, 1982).

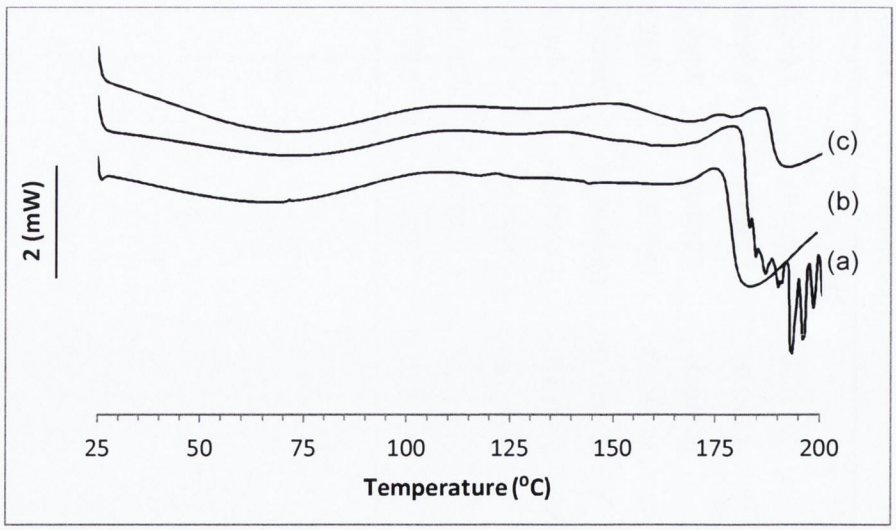

Figure 7.6 DSC scans of spray-dried (a) sCT:Raffinose composite system, (b) sCT:Raffinose:HPβCD 5:57:38 and (c) sCT:Raffinose:HPβCD 5:38:57

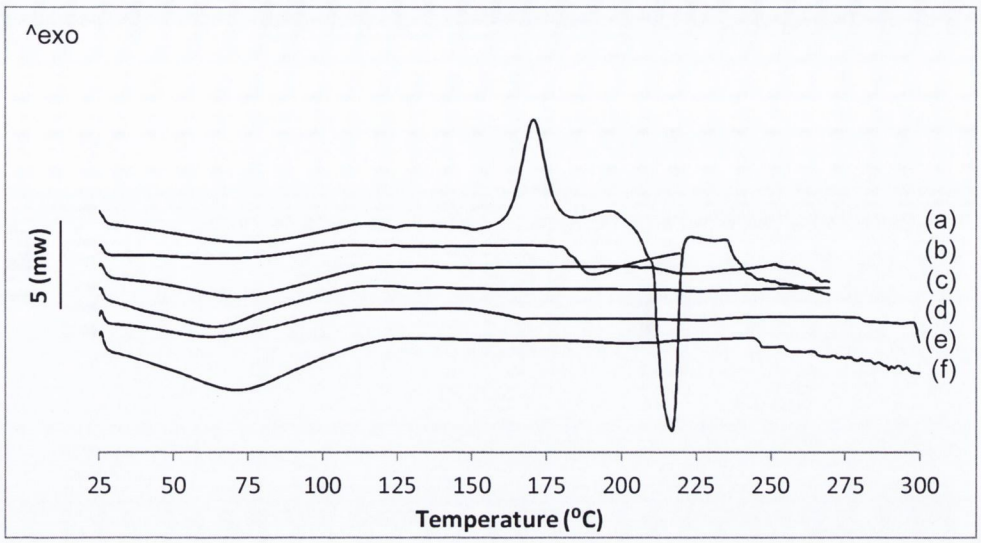

Figure 7.7 DSC scans of spray-dried (a) sCT:Trehalose composite system, (b) sCT:trehalose:raffinose 5:57:38, (c) sCT:trehalose:HPβCD 5:67:28, (d) sCT:trehalose:HPβCD 5:57:38, (e) sCT:trehalose:HPβCD 5:38:57 and (f) sCT:trehalose:HPβCD 5:28:67.

Table 7.3 Glass transition temperature (T_g), recrystallisation temperature and enthalpy (T_c, ΔH_c) and melting temperature and enthalpy (T_m, ΔH_m) of spray-dried sCT:Raffinose and sCT:Trehalose composite systems.

	T_g (°C)	T_c (°C)	ΔH_c (J/g)	T_m(°C)	ΔH_m (J/g)
sCT:R	114.7±0.77	-	-	-	-
sCT:R:HPβCD 5:57:38	144.5±0.44	-	-	-	-
sCT:R:HPβCD 5:38:57	159.2±0.43	-	-	-	-
sCT:T	120.3±1.43	162.7±0.10	88.9±0.21	209.4±0.14	137.6±1.52
sCT:T:R	118.4±1.33	-	-	-	-
sCT:T:HPβCD 5:67:28	139.7±1.49	-	-	-	-
sCT:T:HPβCD 5:57:38	142.5±0.15	-	-	-	-
sCT:T:HPβCD 5:38:57	153.0±0.40	-	-	-	-
sCT:T:HPβCD 5:28:67	182.7±2.76	-	-	-	-

Table 7.4 Residual solvent content (RSC) by TGA and GC-FID for spray-dried sCT:Raffinose and sCT:Trehalose composite systems. MeOH-methanol, BA-butyl acetate, ND – not detected.

	RSC by TGA (% w/w)	RSC by GC-FID (% w/w)		Extrapolated Water content (%)
		MeOH	BA	
sCT:R	2.7±0.45	ND	0.48±0.03	2.22
sCT:R:HPβCD 5:57:38	3.3±0.33	0.09±0.00	1.50±0.01	1.71
sCT:R:HPβCD 5:38:57	3.5±0.6	0.16±0.02	1.72±0.05	1.62
sCT:T	3.4±0.6	0.52±0.00	0.58±0.08	2.3
sCT:T:R	3.3±0.14	0.45±0.00	0.97±0.01	1.88
sCT:T:HPβCD 5:67:28	3.6±0.5	0.73±0.01	1.93±0.01	0.94
sCT:T:HPβCD 5:57:38	5.0±0.4	0.80±0.02	1.55±0.01	2.65
sCT:T:HPβCD 5:38:57	4.2±0.9	0.99±0.01	1.82±0.06	1.39
sCT:T:HPβCD 5:28:67	4.9±0.1	0.88±0.01	1.53±0.04	2.49

7.3.3 Effect of spray drying on sCT stability as determined by FTIR and CD analysis

Freshly spray dried powders were reconstituted into aqueous solutions and analysed by HPLC to determine the peptide loading in the powders. The peptide content in powders is summarised in Table 7.5. Loss of peptide after processing was evident. Variations between formulations are thought to be due to the efficacy of protection of the excipients used on sCT.

7.3.3.1 FTIR

According to Hulse et al. (2008), changes associated with perturbation in the secondary structure of the protein (the α-helix and the β-strand or β-sheets) are reflected in shifting, broadening and reductions in intensity of the amide I band (1660-1670 cm^{-1}) and amide III (1220-1300 cm^{-1}) bands. Native salmon calcitonin appears to comprise a single α-helix, as for its human counterpart, which translates into a prominent band in the amide I region of a FTIR spectrum (Chan et al., 2004; Yang et al., 2006; Tewes et al., 2011). Therefore evaluation of the amide I region by FTIR was undertaken.

FTIR spectra on the amide I region of spray dried powders, when compared to the spectrum of sCT as supplied, showed a small band deviation to lower wavenumbers for sCT:R and for all trehalose composite systems (1657.5 cm^{-1} to 1655.6 cm^{-1}) (Figure 7.8). French et al. (2004) also showed a deviation of the amide I region to lower wavenumbers for spray dried recombinant human granulocyte colony stimulating factor:trehalose and recombinant concensus interferon-α:trehalose powders. Systems composed of cyclodextrin and raffinose presented deviations to higher wavenumbers: 1658.5 cm^{-1} for sCT:R:HPbCD 5:57:38 and 1659.4 cm^{-1} for sCT:R:HPbCD 5:38:57 (Figure 7.8). The latter increase might be due to a more compact solid-state structure of sCT, as reported by Yang et al. (2007) upon spray drying of the peptide on its own. The calculation of area overlap (Table 7.5), demonstrated a small reduction for raffinose composites (6%) that was increased upon addition of HPβCD (8-29%), a greater reduction was seen for trehalose system (70% overlap). The addition of raffinose to sCT:T system increased by 9% the area overlap and, the mixture sCT:T:HPβCD resulted in a higher area overlap for most systems (74 to 80%) as the cyclodextrin proportion was increased, when compared to the sCT:T system.

The reduction in the overlap area reflects a reduction of the α-helix conformation, that is, changes in peptide conformation; such modifications might impair the peptide bioactivity.

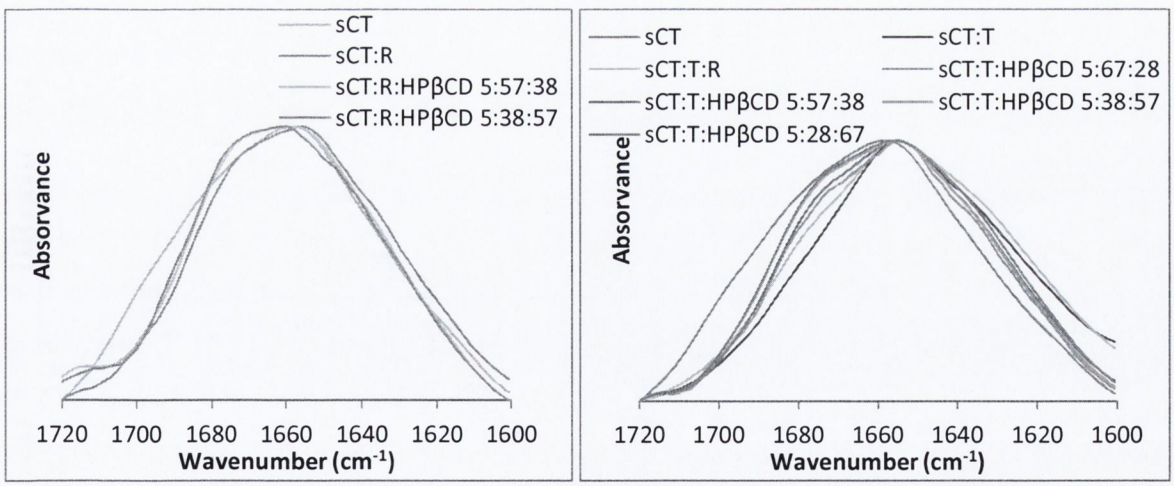

Figure 7.8 FTIR spectra of amide region I of sCT as supplied, (left) sCT:raffinose composite systems and, (right) sCT:trehalose composite systems

Table 7.5 Salmon calcitonin loading in powders by HPLC and Amide I region band area overlap of spray-dried sCT:Raffinose and sCT:Trehalose composite systems with native sCT.

	sCT % (w/w)	Area overlap (%)
sCT:R	5.2±0.03	94
sCT:R:HPβCD 5:57:38	4.8±0.03	92
sCT:R:HPβCD 5:38:57	3.7±0.01	71
sCT:T	4.3±0.07	70
sCT:T:R	4.6±0.06	79
sCT:T:HPβCD 5:67:28	4.0±0.01	69
sCT:T:HPβCD 5:57:38	4.2±0.01	74
sCT:T:HPβCD 5:38:57	4.8±0.01	87
sCT:T:HPβCD 5:28:67	4.4±0.02	80

7.3.3.2 CD

Evaluation of sCT secondary structure by CD was performed by Fatma Farag at University College Cork for sCT:R, sCT:T and sCT:T:R composite systems and on sCT in aqueous solution, methanol and the co-solvent system MeOH:BA, to investigate the solvents effect on peptide conformation. CD spectra of sCT in different solvents and samples reconstituted in water are show in Figure 7.9a and 7.9b, 7.9c and 7.9d, respectively.

sCT in water displayed a random coil arrangement with minimum intensity at 200 nm while in methanol and methanol butyl acetate it showed an α-helix conformation. These results have been previously described by Arvinte and Drake (1993), who compared human (hCT) and salmon calcitonin secondary structure in aqueous and organic solutions, methanol being one of the solvents studied. These authors found that methanol induced an α-helix component in both calcitonins and, in water, neither hCT nor sCT had significant detectable ordered structure (random coil).

For the spray dried powders reconstituted in water sCT, CD spectra indicated a random coil arrangement of sCT. In the case of the sample reconstituted from sCT:T and sCT:T:R a shift to higher wavelength was found; suggesting a possible modification in the peptide conformation.

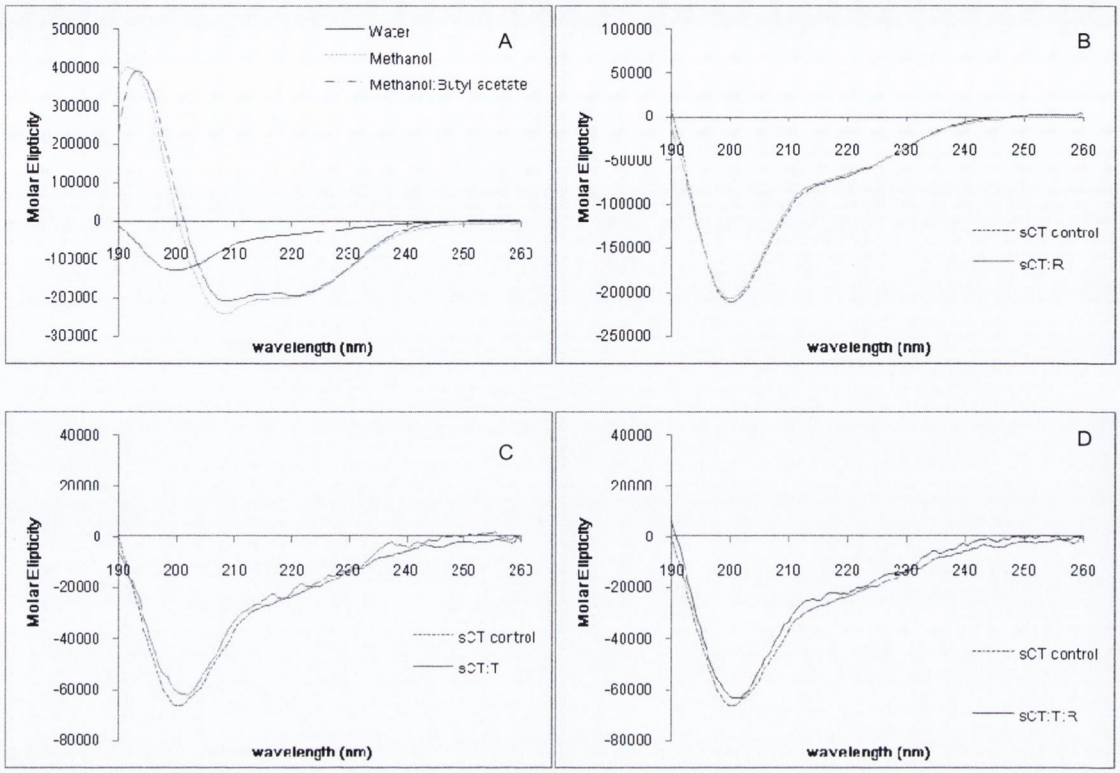

Figure 7.9 CD spectra of (a) sCT in different solvents, (b) sCT:R, (c) sCT:T and (c) sCT:T:R reconstituted in water.

FTIR results showed sCT in the composite systems presented an ordered secondary structure, the α-helix, and that trehalose had less protective power than raffinose or its composite systems, resulting in a possible modification of the peptide conformation. The random coil detected in the reconstituted samples (water as solvent) on CD contradicts the FTIR results. However, the dry powder samples are produced from a MeOH:BA co-solvent system, where sCT secondary structure is stable, presenting the α-helix conformation, with addition of sugars being known to protect this conformation throughout processing according to the recorded FTIR spectra. It is though, upon reconstitution of powders in water, that the protective action of the sugars is lost, due to breaking of the H-bonding between sugar and sCT, resulting in the disordered conformation as confirmed by CD. According to Carpenter and Crowe (1988, 1989) the protective action of the sugar compounds is due to the formation of H-bonding between the excipient and the biomolecule when water is removed, maintaining the structural integrity of the peptide/protein. This theory is known as the water replacement theory. The reconstitution of powders in water, introduces again this element to the peptide, resulting in the observed conformation change.

The shift in the CD spectrum seen for sCT:T sample is probably due to loss of conformation already determined by infra-red spectroscopy studies.

7.3.4 Dynamic vapour sorption

Figure 7.10 and 7.11 represent the sorption and desorption isotherms for each composite system. The solid-state of samples after DVS analysis was evaluated by XRPD.

We have demonstrated that raffinose when exposed to increasing relative humidities recrystallises at 70% RH, retaining water (~10 %) pertaining to the hydrate crystal upon collapse of the amorphous form (Chapter 5, section 5.4.4). When peptide was loaded into raffinose particles the same sorption/desorption profile was recorded; therefore the critical RH was 70 % also. Recrystallisation of the amorphous sCT:R system was evident by XRPD (Figure 6.10a).

The co-spray dried system sCT:R:HPβCD 5:57:38, presented an inflection point at 70 % RH, after which water uptake continued (~19 %). The respective desorption isotherm showed an initial mass loss at higher RH followed by a constant mass loss until 10 % RH, ending with a greater mass loss, resulting in a hysteresis loop. Final moisture uptake was 3.5 %. The inflection point at 70 % could be due to a possible recrystallisation of raffinose, but XRPD analysis showed a typical amorphous halo. As reported for the unloaded particles, recrystallisation may not occur due to insufficient availability of water molecules per raffinose molecule; only 1 mole of water per mole of raffinose was present in the end of the analysis. Studies have reported the dehydration of crystalline raffinose pentahydrate to be a three steps process: 1^{st} loss of one water molecule, 2^{nd} and 3^{rd} loss of two water molecules and, the rehydration leads to the formation of raffinose pentahydrate and raffinose trihydrate (Cheng and Lin, 2006; Chamarthy et al., 2010).

The sorption isotherm of sCT:R:HPβCD 5:38:57 presented an inflection point at RH 80 % with no mass loss and continuous water uptake (~26 %). The desorption isotherm showed complete water desorption. Different hysteresis loops were seen: a loop between 70 and 90 % RH and a second loop between 0 and 70 % RH. The data was fit to the Young-Nelson model to better comprehend these events (Appendix 3). Results of fitting indicated that most water uptake was due to bulk absorption and multilayer adsorption. The absorption events could be attributed to the raffinose fraction, since it has been demonstrated that the interaction of hydroxypropyl-β-cyclodextrin with water vapour results only in the formation of adsorption multilayers (Chapter 5, section 5.4.4). XRPD revealed the system was still amorphous after DVS analysis (Figure 7.12b).

Solid dispersions of sCT:R:HPβCD NPMPs present enhanced physical stability when compared to sCT:R NPMPs; the addition of peptide to the sugar and sugar:polymer systems did not affect the water vapour sorption/desorption behaviour.

Water sorption/desorption isotherms of sCT:T composite system presented the same profile as was described in Chapter 5 for the trehalose NPMPs system (Figure 7.10); an inflection point was registered at 50% RH with no water uptake at higher relative humidities and no water loss throughout desorption with 10.6% water retention (2 moles of water per 1 mole of trehalose) at the end of the cycle. Amorphous trehalose collapsed into its crystalline stable form. XRPD analysis of sample after DVS showed the characteristic peaks of trehalose dihydrate at 8.7° and 23.8° (Nagase H. et al., 2002; Pinto et al., 2006; Ohashi et al., 2007) (Figure 7.12b). The addition of 5 % (w/w) sCT to T NPMPs system did not affect the water sorption behaviour.

Sorption and desorption isotherms for sCT:T:R and sCT:T:HPβCD composite systems are represented in Figure 7.11 The addition of 38 % (w/w) of raffinose and, 28 and 38 % (w/w) of HPβCD increased the critical relative humidity to 60 % RH with a water uptake of 12 to 14 %.

In the case of sCT:T:R, no water uptake was registered above 60 % RH; the desorption isotherm showed a constant water % until 10 % RH after which a drop was registered resulting in a final water content of 8.6 %. XRPD diffractograms (Figure 7.12) presented sharp peaks corresponding to crystalline trehalose (8.7° and 23.8°) and raffinose (10.75° and 21.1°).

For sCT:T:HPβCD samples there was a small mass loss of ~2 % at 70 % RH followed by water uptake. Desorption isotherms showed an initial mass loss at higher RH; from 60 % to 10 % a constant mass and, from 10 to 0 % RH a continuous mass loss. Final moisture uptake was ~3 %. The inflection point at 60 % RH was due to trehalose recrystallisation, evident by XRPD analysis (Figure 7.12b). The remaining water sorption and desorption was due to the cyclodextrin-water interactions.

For spray dried sCT:T:HPβCD 5:28:67 and 5:38:57 moisture uptake was greatly enhanced compared to sCT:T, a 33.7 % mass gain could be achieved, similar to the moisture uptake of spray dried unloaded (without sCT) particles. Different hysteresis loops were seen: a loop between 70 and 90 % RH and a second loop between 0 and 70 % RH. The data was fitted to the Young-Nelson model to better comprehend these events. Moisture uptake was mainly due to mono and multilayer adsorption. A small extent of bulk absorption was registered for sCT:T:HPβCD 5:38:57 (Appendix 3). The latter was attributed to the trehalose fraction, since there was no evidence of this event with

cyclodextrin alone and the main water uptake by trehalose is due to absorption. XRPD after DVS revealed small sharp peaks for the sCT:T:HPβCD 5:38:57 system, meaning that there was some recrystallisation of trehalose; sCT:T:HPβCD 5:28:67 presented an amorphous halo (Figure 7.12b).

Comparing the results to the unloaded (without sCT) particles, similar profiles were obtained; the addition of salmon calcitonin to the systems did not affect their interaction with water vapour.

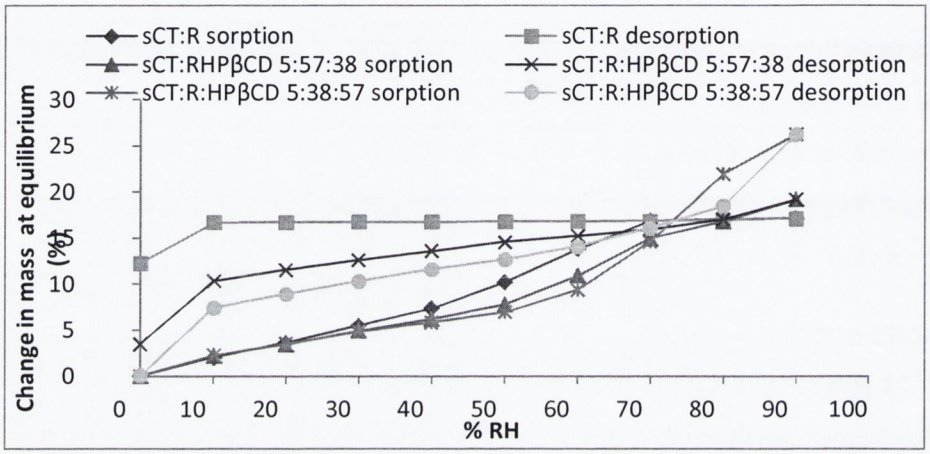

Figure 7.10 Water vapour sorption and desorption isotherms by, DVS, of spray-dried sCT:raffinose composite systems.

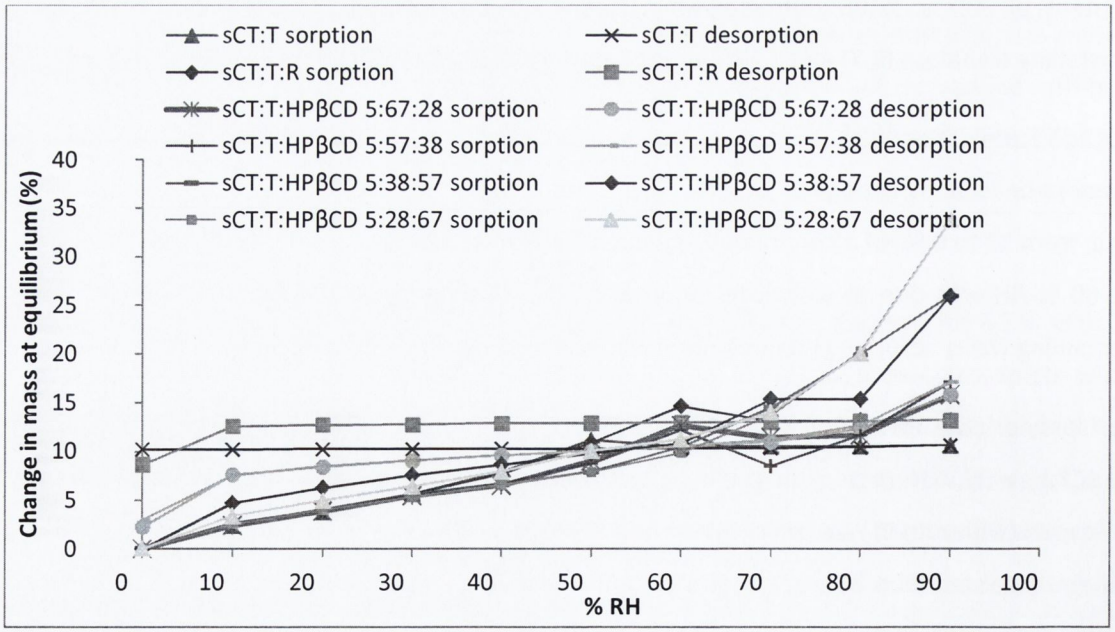

Figure 7.11 Water vapour sorption and desorption isotherms, by DVS, of spray-dried sCT:trehalose composite systems.

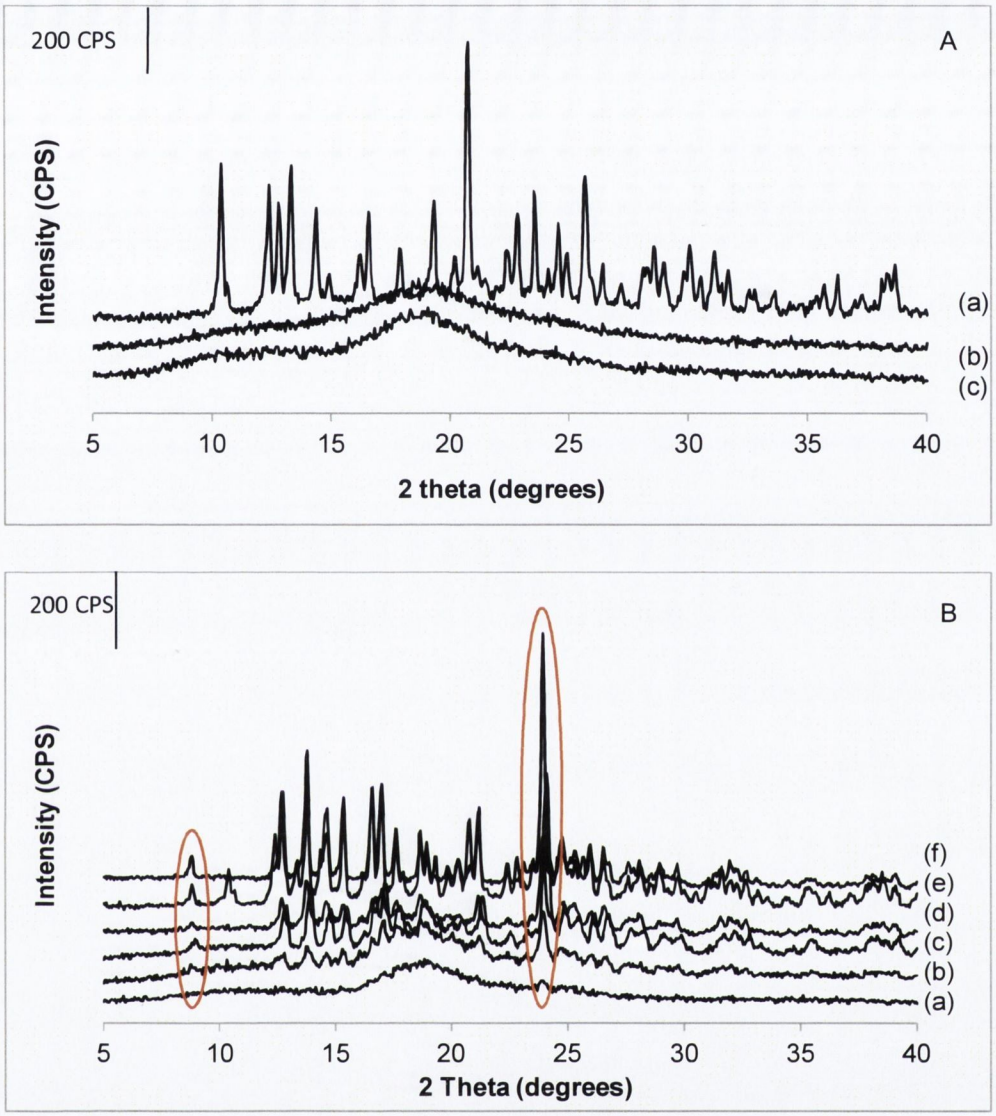

Figure 7.12 XRPD of (A) sCT:raffinose composite systems and (B) sCT:trehalose composite systems after DVS analysis. Red loops indicate trehalose characteristic peaks.

7.3.5 *In vitro* deposition via next generation impactor analysis

Deposition profiles of sCT:sugar composite systems are presented in figures 7.13 and 7.14. There is an evident improvement in powder deposition for the co-spray dried two excipient systems when compared to single excipient systems, as previously seen for the unloaded particles: there was less deposition in the mouthpiece adaptor and induction port; higher deposition on stages 4 to 6, which present lower cut-off points (≤ 2 μm). When raffinose or trehalose was co-spray dried with HPβCD, % recovered emitted dose, fine particle fraction < 3 and 5 μm increased by ~2 fold (Table 7.5 and

7.5). The MMAD values calculated for these composite systems were simillar to the calculated aerodynamic diameters. Hence, possible aggregates are dispersed. This can be atributed to the high SSA (high porosity), since these particles present fewer areas of contact, leading to lower cohesion and easier dispersion (Tabor, 1977).

Statistical analysis of % recovered emitted dose, FPF, MMAD and GSD by ANOVA with Tukey analysis for sCT:R:HPβCD composite systems were significantly different ($p<0.05$) from sCT:R and all composites were similar to one another.

ANOVA with Tukey analysis of sCT:trehalose composite systems also showed % recovered dose, FPF, MMAD and GSD to be significantly different from sCT:T ($p<0.05$). But sample sCT:T:HPβCD 5:67:28 had a different FPF < 5 and 3 μm to the other calcitonin: trehalose:cyclodextrin composite systems.

sCT:T:R system presented a similar deposition profile to sCT:T. Statistically significant differences ($p<0.05$) were only found for the percent of recovered dose (higher) and calculated GSD (smaller). All other parameters were simillar.

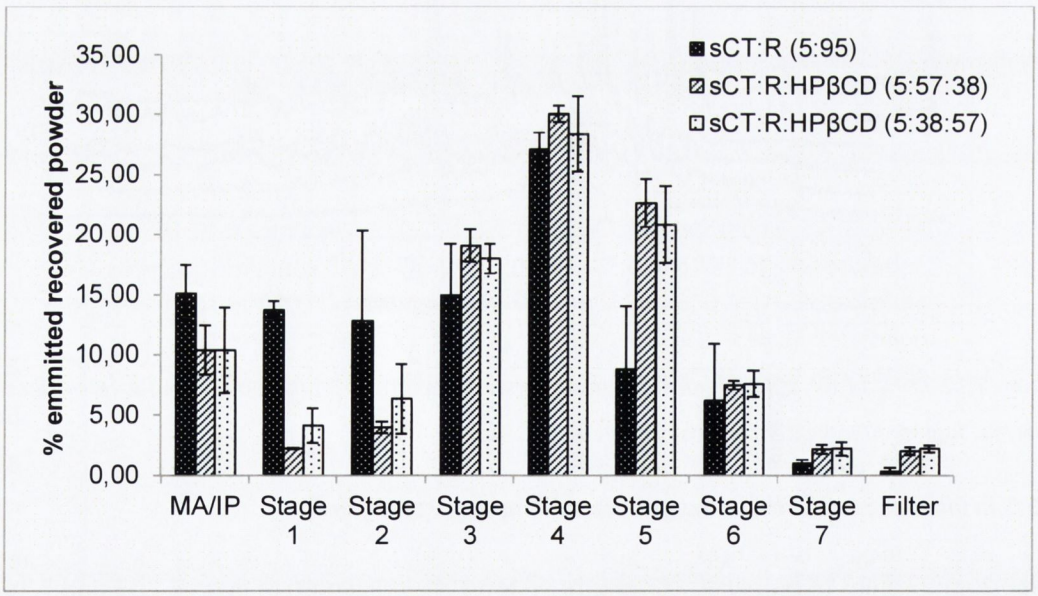

Figure 7.13 *In vitro* aerosol deposition profile by use of a NGI of sCT:raffinose composite systems as calculated % of recovered emitted dose vs. NGI stages. MA – mouth adapter IP – induction port.

Table 7.5 Recovered emitted dose, fine particle fraction (FPF), mass median aerodynamic diameter (MMAD) and geometric standard deviation (GSD) of *in vitro* aerosol deposition of sCT:raffinose composite systems.

	sCT:R	sCT:R:HPβCD 5:57:38	sCT:R:HPβCD 5:38:57
% recovered emitted dose	81.1±5.38	91.5±1.87	91.7±0.77
FPF < 5 μm	62.8±8.21	84.5±2.13	82.1±4.96
< 3 μm	50.5±6.84	81.7±2.19	74.4±3.99
MMAD	2.6±0.05	2.1±0.08	2.3±0.27
GSD	2.0±0.09	2.0±0.02	2.2±0.11

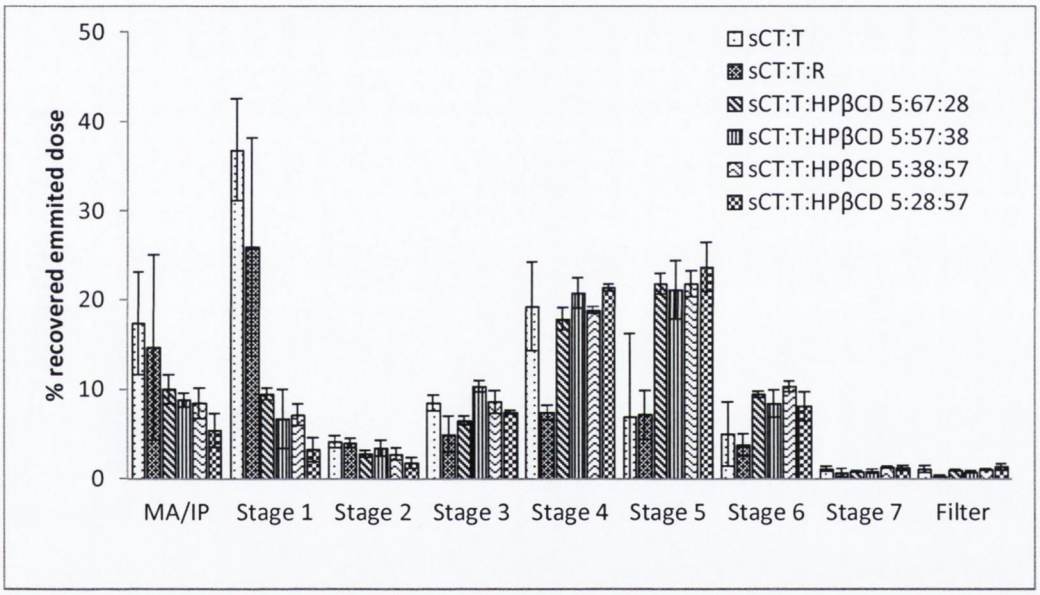

Figure 7.14 *In vitro* aerosol deposition profile by use of a NGI of sCT:trehalose composite systems as calculated % of recovered emitted dose vs. NGI stages. MA – mouth adapter IP – induction port

Table 7.6 Recovered emitted dose, fine particle fraction (FPF), mass median aerodynamic diameter (MMAD) and geometric standard deviation (GSD) of *in vitro* aerosol deposition of sCT:raffinose composite systems.

	sCT:T	sCT:T:R	sCT:T:HPβCD 5:67:28	sCT:T:HPβCD 5:57:38	sCT:T:HPβCD 5:38:57	sCT:T:HPβCD 5:28:67
% recovered emitted dose	48.5±9.04	63.2±8.29	84.6±1.61	87.5±1.88	88.5±1.72	85.3±4.02
FPF < 5 μm	45.5±7.72	45.5±4.40	76.3±1.89	80.7±4.01	80.5±2.22	86.8±3.83
< 3 μm	35.6±0.99	35.6±5.62	69.5±1.54	76.8±6.91	75.2±2.52	83.8±4.99
MMAD	4.7±0.21	4.9±0.62	2.3±0.03	2.3±0.28	2.2±0.08	1.9±0.18
GSD	2.8±0.19	2.5±0.12	2.1±0.02	2.0±0.09	2.1±0.04	1.94±0.04

7.3.6 *In vitro* bioactivity analysis

The cAMP-secreting activities (bioactivity) of sCT and sCT:sugar composite systems were examined using an *in vitro* cAMP assay in T47D cells, which have been reported to possess many calcitonin receptors (Youn et al., 2008). Salmon calcitonin binds to the CT receptor, which belongs to a subfamily of GTP-binding (G)-protein-coupled receptors, activating G-proteins that in turn induce the activation of adenylyl cyclase and phospholipase C to generate the intracellular second messenger molecules, cyclic adenosine 3P,5P-monophosphate (cAMP) (Katayama et al., 2001). Studies by Moe and Keiser (1984), Epand and Epand (1986) and Andreotti et al. (2006), proved the importance of maintaining the secondary structure of sCT, that is, the α-helix, in order to have a fully cAMP-secreting activity (biological activity).

The retained percentage biological activity of all samples after spray drying is shown in figure 7.15 and 7.16. The results show that all sCT:Raffinose composite systems retained 100% activity when compared to unprocessed sCT with no statistically significant difference between samples ($p=0.771$). On the other hand, no spray dried sCT:trehalose composite system retained 100% activity. Due to the great variability in data, no statistically significant differences were found between samples ($p=0.212$).The ability of trehalose to stabilise and protect proteins throughout processing via spray drying has been show by Adler and Lee (1998), Hulse et al. (2008), Yoshii et al. (2008) and Ní Ógáin et al. (2011); in all studies, trehalose had a protective action, where the protein was able to retain 60 to 100% of its activity. Ní Ógáin et al. (2011) also showed the protective effects of raffinose on lysozyme activity, reporting a retained activity of ~94 %.

As previously seen by FTIR and CD, the secondary structure of sCT is protected when spray dried in the presence of raffinose or the co-excipient mixture of raffinose and HPβCD; in the case of trehalose the α-helix was not protected as much throughout processing, but the addition of the cyclodextrin improved the sCT stability. Studies by Sigurjónsdóttir et al. (1999) on the stability of sCT aqueous solutions showed a reduction in aggregation in the presence of HPβCD by formation of inclusion complexes, with the polypeptide aromatic residues protecting the susceptible groups from chemical or enzymatic modification. It is believed the described properties of HPβCD might be the reason for enhancement of sCT protection when this excipient is mixed with trehalose, since the sCT:HPβCD composite system presented good retention of bioactivity.

Based on the collected data and mentioned studies, the variation in the bioactivity of sCT:sugar composite systems is dependent on the protection effectiveness of the excipients used in each formulation.

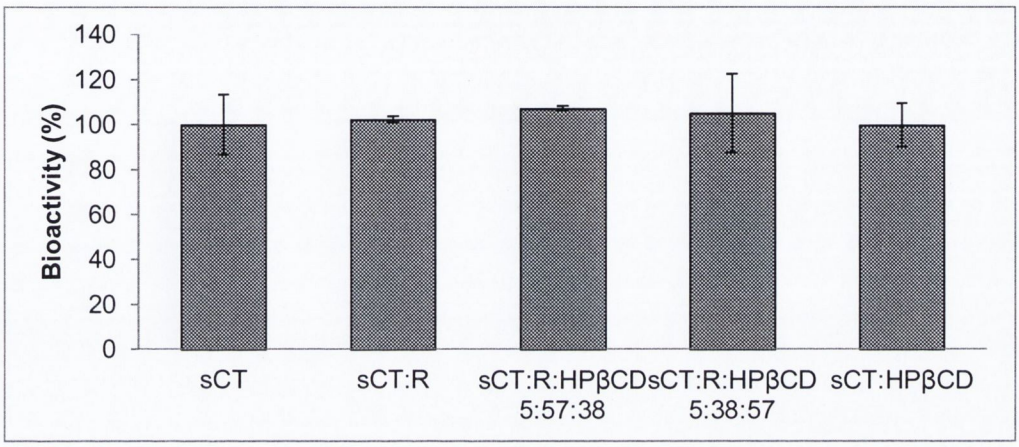

Figure 7.15 Retained salmon calcitonin activity (±SD) for all raffinose composite systems.

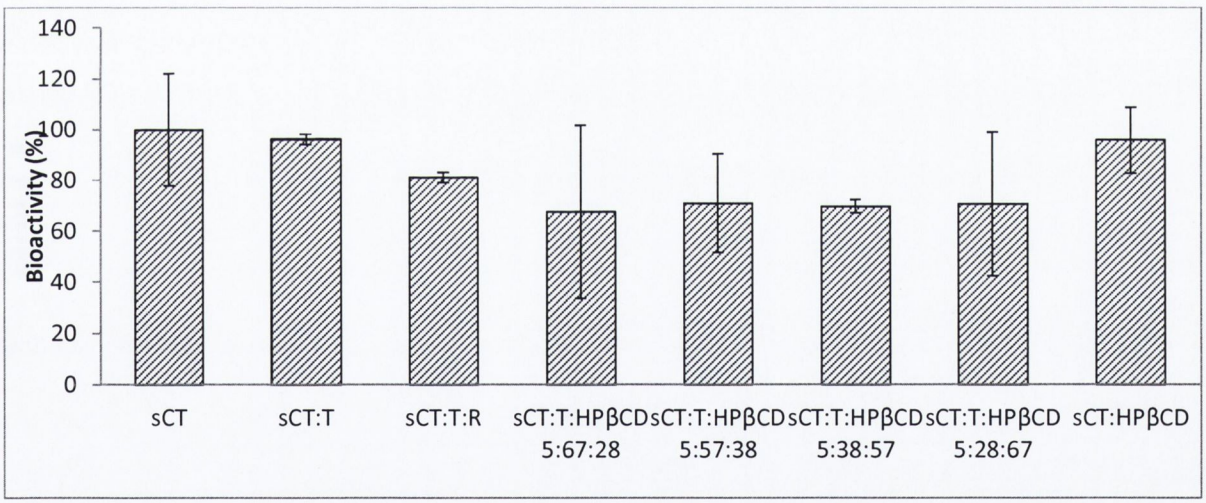

Figure 7.16 Retained salmon calcitonin activity (±SD) for all trehalose composite systems.

7.3.7 Residual solvent levels in salmon calcitonin-loaded spray dried powders

The European Pharmacopeia classifies methanol as a class 2 and butyl acetate as a class 3 residual solvent (organic volatile chemical that is used in the preparation of medicinal products and that have no therapeutic benefit (European Pharmacopoeia 7th Edition, 2012a and European Pharmacopoeia 7th Edition, 2012b). The permitted daily exposure (PDE) and equivalent concentration limit is 30.0 mg/day and 3000 ppm for methanol and, 50.0 mg/day and 5000 ppm for

butyl acetate (European Pharmacopoeia 7th Edition, 2012b). Clark et al. (2008) reported a pulmonary absolute bioavailability ranging from 11 to 18% for sCT and Patton (2000) reported a value of 17%. Salmon calcitonin is commonly used in the treatment of postmenopausal osteoporosis in a dose of 200 units daily intranasally by nasal spray, or in a dose of 100 units daily or every other day by subcutaneous or intramuscular injection; it is also used for the prevention of acute bone loss due to sudden immobilisation, such as in patients with recent osteoporotic fractures. The recommended dose is 100 units daily (or 50 units twice daily) by subcutaneous or intramuscular injection, for 2 to 4 weeks (Martindale, 2011).

To verify the levels of residual solvent in our powders would be within the limits of exposure imposed by the European Pharmacopoeia, the following assumptions were taken: a maximum sCT pulmonary absolute bioavailability value of 18% and sCT dose of 100 IU daily. The sCT used in this study had a potency of 5128.1 IU per mg of powder; sCT content in spray-dried powders was determined by HPLC (Table 7.5); methanol and butyl acetate content were determined by GC-FID. Calculated values are presented in Table 7.7. For a salmon calcitonin daily dose of 100 IU, the sCT:sugar composite systems powders present methanol and butyl acetate concentrations below the limits stated in the European Pharmacopoeia when assuming a sCT absolute pulmonary bioavailability of 18%.

Table 7.7 Concentration (conc) of residual solvents (RS), methanol (MeOH) and butyl acetate (BA), in a salmon calcitonin (sCT) dose of 100 IU.

	sCT (mg/mg powder)	sCT (IU/mg powder)	Powder for sCT dose of 100 IU (mg)	Conc of RS in powder for sCT dose of 100 IU (ppm)	
				MeOH	BA
sCT:R	5.2 x 10-5	0.267	2083	-	10
sCT:R:HPβCD 5:57:38	4.8 x 10-5	0.246	2257	2	31
sCT:R:HPβCD 5:38:57	3.7 x 10-5	0.190	2928	5	50
sCT:T	4.3 x 10-5	0.221	2519	13	15
sCT:T:R	4.6 x 10-5	0.236	2355	11	20
sCT:T:HPβCD 5:67:28	4.0 x 10-5	0.205	2708	20	52
sCT:T:HPβCD 5:57:38	4.2 x 10-5	0.215	2579	21	40
sCT:T:HPβCD 5:38:57	4.8 x 10-5	0.246	2257	22	41
sCT:T:HPβCD 5:28:67	4.4 x 10-5	0.226	2462	22	38

7.4 STORAGE STABILITY

Different studies have reported a rapid water absorption and recrystallisation of amorphous raffinose and trehalose powders when exposed to 60 and 75 % relative humidity (RH) for 24 hours (Hogan and Buckton, 2001; Charmathy et al., 2010; Shebor et al., 2010; Ní Ógáin et al., 2010). Therefore, the conditions 25 °C/< 5 % RH and 4 °C/< 5 % RH were selected for a 24 week storage stability study.

Particle morphology of all composite systems stored under 25 °C/< 5 % RH and sCT:Raffinose composite systems stored under 4 °C/< 5 % RH, was not affected, as can be seen by comparison of SE micrographs taken at week 24 (Appendix 3), with those of the freshly spray-dried powders (Appendix 3). Particle morphology of sCT:Trehalose composite systems changed after 24 weeks storage under 4 °C/ < 5 % RH with the exception of systems sCT:T:HPβCD 5:38:57 and 5:28:67 that maintained their initial morphology (Appendix 3). For other sCT:Trehalose systems, particles lost their characteristic porosity, presenting smooth, smooth with cracks, or rough surfaces (Appendix 3). According to the MSC system, particles changed from type 1BIIIα to type 1AIγ (Paluch et al., 2012).

All sCT:Raffinose and sCT:T:HPβCD composite systems remained XRD-amorphous during the 24-week stability study (Appendix 3). However, the sCT:T composite system presented peaks of small intensity at 17.5°, 20.7°, 22.7° and 25.4°, implying the start of trehalose recrystallisation. DSC of sCT:Raffinose composite systems showed no changes, indicating no crystallisation, under the storage conditions studied for 24 weeks (Appendix 3). Composite systems of sCT:T:HPβCD 5:67:28, 5:38:57 and 5:28:67 stored under 4 °C/ 5% RH for 24 weeks displayed some small changes in the DSC (Appendix 3). Depression of the glass transition temperature was registered after 4 weeks for sCT:T:HPβCD 5:67:28 (T_g ~125 °C) and 5:28:67 (T_g ~170°C) and, after 16 weeks for sCT:T:HPβCD 5:38:57 (T_g ~140 °C). Under the same storage conditions, no differences in the DSC scans were found for the remaining calcitonin:trehalose composite systems. DSC scans of samples stored at 25 °C/< 5%RH only showed differences for the composite system sCT:T:HPβCD 5:28:67, with a reduction of the glass transition temperature after 4 weeks (T_g ~167 °C). sCT:T crystallisation and melting onset occurred at the same temperature in all DSC scans collected and the enthalpy of recrystallisation and fusion were unchanged (T_c ~158 °C, ΔH_c ~89 J/g; T_m ~209 °C, ΔH_m~130 J/g) independently of the storage conditions.

Residual solvent content/moisture content, calculated from TGA, varied over the 24 weeks of study, with increases for sCT:R, sCT:T and sCT:T:R in both storage conditions, (Appendix 3). Previously, by DVS analysis, it was seen that all samples presented a tendency to adsorb and absorb water; at a 5 % RH, raffinose composite systems can uptake water up to 2 % of its mass; for trehalose composite systems water uptake ranged between 2 and 5 %. Hence, the variation seen by TGA during the 24 weeks of study was possibly due to the adsorption and/or absorption of moisture released from the humidity capsule that kept the storage chambers at 5 % RH.

FTIR spectra of the amide region I of each sample was collected at week 4, 12 and 24. Shifts in the amide I band position, throughout storage, were evident for all samples with the exception of the sCT:R system (Appendix); composite systems of sCT:R:HPβCD shifted from 1658 cm^{-1} to ~1656 cm^{-1}, sCT:Trehalose systems from 1655 cm^{-1} to ~1658 cm^{-1}. Table 6.8 presents the calculated area overlap. A decrease in the area overlap was seen for all sCT composite systems; mobility of molecules is thought to have increased with changes in sCT conformation.

Biological activity assay showed good retention of cAMP-secreting activity on storage at 4 and 25 °C/< 5% RH for 24 weeks for all sCT:Raffinose composite systems (Appendix 3), with no statistically significant change compared to freshly spray-dried material. Bioactivity of sCT:Trehalose composite systems at the storage conditions studied, was reduced after 24 weeks (Appendix 3). The reduction of specific activity was only statistically significant for sCT:T, SCT:T:R and sCT:T:HPβCD 5:28:57 systems. The great variability in the remaining samples prevented a determination of whether the reduction was significant or not when compared to freshly spray-dried material. FTIR data indicated salmon calcitonin conformation suffered modifications, with the biological activity of sCT:Trehalose composite systems being compromised after 24-weeks study. Studies by Epand and Epand (1986) and Andreotti et al. (2006) have inferred that structural parameter of sCT α-helix, such as its flexibility and length, can affect its receptor binding affinity, reducing or enlarging sCT biological activity.

Table 7.8 Salmon calcitonin (sCT) loading in powders by HPLC and Amide I region band area overlap with native sCT of spray-dried sCT:raffinose and sCT:trehalose composite systems after storage at 25°C/< 5% RH and 4°C/< 5% RH .

	Freshly Spray-dried	Storage at 4°C/ 5% RH			Storage at 25°C/ 5% RH			sCT loading after 24 weeks storage at 4 °C/< 5 % RH (%, w/w)	sCT loading after 24 weeks storage at 25 °C/< 5 % RH (%, w/w)
		Week 4	Week 12	Week 24	Week 4	Week 12	Week 24		
sCT:R	94	84	74	76	84	85	54	4.4±0.17	3.0±0.00
sCT:R:HPβCD 5:57:38	92	71	71	55	84	56	45	3.0±0.03	2.40±.03
sCT:R:HPβCD 5:38:57	71	54	53	50	54	52	51	2.8±0.01	2.8±0.003
sCT:T	70	72	74	61	79	59	50	3.2±0.01	2.7±0.01
sCT:T:R	79	75	72	71	85	72	58	3.7±0.005	3.2±0.01
sCT:T:HPβCD 5:67:28	69	69	65	66	73	67	54	3.6±0.03	2.9±0.01
sCT:T:HPβCD 5:57:38	74	68	68	66	73	70	67	3.6±0.02	3.6±0.01
sCT:T:HPβCD 5:38:57	87	74	74	56	74	76	57	3.0±0.09	3.0±0.08
sCT:T:HPβCD 5:28:67	80	69	58	37	79	76	51	2.0±0.011	2.7±0.01

7.5 PHARMACOKINETIC STUDIES

A non-compartmental model (moment analysis) was fitted to the data acquired by administration of sCT solution, sCT:Raffinose, sCT:Trehalose and SCT:Raffinose:HPβCD 5:57:38 composite systems. The intravenous sCT plasma concentration versus time curve showed an initial phase of more accentuated decay usually attributed to drug distribution, followed by a second phase that is controlled by drug elimination, that is, a two-exponential decline curve (Figure 7.19). The sCT mean residence time (MRT) was found to be 0.59±0.06h, the terminal half-life was 0.6±0.11 h and the plasma clearance was 0.53±0.11 l/h/kg (0.16±0.03 l/h). In less than an hour, half of the administered drug was eliminated.

Plasma concentration versus time curves for sCT solution and sCT:sugar composite systems after pulmonary administration are shown in Figures 7.37 and 7.38. Calculated pharmacokinetic parameters are presented in Table 7.9.

sCT administered as a solution and as dry powder was rapidly absorbed via the pulmonary route, and peak concentration was reached between 0.07-0.2 h with an observed C_{max} range of 11.0-42.5 μg/l. The drug was eliminated with a terminal half-life ranging from 0.6 to 1.5 h. The absolute bioavailability was calculated and found to vary between 10.1 and 14.9 %. Studies by Youn et al. (2008) on the pulmonary administration of sCT and PEG-sCT also saw a rapid absorption of the unmodified peptide with t_{max} at 0.25 h and a terminal half-life of 0.58±0.13 h. The latter value is within the range of the $t_{1/2\beta}$ mean value found in our studies for the pulmonary sCT delivery as a solution, i.e., 1.5±0.68 h. The t_{max} value was below that in the previously reported study and in work reported by Patton (2000), where sCT delivered via the lungs to rats as a solution formulation presented an absolute bioavailability of 17 % and, the peak concentration was achieved at 0.25 h.

The blood circulation can affect the peak concentration time. Youn et al. (2008) used anaesthetised rats, whereas in the present study rats were injected with an anti-serum to neutralise anesthesia after drug administration to restore the blood circulation to its regular rhythm, resulting in a smaller t_{max} than the one reported by Youn et al. (2008).

The area under the curve for sCT significantly increased ($p=0.049$) when administered as a dry powder in comparison to solution formulation, with the highest value pertaining to the sCT:R:HPβCD formulation (39.5±4.29 μg.h/l). Mean residence time, mean absorption time, absorption and elimination constants, pulmonary clearance and, volumes of distribution of all sCT dry powder and solution formulations were found to be similar (Table 7.9 and Appendix 3). Statistical analysis of this data revealed no difference between these PK parameters. Therefore,

further studies on a larger number of animals should be conducted to increase the statistical robustness of the presented study.

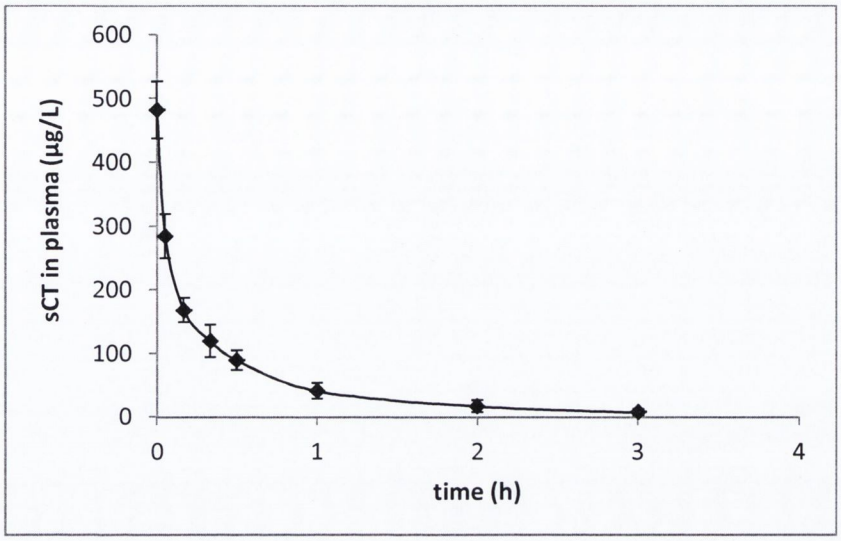

Figure 7.18 Mean plasma sCT vs time profiles in rats following intravenous delivery.

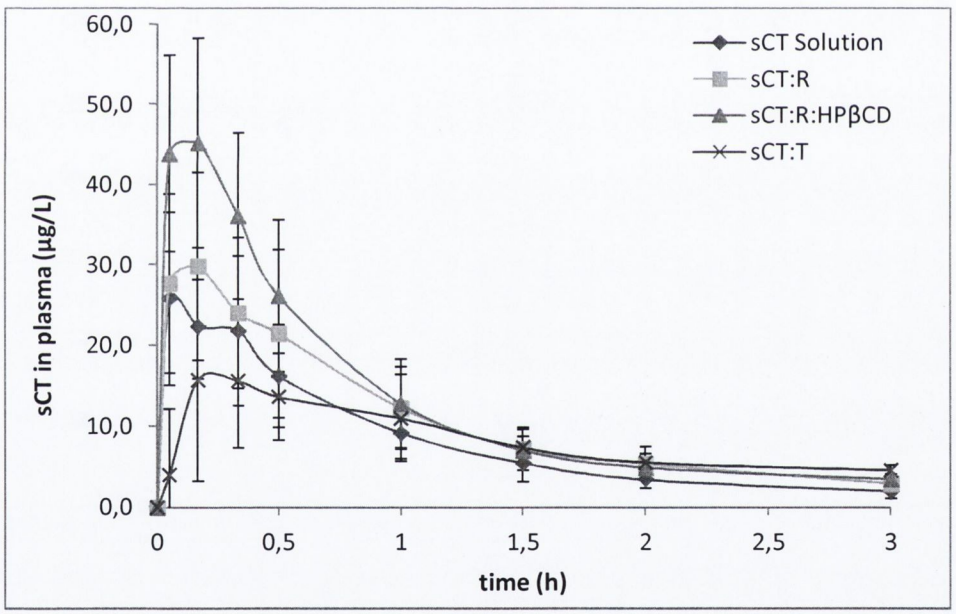

Figure 7.19 Mean plasma sCT vs time profiles in rats following intratracheal delivery.

Table 7.9 Phamacokinetic parameters of sCT in rats after intratracheal delivery (mean ± SD, n=5).

	sCT solution iv	sCT solution pulm	sCT:R 5:95	sCT:R:HPbCD 5:57:38	sCT:T 5:95
Dose (μg/kg)	84±6.95	94±12.3	146±21.3	124±9.9	124±16.9
AUC_0^∞ (μg.h/l)	180.4±37.36	22.4±4.70	36.5±13.80	39.5±4.29	27.8±3.32
C_{max} (μg/l)		15.8±5.06	33.8±12.97	42.5±8.73	11.0±4.14
t_{max} (h)		0.07±0.05	0.1±0.06	0.1±0.06	0.2±0.12
Cl (l/h/kg)	0.53±0.11				
Cl_{pulm} (l/h/kg)		0.05±0.01	0.05±0.01	0.03±0.01	0.05±0.01
MRT (h)	0.59±0.06	2.0±0.73	1.3±0.10	1.3±0.18	2.2±0.93
MAT (h)		1.2±0.97	0.5±0.37	0.6±0.45	1.2±0.93
$t_{1/2\beta}$ (h)	0.6±0.11	1.5±0.68	0.8±0.07	0.9±0.06	0.6±0.48
F_{abs} (%)		11.3±3.01	11.5±3.48	14.9±2.01	10.1±1.37
F_{rel} (%)			104±31.5	135±18.24	74.9±25.91

7.6 CONCLUSION

Salmon calcitonin:sugar composite systems can be produced via the same process conditions as for raffinose and trehalose NPMPs.

Spray dried particles were porous and spherical, with the exception of composites containing a weight fraction >60% of HPβCD in their formulation, which were porous but not as spherical. It was possible to classify these particles within the MSC system (Paluch et al., 2012) as 1BIIIα and 2BIIIα, respectively. Powders were amorphous, as assessed by XRPD and DSC. Surface area and porosity analysis allowed a relationship between average pore diameter and specific surface area to be established, with a decrease of average pore diameter with increasing SSA. The addition of peptide to the systems affected the powder density when compared to unloaded NPMPs. However, this property did not impact on the aerodynamic performance of powders since all sCT:sugar composite systems presented good deposition profiles by NGI assessment, with FPF < 5 μm ranging from 62.8-84.5% for sCT:Raffinose systems and 45.5-86.8% for sCT:Trehalose systems. MMAD ranges were 2.1-2.6 μm and 1.9-4.1 μm for sCT:Raffinose and SCT:Trehalose composite systems, respectively. The MMADs were similar to the calculated aerodynamic diameters. sCT:Raffinose composite systems presented better aerosol deposition than sCT:Trehalose composite systems.

Salmon calcitonin composite system powders presented the same behaviour as their unloaded counterparts when exposed to different relative humidities, as demonstrated by DVS analysis.

FTIR and CD analysis showed the stability of sCT throughout processing. It was found that raffinose and raffinose:cyclodextrin systems have better protective action over the peptide conformation than trehalose and its composite systems. The protective action of the sugars was also tested by sCT bioactivity measurements, where sCT retained full cAMP-secreting activity when spray dried with raffinose or raffinose:cyclodextrin and, a reduction of activity was seen for trehalose and respective composite systems.

All spray dried powders presented a concentration of methanol and butyl acetate below the European Pharmacopoeia limits for a daily dose, being safe, in terms of solvent toxicity, for administration into humans.

Storage stability studies demonstrated that sCT:R and sCT:R:HPβCD systems retained their micromeritic characteristics as well as sCT biological activity over 24 weeks when stored at 4°C/< 5 %RH or 25°C/< 5 % RH. On the other hand, sCT:trehalose composite systems suffered changes in morphology when stored at 4°C/< 5 %RH, with reduction of sCT bioactivity. However, if stored at 25°C/< 5 %RH, the micromeritic properties and sCT cAMP-secreting activity of sCT:T:R and sCT:T:HPβCD systems was preserved. Due to recrystallisation of sCT:T the storage stability of these systems, in either conditions, is compromised, with great reduction of sCT bioactivity.

Preliminary pharmacokinetic studies denoted that sCT dry powder formulations had a similar pharmacokinetic profile to sCT solution. The advantage resides in the use of less excipients to stabilise the peptide in the dry powder formulation versus the solution formulation; additionally DPI are breath actuated contrary to the nebulizers (pulmonary administration of solutions) that require the generation of vapour by a machine.

In conclusion, salmon calcitonin:sugar composite systems presented favourable aerodynamic and micromeritic characteristics, good physical stability and storage stability for sCT delivery to the systemic circulation using the lungs as a port of entry; raffinose systems appears to have better protective action and micromeritic properties than trehalose systems.

CHAPTER 8

GENERAL DISCUSSION

8.1 GENERAL DISCUSSION

This thesis focused on the development of porous microparticulate systems designed for the pulmonary delivery of a therapeutic peptide – salmon calcitonin. The non-reducing sugars trehalose dihydrate and raffinose pentahydrate were selected as stabilising excipients for the NPMPs. Previous studies by Ní Ógáin (2008) centred on the production of raffinose (R) and trehalose (T) nanoporous microparticles (NPMPs) for inhalation, evaluating different ratios of methanol:n-butyl acetate (MeOH:BA) solvent system and concluding that NPMPs spray dried from 80:20 (v/v) MeOH:BA displayed favourable micromeritic characteristics, suggesting potential suitability for pulmonary delivery. In addition, Ní Ógaín (2008) highlighted problems with the spray drying process such as low yields and powder deposits on cyclone walls. Therefore, before producing peptide-loaded sugar NPMPs, the research in this thesis concentrated primarily on fully understanding the spray drying process for the production and optimisation of raffinose and trehalose NPMPs.

8.1.1 Production and spray drying of sugar NPMPs

Chapter 3 and 4 discussed the optimisation of the spray drying process for the production of sugar NPMPs, a one-factor-at-a-time (OFAT) (Chapter 3) and a statistical design of experiment (DOE) approach (Chapter 4) were the methods selected. The effect of the spray drying parameters inlet temperature(T_{inlet}) , feed rate (pump) and feed solution concentration on the powder yield, particle size (d_{50}), residual solvent content (RSC), and process outlet temperature (T_{outlet}) for raffinose and trehalose NPMPs were investigated. The DOE also evaluated the effect of the gas flow on powder characteristics and the additional outcome, specific surface area (SSA).

Maury et al. (2005) published an OFAT study to improve the yield on spray drying aqueous solutions of trehalose dihydrate using a laboratory-scale spray drier (Büchi Model 191). This study showed that the powder yield increased with higher process temperatures, with a maximum being reached at T_{inlet} = 100 °C, after which it decreased sharply. The decrease observed was thought to be caused by heating of the cyclone wall above the so-called 'sticky point' of trehalose, resulting in increased particle deposits on the walls of the tower and cyclone. Increasing liquid feed flow rate or decreasing atomizing air flow rate was found to be detrimental to powder yield; it was determined that the drying air flow rate should be as high as possible to ensure sufficient heat transfer to dry the trehalose adequately to give a high powder yield.

Moran and Buckton (2007) studied the impact of concentration of aqueous trehalose dihydrate on spray dried particle size and powder recrystallisation. Amorphous spheres were produced. Those from the highest feed concentration were found to have the largest particle size (due to more rapid onset of drying), whereas the lowest feed concentration resulted in the smallest particles. The high feed concentration resulted in material that reproducibly and readily crystallised when exposed to water vapour. The most dilute feed concentration resulted in samples that exhibited great variability between batches, often requiring a larger mass of water to be sorbed before the crystallisation would begin than was needed for samples from higher feed concentrations. A compromise was found with the material resulting from intermediate feed concentration, which showed less variability than seen for low feed materials and greater dissipation of desorbed water than for high feed material. Moran and Buckton (2007) concluded that the properties of amorphous trehalose are altered as a consequence of processing and care must be taken to optimise this when attempting to stabilise macromolecular drugs.

All spray dried raffinose and trehalose NPMPs powders (chapter 3 and 4) were amorphous by XRPD analysis and constituted by spherical and porous particles type 1BIIIα according to the new MCS developed by Paluch et al. (2012). The amorphous nature of trehalose after spray drying has been reported in a variety of studies such those presented by Maury et al. (2005), Moran and Buckton (2007), Ní Ógaín et al. (2010), among others. On the other hand, the amorphous nature of raffinose has been well studied (Kajiwara et al., 1999; Davidson and Sun, 2001; Hogan and Buckton, 2001; Buera et al., 2005; Charmathy et al., 2010), however, studies of spray dried powders solely constituted by raffinose have only been reported by Ní Ógaín et al. (2010), with produced powders being amorphous as well those presented in this thesis. In addition, the studies in Chapter 3 and 4 studied thoroughly the effect of the process variables on raffinose powders, which has not been published to date.

In chapter 3, similar to what was reported by Maury et al. (2005), powder yield of both sugar NPMPs was seen to increase with increasing inlet temperature until a setting of 120 °C, after which a reduction was seen. However, contrary to Maury et al. (2005), increasing pump setting led to higher yields but this was not statistically significant. The particle size of sugar NPMPs was significantly affected by feed concentration, as was found in the studies by Moran and Buckton (2007). Residual solvent content and outlet temperature were found to be affected by the inlet temperature and pump setting. In Chapter 4, it was seen that raffinose and trehalose yields were mainly affected by the gas flow (a parameter which was not studied in Chapter 3) and by the pump and feed concentration, with trehalose NPMPs yield also being affected by the inlet

temperature. Particle size of raffinose NPMPs was affected by the gas flow and feed concentration and trehalose NPMPs by the gas flow, pump and feed concentration. The inlet temperature and pump setting affected residual solvent content and outlet temperature of trehalose NPMPs. Raffinose NPMPs residual solvent content was affected only by the inlet temperature and the process outlet temperature by the inlet temperature, gas flow and pump setting. Additionally, the effect of interactions between spray drying parameters was identified for both sugar NPMPs.

For most outcomes the effects of different parameters were identical by both methodologies used. However, the DOE method appears to be more robust, since it was possible to identify more statistically significant effects. For example, in both methodologies a trend of increasing yield with increasing pump setting was identified, but it was only determined to be significant when applying the DOE method. The DOE also allowed differences in raffinose and trehalose NPMPs processing to be determined. In Tables 4.4 and 4.5 (Chapter 4), it is evident that each material is affected differently by the spray dryer parameters. For example, increasing feed concentration increased raffinose NPMP yields and decreased trehalose NPMP yields. Also the existence of more parameter interactions, when spray drying trehalose, suggests this process is more complex than spray drying raffinose.

The DOE method gave a greater insight into the raffinose and trehalose NPMPs spray drying process than the OFAT method. According to Montgomery (1997), an OFAT allows straightforward conclusions on the studied parameter effects; nevertheless, this type of experiment is known to be unable to establish the existence of possible interactions between process parameters. The DOE methodology, in comparison to the OFAT method, presents the advantage of estimation of interactions between parameters. For example, the residual solvent content of both sugar powders was affected by interactions between two and three variables. In the OFAT the process optimisation is based on selection of the best result attained for each parameter. In contrast, the DOE allows the establishment of model equations that provide a tool to estimate the effect of a parameter within several levels of the other parameters and makes process optimisation more efficient because the optimal solution is searched over the entire design space (Montgomery, 1997). Table 8.1 presents the optimised conditions from OFAT and DOE studies for the spray drying of raffinose and trehalose NPMPs.

The conditions predicted differ depending on the method used, with the exception of the aspirator setting (kept constant in both studies), the predicted trehalose feed solution concentration and the predicted pump rate to be used for raffinose spray drying. The gas flow

was determined by the DOE studies to be the parameter that impacted most on powder characteristics. This parameter was not evaluated in the OFAT, where it was kept constant, hence the difference. There was a 30 °C difference in predicted optimised inlet temperature depending on the methodology applied; such a discrepancy will affect powder residual solvent content, as it was defined by both studies to be a parameter with a strong impact.

Tabel 8.1 Optimised process conditions by one-factor-at-a-time (OFAT) and design of experiment (DOE) studies for raffinose and trehalose NPMPs spray drying.

Parameter	Predicted setting for optimised samples			
	OFAT		DOE	
	Raffinose	Trehalose	Raffinose	Trehalose
Aspirator (%)	100	100	100	100
Gas flow rate (mm)	40 (667 L/h)	40 (667 L/h)	50 (1020 L/h)	50 (1020 L/h)
Inlet temperature (°C)	120	120	150	150
Pump rate (%)	30	35	30	40
Feed solution concentration (%)	2	1	2.9	1

Ní Ógáin (2008) spray dried raffinose NPMPs under the following conditions: T_{inlet} 100 °C, gas flow rate 40 mm (667 l/h) and pump rate 30 % (8.5 ml/min). The total solid concentration in the feed solution was 1 % for raffinose and 0.5 %.for trehalose.

Table 8.2 details the characteristics of the spray dried powders obtained by spray drying raffinose and trehalose at the predicted optimised conditions described above. The data indicated an increase in the collected yield and specific surface area (for trehalose only) and a reduction in the geometric median particle size and residual solvent content with application of the OFAT and DOE methodologies compared to the studies reported by Ní Ógáin (2008). The spray drying gas flow rate is the main parameter affecting the SSA (chapter 4). The DOE model equations predicted the use of a gas flow of 50 mm (1052 l/h), higher than the gas flow used in the preceding studies, resulting in the increase seen in the trehalose powder SSA. The inlet temperature was increased from 100 to 120 °C (OFAT) and 150 °C (DOE), resulting in drier powders, hence the reduction in the RSC, and less powder sticking to the cyclone walls, increasing the collected yields. Even though the feed solution concentration was increased, the median particle size was reduced compared to the previous studies by Ní Ógain (2008). Particle size in spray drying is primarily regulated by the air/liquid mass ratio (ALR). The ALR calculated for the studies undertaken by Ní Ógáin (2008) was 0.9 and 1.0 for raffinose and trehalose NPMPs respectively. For the optimised conditions as determined by the OFAT study, the ALR was 0.6 for

raffinose NPMPs and 0.7 for trehalose NPMPs. In the case of the DOE study optimised conditions indicated an ALR of 1.2 and 1.0 for raffinose and trehalose NPMPs respectively. The inlet temperature can also influence the particle size, since a higher inlet temperature leads to more efficient droplet drying resulting in drier particles with reduced tendency to adhesion (Vehring, 2007; Nandiyanto and Okuyama, 2011).

Based on the calculated ALR, the geometric mean particle size of the sugar NPMPs spray dried under the conditions defined by the OFAT method should be higher than the results obtained by Ní Ógáin (2008), since ALR was smaller and the concentration of the feed solutions was higher. Trehalose NPMPs presented similar particle size and RSC, but raffinose NPMPs presented a smaller d_{50} (Table 8.2). It is believed that, when spray drying at 100 °C (Ní Ógáin, 2008) particles are not efficiently dried, as the raffinose powder RSC was ~4 %. This may result in particle adhesion producing agglomerates that are not broken during particle size analysis by laser diffraction; while in the OFAT and DOE the inlet temperature was higher, resulting in a powder with low RSC and no agglomerates. Calculated ALR for optimised conditions via DOE was higher for raffinose. In the case of trehalose NPMPs, calculated ALR for optimised contidions was higher when compared to OFAT, but equal to the value reported by Ní Ógáin (2008). Particle size was reduced by ~1 μm and powder residual solvent was < 3 % compared to preceding studies. In this case the higher air liquid mass ratio led to the formation of droplets of smaller size, that after a more efficient drying (lower RSC) resulted in particles with a mean geometric diameter < 2 μm, presenting a preferable diameter for particles that are intended to be delivered into the deep lung ((airways with a diameter of 1-3 μm) (Hickey, 2006)).

Table 8.2 Collected data from raffinose and trehalose NPMPs spray drying by Ní Ógáin (2008), following one-factor-at-a-time (OFAT) optimised conditions and, following the factorial experimental design (DOE) optimised conditions . d_{50} – geometric median particle size, RSC –residual solvent content, SSA – specific surface area.

	Ní Ógáin (2008)		OFAT		DOE	
	Raffinose	Trehalose	Raffinose	Trehalose	Raffinose	Trehalose
Yield (%)	2.5-27%	~50%	57.7±0.33	61.1±0.85	57.7±1.6	57.1±2.4
d_{50} (μm)	3.0±0.05	2.5±0.04	2.4±0.01	2.4±0.05	1.8±0.02	1.6±0.04
RSC (%)	~4%	3-4%	2.3±0.65	3.8±0.30	2.6±0.34	2.5±0.49
SSA (m^2/g)	44.49±0.49	44.30±1.58	44.43±1.34	47.64±0.15	58.16±0.51	51.44±0.49
T_{oulet} (°C)	60-64	61-65	71±1.4	69±2.8	85±1.4	86±0.0

The use of a DOE method appeared to be more robust (good statistical significance) than the OFAT method, and enabled estimation of optimised spray drying conditions, allowing the

production of raffinose and trehalose NPMPs with improved characteristics in relation to their intended use as drug carriers for pulmonary delivery. Compared to the OFAT approach, the DOE allows for less time consuming and better understanding of a process; experimental runs are well established within a matrix, where variables are set at different levels in order to establish their possible effects on the studied outcome. Studies on the effects of a variable via an OFAT methodology are time consuming, as the effect is only evaluated from one perspective and not as by evaluating combinatory effects of variables as in the DOE; with no evaluation of possible interactions between process variables. In the DOE the presence or absence of interactions between variables is already taken into account in the design of the study, since in a run more than one variable is being evaluated. Moreover, the construction of models that enable process outcome prediction minimises experimental work, by aiding the researcher in the selection of runs. Thus, from the findings of the studies presented here, the use of a DOE is recommended in future spray drying studies orinvestigations of other types of processing techniques, in order to gain a thorough understanding, of the process.

The next step in understanding process of spray drying the sugars was to test the feasibility of producing NPMPs using different spray dryers. Studies presented in Chapter 6 addressed this question. Raffinose NPMP spray drying was studied in two different spray dryers: Niro SDMicro (laboratory scale) and Niro Mobile Minor (pilot scale). Raffinose was selected as the material to be spray dried, since fewer effects from the process variables impacted on powder characteristics, as discussed above, and due to the novelty in spray drying this material at a larger scale.

The atomisation step, the geometry of the nozzle, drying chamber and cyclone and the thermal exchange are key to the scale-up process (Rafin et al., 2006; Thybo et al., 2008). The process outlet temperature, vapour concentration in the drying gas and droplet size should be kept constant in order to produce particles of the same size (Rafin et al., 2006; Thybo et al., 2008; Gil et al., 2010). It was possible to keep the outlet temperature for the Niro SD Micro constant, by balancing the setting of the inlet temperature with the pump setting (samples SDM4, SDM5 and SDM7). The process and atomisation gas flow also affect the outlet temperature, as shown in the DOE (section 6.4 of Chapter 6). However the inlet setting was higher than the temperature used in the Büchi Mini spray dryer. The larger dimensions of the Niro SDMicro result in a different thermal flow in the drying chamber and cyclone when compared to the Büchi's drying chamber, requiring a larger thermal energy output and hence an increase in the inlet temperature.

The outlet temperatures of the experimental runs of samples MM2, MM4, MM5 and MM6 from the Niro Mobile Minor were also similar values to the corresponding T_{outlet} of the Büchi Mini spray dryer. Also, in this case there was an interaction between inlet temperature, pump and atomisation gas flow. The inlet temperature was set between 110 and 125 °C, close to the T_{inlet} of 120 °C set in the Büchi Mini spray dryer. Although there was a difference in scale, it was possible to achieve the same outlet temperature without increasing the thermal energy output (T_{inlet} - T_{outlet}), which, according to Masters (2002), makes the process more cost effective.

Nevertheless, it would be expected that by keeping the outlet temperature constant the resulting residual solvent content would also be similar. This was not observed for powders produced in the Niro SD Micro. These presented higher residual solvent contents, indicating that the process was not as efficient as in the Büchi Mini spray dryer. This parameter is affected by the inlet temperature, pump setting and gas flow, as discussed in Chapter 4 and 6, which are also responsible for the outlet temperature achieved. Due to the larger dimensions of this spray dryer it is thought that the thermal exchange throughout particle drying is different, due to different thermal flow, as mentioned previously. In addition, particles produced are larger, indicating that bigger droplets were produced, which would contain higher solvent compared to smaller droplets. Figure 8.1 presents the correlation between geometric median particle size (d_{50}) and residual solvent content (only samples produced at equivalent T_{outlet} to Büchi Spray dryer were used to generate the plot). For the Niro Mobile Minor, samples presented similar residual solvent content to Büchi samples.

Particle size was larger for powders processed in both Niro spray dryers when compared to the Büchi spray dryer. The use of different nozzles and the difference in the gas and feed flow rate would be expected to result in different droplet sizes. Variation in specific surface area was also evident, with results being lower for powders prepared on the Niro SDMicro. This micromeritic characteristic is dependent on the evaporation rate and thermal exchange between the droplet and drying air, since the nanoparticulates are formed as the solvent evaporates and the space between these results in the porosity of the particles that leads to the high surface area. Another factor impacting on particle size is the particle residence time, which is modified with the geometry of the drying chamber and cyclone (Maa et al., 1998). SEM micrographs of particles spray dryed using the Niro SDMicro, showed some particles to be porous but with fused surfaces (samples SDM3 and SDM6), hence the smaller surface area. These samples were spray dried with a low process gas pressure, high atomisation (high nozzle pressure) and pump setting of 15 and 20 %. It is thought that the reduction of droplet size due to high atomisation, higher

solid content due to higher pump setting and low flow of drying gas did not achieve a good solvent evaporation and diffusion rate, necessary for the formation of small and separate nanoparticulates, creating instead large fused particles, with a sponge-like structure.

Although there were differences in the micromeritic properties of the raffinose NPMPs produced in the Niro SDMicro and Niro Mobile Minor, these powders demonstrated equivalent *in vitro* deposition to the raffinose NPMPs powders produced using the Büchi B-290 Mini Spray Dryer, showing that it is possible to produce raffinose NPMPs at the pilot scale and in different laboratory scale spray dryers.

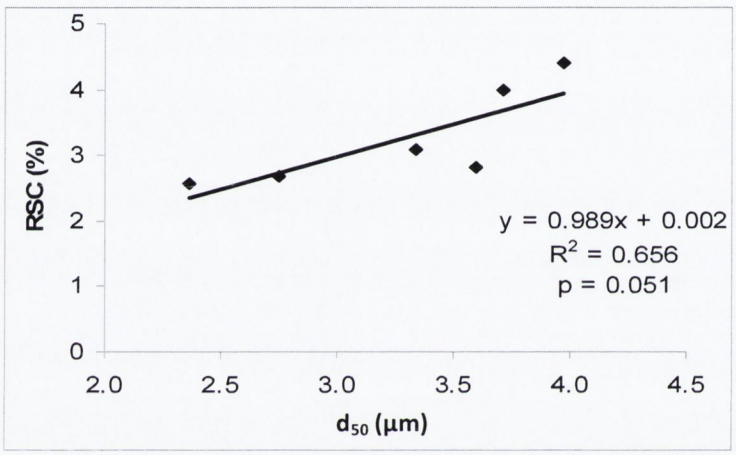

Figure 8.1 Relationship between geometric median particle size (d_{50}) and the residual solvent content (RSC) of raffinose powders spray dried using the Niro SDMicro.

All powders produced presented residual butyl acetate content, which could be reduced by drying for 24 hours at 25 °C under a nitrogen purge. Consequently, spray drying from methanol:propyl-acetate (MeOH:PA) solutions was investigated (Chapter 4). Different systems were investigated. Although NPMPs of both raffinose and trehalose could be produced, , the powders contained higher content of PA than BA (for the powders spray dried from MeOH:BA solutions). Another interesting observation was the different morphology of particles when spray dried from solutions of 80:20 MeOH:PA compared to particles spray dried from MeOH:BA 80:20 and that increasing fraction of propyl acetate in the solvent composition led to the production of NPMPs.

Paluch et al. (2012) found that on spray drying hydrophilic chlorothiazide sodium (CTZNa) and chlorothiazide potassium (CTZK) from MeOH:BA solutions, varying the solvent proportions resulted in different types of particle morphology. Spherical particles composed of nanoparticulate agglomerates were produced when solutions with higher content of butyl acetate were spray dried. Butyl acetate and propyl acetate are anti-solvents, promoting the

precipitation of the excipient/drug upon evaporation of methanol followed by the acetate, leading to formation of the nanoparticulates. For propyl acetate, the particle morphology improved with the inclusion of a higher proportion of this solvent in the MeOH:PA mixed solvent system resulting in the formation of NPMPs (particles type 1BIIIα). Paluch et al. (2012) also observed the same effect when changing the butyl acetate proportion for spray dried chlorothiazide sodium or potassium from MeoH:BA. However, studies by Ní Ógaín (2008) showed that in spray drying sugar NPMPs the optimum MeOH:BA ratio was 4:1 (evaluated ratios were 1:1, 7:3, 4:1 and 9:1), and that a lower BA proportion in the mixed solvent was necessary to produce spherical particles with high surface area, which is in contrast to the results of Paluch et al. (2012) and to experiments reported here using the MeOH:PA solvent system. Hence, it is though that the morphology of spray dried particles is not only dependent on the type and proportion of anti-solvent used, but also on the solubility of the solute in the anti-solvent. Based on the presented studies it is hypothesised that raffinose and trehalose solubility in butyl acetate is lower than in propyl acetate, since higher proportions of propyl acetate were required to achieve the NPMPs morphology, since the formation of this type of particle is based on the precipitation of the solute in the anti-solvent (BA and PA) when the solvent in which is more soluble evaporates (MeOH).

In conclusion, the sugar NPMPs production by spray drying appear to be largely dependent on the solvent ratio of the co-solvent system and on the process parameter settings. The latter will affect the evaporation of the solvent from the droplets. The combination of the studies presented in this thesis with those presented by Ní Ógáin (2008) and Paluch et al. (2012) indicate that the morphology of materials spray dried from MeOH:BA co-solvent system rely primarily on the solvent drying and secondarily on the solubility of the material in the co-solvent system, since it has been shown in Chapter 3 and 4 that solutions with different concentrations can result in NPMPs and that the surface area that reflects the porosity and morphology of the particles is dependent on the process parameters.

8.1.2 Salmon calcitonin: sugar NPMPs – process and storage stability

Stability is of vital importance in drug development. Changes in drug/formulation stability could risk patient safety, since the dosage amount to the patient may be lower than expected and toxic degradants might form. The evaluation of the drug and excipients chemical, physical and storage stability is a requirement in order to support new formulation pharmaceutical applications (Huynh-Ba, 2009). The amorphous state is not a thermodynamic equilibrium state,

as is the crystalline state, and thus amorphous materials tend to revert back to the stable crystalline form (Liu et al., 2006).

FTIR spectra of all spray dried two excipient composite systems showed interactions between molecules. A broad band between 3600-3000 cm^{-1} was attributed to the stretching vibration of the OH groups, indicating a wide range of hydrogen-bond lengths and orientations; bands between 1200-900 cm^{-1}, attributed to the combination of CO stretching and OH bending vibrations, presented a shift to higher wavenumbers; and the bands of the sugars glycosidic bond (~998 cm^{-1}) also presented modifications. The shifting in the OH bending vibrations is indicative of modification of the level of hydrogen bonding of the C–O–H groups (Wolkers et al., 2004). All molecules (HPβCD, raffinose and trehalose) are good H-bond donors and accepters (hydroxyl groups). Modifications in the OH bands are thus expected and may be attributed to the formation of H-bonds between trehalose and raffinose, trehalose and HPβCD and raffinose and HPβCD. The modification of the band related to the sugar's glycosidic bond is indicative of a conformation change of the molecule caused by the new hydrogen bonds (Akao et al., 2001).

The hydrogen bonds between the non-reducing sugars and the cyclodextrin are established on the external surface of the latter, which is polar (hydrophilic) due to the presence of secondary and primary hydroxyls at the edge of the ring. The inner part of the cyclodextrin is made apolar (hydrophobic) by glycosidic oxygens and methane protons (Martin Del Valle, 2004). Hence, it will not establish H-bonds with the sugars. Furthermore, inclusion complexes should not be formed, since the sugars are not hydrophobic and present a molecular diameter larger than the cyclodextrin cavity diameter (11.4 Å for raffinose, 12.2 Å for trehalose and 7.8 Å for the HPβCD cavity (Clinkenbeard and Thiessen, 1991; Brewster and Loftsson, 2007; Nagase et al., 2008)).

Interactions between the components of a mixture can also be identified by the thermal behaviour of the mixture, that is, by the existence of a single T_g and delay or inhibition of crystallisation, when mixtures are analysed by DSC (Vasconcelos et al., 2007). The spray drying of mixtures of sugars and the oligossacharide resulted in powders with a single T_g, higher than that of the single sugar systems, and resulted in the inhibition of trehalose crystallisation on heating in the DSC. These composite systems were thus more physically stable when subjected to increasing temperature on the DSC than raffinose and trehalose spray dried alone.

The Gordon-Taylor equation was used to predict the T of the spray dried systems without sCT. However, the glass transition of the spray dried two excipient composite systems did not follow the Gordon-Taylor equation, presenting negative deviations. Therefore, other approaches, which

are less commonly used, were applied for the T_g prediction: Fox and Kwei equations. The T_g data was successfully fitted by the Kwei equation (Figure 5, Chapter 5). The Gordon-Taylor and Fox equations do not account for interactions between the mixture components, whereas the Kwei equation is used in cases of strong interactions between components (Kalichevsky et al., 1992; Tajber et al., 2005). According to Taylor and Zografi (1998) the existence of hydrogen bonding between components of a mixture will affect the glass transition of the system and the experimental T_g value will be lower (negative deviation) than that predicted by the Gordon-Taylor equation. Taylor and Zografi's studies focused on PVP blends with the non-reducing sugars sucrose, trehalose and raffinose. By FTIR analysis of the spray dried systems in the current work, the existence of hydrogen bonds was identified between the sugars and sugars:oligossacharide, resulting in a negative deviation of experimental compared to predicted T_g values by the Gordon-Taylor and Fox equations. In addition, the constant q of Kwei equation presented a high value for all systems indicating/confirming the formation of hydrogen bonds between excipients.

DSC scans of sCT composite systems (Chapter 6) also presented a single glass transition event as their unloaded composite conterpart. Student's t-test was used to compare the T_g of the unloaded and loaded particles. P-values were found to be >0.05, meaning no differences between the mean values were found. The co-spray drying of sCT with a sugar or combination of two sugars or sugar:oligossacharide, did not affect the powder's glass transition temperature.

Carpenter and Crowe (1988, 1989) suggested the water replacement theory to explain the protective action of the sugar compounds, where the formation of H-bonding between the excipient and the biomolecule occurs when water is removed, maintaining the structural integrity of the peptide/protein. FTIR spectra of sCT composite systems presented a wide band between 3600-3000 cm^{-1} (OH stretching) and modification of bands between 1200-900 cm^{-1} (OH bonding) that are attributed to formation of H-bonds between molecules. Salmon calcitonin, raffinose, trehalose and HPβCD are good H-bond donors and acceptors (Table 8.3). The obtained results reinforce the theory of Carpenter and Crowe.

Table 8.3 Number of H-bond donors and receptors in the materials spray dried (http://pubchem.ncbi.nlm.nih.gov/).

	H-Bond donor	H-Bond acceptor
Salmon calcitonin (acetate)	53	57
Raffinose pentahydrate	11	16
Trehalose dihydrate	10	13
Hydroxypropyl-β-cyclodextrin	25	39

A second theory of protein protection through the use of such sugars was proposed by Franks et al. (1991) based on the formation of an amorphous glass during drying, which provides a rigid matrix around the protein molecules to restrict and stabilise their motion. All composite systems were amorphous and presented high glass transition temperatures. However, amorphous sugars present a strong tendency to sorb (adsorb and absorb) water. This hygroscopicity may cause crystallisation of that sugar and compromise the stability of the pharmaceutical formulation, e.g., loss of bioactivity of the peptide (Hancock and Shamblin, 1998). Amorphous raffinose and trehalose are known to be susceptible to moisture-induced crystallisation. Mazzobre et al. (1997) evaluated the effect of delaying crystallisation of trehalose in trehalose:lactase systems by the addition of maltodextrin in a ratio of 80:20 (maltodextrin:trehalose). Results showed an increase in the T_g of the system and a delay in trehalose recrystallisation, with improvement of lactase stability at relatively high RH (75 %). Constantino et al. (1998) co-lyophilised different ratios of recombinant humanised monoclonal antibody (rhGH) with trehalose, reporting rhGH to act as a trehalose recrystallisation inhibitor, confirmed by water vapour sorption studies. When exposed to increasing RH, systems with 25:75 and 40:60 protein:peptide ratio (w/w) delayed the trehalose recrystallisation from 50 % to 70 % and 80 % RH, respectively. For mixtures presenting equal ratio of protein:trehalose no recrystallisation was seen. It was suggested that interaction between rhGH and trehalose provided resistance to crystallisation.

DVS analysis on the single and two excipient composite systems (unloaded particles) and salmon calcitonin composite systems (loaded particles) presented similar profiles (Chapter 5 and 7). The addition of the peptide to the single excipient and two excipients composite system did not affect the water sorption behaviour for these peptide-sugar formulations, probably due to the low loading of 5 % w/w peptide. From the sCT composite systems, those that presented inhibition of raffinose and trehalose crystallisation were: sCT:R:HPβCD 5:38:57, sCT:T HPβCD 5:38:57 and sCT:T HPβCD 5:28:67, which all presented an enhanced physical stability when compared to systems constituted by sCT:R and sCT:T. As in the studies of Mazzobre et al. (1997),

a delay and inhibition of trehalose crystallisation was achieved by the addition of the oligossacharide. In the case of the systems investigated here no effect of the peptide on sugar crystallisation was seen. The reduced percentage of peptide loading may not allow effects such as those described by Constatino et al. (1998) to be determined.

The chemical stability of salmon calcitonin throughout processing was evaluated by means of HPLC (quantification of the peptide) and by measurement of its bioactivity by a cAMP assay (Chapter 7). FTIR and CD were used to evaluate the retention of sCT native conformation. HPLC data showed sCT loading varied between 4 and 5 % for most systems, suggesting possible loss of peptide during processing. Raffinose and the mixture raffinose:cyclodextrin presented excellent protective action of the peptide conformation (full retention of the α-helix). Trehalose powders presented lower protection of the peptide structure, resulting in a lower loading and bioactivity (Figure 7.15 and 7.16, table 7.5; Chapter 7). CD evaluation also showed that sCT conformation was not affected by the chosen organic solvent system for spray drying.

Storage stability studies (Chapter 6) further demonstrated the protective action of raffinose and the mixture raffinose:cyclodextrin, since, after 24 weeks storage at 4° C/5% RH and 25 °C/5% RH the sCT systems retained their morphology as well as sCT biological activity. The mixing of trehalose with raffinose or HPβCD proved to increase the stability of trehalose only at the storage conditions 25 °C/5% RH, with retention of particle morphology and sCT bioactivity.

8.1.3 Suitability of sugar and sCT:sugar NPMPs for pulmonary delivery

Studies by Vanbever et al. (1999), Healy et al. (2008), Nolan et al. (2010) and Ní Ógáin et al. (2010) have reported the suitability of porous particles for pulmonary delivery of drugs, focusing on their aerosolisation properties.

Vanbever et al. (1999) reported that large porous particles, produced by spray drying aqueous solutions including a lung surfactant responsible for pore formation, with a d_{50} between 3 and 15 μm achieved an emitted dose of 96% and a fine particle fraction (<5 μm) between 49 and 92 %. Nolan et al. (2010) showed sodium cromoglicate NPMPs to present emitted dose between 42 and 64 % and a FPF <5 μm between 40 and 62 %. Ní Ógaín et al. (2010) reported for raffinose and trehalose NPMPs an emitted dose of ~80 % and a fine particle faction <5 μm of ~55 % for raffinose and ~40 % for trehalose.

The powder characteristics, such as particle size and morphology, density, specific surface area and *in vitro* deposition behaviour of selected samples were investigated in the present work (Chapter 4, 5 and 7). The fine particle fraction < 5 and 3 μm, mass median aerodynamic diameter

(MMAD) and the geometric standard deviation (GSD) are the main characterising parameters of the aerosol deposition.

The majority of spray dried particles were spherical and porous, type 1BIIIα as classified by Paluch et al. (2012). Irregular shaped particle morphology was identified in powders resulting from raffinose:HPβCD, with a HPβCD content greater than 40 %, but the characteristic porosity of the NPMPs was maintained. The main difficulty associated with inhalation of drug powders and their efficient delivery is the strong interparticle forces which make the cohesive bulk powder agglomerate; these interparticle forces are generally affected by surface roughness, geometrical structure and deformation of individual particles (Daniher and Zhu, 2008). The ANOVA evaluation of the aerosol parameters showed no difference between raffinose:HPβCD powders (Chapter 5). Tabor (1977) reported that when particles present fewer areas of contact, interparticle forces are lower, leading to a reduction of powder cohesion and easier dispersion. Composite particles with a cyclodextrin content over 40% presented high values of specific surface area (highest for ratio 60:40 R:HPβCD), resulting in powders comprising particles with few areas of contact. Nolan et al. (2010) reported that irregular shaped sodium cromoglicate NPMPs had lower FPF < 5 μm than spherical shaped NPMPs and lower specific surface area, which is the opposite of what was found for the raffinose and trehalose composite systems studied here, since raffinose:cyclodextrin particles presented a more irregular shape when compared to a spherical particle Hence, it is possible that specific surface area compared to particle morphology, presents a greater influence on particle deposition, especially for raffinose:cyclodextrin composites.

Chapter 4 discussed the relationship between specific surface area and fine particle fraction, reporting that for particles presenting a similar geometric median particle size, the FPF < 5μm increases with increasing SSA. Spray dried systems which were evaluated in terms of aerosol deposition, presented a geometric median diameter between 1.5 and 1.8 μm. For these systems an increase in FPF < 5 and 3 μm with increasing powder specific surface area was observed, independently of the presence or absence of peptide in the formulation (Chapter 5 and 6). A correlation between SSA and FPF was investigated (Appendix 3). Trehalose:raffinose composite systems did not present a significant correlation, a larger number of samples might be necessary to prove significance of the trend, whereas all remaining composites presented significant correlations. It can be postulated that, for the majority of samples the composition (single, two excipient and peptide:excipients composites) does not affect the studied trend and, as discussed previously, particle morphology effect on aerosol deposition can be disregarded. However, it

should be borne in mind that the specific surface area was seen to vary with the system composition (Chapter 5 and 6).

The aerosol deposition of the systems comprising salmon calcitonin was discussed in Chapter 7. Student's t-test was used to compare the aerosol parameters FPF <5 and 3 μm, MMAD and GSD of the loaded and unloaded powders. Table 8.4 presents the p-values for each pair of systems. It was found, for the majority of powders, that the inclusion of the peptide in the formulation did not significantly affect the aerosol deposition. The composite system T:HPβCD presented significant differences in the FPF <5 and 3 μm from its salmon calcitonin-loaded counterpart. In this case it was seen that the inclusion of the peptide resulted in a reduction of the fine particle fraction. The main differences found between powder characteristics were in terms of the bulk and tap density. Particles with lower bulk and tap density are advantageous for pulmonary drug delivery where they present improved dispersibility and delivery efficiency (Vehring, 2007). The salmon calcitonin composite presented higher bulk and tap density, resulting in a lower fine particle fraction.

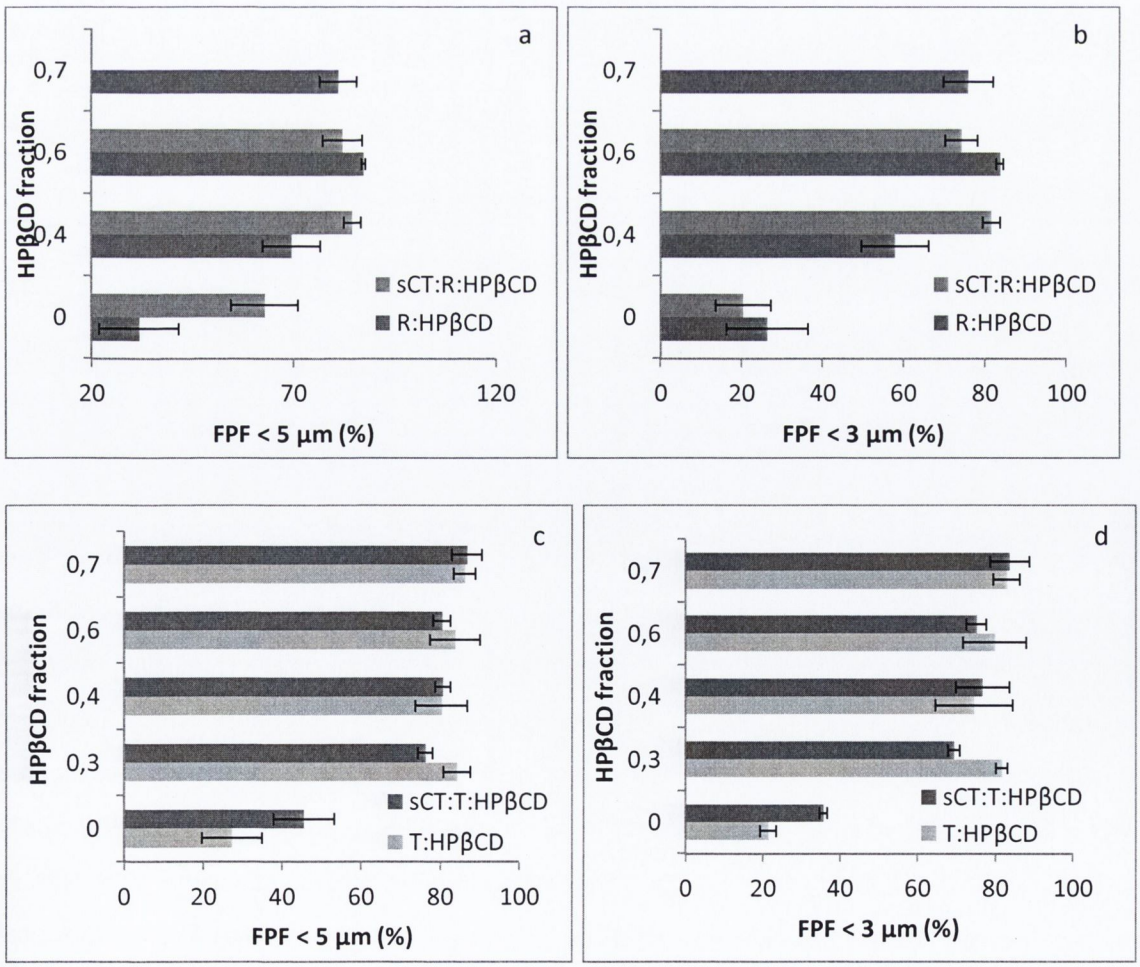

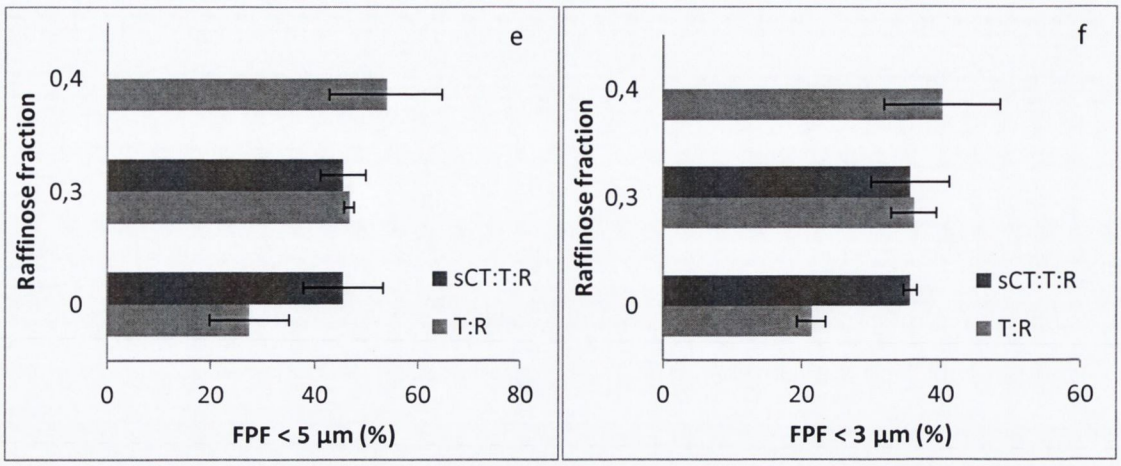

Figure 8.2 Fine particle fraction <5 and <3 µm of (a, b) raffinose composite systems, (c, d) trehalose:cyclodextrin composite systems and (e, f) trehalose:raffinose composite systems.

Table 8.4 Student's t-test p-values (confidence level 95%) of the comparison of aerosol parameters between loaded and unloaded systems.

	FPF < 5 µm	FPF < 3 µm	MMAD	GSD
	p-value	p-value	p-value	p-value
R/sCT:R	0.181	0.217	0.132	0.691
R:HPβCD 60:40 / sCT:R:HPβCD 5:57:38	0.212	0.157	0.037	0.179
R:HPβCD 40:60 / sCT:R:HPβCD 5:38:57	0.210	0.059	0.763	0.160
T / sCT:R	0.237	0.074	0.173	0.323
T:R /sCT:T:R	0.461	0.381	0.080	0.699
T:HPβCD 70:30 / sCT:T:HPβCD 5:67:28	0.002	0.002	0.051	0.127
T:HPβCD 60:40 / sCT:T:HPβCD 5:57:38	0.880	0.775	0.919	0.197
T:HPβCD 40:60 / sCT:T:HPβCD 5:38:57	0.542	0.435	0.718	0.621
T:HPβCD 30:70 / sCT:T:HPβCD 5:28:57	0.776	0.399	0.271	0.315

Considering all the salmon calcitonin composite systems, those with cyclodextrin in their formulation resulted in improved deposition profiles, with very high fine particle fractions being achieved: >80% (< 5 µm) and >70% (< 3 µm). Studies by Vanbever et al. (1999) (described previously in text) and Dellamary et al. (1999) reported porous particles formulations that achieved a high fine particle fraction in *in vitro* deposition studies. The latter authors presented different drug formulations of hollow porous microspheres (PulmoSpheres^{TM}), with a FPF ~ 68%. Hence, in terms of pulmonary delivery the salmon calcitonin sugar:cyclodextrin NPMPs composites are more promising as powders for delivery into the deep lung than composites comprising only sCT and sugar.

The pharmacokinetic study demonstrated that sCT dry powder formulations had a similar pharmacokinetic profile to sCT solution, with the formulation sCT:R:HPβCD 5:57:38 resulting in higher bioavailability. HPβCD is a known non-toxic permeability enhancer (Brewster and Loftsson, 2007); its addition to raffinose formulation may be the cause of the resulting higher bioavailability of the sCT:R:HPβCD 5:57:38 composite system.

Although the administration was intratracheal, overcoming deposition in the high airways, the increase in bioavailability is thought to be related to the aerosol deposition of this type of powder, since it was seen that sCT:R:HPβCD 5:57:38 presented elevated FPF < 5 and 3 μm ~85 % and ~82 %, respectively, and these diameters are related to the low airways, where blood circulation is elevated.

In conclusion, raffinose NPMPs appear to be more robust to spray dry than trehalose NPMPs, since fewer effects of spray drying parameters were detected. This characteristic allowed the successful spray drying at larger scale with the Niro Mobile Minor where powders with similar characteristics to those produced using the Buchi B-290 Mini spray dryer were obtained that presented good *in vitro* deposition properties. Such studies have never been published to date. Additionally, raffinose NPMPs and its composite systems presented better physical and storage stability than trehalose and its composite NPMPs systems, suggesting once more that raffinose is a more promising protective agent of peptides and proteins compared to trehalose. Aerosol deposition of raffinose composite systems was better than trehalose composite systems. The FPF of both sugar powders was enhanced with the inclusion of HPβCD in the NPMPs formulation, resulting in FPF greater than 80%. R:HPβCD composite systems were found to be superior to T:HPβCD composite systems due to their better preservation of the peptide conformation and bioactivity upon spray drying and during powder storage at 4 and 25°C/< 5 % RH. This combination of excipients has not been published to date, only trehalose and maltodextrin have been reported by Mazzobre et al. (1997). The use of HPβCD in combination with the non-reducing sugars is a novel and efficient way (producing high yields and improved aerosol deposition) of overcoming the issue of high hygroscopicity of these sugars, which has been regarded as the main downside of their use, leading to their reduced stability.

8.2 MAIN FINDINGS OF THE THESIS

- The production of NPMPs of raffinose and trehalose by a spray drying process was successfully optimised by means of an experimental design in order to achieve desirable micromeritic characteristics for pulmonary delivery. No previous description in the literature had been made on the impact of spray drying parameters on raffinose powders.
- By means of the DOE studies it was possible to establish that powder aerosol deposition in terms of fine particle fraction can be improved by modification of powder specific surface area.
- NPMPs of raffinose and trehalose can also be produced by using the co-solvent system MeOH:PA, suggesting potential for further development of these systems.
- NPMP composites comprised of raffinose or trehalose with hydroxypropyl-β-cyclodextrin and of trehalose with raffinose were spray dried. These systems potentially represent an improved carrier system for peptides or other drug compounds when compared to the single excipient systems, showing increased physical and storage stability. There was an enhancement of powder fine particle fraction when HPβCD was included in the formulation.
- Salmon calcitonin NPMPs composite systems were spray dried and were shown to have suitable physicochemical characteristics, physical and storage stability and aerosol deposition profiles for pulmonary delivery. Pharmacokinetic studies proved the applicability of such powders for systemic delivery of peptides or other drug compounds.
- Spray drying of raffinose and raffinose:HPβCD NPMPs is feasible in larger scale spray dryers.

8.3 PROPOSED FUTURE WORK

- Investigation of the production of sCT:sugar NPMPs with higher peptide loading.
- Investigation of the distribution within the co-spray dried system particles of the various components, focusing on the peptide. By measuring surface energies, it may be possible to map the surface of particles.
- Evaluation of the aerosol deposition of the develop systems at different flow rates, e.g., those representing elderly and compromised lung function.
- Development of the spray dried systems from MeOH:PA, by means of a more comprehensive spray drying study in order to reduce their residual solvent content.
- Further investigations on the *in-vivo* delivery of the sCT systems are necessary. Earlier times of collection would be ideal in order to gain a better insight on the drug absorption.
- Investigation of the production of sCT: anti-trypsin: sugar NPMPs with intension of improving sCT bioavailability.
- Addition of a radiolabel to the sCT:sugars NPMP formulations for pulmonary deposition would enable imaging and quantification by single photon emission computed tomography (SPECT), computed tomography (CT), high resolution computed tomography (HRCT) or positron emission tomography (PET).
- Studies on the application of raffinose and trehalose NPMPs systems for the delivery of drugs, such as antibiotics and anti-inflammatories, for local action in the lungs.

REFERENCES

Abdul-Fattah, A.M., Kalonia, D.S., Pikal, M.J., 2007. The Challenge of Drying Method Selection for Protein Pharmaceuticals: Product Quality Implications. Journal of Pharmaceutical Sciences, 96 (8), pp. 1886-1916.

Adler, M. and Lee, G., 1998. Stability and surface activity of lactate dehydrogenase in spray-dried trehalose. Journal of Pharmaceutical Sciences, 88 (2), pp. 199-208.

Andreotti, G., Méndez, B.L., Amodeo, P., Morelli, M.A.C., Nakamuta, H., Motta, A., 2006. Structural determinants of salmon calcitonin bioactivity – The role of the Leu-based amphipathic α-Helix. The Journal of Biological chemistry, 28 (34), pp. 24193-24203.

Al-Asheh, S., Jumah, R., Banat, F., Hammad, S., 2003. The use of experimental factorial design for analysing the effect of spray dryer operating variables on the production of tomato powder. Trans IchemE, 81 (C), pp. 81-88.

Akao, K., Okubo, Y., Asakawa, N., Inoue, Y., Sakurai, M., 2001. Infrared spectroscopic study on the properties of the anhydrous from II of trehalose. Implications for the functional mechanism of trehalose as a biostabilizer. Carbohydrate research, 334, pp. 233-241.

Arvine, T. and Drake, A. F., 1993. Comparative study of human and salmon calcitonin secondary structure in solutions with low dielectric constants. Journal of Biological chemistry, 268, pp. 6408-6414.

Baird, A.J. and Taylor, S.L., 2011. Evaluation of amorphous solid dispersion properties using thermal analysis techniques. Advanced Drug Delivery Reviews, 64 (5), pp. 396-421.

Baldinger, A., Clerdent, L., Rantanen, J., Yang, M., Grohganz, H., 2011. Quality by design approach in the optimization of the spray-drying process. Pharmaceutical Development and Technology, 17 (4), pp. 389-97.

Bhandari, B.R., Datta, N., Howes, T., 1997. Problems associated with spray drying of sugar-rich foods. Drying Technology, 15 (2), pp. 671-684.

Branchu, S., Forbes, R.T., York, P., Petrén, S., Nyqvist, H., Camber, O., 1999. Hydroxypropyl-β-cyclodextrin inhibits spray-drying-induced inactivation of β-galactosidase. Journal of Pharmaceutical Sciences, 88 (9), pp. 905-911.

Bravo-Osuna, I., Ferrero, C., Jiménez-Castellanos, M.R., 2005. Water sorption-desorption behaviour of methyacrylate-starch copolymers: effect of hydrophobic graft nad drying method. European Journal of Pharmaceutics and Biopharmaceutics, 59, pp. 537-548.

Billon, A., Bataille, B., Cassanas, G., Jacob, M., 2000. Development of spray-dried acetaminophen microparticles using experimental designs. International Journal of Pharmaceutics, 203, pp.159-168.

Bosquillon, C., Lombry, C., Préat, V., Vanbever, 2001. Influence of formulation excipients and physical characteristics of inhalation dry powders on their aerosolisation performance. Journal of Controlled Release, 70, pp. 329-339.

Bosquillon, C., Rouxhet, P.G., Ahimou, F., Simon, D., Culot, C., Préat, V., Vanbever, R., 2004. Aerosolization properties, surface composition and physical state of spray dried protein powders. Journal of Controlled Release, 99, pp. 357-367.

Brandenberger, H., 2003. Development of a novel high-performance cyclone toincrease the yield in a mini spray dryer. Best@buchi Evaporation and Life science Information Bulletin, 27.

Buera, P., Shebor, C., Elizalde, B., 2005. Effects of carbohydrate crystallization on stability of dehydrated foods and ingrediente formulations. Journal of Food Engineering, 67, pp.157-165.

Burnett, D., Thielmann, F., 2008. Application note 33: Impact of Protein Concentration on the Moisture-Induced Phase Transitions of Protein-Sugar Formulations. Surface Measurements Systems Ltd, London, UK.

Carpenter, J. F., Crowe, J. H., 1989. Infrared spectroscopic studies on the interaction of carbohydrates with dried proteins. Biochemistry, 28, pp. 3916-3922.

Carpenter, J.F., Crowe, J.H., 1988. The mechanism of cryoprotection of proteins by solutes. Cryobiology 25, pp. 244–255.

Chan, H.K., Clark, A.R., Feeley, J.C., Kuo, MC., Lehrman, S.R., Pikal-Cleland, K., Miller, D.P., Vehring,R., Lechuga-Ballesteros, D., 2004. Physical stability of salmon calcitonin spray-dried powders for inhalation. Journal of Pharmceutical Sciences, 93 (3), pp. 792-804.

Chan, H.K., 2006. Dry powder aerosol delivery systems: current and future research directions. Journal of Aerosol Mededicine, 19, pp. 21-27.

Chamarthy, S.P., Khalef, N., Trasi, N., Bakri, A, Carvajal, M.T., Pinal, R., 2010. The effect of dehydration conditions on the functionality of anhydrous amorphous raffinose. European Journal of Pharmaceutical Sciences , 40 (3), pp. 171-178.

Chen, T., Bhowmick, S., Sputtek, A., Fowler, A., Toner, M., 2002. The glass transition temperature of mixtures of trehalose and hydroxyethyl starch. Cryobiology, 44, pp. 301-306.

Cheng, W.T. and Lin, S.Y., 2006. Processes of dehydration and rehydration of raffinose pentahydrate investigated by thermal analysis and FT-IR/DSC microscopic system. Carbohydrate Polymoers, 64 (2), pp. 212–217.

Chew, N.Y., Bagster, D.F., Chan, H.K., 2000. Effect of particle size, air flow and inhaler device on the aerosolisation of disodium cromoglycate powders, International Journal of Pharmaceutics, 206 (1-2), pp. 75-83.

Chow, A., Tong, H., Chattopadhyay, P., Shekunov, B., 2007. Particle engineering for pulmonary drug delivery. Pharmaceutical Research, 24, pp. 411-437.

Clark, A., Kuo, M.C., Newman, S., Hirst, P., Pitcairn, G., Pickford, M., 2008. A comparison o pulmonary bioavailability of powder and liquid aerosol formulations of salmon calcitonin. Pharmaceutical Research, 25 (7), pp. 1583-1590.

Clas, C.D., Dalton, C.R., Hancock, B., 1999. Differential scanning calorimetry: applications in drug development. Pharmaceutical Science and Technology Today, 2, pp. 311-320.

Cleland, J.L., Daugherty, A., Mrsny, R., 2001. Emerging protein delivery methods. Current Opinion in Biotechnology, 12, pp. 212–219.

Clinkenbeard, K.D., Thiessen, A.E., 1991. Mechanism of action of Moraxella bovis hemolysin. Infection and Immunity, 59(3), pp. 1148-52.

Colaco, C., Sen, S., Thangavelu, M., Pinder, S., Roser, B., 1992. Extraordinary stability of enzymes dried in trehalose: Simplified molecular biology. Biotechnology, 10, pp. 1007-1011.

Creighton, T.E., 2010. Insulin Delivery - Biophysical Chemistry of Nucleic Acids and Proteins- Helvetian Press. http://www.knovel.com/web/portal/browse/display?_EXT_KNOVEL_DISPLAY_bookid=4299

Daniher, D.I. and Zhu, J., 2008. Dry powder platform for pulmonary drug delivery. Particuology 6, pp. 225-238.

Davidson, P. and Sun, W., 1998. Protein inactivation in amorphous sucrose and trehalose matrices: effects of phase separation and crystallization. Biochimica et Biophysica Acta, 1425, pp. 235-244.

Davidson, P. and Sun, W, 2001. Effect of sucrose/raffinose mass ratios on the stability of co-lyophilized protein during storage above Tg. Pharmaceutical Research, 18 (4), pp. 474-479.

Davis, M.E. and Brewster, M.E., 2004. Cyclodextrins – based pharmaceutics: past, present and future. Nature Reviews Drug Discovery, 3, pp. 1023-1035.

Elversson, J. and Millqvist-Fureby, M., 2005. Particle size and density in spray drying-effects of carbohydrates properties. Journal of Pharmaceutical Sciences, 94, pp. 2049–2060.

Epand, R.M. and Epand, R.F., 1986. Conformational flexibility and biological activity of salmon calcitonin. Biochemistry, 25 pp. 1964-1968.

Esposito, E., Roncarati, R., Cortesi, R., Cervellati, F., Nastruzzi, C., 2000. Production of eudragit microparticles by spray-drying technique: influence of experimental parameters on morphological and dimensional characteristics. Pharmaceutical Development and Technology, 5 (2), pp. 267-278.

European Pharmacopoeia, 2012a, European Pharmacopoeia: Preparations for Inhalation: Aerodynamic Assessment of Fine Particles (7th edition) Council of Europe, Strasbourg, pp. 274–284.

European Pharmacopoeia, 2012b, European Pharmacopoeia: Residual Solvents (7th edition) Council of Europe, Strasbourg, pp. 583–590.

European pharmacopoeia, 2012. Bulk density and tap density of powders. 7th Edition, Strasbourg, pp.

European pharmacopoeia, 2012. Preparations for inhalation: Aerodynamic assessment of fine particles. 7th Edition, Strasbourg, pp. 274-284.

European pharmacopoeia, 2012. Methods of analysis: 2.9.26 Specific Surface Area by Gas Adsorption. 7th Edition, Strasbourg, pp. 260-263.

Fournier, E., 2001. Colorimetric Quantification of Carbohydrates. Current Protocols in Food Analytical Chemistry. John Wiley and Sons, Inc.

Fischer, S., Hopkinson, D., Liu, M., MacLean, A.A., Edwards, V., Cutz, E., Keshavjee, S., 2001. Raffinose improves 24-hour lung preservation in low potassium dextran glucose solution: a histologic and ultrastructural analysis. The Annals of Thoracic Surgery, 71 (4), pp. 1140–1145.

Foster, T.M., Dormish, J.J., Narahari, U., Meyer, J.D., Vrkljan, M., Henkin, J., Porter, W.R., Staack, H., Carpenter, J.F., 1996. Thermal stability of low molecular weight urokinase during heat treatment III: Effect of salts, sugars and Tween 80. International Journal of Pharmaceutics, 134 (1–2), pp. 193–201.

Franks, F., Hatley, R. H. M., Mathias, S. F., 1991. Material science and the production of shelf stable biologicals. BioPharm, 4, pp. 38-55.

French, D.L., Arakawa, T., Li, T., 2004. Fourier transformed infrared spectroscopic investigation of protein conformation in spray-dried protein/trehalose powders. Biopolymers, 73, pp. 524-531.

Gil, M., Vicente, J., Gaspar, F., 2010. Scale-up methodology for pharmaceutical spray drying. Chemistry Today, 28 (4), pp. 18-22.

Goula, A.M., Adamapoulos, K.G., 2005. Spray drying of tomato pulp in dehumidified air: II. The effect on powder properties. Journal of Food Engineering, 66, pp. 35-42.

Gregg, S.J. and Sing, K.S.W., 1982. Adsorption, Surface Area and Porosity. 2nd Edition, Academic Press, London.

Hancock, B.C. and Shamblin, S.L., 1998. Water vapour sorption by pharmaceutical sugars. Pharmaceutical Science and Technology Today, 1 (8), pp. 345-351.

Hancock, B.C., 2007. Amorphous pharmaceutical systems In: Encyclopedia of pharmaceutical Technology. Informa Healthcare USA, Inc.

Healy, A.M., McDonald, B.F., Tajber, L., Corrigan O.I., 2008. Characterisation of excipient-free nanoporous microparticles (NPMPs) of bendroflumethiazide. European Journal of Pharmaceutics and Biopharmaceutics, 69, pp.1182 –1186.

Hickey, A.J., Martonen, T.B., Yang, Y., 1996. Theoretical relationship of lung deposition of the fine particle fraction of inhalation aerosols. Pharmaceutica Acta Helvetiae, 7 (1), pp. 185- 190.

Higashiyam, T., 2012. Novel functions and applications of trehalose. Pure Applied Chemistry, 74 (7), pp. 1263 -1269.

Hogan, S. and Buckton, G., 2001. Water sorption/desorption – near IR and calorimetric study of crystalline and amorphous raffinose. International Journal of Pharmaceutics, 227, pp. 57-69.

Howard, S.A., 2007. Solids: Flow Properties. Encyclopedia of Pharmaceutical Technology. Informa Healthcare USA, Inc., pp. 3275-3296.

Hulse, W.L., Forbes, R.T., Bonner, C.M., 2008. Do co-spray dried excipients offer better lysozyme stabilization than single excipients? European Journal of Pharmaceutical Sciences, 33, pp. 294-305.

Huynh-Ba, K., 2009. Handbook of stability testing in pharmaceutical development. Springer, New York.

Johnson, K.A., 1997. Preparation of peptide and protein powders for inhalation. Advance Drug Delivery Reviews, 26, pp. 3-15.

Jeffrey, G.A. and Huang, D., 1990. The hydrogen bonding in the crystal structure of raffinose pentahydrate. Carbohydrate Research, 204, pp. 173-182.

Kajiwara, K., Franks, F., Echlin, P., Greer, A.L., 1999. Structural and dynamic properties of crystalline and amorphous phases in raffinose-water mixtures. Pharmaceutical research, 16 (9), pp. 1441-1448.

Kalichevsky, M.T., Jaroszkiewicz, E.M., Blanshard, J.M.V., 1993. A study of the glass transition of amylpectin-sugar mixtures. Polymer, 34(2), pp. 346-358.

Katayama, T., Furuya, M., Yamaichi, K., Konishi, K., Sugiura, N., Murafuji, H., Magota, K., Saito, M., Tanaka, S., Oikawa, S., 2001. Discovery of a nonpeptide small molecule that selectively mimics the biological actions of calcitonin, Biochimic and Biophysic Acta, 1526, pp. 183–190.

Koushik, K. and Kompella, U.B., 2004. Particle and device engineering for inhalation drug delivery. Drug Delivery Technology, 4, pp. 40-50.

Kunda, N.K., Somavarapu, S., Gordon, S.B., Hutcheon, G.A., Saleem, I.Y., 2012. Nanocarriers Targeting Dendritic Cells for Pulmonary Vaccine Delivery. Pharmaceutical research. DOI 10.1007/s11095-012-0891-5.

Kwei, T.K., 1984. The effect of hydrogen bonding on the glass transition temperatures of polymer mixtures. Journal of Polymer Science – Part B - Polymer Letters, 22, pp. 307–313.

Leinen, K.M. and Labuza, T.P., 2006. Crystallization inhibition of an amorphous sucrose system using raffinose. Journal of Zhejiang University SCIENCE B, 7 (2), pp. 85-89.

Liu, Y., Bhandari, B., Zhou, W., 2006. Glass transition and enthalpy relaxation of amorphous food saccharides: a review. Journal of Agriculture and Food Chemistry, 54 (16) , pp. 5701-5717.

Loftsson, T. and Brewster, M.E., 1996. Pharmaceutical Applications of Cyclodextrins. 1. Drug Solubilization and Stabilization. Journal of pharmaceutical sciences, 85 (10), pp. 1017-1025.

López-Díez, E.C. and Bone, S., 2004. The interaction of trypsin with trehalose: an investigation of protein preservation mechanisms. Biochimic and Biophysic Acta, 673, pp. 139-148.

Maa, Y.F., Nguyen, P.A., Sit, K., Hsu, C.C., 1998. Spray drying performance of a bench-top spray dryer for protein aerosol powder preparation. Biotechnology and Bioengineering, 60 (3), pp. 301-309.

Maa, Y.F., Constantino, H.R., Nguyen, P.A., Hsu, C.C., 1997. The effect of operating and formulation variables on the morphology of spray dried particles. Pharmaceutical Development and Technology, 2, pp. 213-223.

Maltesen, M.J., Bjerregaard, S., Hovgaard, L., Havelund, S., Van de Weert, M., 2008. Quality by design – Spray drying of insulin intended for inhalation. European Journal of Pharmaceutics and Biopharmaceutics, 70, pp. 828-838.

Martin Del Valle, E.M., 2004. Cyclodextrin-based pharmaceutics: past, present and future. Nature Reviews Drug Discovery, 3, pp. 1023–1035.

Martindale, W. and Sweetman, S.C., 2011. Martindale: the complete drug reference, 37th Edition London, Pharmaceutical Press.

Masters, K., 1991. Spray drying handbook, 5th Edition, Longman, New York.

Masters, K., 2002. Spray drying in practice. Spray Dry Consult international ApS, Denmark.

Masuko, T., Minami, A., Iwasaki, N., Majima, T., Nishimura, S.I., Lee, Y.C., 2005. Carbohydrate analysis by a phenol-sulfuric acid method in microplate format. Analytical Chemistry, 339, pp. 69-72.

Maury, M., Murphy, K., Sandeep, K., Shi, L., Lee, G., 2004. Spray-drying of proteins: effects of sorbitol and trehalose o aggregation and FT-IR amide I spectrum of an immunoglobulin G. European Journal of Pharmaceutics and Biopharmaceutics, 59, pp. 251-261.

Maury, M., Murphy, K., Sandeep, K., Shi, L., Lee, G., 2005. Effects of process variables on the powder yield of spray-dried trehalose on a laboratory spray-dryer. European Journal of Pharmaceutics and Biopharmaceutics, 59, pp. 565–573.

Mazzobre, M.F., Buera, M.P., Chirife, J., 1997. Protective role of trehalose on termal stability of lactase in relation to its glass and crystal forming properties and effect of delaying crystallization. Lebensmittel-Wissenschaft und Technologie, 30, pp. 324-329.

Misiuk, W. and Zalewska, M., 2009. Investigation of inclusion complex of trazodone hydrochloride with hydroxypropyl-β-cyclodextrin. Carbohydrate Polymers, 77, pp 482-488.

Moe, G.R. and Kaiser, E.T., 1985. Design, Synthesis, and Characterization of a Model Peptide Having Potent Calcitonin-like Biological Activity: Implications for Calcitonin Structure/ Activity. Biochemistry, 24, pp. 1971-1976

Montgomery, C.D., 1997. Design and Analysis of Experiments, 5th Edition. John Wileyand Sons, New York.

Moran, A. and Buckton, G., 2007. Adjusting and understanding the properties and crystallization behavior of amorphous trehalose as a function of spray drying feed concentration. International Journal of Pharmaceutics, 343, pp. 12-17.

Motta, A., Andreotti, G., Amodeo, P., Strazzullo, G., Morelli, M.A.C., 1998. Solution Structure of Human Calcitonin in Membrane-Mimetic Environment: The Role of the Amphipathic Helix. PROTEINS: Structure, Function and Genetics, 32, pp. 314–323.

Nandiyanto, A.B.D. and Okuyama, K., 2011. Progress in developing spray-drying methods for the production of controlled morphology particles: From the nanometer to submicrometer size ranges. Advanced Powder Technology, 22 (1), pp. 1-19.

Nagase, H., Endo, T., Ueda, N.M., 2002. An anhydrous polymorphic form of trehalose. Carbohydrate Research, 337, pp. 167-173.

Newman, A., Knipp, G., Zografi, G., 2012. Assessing the performance of amorphous solid dispertions. Journal of Pharmaceutical Sciences, 101, 4, pp. 1355-1377.

Ní Ógáin, O., Li, J., Tajber, L., Corrigan, O.I., Healy, A.M., 2011. Particle engineering of materials for oral inhalation by dry powder inhalers. I – Particles of sugar excipients (trehalose and raffinose) incorporating a model protein. International Journal Pharmaceutics, 405, pp. 23-25.

Ní Ógáin, O., 2008. Investigations of a spray-drying method for producing nanoporous/nano-particulate microparticles (NPMPs) of proteins and protein-excipient composites. School of Pharmacy. Dublin, Trinity College Dublin. PhD.

Nolan, L.M., Li, J., Tajber, L., Corrigan, O.I., Healy, A.M., 2011. Particle engineering of materials for oral inhalation by dry powder inhalers. II-Sodium cromoglicate. International Journal of Pharmaceutics, 405 (1-2), pp. 36-46.

Ohashi, T., Yoshii, H., Furuta, T., 2007. Innovative crystal transformation of dihydrate trehalose to anhydrous trehalose using ethanol. Carbohydrate Research, 342, pp. 819-825.

Ohtake, S. and Wang, Y.J., 2011. Trehalose: current use and future applications. Journal of Pharmaceutical Sciences, 100 (6), pp. 2020-2053.

Paluch, K.J., Tajber,L. Corrigan, O.I., Healy, A.M., 2012. Impact of process variables on the micromeritic and physicochemical properties of spray dried porous microparticles Part I- Introduction of a new Morphology Classification System. Journal of Pharmacy and Pharmacology, 64 (11), pp. 1570-1582.

Papelis, C., Um, W., Russel, C.E., Chapman, J.B., 2003. Measuring the specific surface area of natural and manmade glasses: effects of formation process, morphology, and particle size. Colloids and Surfaces A: Physicochemical and Engineering Aspects, 215, pp.221-239.

Patton, J.S., Bukar, J., Nagarajan, S., 1999. Inhaled insulin. Advanced Drug Delivery Reviews, 35 (2–3), pp. 235–247.

Paudel, A. and Mooter, G.V., 2012. Influence of solvent composition on the miscibility and physical stability of naproxen/pvp k 25 solid dispersions prepared by co-solvent spray drying. Pharmaceutical Research, 29, pp. 251-270.

Pinto, S., Diogo, H., Moura-Ramos, J., 2006. Crystalline anhydrous α,α-trehalose (polymorph β) and crystalline dihydrate α,α-trehalose: A calorimetric study. Journal of Chemical Thermodynamics, 38, pp. 1130-1138.

Prinn, K.B., Constantino, H.R., Tracy, M., 2002. Statistical modelling of protein spray drying at the lab scale. AAPS PharmSciTech 3, E4.

Raffin, R.P., Jornada, D.S., Ré, M.I., Pohlman, A.R., Guterres, S.S., 2006. Sodium pantoprazole-loaded enteric microparticles prepared by spray drying by spray drying: Effect of the scale production on process validation. International Journal of Pharmaceutics, 324, pp 10-18.

Ryan, S., Wang, X., Mantovani, G., Sayers, C., Haddleton, D., Brayden, D., 2009. Conjugation of salmon calcitonin to a combed-shaped and functionalized poly(poly(ethylene glycol) methyl ether methacrylate) yields a bioactive stable conjugate. Journal of Controlled Release, 135, pp. 51-59.

Scheuch, G., Kohlhaeufl, M.J., Brand, P., Siekmeier, R., 2006. Clinical perspectives on pulmonary systemic and macromolecular delivery. Advanced Drug Delivery Reviews, 58, pp. 996–1008.

Schneider, H.A., 1997. The glass transition temperature of random copolymers: 2. Extension of the Gordon-Taylor equation for asymmetric T_g vs composition curves. Polymer, 38 (6), pp. 1323-1337.

Seidell, A., 2010. Solubilities of inorganic and organic compounds: a compilation of quantitative solubility data from the periodical literature. Vol. 1, 2nd Edition, Nabu Press.

Shambiln, S., Taylor, L.S., Zographi, G., 1998. Mixing behavior of colyophilized binary systems. Journal of Pharmaceutical Sciences, 87 (6), pp. 694-701.

Shao, Z., Krishnamoorthy, R., Mitra, A.K., 1992. Cyclodextrins as nasal absorption promoters of insulin: mechanistic evaluations. Pharmaceutical Research, 9, pp. 1157–1163.

Shebor, C., Mazzobre, M.F., Buera, M.P., 2010. Glass transition and time-dependent crystallization behavior of dehydration bioprotectant sugars. Carbohydrate Research, 345, pp. 303-308.

Shekunov, B.Y., Chattopadhyay, P., Tong, H.H.Y., Chow, A.H.L., 2007. Particle size analysis in pharmaceutics: principles, methods and applications. Pharmaceutical Research, 24, pp. 203-227.

Sigurjónsdóttir, J.F. and Loftsson, T.M, 1999. Influence of cyclodextrins on the stability of the peptide salmon calcitonin in aqueous solution. International Journal of Pharmaceutics, 186, pp. 205–213.

Sinha, S., Baboota, S., Ali, M., Kumar, A., Ali, J., 2009. Solid dispersion: an alternative technique for bioavailability enhancement of poorly soluble drugs. Journal of Dispersion Science and Technology, 30, pp. 1458-1473.

Stähl, K., Claesson, M., Lilliehorn, P., Lindén, H., Bäckström, K., 2002. The effect of process variables on the degradation and physical properties of spray dried insulin intended for inhalation. International Journal of Pharmaceutical, 233, pp. 227-237.

Stuart, B.O., 1976. Deposition and Clearence of inhaled particles. Environmental Health Prespectives, 16, pp. 41-53.

Sussich, F., Princivalle, F., Cesàro, A., 1999.The interplay of the rate of water removal in the dehydration of α,α-trehalose. Carbohydrate Research, 322, pp. 113-119.

Sussich, F. and Cesàro, A., 2008. Trehalose amorphisation and recrystallisation. Carbohydrate Research 343, pp. 2667-2674.

Tabor, D., 1977. Surface Forces and surface Interactions. Journal of Colloid and Interface Science, 58, pp. 2-13.

Taylor, L.S. and York, P., 1998. Characterization of the phase transitions of trehalose dehydrate on heating and subsequent dehydration. Journal of Pharmaceutical Sciences, 87 (3), pp. 347-355.

Taylor, L.S. and Zografi, G., 1998. Sugar-polymer hydrogen bond interactions in lyophilized amorphous mixtures. Journal of Pharmaceutical Sciences, 87 (12), pp. 1615-1621.

Tajber, L., Corrigan, O.I., Healy, A.M., 2009. Spray drying of budesonide, formoterol fumarate and their composites—II. Statistical factorial design and in vitro deposition properties. International Journal of Pharmaceutics, 367, pp. 86–96.

Technical data Büchi B-290, available at: www.buchi.com, Drying, Mini Spray Dryer B-290. Data accessed Jan. 15, 2009.

Telko, M.J., Hickey, A.J., 2005. Dry powder inhaler formulation. American Journal of Respiratory and Critical Care Medicine, 50, pp.1209–1227.

Tewes, F., Tajber, L., Corrigan, O.I., Ehrhardt, C., Healy, A.M., 2010. Development and characterisation of soluble polymeric particles for pulmonary peptide delivery. European Journal of Pharmaceutical Sciences, 41, pp. 337-352.

Tewes, F., Gobbo, O. L., Amaro, M.I., Tajber, L., Corrigan, O.I., Ehrhardt, C., Healy, A.M., 2011. Evaluation of HPβCD-PEG microparticles for salmon calcitonin administration via pulmonary delivery. Molecular pharmaceutics, 8, pp. 1887-1898.

Thybo, P., Hovgaard, L., Lindeløv, J.S., Brask, A., Andersen, S.K., 2008. Scaling up the spray drying process from pilot to production scale using an atomized droplet size criterion. Pharmaceutical Research, 25 (7), pp. 1610-1620.

Thybo, P. and Hovgaard, L., 2008. Droplet size measurements for spray dryer scale-up. Pharmaceutical Development and Technology, 13, pp. 93-104.

Ungaro, F., Rosa, G., Miro, A., Quaglia, F., Rotonda, M.I., 2006. Cyclodextrins in the production of large porous particles: developmet of dry powders for sustained release of insulin to the lungs. European Journal of Pharmaceutical Sciences, 28, pp. 423-432.

Vanbever, R., Mintzes, J.D., Wang, J., Nice, J., Chen, D., Batycky, R., Langer, R., Edwards, D.A., 1999. Formulation and physical characterisation of large porous particles for inhalation. Pharmaceutical Research, 16 (11), pp. 1735-1742.

Van de Weert, M., Haris, P.I., Hennik, W.E., Crommelin, D.J.A., 2001. Fourier Transform Infrared Spectrometric Analysis of Protein Conformation: Effect of Sampling Method and Stress Factors. Analytical Biochemistry, 297 (2), pp. 160-169.

Vasconcelos, T., Sarmento, B., Costa, P., 2007. Solid dispersions as strategy to improve oral bioavailability of poor water soluble drugs. Drug discovery today, 12 (23/24), pp.1068-1075.

Vehring, R., Foss, W.R:, Lechuga-Ballesteros, D., 2007. Particle formation in spray drying. Aerosol Science, 38, pp. 728 – 746.

Webb, P.A., 2001. Volume and Density Determinations for Particle Technologists. Micromeritics Instrument Corp., available at: www.micromeritics.com. Data accessed Feb. 25, 2009.

Williams III, R.O., Mahaguna, V., Sriwongjanya, M., 1998. Characterization of an inclusion complex of cholesterol and hydroxypropyl-β-cyclodextrin. European Journal of Pharmaceutics and Biopharmaceutics, 46, pp. 355-360.

Wolkers, W.F., Oldenhof, H., Alberda, M., Hoeska, F.A., 1998. A Fourier transform infrared microspectroscopy study of sugar glasses: application to anhydrobiotic higher plant cells. Biochimica et Biophysica Acta, 1379, pp. 83-96.

Wolkers, W.F., Oliver, A. E., Tablin, F., Crowe, J.H., 2004. A Fourier-transform infrared spectroscopy of sugar glasses. Carbohydrate Research, 339 (6), pp. 1077-1085.

Wu, H., Liang, H., Yuan, Q., Wang, T., Yan, X., 2010. Preperation and stability investigation of the inclusion complex of sulforaphane with hydroxypropyl-β-cyclodextrin. Carbohydrate polymers, 82, pp. 623-627.

Yang, M., Velaga, S., Yamamoto, H., Takeuchi, H., Kawashima, Y., Hovgaard, L., van de Weert, M., Frokjaer, S., 2007. Characterisation of salmon calcitonin in spray-dried powder for inhalation: Effect of chitosan. Ineternational Journal of Pharmaceutics, 331, pp. 176-181.

Yavuz, B., Bilensoy,E., Vural, I., Sumnu, M., 2010. Alternative oral exemestane formulation: Improved dissolution and permeation. International Journal of Pharmaceutics, 398, pp. 137–145

Yoshii, H., Buche, F., Takeuchi, N., Terrol, C., Ohgawana, M., Furuta, T., 2008. Effects of protein on retention of ADH enzyme activity encapsulated in trehalose matrices by spray drying. Journal of Food Engineering, 87, pp.37-39.

Youn, Y.S., Kwon, M.J., Na, D.H., Chae, S.Y., Lee, S., Lee, K.C., 2008. Improved intrapulmonary delivery of site-specific PEGylated salmon calcitonin: Optimization by PEG size selection. Journal of Controlled Release, 125, pp. 98-75.

Yu, L., 2001. Amorphous pharmaceutical solids: preparation, characterization and stabilization. Advanced Drug Reviews, 48, pp. 27-42.

Zeng, M.X., Martin, G.P, Marriott, C., 2003. Particle interactions in dry powder formulations for inhalation. Taylor and Francis, 3rd Edition, London and New York.

APPENDICES

System	Solvent				Drying gas	Mode	Feed Conc (%)	T_{inlet} (°C)	T_{outlet} (°C)	Aspirator (%)	Gas flow (cm)	Pump (%)	Porous/non-porous
	%	name	%	name									
Raffinose	80	MeOH	20	BA		CM/suck	1	90	50-54	100	4	30	porous
Raffinose	80	MeOH	20	BA		CM/suck	1	100	57-60	100	4	30	porous
Raffinose	80	MeOH	20	BA		CM/suck	1	110	68-69	100	4	30	porous
Raffinose	80	MeOH	20	BA		CM/suck	1	120	71-73	100	4	30	porous
Raffinose	80	MeOH	20	BA		CM/suck	1	130	71-75	100	4	30	porous
Raffinose	80	MeOH	20	BA		CM/suck	1	140	78	100	4	30	porous
Raffinose	80	MeOH	20	BA		CM/suck	1	120	72-74	100	4	20	porous
Raffinose	80	MeOH	20	BA	N_2	CM/suck	1	120	72	100	4	35	porous
Raffinose	80	MeOH	20	BA		CM/suck	1	120	69-70	100	4	35	porous
Raffinose	80	MeOH	20	BA		CM/suck	2	120	70	100	4	30	porous
Raffinose	80	MeOH	20	BA		CM/suck	3	120	63	100	4	30	porous
Raffinose	80	MeOH	20	BA		CM/suck	3.5	120	64	100	4	30	porous
Raffinose	85	MeOH	15	BA		CM/suck	2	120	71	100	4	30	porous
Raffinose	85	MeOH	15	BA		CM/suck	4	120	71	100	4	30	porous
Raffinose	90	MeOH	10	BA		CM/suck	2	120	67	100	4	30	Non-porous

System	Solvent				Drying gas	Mode	Feed Conc (%)	T_{inlet} (°C)	T_{outlet} (°C)	Aspirator (%)	Gas flow (cm)	Pump (%)	Porous/non-porous
	%	name	%	name									
Raffinose	80	MeOH	20	BA	N_2	CM/suck	1	150	94-96	100	5	15	Porous
Raffinose	80	MeOH	20	BA		CM/suck	3.5	90	56-58	100	5	15	Porous
Raffinose	80	MeOH	20	BA		CM/suck	3.5	90	52	100	3	40	Porous
Raffinose	80	MeOH	20	BA		CM/suck	1	150	82-84	100	5	40	Porous
Raffinose	80	MeOH	20	BA		CM/suck	1	90	51	100	3	40	Porous
Raffinose	80	MeOH	20	BA		CM/suck	3.5	150	85-89	100	5	40	Porous
Raffinose	80	MeOH	20	BA		CM/suck	1	150	89-90	100	3	40	Porous
Raffinose	80	MeOH	20	BA		CM/suck	3.5	150	92-93	100	5	15	Porous
Raffinose	80	MeOH	20	BA		CM/suck	1	90	49-50	100	5	40	Porous
Raffinose	80	MeOH	20	BA		CM/suck	3.5	90	60-62	100	3	15	Porous
Raffinose	80	MeOH	20	BA		CM/suck	3.5	150	89	100	3	40	Porous
Raffinose	80	MeOH	20	BA		CM/suck	1	150	99	100	3	15	Porous
Raffinose	80	MeOH	20	BA		CM/suck	1	90	60-61	100	3	15	Porous
Raffinose	80	MeOH	20	BA		CM/suck	3.5	90	48	100	5	40	Porous

System	Solvent				Drying gas	Mode	Feed Conc (%)	T_{inlet} (°C)	T_{outlet} (°C)	Aspirator (%)	Gas flow (cm)	Pump (%)	Porous/non-porous
	%	name	%	name									
Raffinose	80	MeOH	20	BA	N_2	CM/suck	3.5	150	94-101	100	3	15	porous
Raffinose	80	MeOH	20	BA		CM/suck	1	90	57-58	100	5	15	porous
Raffinose	80	MeOH	20	BA		CM/suck	2	150	87	100	5	4	porous
Raffinose	80	MeOH	20	BA		CM/suck	2.9	150	84-86	100	5	3	porous
Raffinose	65	MeOH	35	PA		CM/suck	2.9	150	86-87	100	5	3	porous
Raffinose	70	MeOH	30	PA		CM/suck	2.9	150	88-88	100	5	3	porous
Raffinose	80	MeOH	30	PA		CM/suck	2.9	150	87-89	100	5	3	porous
R:HPβCD (80:20)	80	MeOH	20	BA		CM/suck	2.9	150	87-93	100	5	3	porous
R:HPβCD (70:30)	80	MeOH	20	BA		CM/suck	2.9	150	87-88	100	5	3	porous
R:HPβCD (60:40)	80	MeOH	20	BA		CM/suck	2.9	150	81-93	100	5	3	porous
R:HPβCD (40:60)	80	MeOH	20	BA		CM/suck	2.9	150	83-89	100	5	3	porous
R:HPβCD (30:70)	80	MeOH	20	BA		CM/suck	2.9	150	86	100	5	3	porous
R:HPβCD (20:80)	80	MeOH	20	BA		CM/suck	2.9	150	89	100	5	3	porous
sCT:R (5:95)	80	MeOH	20	BA		CM/suck	2.9	150	86-88	100	5	3	porous
sCT:R: HPβCD (5:57:38)	80	MeOH	20	BA		CM/suck	2.9	150	81-93	100	5	3	porous
sCT:T: HPβCD (5:38:57)	80	MeOH	20	BA		CM/suck	2.9	150	83-89	100	5	3	porous

System	Solvent				Drying gas	Mode	Feed Conc (%)	T_{inlet} (°C)	T_{outlet} (°C)	Aspirator (%)	Gas flow (cm)	Pump (%)	Porous/non-porous
	%	name	%	name									
Trehalose	80	MeOH	20	BA		CM/suck	0.5	90	49-55	100	4	30	porous
Trehalose	80	MeOH	20	BA		CM/suck	0.5	100	59-60	100	4	30	porous
Trehalose	80	MeOH	20	BA		CM/suck	0.5	110	65-68	100	4	30	porous
Trehalose	80	MeOH	20	BA		CM/suck	0.5	120	70-73	100	4	30	porous
Trehalose	80	MeOH	20	BA		CM/suck	0.5	130	73-79	100	4	30	porous
Trehalose	80	MeOH	20	BA		CM/suck	0.5	140	81-86	100	4	30	porous
Trehalose	80	MeOH	20	BA		CM/suck	0.5	120	73-74	100	4	25	porous
Trehalose	80	MeOH	20	BA	N_2	CM/suck	0.5	120	68-69	100	4	35	porous
Trehalose	80	MeOH	20	BA		CM/suck	1	120	67-68	100	4	35	porous
Trehalose	80	MeOH	20	BA		CM/suck	1.5	120	69	100	4	35	porous
Trehalose	85	MeOH	15	BA		CM/suck	1	120	70	100	4	35	porous
Trehalose	90	MeOH	10	BA		CM/suck	1.5	120	63	100	4	35	Non-porous
Trehalose	80	MeOH	20	BA		CM/suck	1.5	150	84-85	100	5	40	porous
Trehalose	80	MeOH	20	BA		CM/suck	0.5	90	49	100	5	40	porous
Trehalose	80	MeOH	20	BA		CM/suck	0.5	90	50	100	3	40	porous

System	Solvent				Drying gas	Mode	Feed Conc (%)	T_{inlet} (°C)	T_{outlet} (°C)	Aspirator (%)	Gas flow (cm)	Pump (%)	Porous/non-porous
	%	name	%	name									
Trehalose	80	MeOH	20	BA		CM/suck	1.5	150	97-98	100	3	15	porous
Trehalose	80	MeOH	20	BA		CM/suck	0.5	150	95-103	100	5	15	porous
Trehalose	80	MeOH	20	BA		CM/suck	1.5	90	50- 53	100	3	40	porous
Trehalose	80	MeOH	20	BA		CM/suck	1.5	90	52-57	100	5	40	porous
Trehalose	80	MeOH	20	BA		CM/suck	1.5	90	59-60	100	3	15	porous
Trehalose	80	MeOH	20	BA		CM/suck	0.5	150	81-86	100	5	40	porous
Trehalose	80	MeOH	20	BA		CM/suck	1.5	150	91-94	100	5	15	porous
Trehalose	80	MeOH	20	BA		CM/suck	1.5	90	54-61	100	5	15	porous
Trehalose	80	MeOH	20	BA		CM/suck	1.5	150	85-86	100	3	40	porous
Trehalose	80	MeOH	20	BA		CM/suck	0.5	150	99-103	100	3	15	porous
Trehalose	80	MeOH	20	BA		CM/suck	0.5	90	60-61	100	3	15	porous
Trehalose	80	MeOH	20	BA		CM/suck	0.5	90	57-58	100	5	15	porous
Trehalose	80	MeOH	20	BA		CM/suck	0.5	150	86-87	100	3	40	porous

System	Solvent				Dry. gas	Mode	Feed Conc (%)	T_{inlet} (°C)	T_{outlet} (°C)	Aspirator (%)	Gas flow (cm)	Pump (%)	Porous/non-porous
	%	name	%	name									
Trehalose	80	MeOH	20	BA	N_2	CM/suck	1	150	86	100	5	40	porous
Trehalose	80	MeOH	20	BA		CM/suck	1	116	77-79	100	3	15	porous
Trehalose	65	MeOH	35	PA		CM/suck	1	150	86-87	100	5	40	porous
Trehalose	70	MeOH	30	PA		CM/suck	1	150	83	100	5	40	porous
Trehalose	80	MeOH	30	PA		CM/suck	1	150	85-87	100	5	40	Porous
T:R (80:20)	80	MeOH	20	BA		CM/suck	1	150	84-87	100	5	40	Porous
T:R (70:30)	80	MeOH	20	BA		CM/suck	1	150	83-86	100	5	40	Porous
T:R (60:40)	80	MeOH	20	BA		CM/suck	1	150	84-88	100	5	40	Porous
T:R(40:60)	80	MeOH	20	BA		CM/suck	1	150	83	100	5	40	Porous
T:R (30:70)	80	MeOH	20	BA		CM/suck	1	150	86-90	100	5	40	Porous
T:R(20:80)	80	MeOH	20	BA		CM/suck	1	150	84-89	100	5	40	Porous
T:HPβCD (80:20)	80	MeOH	20	BA		CM/suck	1	150	87-88	100	5	40	Porous
T:HPβCD (70:30)	80	MeOH	20	BA		CM/suck	1	150	87-89	100	5	40	Porous

System	Solvent				Drying gas	Mode	Feed Conc (%)	T_{inlet} (°C)	T_{outlet} (°C)	Aspirator (%)	Gas flow (cm)	Pump (%)	Porous/non-porous
	%	name	%	name									
Raffinose	80	MeOH	20	BA	N_2	CM/suck	1	90	50-54	100	4	30	porous
Raffinose	80	MeOH	20	BA		CM/suck	1	100	57-60	100	4	30	porous
Raffinose	80	MeOH	20	BA		CM/suck	1	110	68-69	100	4	30	porous
Raffinose	80	MeOH	20	BA		CM/suck	1	120	71-73	100	4	30	porous
Raffinose	80	MeOH	20	BA		CM/suck	1	130	71-75	100	4	30	porous
Raffinose	80	MeOH	20	BA		CM/suck	1	140	78	100	4	30	porous
Raffinose	80	MeOH	20	BA		CM/suck	1	120	72-74	100	4	20	porous
Raffinose	80	MeOH	20	BA		CM/suck	1	120	72	100	4	35	porous
Raffinose	80	MeOH	20	BA		CM/suck	1	120	69-70	100	4	35	porous
Raffinose	80	MeOH	20	BA		CM/suck	2	120	70	100	4	30	porous
Raffinose	80	MeOH	20	BA		CM/suck	3	120	63	100	4	30	porous
Raffinose	80	MeOH	20	BA		CM/suck	3.5	120	64	100	4	30	porous
Raffinose	85	MeOH	15	BA		CM/suck	2	120	71	100	4	30	porous
Raffinose	85	MeOH	15	BA		CM/suck	4	120	71	100	4	30	porous
Raffinose	90	MeOH	10	BA		CM/suck	2	120	67	100	4	30	Non-porous

System	Solvent				Drying gas	Mode	Feed Conc (%)	T_{inlet} (°C)	T_{outlet} (°C)	Aspirator (%)	Gas flow (cm)	Pump (%)	Porous/non-porous
	%	name	%	name									
Raffinose	80	MeOH	20	BA	N_2	CM/suck	1	150	94-96	100	5	15	Porous
Raffinose	80	MeOH	20	BA		CM/suck	3.5	90	56-58	100	5	15	Porous
Raffinose	80	MeOH	20	BA		CM/suck	3.5	90	52	100	3	40	Porous
Raffinose	80	MeOH	20	BA		CM/suck	1	150	82-84	100	5	40	Porous
Raffinose	80	MeOH	20	BA		CM/suck	1	90	51	100	3	40	Porous
Raffinose	80	MeOH	20	BA		CM/suck	3.5	150	85-89	100	5	40	Porous
Raffinose	80	MeOH	20	BA		CM/suck	1	150	89-90	100	3	40	Porous
Raffinose	80	MeOH	20	BA		CM/suck	3.5	150	92-93	100	5	15	Porous
Raffinose	80	MeOH	20	BA		CM/suck	1	90	49-50	100	5	40	Porous
Raffinose	80	MeOH	20	BA		CM/suck	3.5	90	60-62	100	3	15	Porous
Raffinose	80	MeOH	20	BA		CM/suck	3.5	150	89	100	3	40	Porous
Raffinose	80	MeOH	20	BA		CM/suck	1	150	99	100	3	15	Porous
Raffinose	80	MeOH	20	BA		CM/suck	1	90	60-61	100	3	15	Porous
Raffinose	80	MeOH	20	BA		CM/suck	3.5	90	48	100	5	40	Porous

System	Solvent				Drying gas	Mode	Feed Conc (%)	T_{inlet} (°C)	T_{outlet} (°C)	Aspirator (%)	Gas flow (cm)	Pump (%)	Porous/non-porous
	%	name	%	name									
Raffinose	80	MeOH	20	BA	N_2	CM/suck	3.5	150	94-101	100	3	15	porous
Raffinose	80	MeOH	20	BA		CM/suck	1	90	57-58	100	5	15	porous
Raffinose	80	MeOH	20	BA		CM/suck	2	150	87	100	5	4	porous
Raffinose	80	MeOH	20	BA		CM/suck	2.9	150	84-86	100	5	3	porous
Raffinose	65	MeOH	35	PA		CM/suck	2.9	150	86-87	100	5	3	porous
Raffinose	70	MeOH	30	PA		CM/suck	2.9	150	88-88	100	5	3	porous
Raffinose	80	MeOH	30	PA		CM/suck	2.9	150	87-89	100	5	3	porous
R:HPβCD (80:20)	80	MeOH	20	BA		CM/suck	2.9	150	87-93	100	5	3	porous
R:HPβCD (70:30)	80	MeOH	20	BA		CM/suck	2.9	150	87-88	100	5	3	porous
R:HPβCD (60:40)	80	MeOH	20	BA		CM/suck	2.9	150	81-93	100	5	3	porous
R:HPβCD (40:60)	80	MeOH	20	BA		CM/suck	2.9	150	83-89	100	5	3	porous
R:HPβCD (30:70)	80	MeOH	20	BA		CM/suck	2.9	150	86	100	5	3	porous
R:HPβCD (20:80)	80	MeOH	20	BA		CM/suck	2.9	150	89	100	5	3	porous
sCT:R (5:95)	80	MeOH	20	BA		CM/suck	2.9	150	86-88	100	5	3	porous
sCT:R: HPβCD (5:57:38)	80	MeOH	20	BA		CM/suck	2.9	150	81-93	100	5	3	porous
sCT:T: HPβCD (5:38:57)	80	MeOH	20	BA		CM/suck	2.9	150	83-89	100	5	3	porous

System	Solvent				Drying gas	Mode	Feed Conc (%)	T_{inlet} (°C)	T_{outlet} (°C)	Aspirator (%)	Gas flow (cm)	Pump (%)	Porous/non-porous
	%	name	%	name									
Trehalose	80	MeOH	20	BA		CM/suck	0.5	90	49-55	100	4	30	porous
Trehalose	80	MeOH	20	BA		CM/suck	0.5	100	59-60	100	4	30	porous
Trehalose	80	MeOH	20	BA		CM/suck	0.5	110	65-68	100	4	30	porous
Trehalose	80	MeOH	20	BA		CM/suck	0.5	120	70-73	100	4	30	porous
Trehalose	80	MeOH	20	BA		CM/suck	0.5	130	73-79	100	4	30	porous
Trehalose	80	MeOH	20	BA		CM/suck	0.5	140	81-86	100	4	30	porous
Trehalose	80	MeOH	20	BA		CM/suck	0.5	120	73-74	100	4	25	porous
Trehalose	80	MeOH	20	BA	N_2	CM/suck	0.5	120	68-69	100	4	35	porous
Trehalose	80	MeOH	20	BA		CM/suck	1	120	67-68	100	4	35	porous
Trehalose	80	MeOH	20	BA		CM/suck	1.5	120	69	100	4	35	porous
Trehalose	85	MeOH	15	BA		CM/suck	1	120	70	100	4	35	porous
Trehalose	90	MeOH	10	BA		CM/suck	1.5	120	63	100	4	35	Non-porous
Trehalose	80	MeOH	20	BA		CM/suck	1.5	150	84-85	100	5	40	porous
Trehalose	80	MeOH	20	BA		CM/suck	0.5	90	49	100	5	40	porous
Trehalose	80	MeOH	20	BA		CM/suck	0.5	90	50	100	3	40	porous

System	Solvent				Drying gas	Mode	Feed Conc (%)	T_{inlet} (°C)	T_{outlet} (°C)	Aspirator (%)	Gas flow (cm)	Pump (%)	Porous/non-porous
	%	name	%	name									
Trehalose	80	MeOH	20	BA		CM/suck	1.5	150	97-98	100	3	15	porous
Trehalose	80	MeOH	20	BA		CM/suck	0.5	150	95-103	100	5	15	porous
Trehalose	80	MeOH	20	BA		CM/suck	1.5	90	50- 53	100	3	40	porous
Trehalose	80	MeOH	20	BA		CM/suck	1.5	90	52-57	100	5	40	porous
Trehalose	80	MeOH	20	BA		CM/suck	1.5	90	59-60	100	3	15	porous
Trehalose	80	MeOH	20	BA		CM/suck	0.5	150	81-86	100	5	40	porous
Trehalose	80	MeOH	20	BA		CM/suck	1.5	150	91-94	100	5	15	porous
Trehalose	80	MeOH	20	BA		CM/suck	1.5	90	54-61	100	5	15	porous
Trehalose	80	MeOH	20	BA		CM/suck	1.5	150	85-86	100	3	40	porous
Trehalose	80	MeOH	20	BA		CM/suck	0.5	150	99-103	100	3	15	porous
Trehalose	80	MeOH	20	BA		CM/suck	0.5	90	60-61	100	3	15	porous
Trehalose	80	MeOH	20	BA		CM/suck	0.5	90	57-58	100	5	15	porous
Trehalose	80	MeOH	20	BA		CM/suck	0.5	150	86-87	100	3	40	porous

System	Solvent				Dry. gas	Mode	Feed Conc (%)	T_{inlet} (°C)	T_{outlet} (°C)	Aspirator (%)	Gas flow (cm)	Pump (%)	Porous/non-porous
	%	name	%	name									
Trehalose	80	MeOH	20	BA	N_2	CM/suck	1	150	86	100	5	40	porous
Trehalose	80	MeOH	20	BA		CM/suck	1	116	77-79	100	3	15	porous
Trehalose	65	MeOH	35	PA		CM/suck	1	150	86-87	100	5	40	porous
Trehalose	70	MeOH	30	PA		CM/suck	1	150	83	100	5	40	porous
Trehalose	80	MeOH	30	PA		CM/suck	1	150	85-87	100	5	40	Porous
T:R (80:20)	80	MeOH	20	BA		CM/suck	1	150	84-87	100	5	40	Porous
T:R (70:30)	80	MeOH	20	BA		CM/suck	1	150	83-86	100	5	40	Porous
T:R (60:40)	80	MeOH	20	BA		CM/suck	1	150	84-88	100	5	40	Porous
T:R(40:60)	80	MeOH	20	BA		CM/suck	1	150	83	100	5	40	Porous
T:R (30:70)	80	MeOH	20	BA		CM/suck	1	150	86-90	100	5	40	Porous
T:R(20:80)	80	MeOH	20	BA		CM/suck	1	150	84-89	100	5	40	Porous
T:HPβCD (80:20)	80	MeOH	20	BA		CM/suck	1	150	87-88	100	5	40	Porous
T:HPβCD (70:30)	80	MeOH	20	BA		CM/suck	1	150	87-89	100	5	40	Porous

System	Solvent				Drying gas	Mode	Feed Conc (%)	T_{inlet} (°C)	T_{outlet} (°C)	Aspirator (%)	Gas flow (cm)	Pump (%)	Porous/non-porous
	%	Name	%	Name									
T:HPβCD (60:40)	80	MeOH	20	BA	N_2	CM/suck	1	150	89-91	100	5	40	porous
T:HPβCD (40:60)	80	MeOH	20	BA		CM/suck	1	150	83-87	100	5	40	porous
T:HPβCD (30:70)	80	MeOH	20	BA		CM/suck	1	150	82-86	100	5	40	porous
T:HPβCD (20:80)	80	MeOH	20	BA		CM/suck	1	150	85	100	5	40	porous
sCT:T (5:95)	80	MeOH	20	BA		CM/suck	1	150	86-88	100	5	40	Porous
sCT:T:R (5:57:38)	80	MeOH	20	BA		CM/suck	1	150	84-88	100	5	40	Porous
sCT:T: HPβCD (5:67:28)	80	MeOH	20	BA		CM/suck	1	150	87-89	100	5	40	Porous
sCT:T: HPβCD (5:57:38)	80	MeOH	20	BA		CM/suck	1	150	89-91	100	5	40	Porous
sCT:T: HPβCD (5:38:57)	80	MeOH	20	BA		CM/suck	1	150	83-87	100	5	40	Porous
sCT:T: HPβCD (5:28:67)	80	MeOH	20	BA		CM/suck	1	150	82-86	100	5	40	Porous

System	Solvent				Drying gas	Mode	Feed conc (%)	T_{inlet} (°C)	T_{outlet} (°C)	Process gas pressure (bar)	Nozzle gas pressure (bar)	Pump (%)	Porous/non-porous
	%	name	%	name									
Raffinose	80	MeOH	20	BA	N_2	Blow	2.9	180	82-84	1	1	15	Porous
Raffinose	80	MeOH	20	BA		Blow	2.9	180	79-75	0.8	1.2	15	porous
Raffinose	80	MeOH	20	BA		Blow	2.9	180	81-83	0.8	1.4	15	porous
Raffinose	80	MeOH	20	BA		Blow	2.9	180	93	1	1	10	Non-porous
Raffinose	80	MeOH	20	BA		Blow	2.9	180	82	1	1	20	Non-porous
Raffinose	80	MeOH	20	BA		Blow	2.9	180	83	0.8	1.4	20	porous
Raffinose	80	MeOH	20	BA		Blow	2.9	180	83-85	1	1	10	porous
Raffinose	80	MeOH	20	BA		Blow	2.9	180	83-90	1.2	1.4	15	porous
Raffinose	80	MeOH	20	BA		Blow	2.9	180	78-82	0.8	0.8	15	porous
Raffinose	80	MeOH	20	BA		Blow	2.9	180	98	1.2	0.8	15	porous
Raffinose	80	MeOH	20	BA		Blow	2.9	180	69-73	0.8	1.4	15	porous
R:HPβCD (60:40)	80	MeOH	20	BA		Blow	2.9	180	78-87	1.2	1.4	15	porous
R:HPβCD (40:60)	80	MeOH	20	BA		Blow	2.9	180	78-87	1.2	1.4	15	porous

System	Solvent				Drying gas	Mode	Feed conc (%)	T_{inlet} (°C)	T_{outlet} (°C)	Atomization pressure (bar)	Pump (kg/h)	Porous/non-porous
	%	name	%	name								
Raffinose	80	MeOH	20	BA	N_2	CM/suck	2	125	80	1	0.8	porous
Raffinose	80	MeOH	20	BA		CM/suck	2	110	70	1	0.8	porous
Raffinose	80	MeOH	20	BA		CM/suck	2	90	60	1	0.8	porous
Raffinose	80	MeOH	20	BA		CM/suck	2	125	70	2	1.4	porous
Raffinose	80	MeOH	20	BA		CM/suck	2	125	70	3	1.2	porous
Raffinose	80	MeOH	20	BA		CM/suck	2	125	70	1	1.8	porous
Raffinose	80	MeOH	20	BA		CM/suck	2	150	80	1	2.0	porous
Raffinose	80	MeOH	20	BA		CM/suck	2	180	80	2	3.2	porous
Raffinose	80	MeOH	20	BA		CM/suck	2	150	80	1	2.0	porous
Raffinose	80	MeOH	20	BA		CM/suck	2	180	80	1	3.4	porous
Raffinose	90	MeOH	10	BA		CM/suck	2.5	125	80	1	1.0	Non-porous
Raffinose	70	MeOH	30	BA		CM/suck	1.5	125	80	1	2.9	Non-porous

- **Cyclone cut-off diameter calculation as reported by Maury et al. (2005):**

The downward spiralling vortex of air in a high performance cyclone exerts two opposite forces on a suspended particle: the centrifugal force acting outwards towards to cyclone wall at $x = r_a$, and the drag force acting inwards towards the inner edge of the vortex approximated by the radius of the exit duct, $x = r_i$. A particle rotating at $x = r_i$ with zero radial velocity,$\partial r(x,t)/\partial t|x = r1$, represents the low limit of particle size that can be separated from the air vortex. Barth equated the centrifugal and drag forces acting on this particle of limiting diameter $\bar{d}$, to obtain (Maury et al. (2005).

Barth's model as described by Maury et al. (2005): $\bar{d}^2 = \frac{9\eta Q}{(v_t^{-p})\rho_p \pi h_i}$, where η is air viscosity (pa s), Q is the air flow rate (m^3/s), ρ_p particle density (kg/m^3), and h_i vortex height (m). $v_t^{-p} = v_{in}\left(\frac{r_a}{r_i}\right)^{1/2}$ with $v_{in} = \frac{Q}{(\pi/4)r_a^2}$, v_t^{-p} is the tangencial particle velocity (m/s), r_a is the cyclone radius (m), r_i radius of the exit duct (m).

	h_i (mm)	r_a (mm)	r_i (mm)
HP cyclone	150	19	7

Q = 35 m^3/h = 9.72 x 10^{-3} m^3/s
ηs = 9.72 x 10 exit duct (m).elocity (m/s),$^{-5}$ Pa s
ρ_p(TRE)= 1.4 g/cm^3 = 1400 kg/m^3
ρ_p(RAF)= 1.6 g/cm^3 = 1600 kg/m^3

1. Find v_{in}: $v_{in} = \frac{9.72\,10^{-3}}{(\pi/4)0.019^2}$= 34.72 m/s

2. Find v_t^{-p}: $v_t^{-p} = 34.72\left(\frac{0.019}{0.007}\right)^{1/2}$ = 57.20 m/s

3. Find $\bar{d}^2$ for raffinose: $\bar{d}^2 = \frac{9\,or\,raffi10^{-5}\,5or\,ra10^{-3}}{57.20raffin\pi\times0.15}$ =0.36 ff^2

4. Find $\bar{d}^2$ for trehalose: $\bar{d}^2 = \frac{9\,or\,treha10^{-5}\,5or\,tr10^{-3}}{57.20trehal\pi\times0.15}$ = 0.377 al^2

5. Find $\bar{d}$ for raffinose and trehalose: $\overline{d_R}$ = $\sqrt{0.36}$ = 0.6 ff $\overline{d_T}$ = $\sqrt{0.377}$ = 0.61 fi

- **Example of *in-vitro* aerosol deposition calculations**

Part	Fluorescence	Volume	mg
Device	1295	25	1.264
Capsule	737	25	0.720
Mouth/IP	1900	25	1.855
Stage 1	1231	25	1.202
Stage 2	459	25	0.448
Stage 3	1696	25	1.656
Stage 4	3890	25	3.798
Stage 5	5174	25	5.052
Stage 6	1594	25	1.556
Stage 7	1384	5	0.270
Filter	1422	5	0.278
Weight recovered			**18.10**
Weight of powder in capsule			**19.92**
% recovery			**90.88**
Emitted dose			**16.12**
Emitted fraction (as per cent)			**89.04**
Non-emitted fraction			**3.84**

Stage	60 l/m	Actual airflow
		45.6
Stage 1	8.06	9.35
Stage 2	4.46	5.14
Stage 3	2.82	3.23
Stage 4	1.66	1.89
Stage 5	0.94	1.09
Stage 6	0.55	0.65
Stage 7	0.34	0.41
Filter		

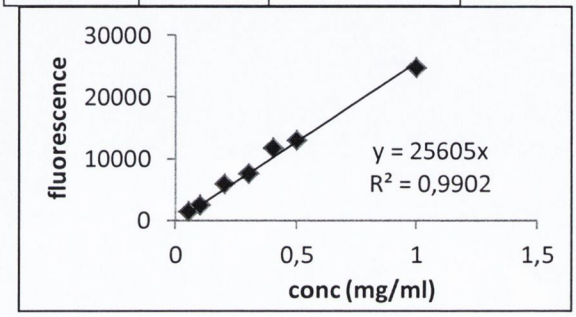

	Weight (mg)	Percentage (%)	
Weight of Powder in the Capsule (Nominal)	19.92	100	**Nominal dose**
Total weight of powder recovered	18.10	90.88	**conforms to B.P.**
Emitted weight of powder recovered (no capsule and device)	16.115	89.04	**Total recovered**
Mass of drug recovered from stages -1 to F only	14.260	78.79	**Emitted recovered**
Fine Particle Dose (FPD) below 5 um	12.95		
Fine Particle Dose (FPD) below 3 um	12.22		
Fine Particle Fraction as per nominal dose		65.01	
Fine Particle Fraction as per total recovered dose		71.54	
FPF <5 as per emitted recovered dose		80.34	
FPF < 3 as per emitted recovered dose		75.81	
MMAD (um)	2.050		
GSD (um)	2.042		
NGI Components		**Mass (mg)**	
Stage 1		1.202	
Stage 2		0.448	
Stage 3		1.656	
Stage 4		3.798	
Stage 5		5.052	
Stage 6		1.556	
Stage 7		0.270	
Filter		0.278	
Mass of drug recovered from stages 1 to F		**14.26**	
Mass of drug captured in the app.FP size range (Stages 2-F)		**13.06**	

NGI Components	ECD (Effective Cut-Off Diameter)	Stage collection (%)	Cumulative mass (mg)	Cumulative fraction (%)
Filter		1.95	0.00	0.00
Stage 7	0.41	1.90	0.27	1.95
Stage 6	0.65	10.91	1.83	3.84
Stage 5	1.09	35.43	6.88	14.76
Stage 4	1.89	26.63	10.68	50.18
Stage 3	3.23	11.61	12.33	76.82
Stage 2	5.14	3.14	12.78	88.43
Stage 1	9.35	8.43	13.98	91.57

Calculation of Fine Particle Dose (FPD)				
Cumulative mass (mg)	**zscore**	**ECD**	**ln(ECD)**	
0.00	#NÚM!			Filter
0.27	-2.7818	0.41	-0.8949	Stage 7
1.83	-2.0910	0.65	-0.4332	Stage 6
6.88	-1.4849	1.09	0.0836	Stage 5
10.68	-1.2439	1.89	0.6358	Stage 4
12.33	-1.1585	3.23	1.1740	Stage 3
12.78	-1.1368	5.14	1.6379	Stage 2
13.98	-1.0811	9.35	2.2351	Stage 1

Slope and intercept estimated on the stages 3 to 1 only!	
	Coefficients
Intercept	16.443
Slope	13.114
FPD (below 5.0 um)	**12.95**
	12.22

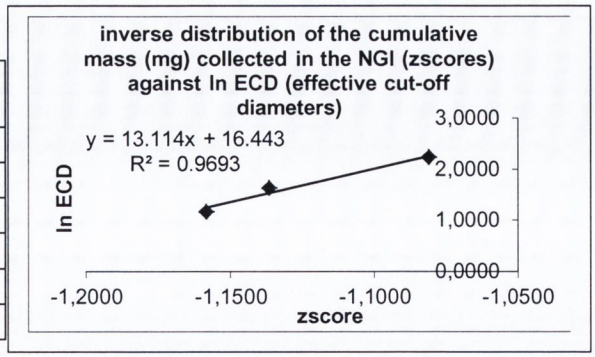

Calculation of Mass Median Aerodynamic Diameter and the Geometric Standard Deviation				
Cumulative fraction (%)	**zscore**	**ECD**	**ln(ECD)**	
0.00	#NÚM!			Filter
1.95	-2.0648	0.408633352	-0.8949	Stage 7
3.84	-1.7693	0.648447073	-0.4332	Stage 6
14.76	-1.0469	1.087167972	0.0836	Stage 5
50.18	0.0046	1.888537877	0.6358	Stage 4
76.82	0.7328	3.234761848	1.1740	Stage 3
88.43	1.1967	5.144128287	1.6379	Stage 2
91.57	1.3768	9.347504911	2.2351	Stage 1

	Coefficients	
Intercept	0.718	
Slope	0.714	
MMAD	**2.050**	**Um**
GSD	**2.042**	**Um**

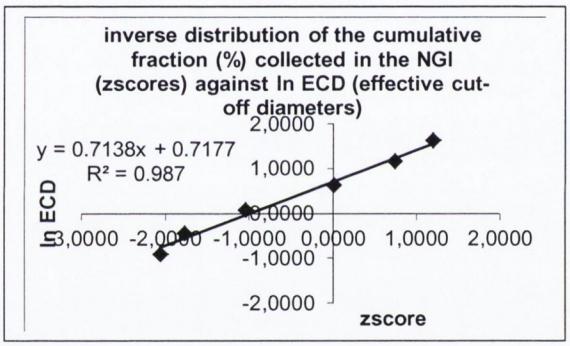

- **Example of sCT Bioactivity calculation**

	pmol/ml		**od**	**average**	**corrected**	**%B/Bo**
	Nsb	log	0.009			
			0.018	0.014		
s0	0.00		0.623			
			0.667	0.645	0.632	
s1	3.75	0.574031	0.583			
			0.578	0.581	0.567	89.77363
s2	7.5	0.875061	0.605			
			0.593	0.599	0.585	92.60725
s3	15.00	1.176091	0.425			
			0.384	0.405	0.391	61.89647
s4	30.00	1.477121	0.381			
			0.316	0.349	0.335	53.07108
s5	60.00	1.778151	0.211			
			0.217	0.214	0.201	31.78724
s6	120.00	2.079181	0.137			
			0.153	0.145	0.131	20.76144
s7	240.00	2.380211	0.102			
			0.094	0.098	0.084	13.35286

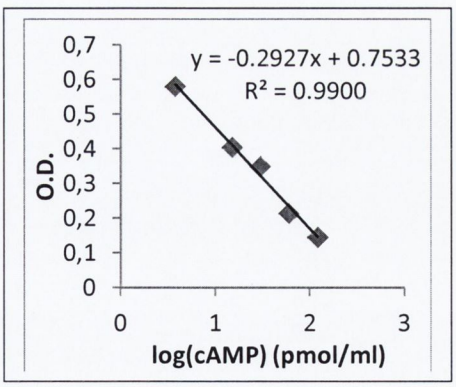

		average	corrected	cAMP	% activity		
Sct	0.260		0.247	53.84235	109.529		
	0.284	0.272	0.271	44.47376	90.47095		
	0.376		0.362	21.68605	44.11494	100	13.47611
T	0.275	0.325	0.261	48.03804	97.72159		
	0.548		0.535	5.578252	11.34758		
	0.278	0.413	0.265	46.62326	94.84359	96.28259	2.035059
R	0.319		0.306	33.87615	68.91272		
	0.406	0.363	0.393	17.05996	34.70431		
	0.260		0.246	53.92713	109.7015	89.30711	28.84203
average sCT		32.00883					

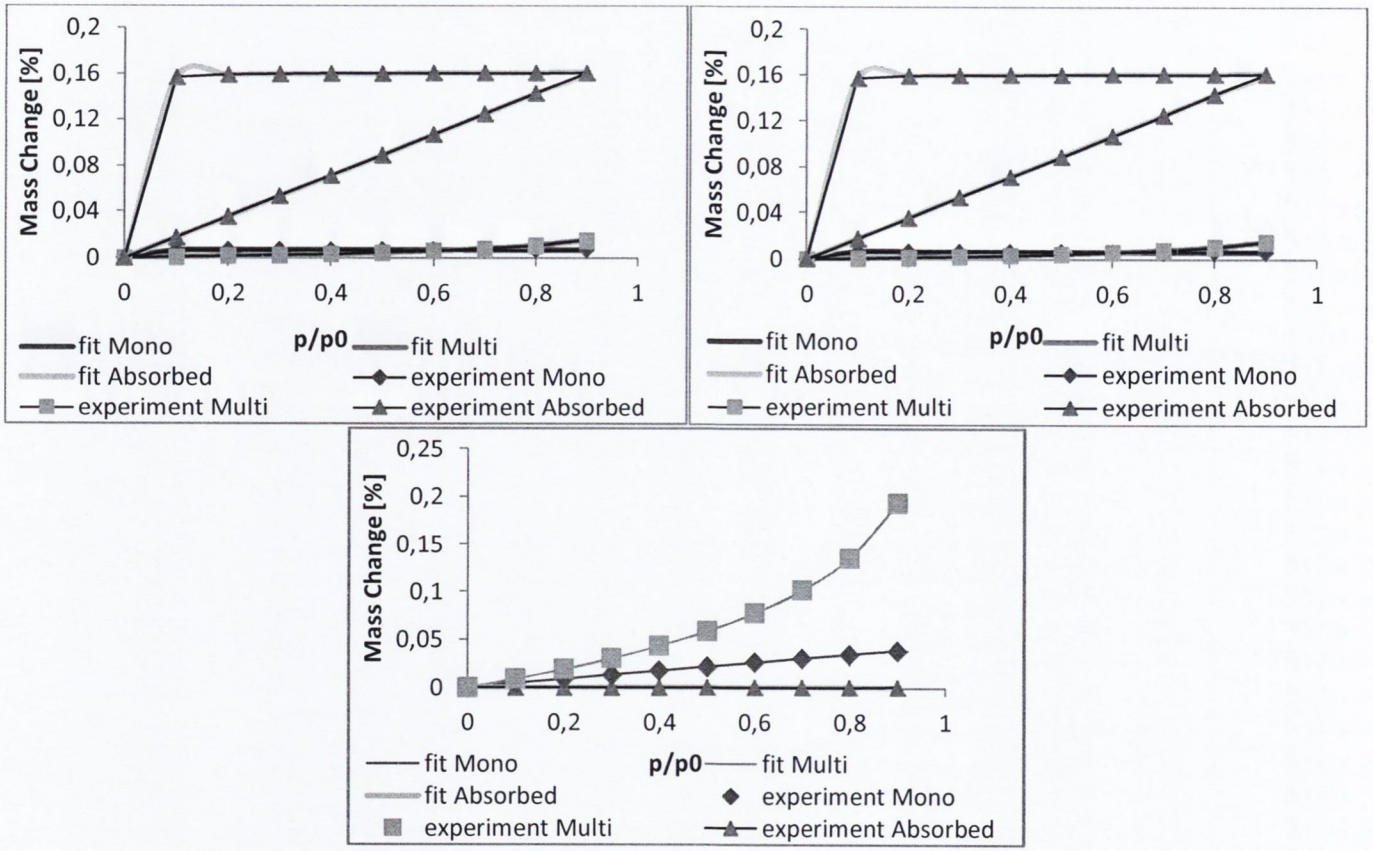

Chapter 5 Young-Nelson component plot of spray dried excipients alone (a) Trehalose (B) raffinose (c) HPβCD.

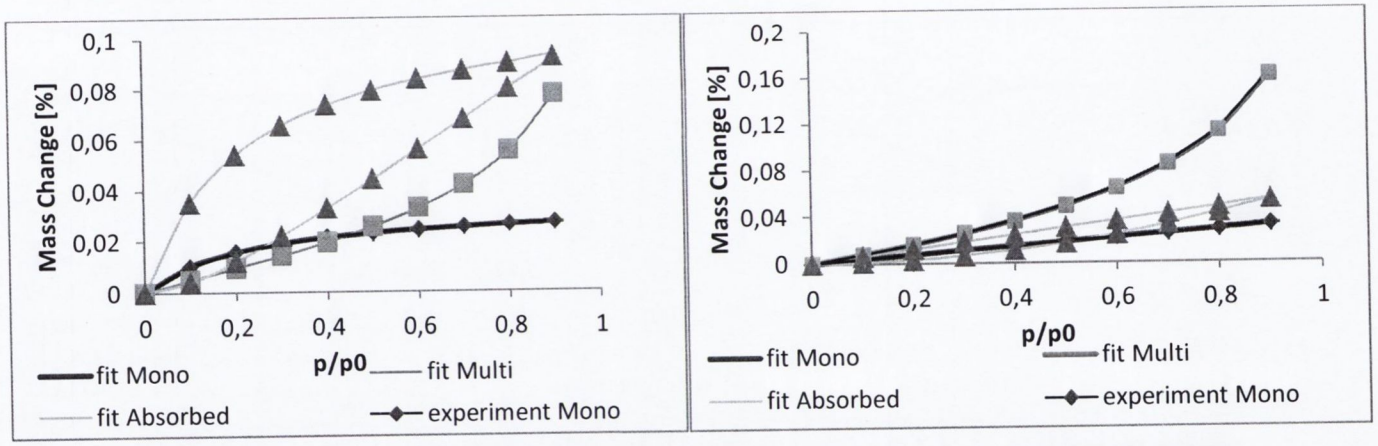

Chapter 5 Young-Nelson model component plot of R:HPβCD (a) 40:60 and (b) 30:70 composite systems.

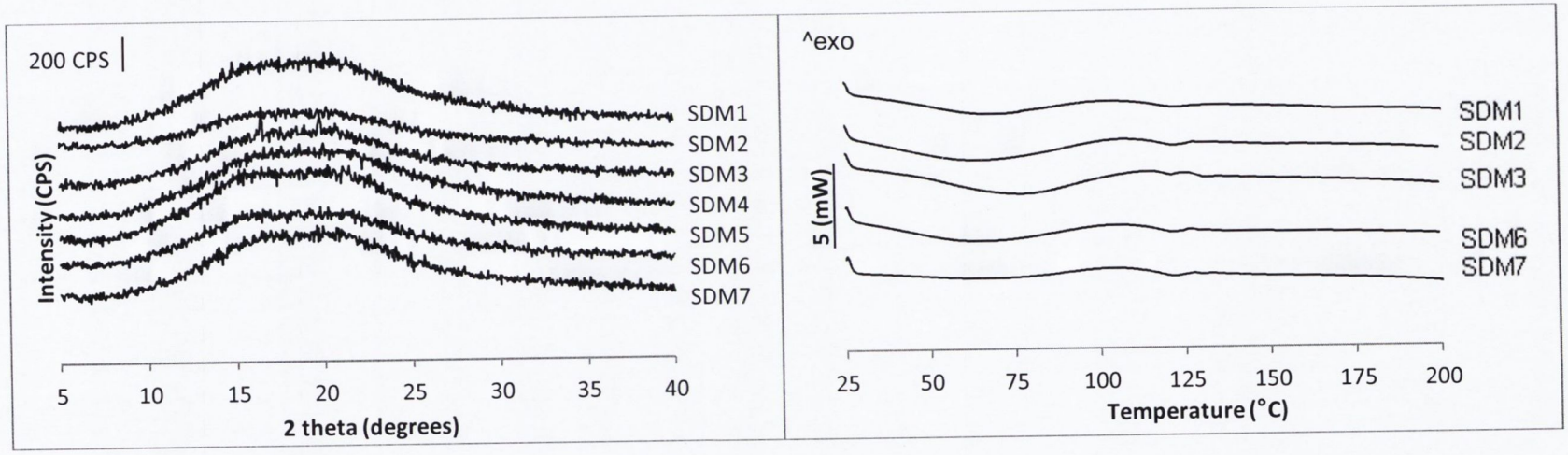

Chapter 6 (a) XRPD diffractograms and (b) DSC scans of spray dried raffinose powders prepared using the Niro SDMicro

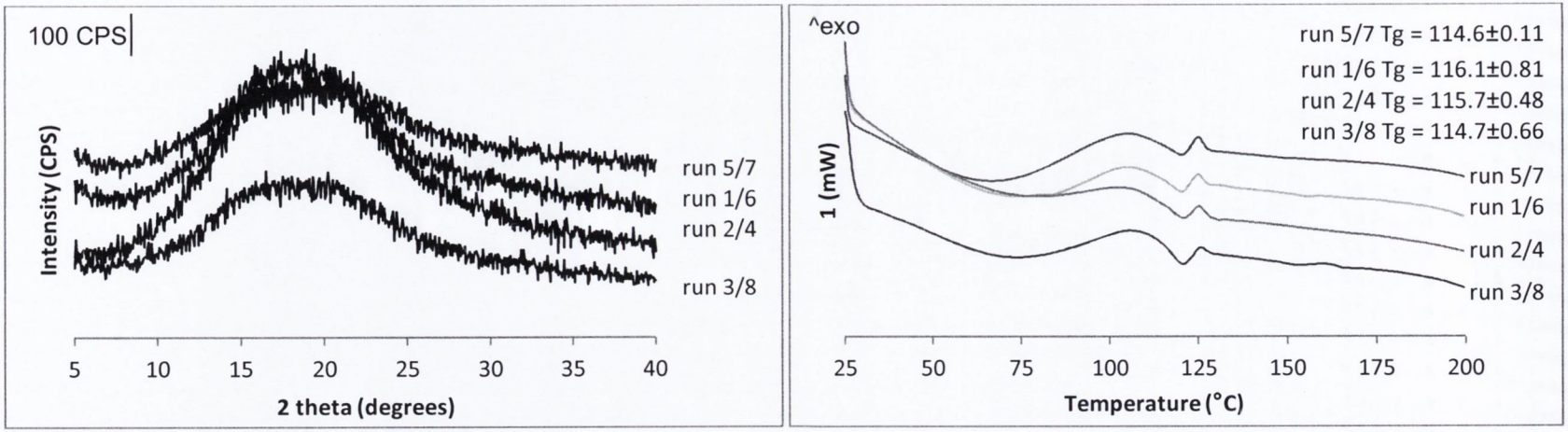

Chapter 6 (a) XRPD diffractograms and (b) DSC scans of spray dried raffinose powders according the DOE using the Niro SDMicro.

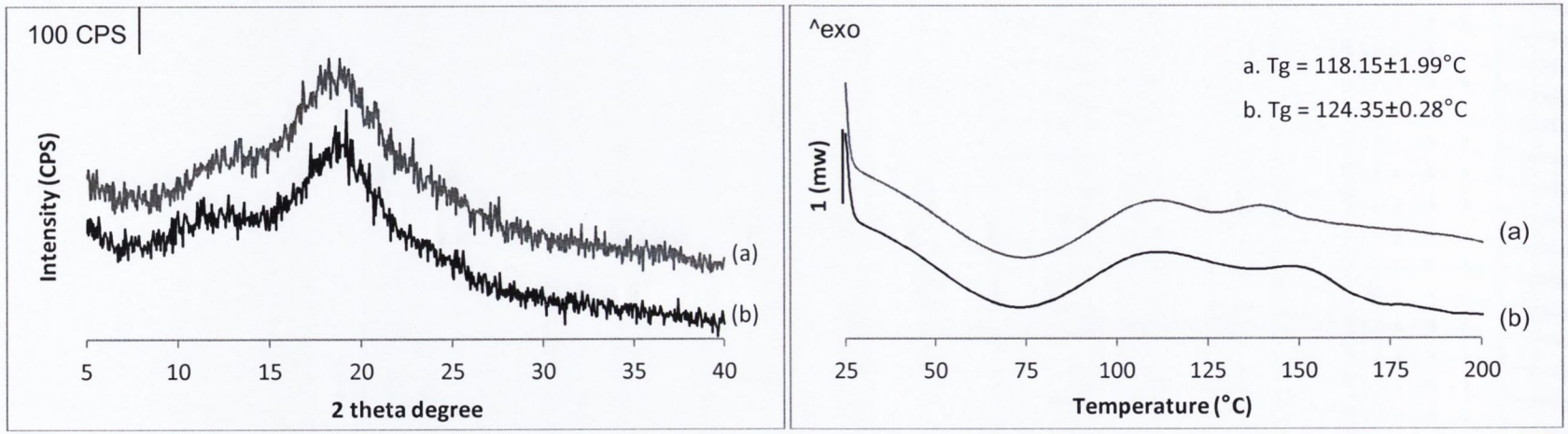

Chapter 6 (a) XRPD of spray dried and (b) DSC scans of raffinose:HPβCD composite systems with ratios (a) 60:40 and (b) 40:60.

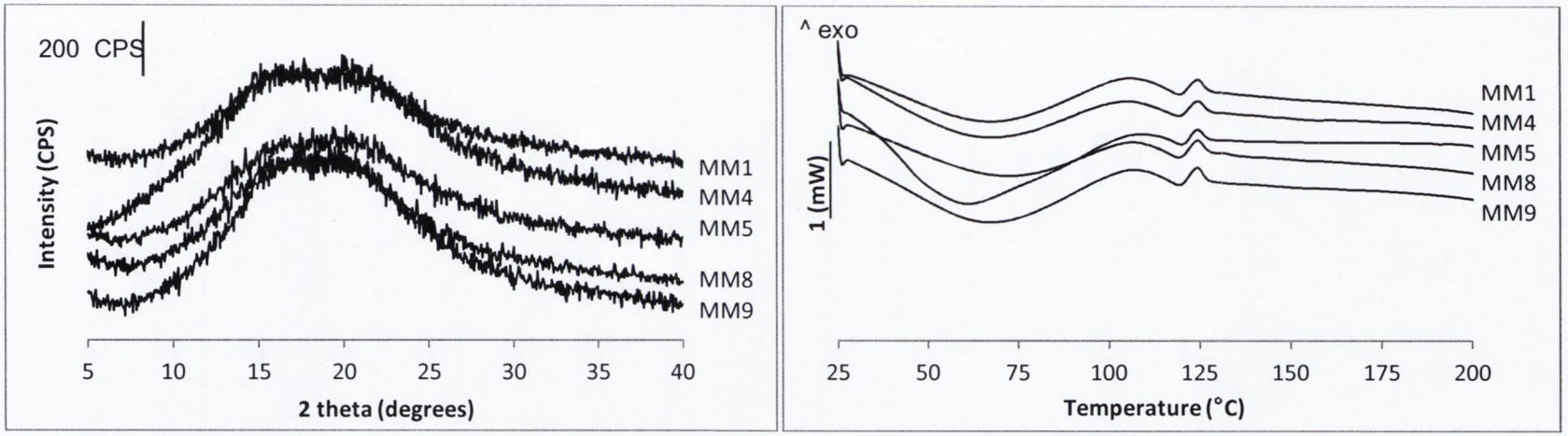

Chapter 6 (a) XRPD diffractograms and (b) DSC scans of spray dried raffinose powders prepared using the Niro Mobile Minor

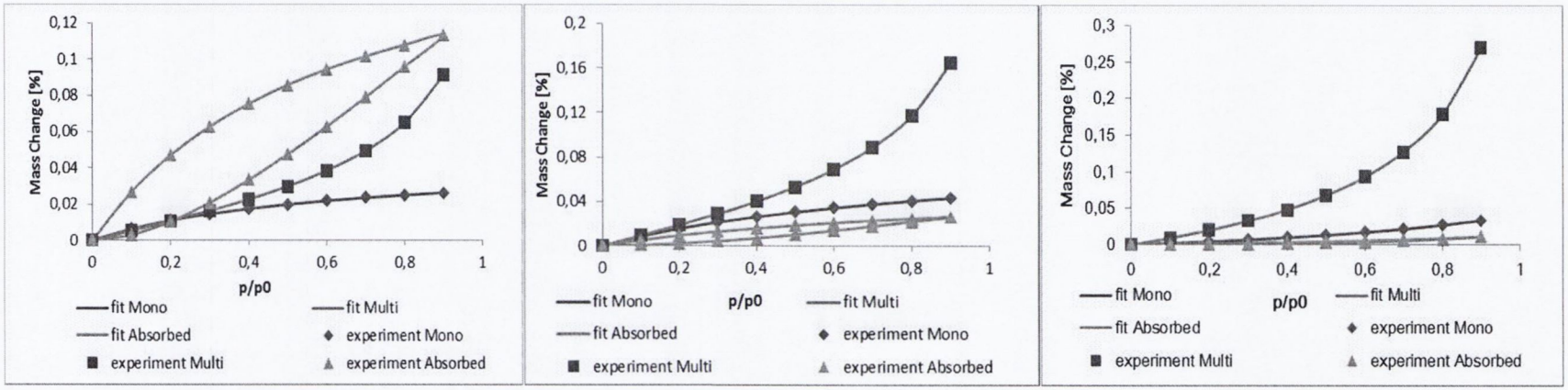

Chapter 6 Young-Nelson model component plot of (a) sCT:T, (b) sCT:T:HPβCD 5:38:57 and (c) sCT:T:HPβCD 5:28:67.

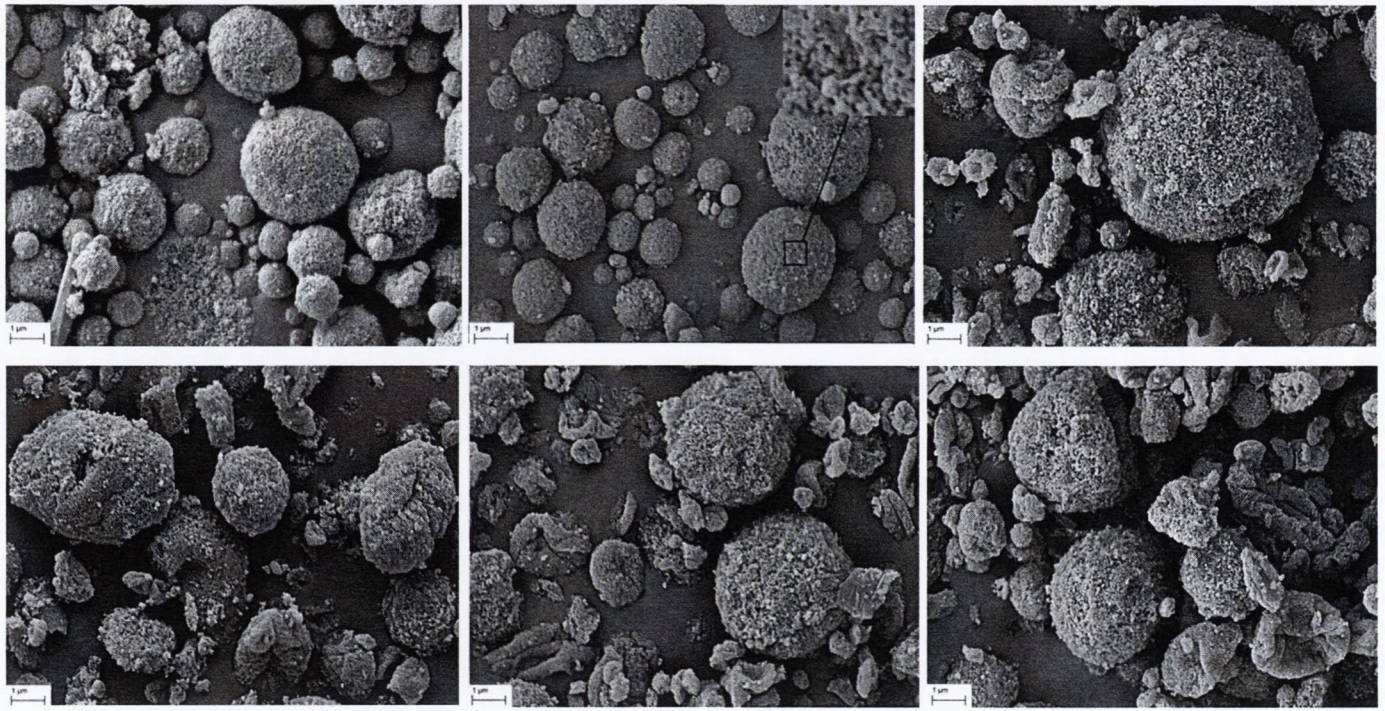

Chapter 7 SE micrographs of spray-dried (a) sCT:R, (c) sCT:R:HPβCD 5:57:38 and (e) sCT:R:HPβCD 5:38:57 after 24-weeks storage at 25 °C/< 5% RH; and of spray-dried (b) sCT:R, (d) sCT:R:HPβCD 5:57:38 and (f) sCT:R:HPβCD 5:38:57 after 24-weeks storage at 4 °C/< 5% RH.

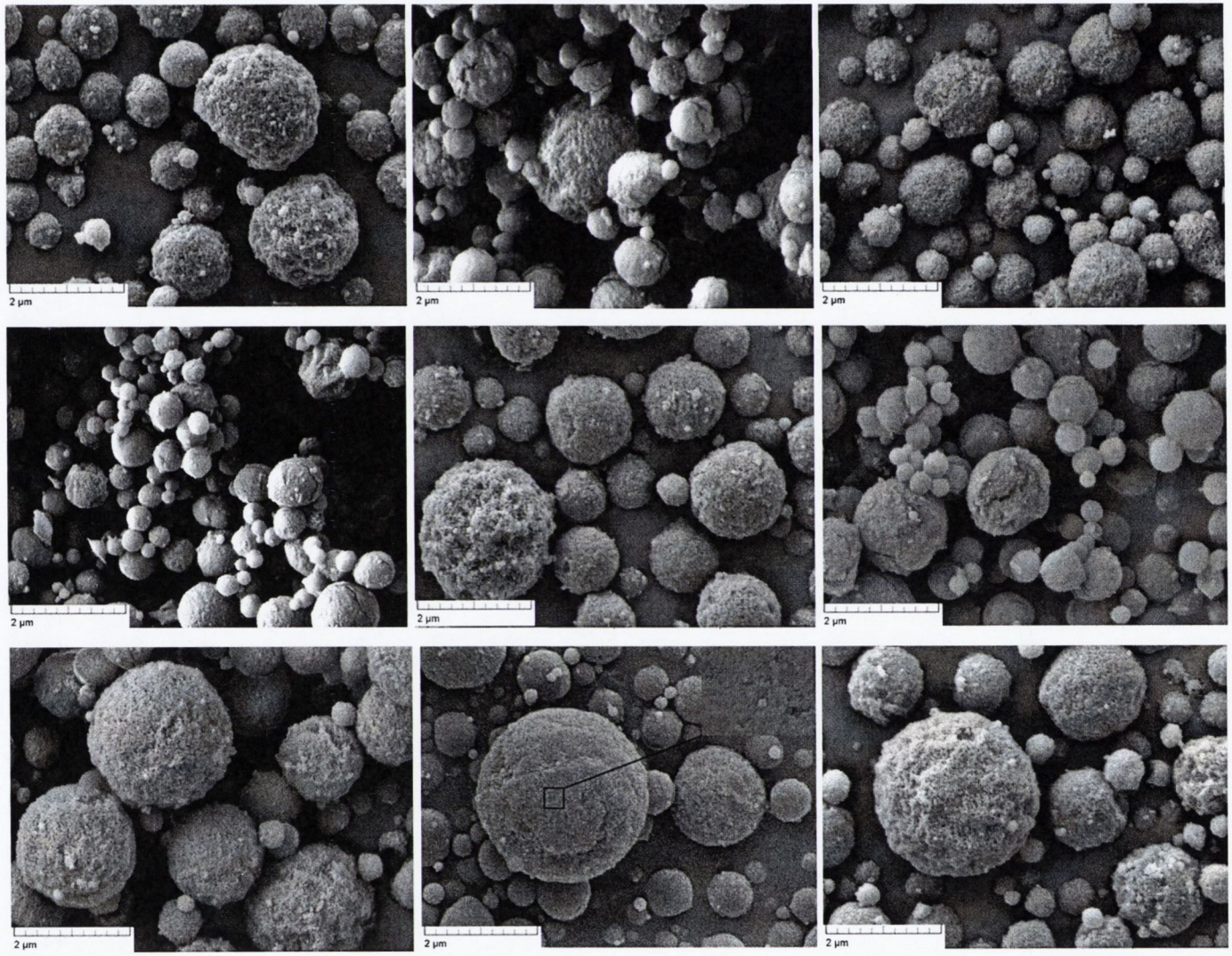
2 µm
2 µm
2 µm
2 µm
2 µm
2 µm
2 µm
2 µm
2 µm

Chapter 7 SE micrographs of spray-dried (a) sCT:T, (c) sCT:T:R, (e) sCT:T:HPβCD 5:67:28, (g) sCT:T:HPβCD 5:57:38, (i) sCT:T:HPβCD 5:38:57 and (k) sCT:T:HPβCD 5:28:67 after 24-weeks storage at 25 °C/< 5% RH; and of spray-dried (b) sCT:T, (d) sCT:T:R, (f) sCT:R:HPβCD 5:67:28, (h) sCT:R:HPβCD 5:57:38, (j) sCT:T:HPβCD 5:38:57 and (l) sCT:T:HPβCD 5:28:67 after 24-weeks storage at 4 °C/< 5% RH.

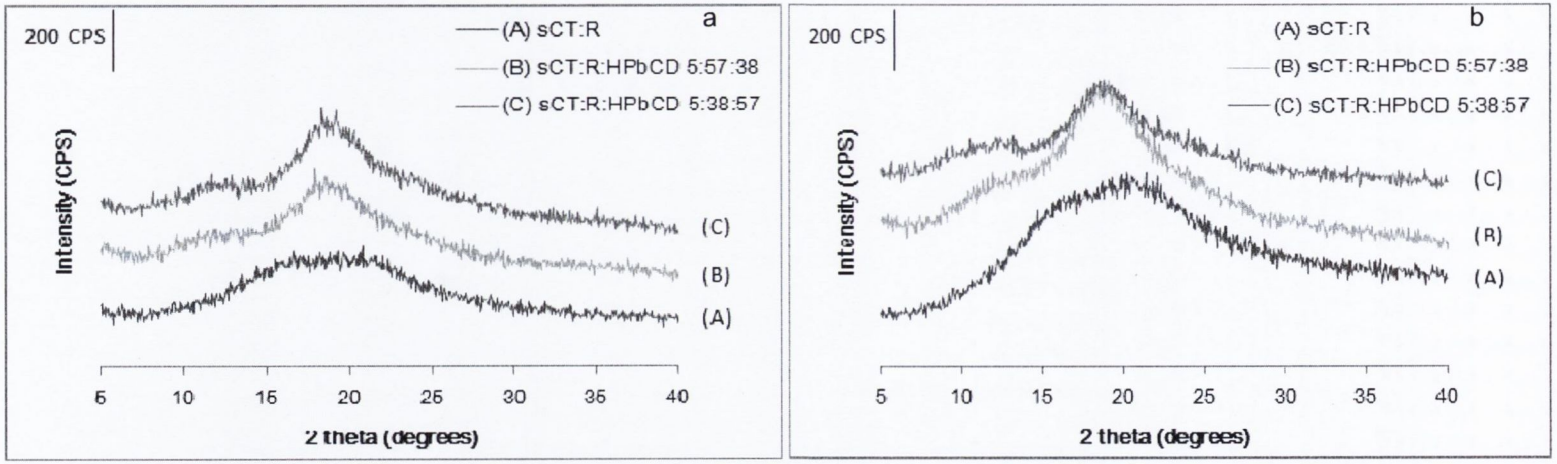

Chapter 7 XRPD of spray-dried sCT:raffinose composite systems after storage at (a) 25 °C/ 5% RH and (b)) 4 °C/ 5% RH. HPbCD – Hydroxypropyl-β-cyclodextrin

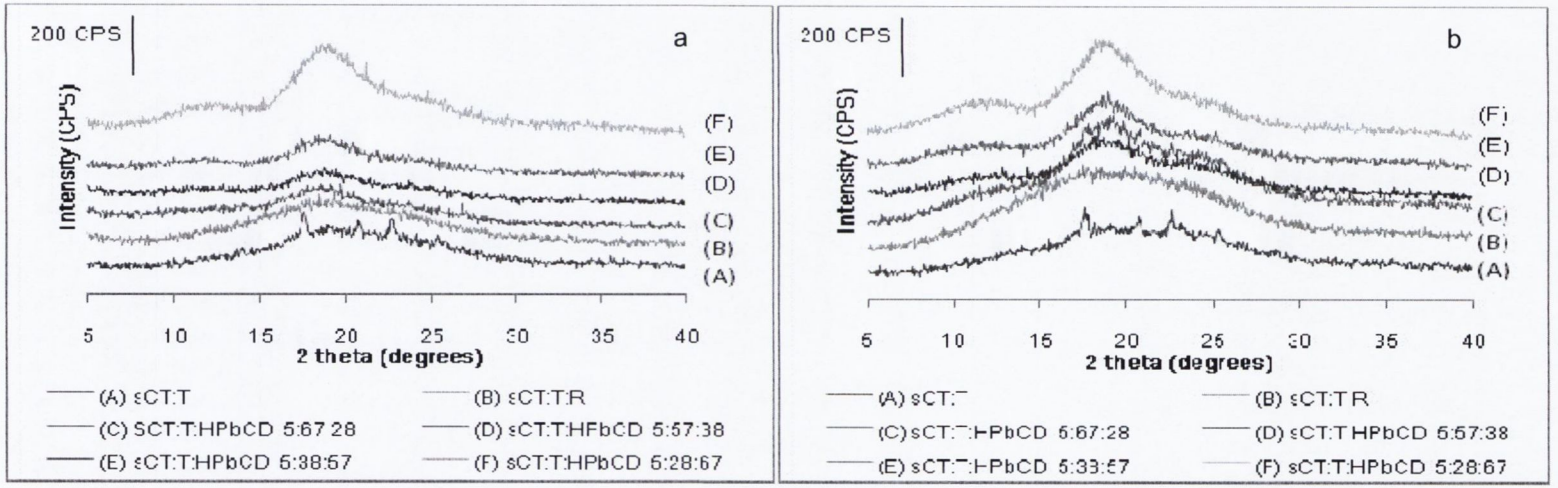

Chapter 7 XRPD of spray-dried sCT:trehalose composite systems after storage at (a) 25 °C/ 5% RH and (b)) 4 °C/ 5% RH. HPbCD – Hydroxypropyl-β-cyclodextrin

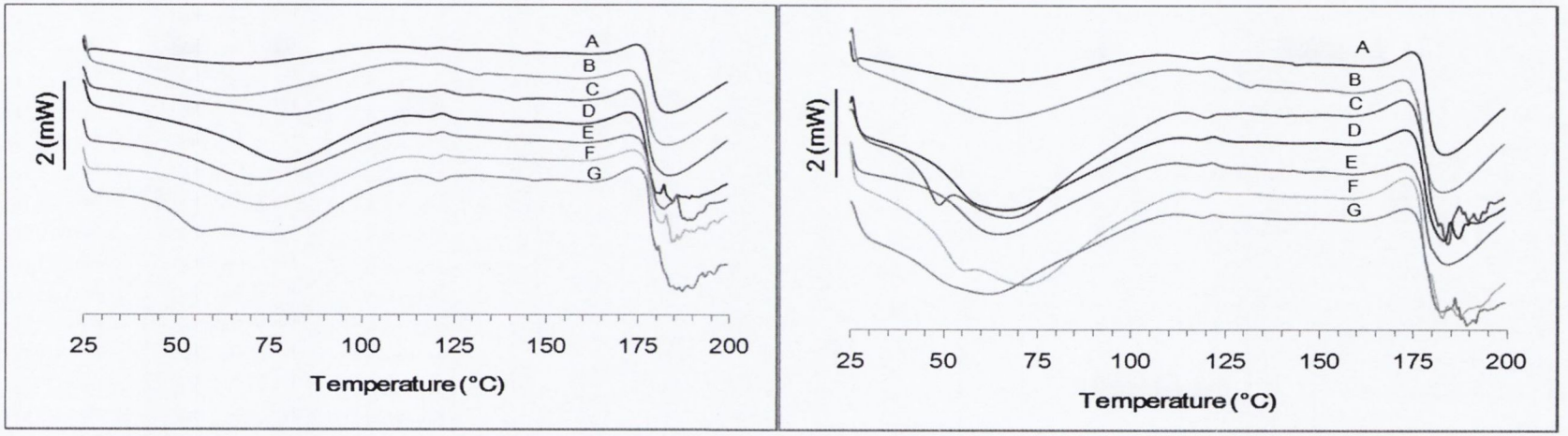

Chapter 7 DSC scan of sCT:R stored at (left) 25 °C/5% RH and (right) 4 °C/5% RH at weeks 4 (B), 8 (C),12 (D), 16 (E), 20 (F) and 24 (F) and, freshly spray dried powder (A).

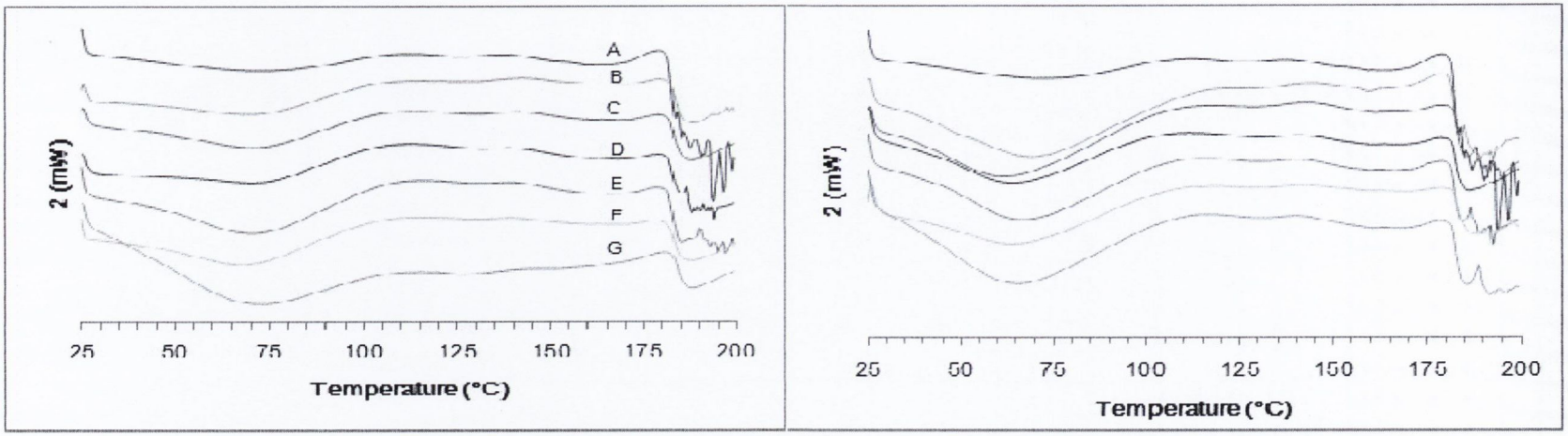

Chapter 7 DSC scans sCT:R:HPβCD 5:57:38 stored at (left) 25 °C/5% RH and (right) 4 °C/5% RH at weeks 4 (B), 8 (C),12 (D), 16 (E), 20 (F) and 24 (F) and, freshly spray dried powder (A).

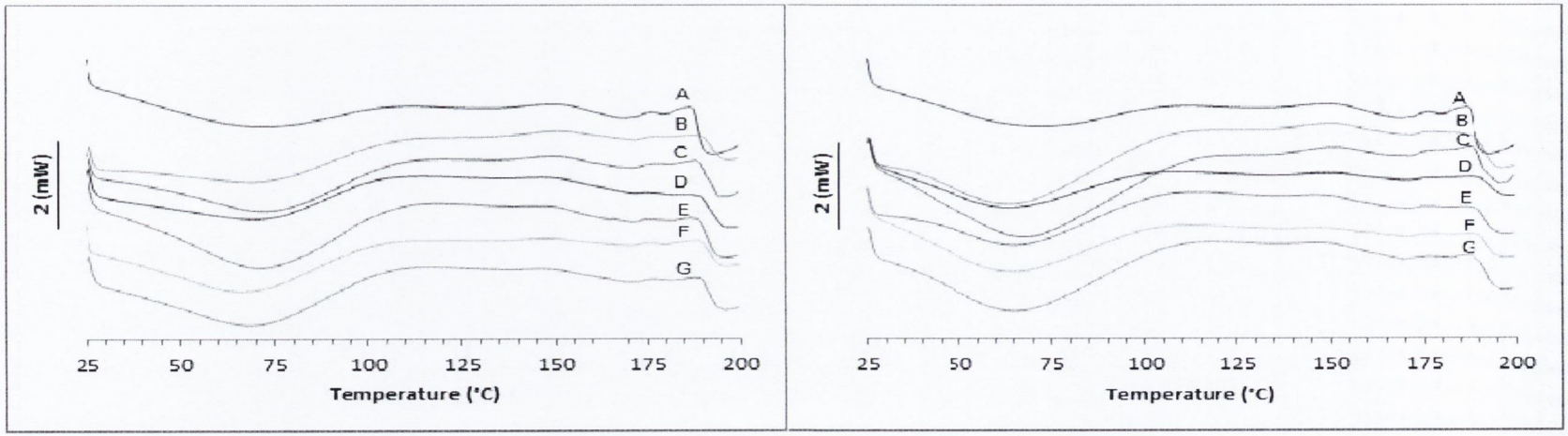

Chapter 7 DSC scans of sCT:R:HPβCD 5:38:57 stored at (left) 25 °C/5% RH and (right) 4 °C/5% RH at weeks 4 (B), 8 (C),12 (D), 16 (E), 20 (F) and 24 (F) and, freshly spray dried powder (A).

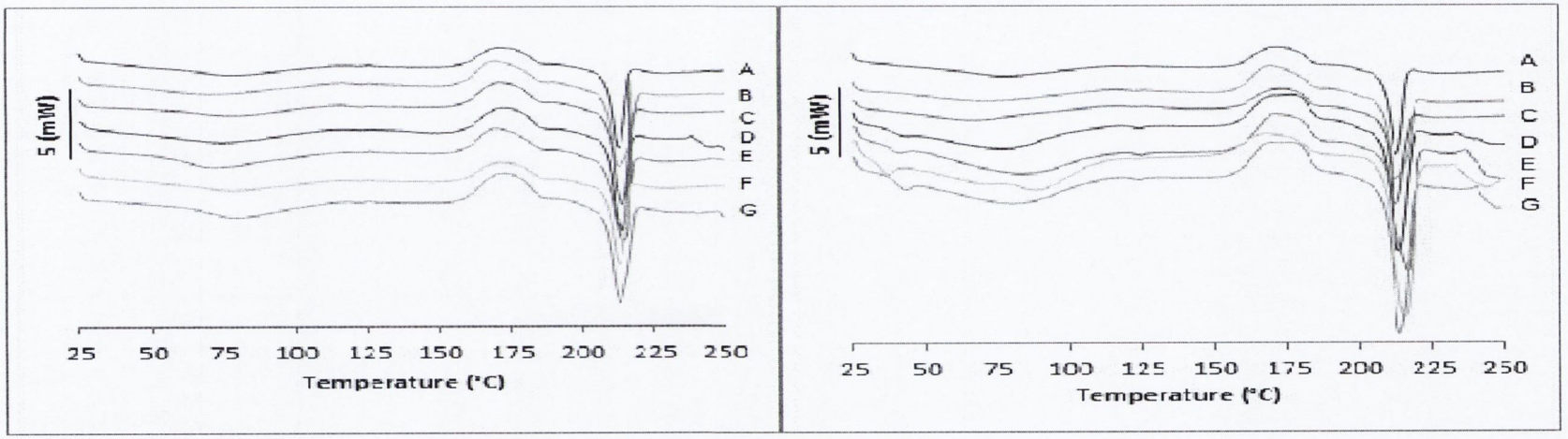

Chapter 7 DSC scans of sCT:T stored at (left) 25 °C/5% RH and (right) 4 °C/5% RH at weeks 4 (B), 8 (C),12 (D), 16 (E), 20 (F) and 24 (F) and, freshly spray dried powder.

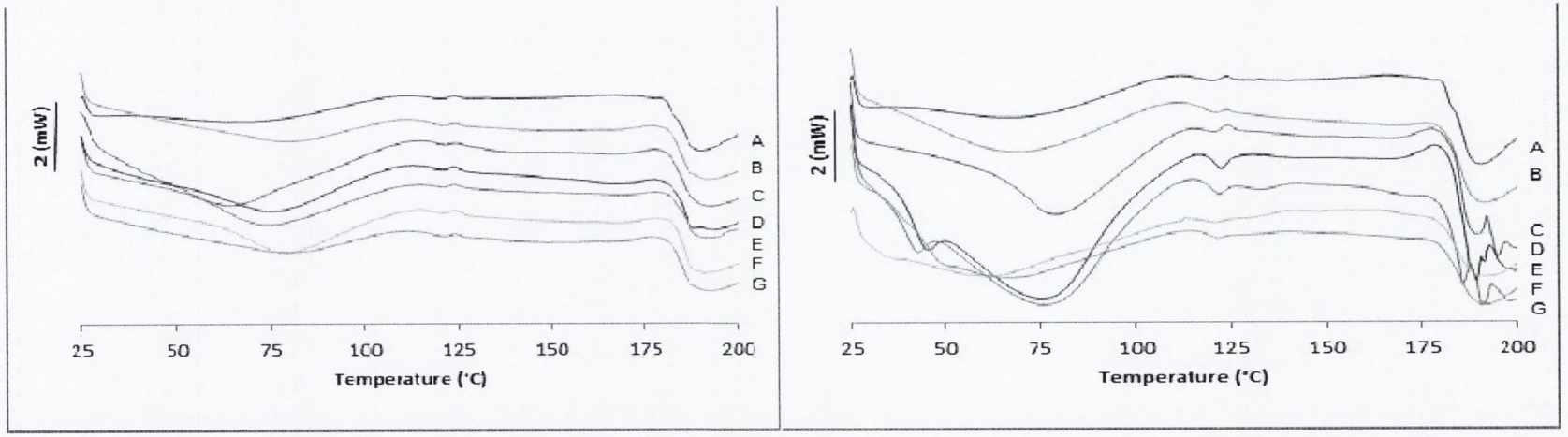

Chapter 7 DSC scans of sCT:T:R stored at (left) 25 °C/5% RH and (right) 4 °C/5% RH at weeks 4 (B), 8 (C),12 (D), 16 (E), 20 (F) and 24 (F) and, freshly spray dried powder (A).

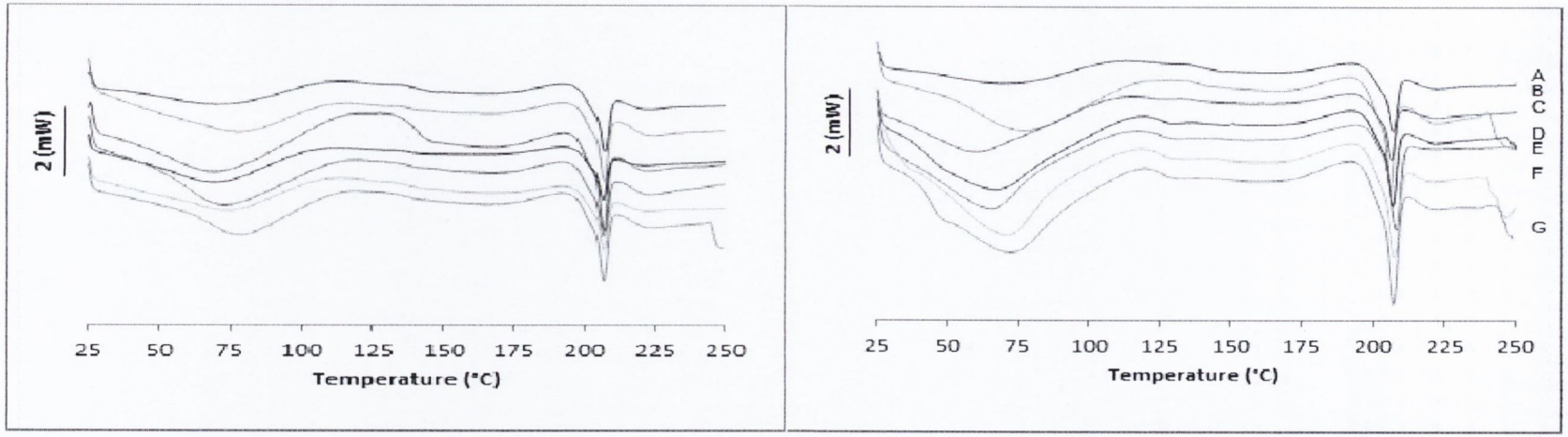

Chapter 7 DSC scans of sCT:T:HPβCD 5:67:28 stored at (left) 25 °C/5% RH and (right) 4 °C/5% RH at weeks 4 (B), 8 (C),12 (D), 16 (E), 20 (F) and 24 (F) and, freshly spray dried powder (A).

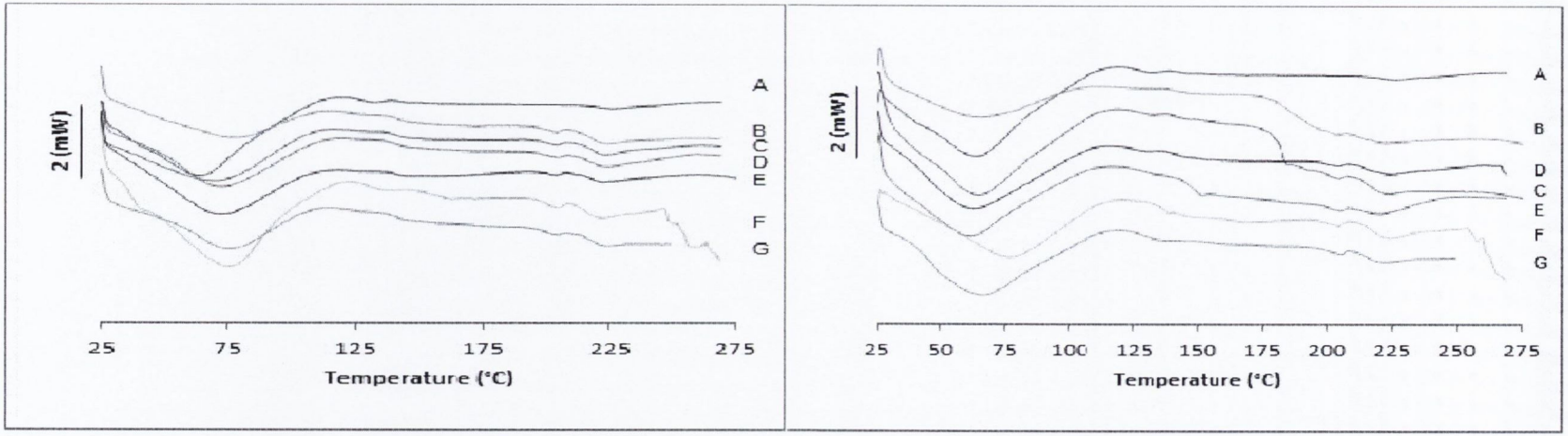

Chapter 7 DSC scans of sCT:T:HPβCD 5:57:38 stored at (left) 25 °C/5% RH and (right) 4 °C/5% RH at weeks 4 (B), 8 (C),12 (D), 16 (E), 20 (F) and 24 (F) and, freshly spray dried powder (A).

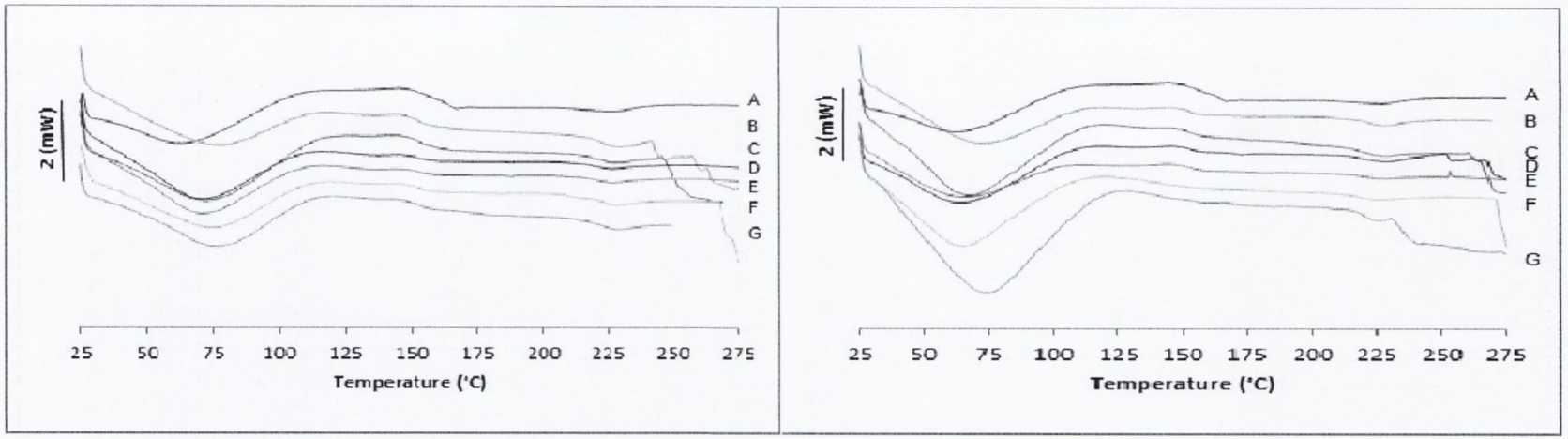

Chapter 7 DSC scans of sCT:T:HPβCD 5:38:57 stored at (left) 25 °C/5% RH and (right) 4 °C/5% RH at weeks 4 (B), 8 (C),12 (D), 16 (E), 20 (F) and 24 (F) and, freshly spray dried powder (A).

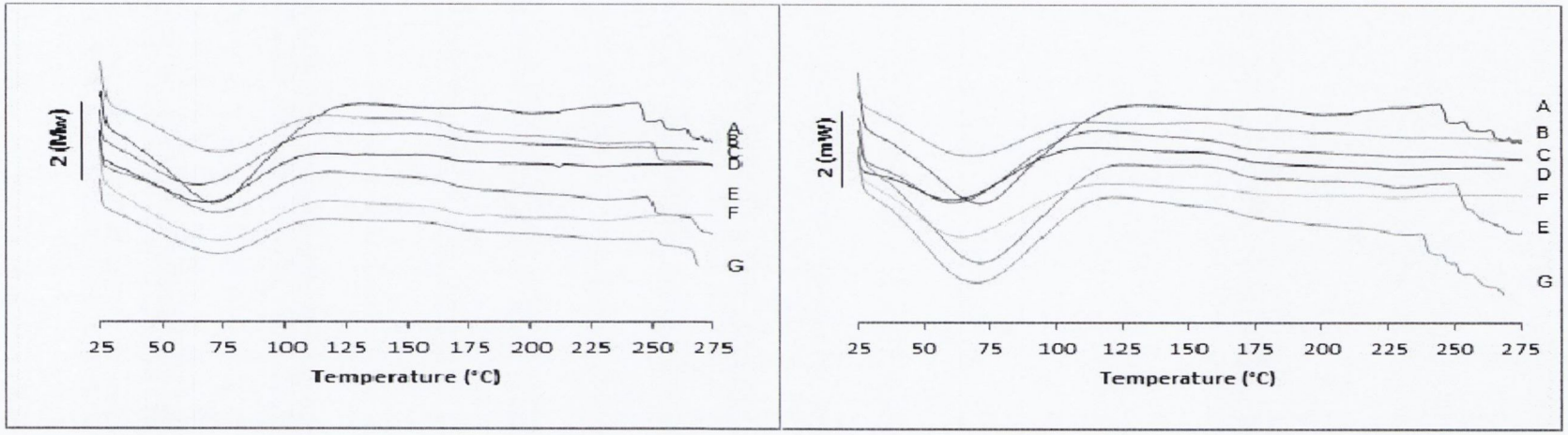

Chapter 6 DSC scans of sCT:T:HPβCD 5:28:67 stored at (left) 25 °C/5% RH and (right) 4 °C/5% RH at weeks 4 (B), 8 (C),12 (D), 16 (E), 20 (F) and 24 (F) and, freshly spray dried powder (A).

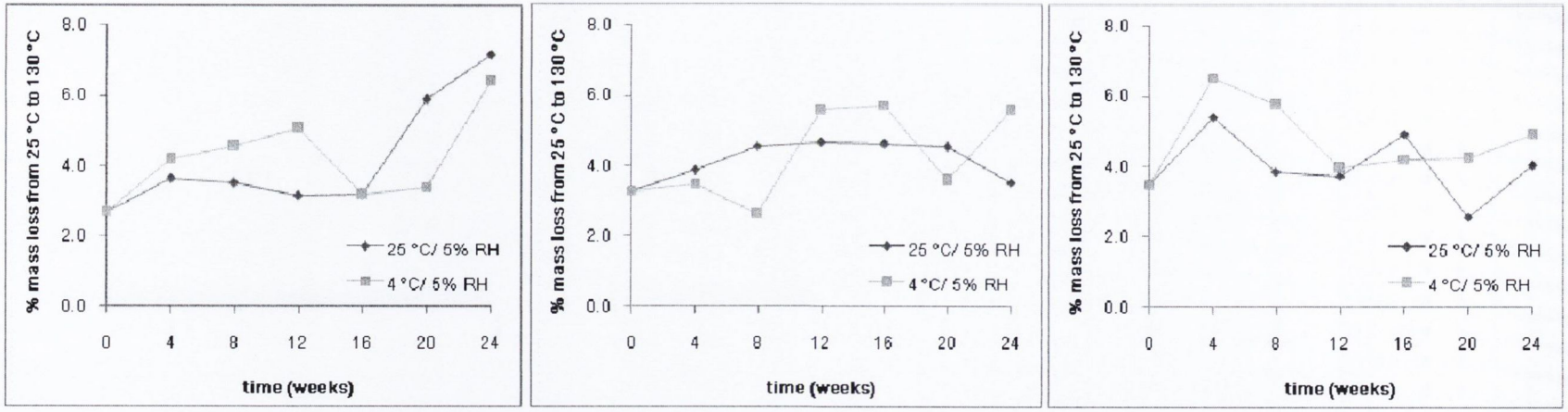

Chapter 7 Percentage of mass loss from 25°C to 130°C by TGA of (left) sCT:R, (middle) sCT:R:HPβCD 5:57:38 and (right) sCT:R:HPβCD 5:38:57 during storage.

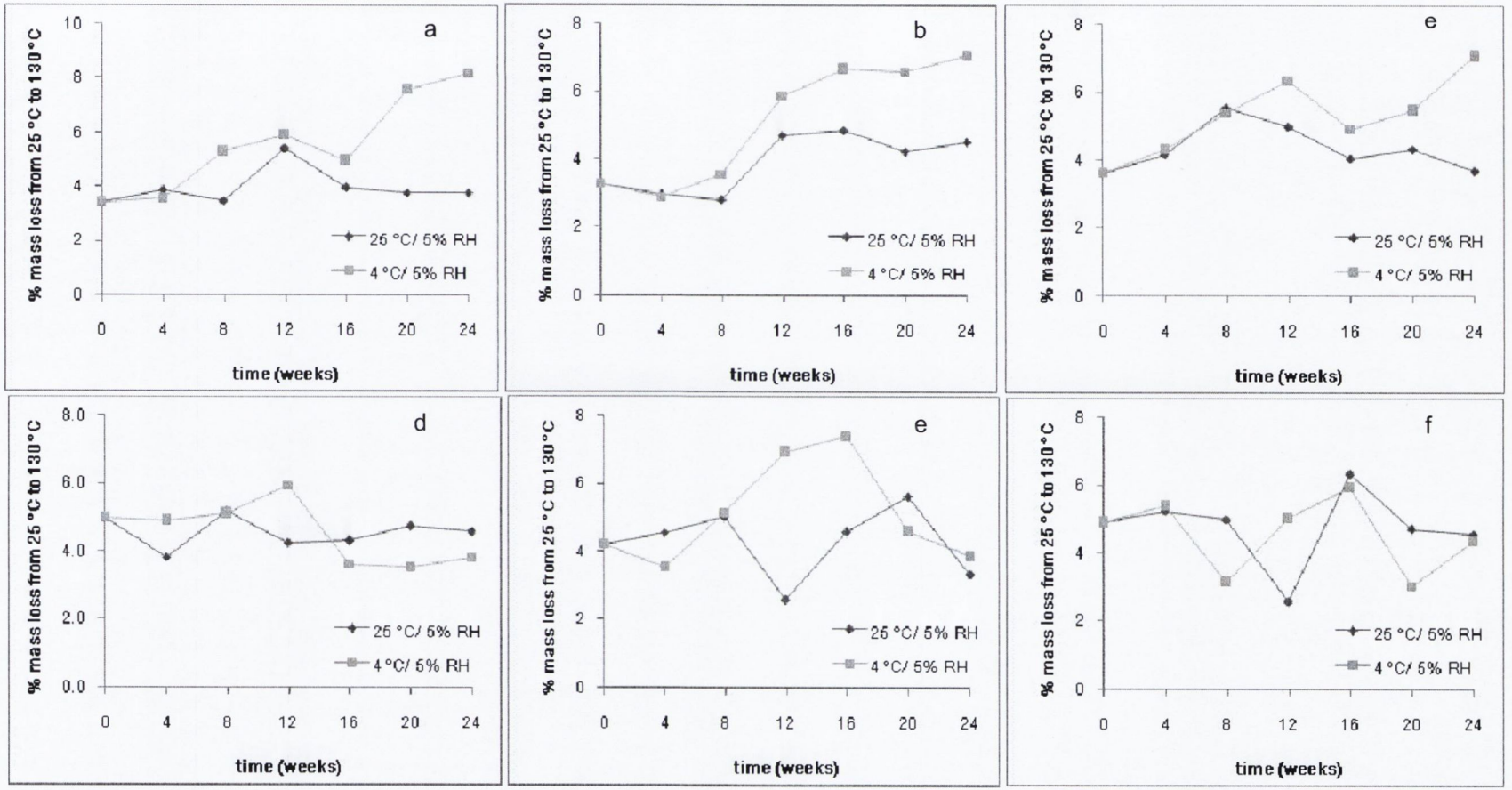

Chapter 7 Percentage of mass loss from 25°C to 130°C by TGA of (a) sCT:T, (b) sCT:T:R, (c) sCT:R:HPβCD 5:67:28, (d) sCT:R:HPβCD 5:57:38, (e) sCT:R:HPβCD 5:38:57 and (f) sCT:R:HPβCD 5:28:67 during storage.

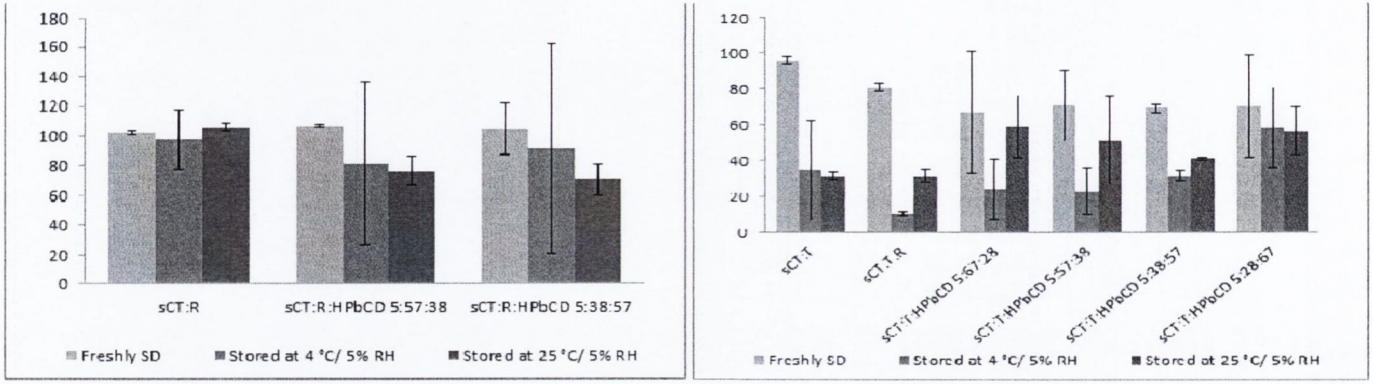

Chapter 7 Retained salmon calcitonin activity (±SD) for (a) all raffinose composite systems and (b) all trehalose composite systems after 24 weeks storage.

Chapter 7 Phamacokinetic parameters of sCT in rats after intratracheal delivery (mean ±SD, n=5).

	sCT solution iv	sCT solution pulm	sCT:R 5:95	sCT:R:HPbCD 5:57:38	sCT:T 5:95
Dose (µg/Kg)	84±6.95	94±12.3	146±21.3	124±9.9	124±16.9
AUC0∞ (µg.h/L)	180.4±37.36	22.4±4.70	36.5±13.80	39.5±4.29	27.8±3.32
Cmax (µg/L)		15.8±5.06	33.8±12.97	42.5±8.73	11.0±4.14
tmax (h)		0.07±0.05	0.1±0.06	0.1±0.06	0.2±0.12
Cl (L/h/Kg)	0.53±0.11				
Clpulm (L/h/Kg)		0.05±0.01	0.05±0.01	0.03±0.01	0.05±0.01
MRT (h)	0.59±0.06	2.0±0.73	1.3±0.10	1.3±0.18	2.2±0.93
MAT (h)		1.2±0.97	0.5±0.37	0.6±0.45	1.2±0.93
ke (h-1)	1.04±0.16	0.6±0.18	0.8±0.06	0.8±0.10	0.6±0.29
ka (h-1)		1.6±1.03	2.74±1.32	3.7±2.82	0.9±0.51
t1/2β (h)	0.6±0.11	1.5±0.68	0.8±0.07	0.9±0.06	0.6±0.48
Fabs (%)		11.3±3.01	11.5±3.48	14.9±2.01	10.1±1.37
Frel (%)			104±31.5	135±18.24	74.9±25.91
Vss (L/Kg)	0.4±0.12	0.1±0.04	0.1±0.02	0.03±0.02	0.1±0.07
Vdβ (L/Kg)	0.4±0.05	0.1±0.06	0.1±0.02	0.04±0.004	0.1±0.05